OPEN ACCESS

University of BRISTOL

This electronic thesis or dissertation has been downloaded from Explore Bristol Research, http://research-information.bristol.ac.uk

Author:
Jervis, Mark T

Title:
Some effects of surface tension on water waves at a wall.

General rights
Access to the thesis is subject to the Creative Commons Attribution - NonCommercial-No Derivatives 4.0 International Public License. A copy of this may be found at https://creativecommons.org/licenses/by-nc-nd/4.0/legalcode This license sets out your rights and the restrictions that apply to your access to the thesis so it is important you read this before proceeding.

Take down policy
Some pages of this thesis may have been removed for copyright restrictions prior to having it been deposited in Explore Bristol Research. However, if you have discovered material within the thesis that you consider to be unlawful e.g. breaches of copyright (either yours or that of a third party) or any other law, including but not limited to those relating to patent, trademark, confidentiality, data protection, obscenity, defamation, libel, then please contact collections-metadata@bristol.ac.uk and include the following information in your message:

• Your contact details
• Bibliographic details for the item, including a URL
• An outline nature of the complaint

Your claim will be investigated and, where appropriate, the item in question will be removed from public view as soon as possible.

Some Effects of Surface Tension on Water Waves and Water Waves at a Wall

Mark T. Jervis

School of Mathematics
University of Bristol

A Thesis submitted to The University of Bristol
for the degree of Doctor of Philosophy
in the Faculty of Science

September 1996

Abstract

The work presented here mainly concerns the effects of surface tension on steep gravity waves. These are investigated by extending a numerical program to include surface tension. The work has been influenced by contact with coastal engineers, and as a result the third chapter is devoted to the study of waves near a wall, in particular on shallow water. The two themes are brought together in the final substantial chapter which has significant implications for the extrapolation of results from small scale experiments to prototype scale.

Chapter 1 introduces capillary waves. In chapter 2, results from the potential flow solver for nonlinear almost steady waves are compared with the theoretical work of Longuet-Higgins (1963, 1995) and experiments Perlin, Ting & Lin (1993) and found generally to be in agreement. Some differences between our numerical results and the work of these authors are highlighted and explained.

Chapter 3 relates to coastal engineering applications and considers a different type of surface wave, the gravity waves found in front of coastal structures. The study focuses on the hydrodynamic parameters on the bed under such waves. In particular, trends as the water depth is decreased and the failure of linear theory on shallow depths.

Study of the interaction of such waves with coastal structures is continued in chapter 4. The flow of water due to the overtopping of a vertical wall by waves is modelled. Results for overtopping volume per wave are in general agreement with experimental data on overtopping rates. The model is used to investigate the effect of different shapes for bed geometry in front of the wall.

The preceding chapters are brought together in the final sections. The inclusion of surface tension allows us to perform overtopping calculations for the small scale waves often used in wave experiments. We find that surface tension can significantly affect the overtopping volumes and run-up heights.

Acknowledgements

I would like to thank Prof. Howell Peregrine in particular for his help and guidance during this study, and Geoff Mercer and David Smith at University College, Canberra, Australia for the provision of standing wave profiles.

I would also like to thank all my family and Kate Bower for continued encouragement and support without which I would have not completed this thesis. Thanks must also go to Diki Porter and Tim Barnes for help with LaTeX and IDL as well as Johnny Fathers, Richie Jones, Dave Donaghy and the rest of the Mathematics Department postgraduates for their various morale boosting antics.

I acknowledge support from the U.K. Engineering and Physical Sciences Research Council and from the Commission of the European Communities, Directorate General for Science, Research and Development under MAST Contract MAS2-CT92-0047.

Author's Declaration

The work described in this dissertation was carried out in the School of Mathematics, University of Bristol and has not been submitted for any other degree or diploma of any examining body. All the material described herein is the original work of the author, except where otherwise acknowledged.

M.T. Jervis

Contents

1 Introduction **1**

1.1 Capillary waves 1

1.2 Basic equations 3

1.2.1 Numerical and analytical studies of capillary-gravity waves . . 7

1.2.2 Pure capillary waves 11

1.3 Summary of chapter 2 13

1.4 Summary of later chapters 13

2 Surface Tension Effects On Steady Gravity Waves **16**

2.1 'Parasitic' capillary waves 16

2.1.1 A dynamical theory of parasitic capillary waves 17

2.1.2 Energy of parasitic capillaries 19

2.1.3 Generation of vorticity by parasitic capillaries 20

2.1.4 Blocking of capillary waves 21

2.1.5 Three- and four-wave interactions 22

2.1.6 Breaking of parasitic capillary waves 24

2.1.7 Origin of parasitic capillary waves 25

2.2 Current work on parasitic capillaries 26

2.2.1 Numerical formulation 26

2.2.2 Basic numerical model 26

2.2.3 Length scales and the choice of σ 31

2.2.4 Numerical instabilities and smoothing 32
2.2.5 Surface energy 34
2.2.6 Effect of smoothing on energy 34
2.2.7 Other effects of point number 38
2.2.8 Resolution of capillary waves 41
2.2.9 Regridding the surface 42
2.3 Numerical calculations 44
2.3.1 Quasi-steady capillary gravity waves 44
2.4 Comparison with other numerical calculations 48
2.4.1 Longuet-Higgins (1995) 48
2.4.2 Comparisons with Perlin, Lin & Ting (1993) 58
2.5 Very steep gravity waves 69
2.6 Short capillary-gravity waves 73
2.7 Solitary-type capillary-gravity waves 74
2.7.1 Blocking on solitary waves 79
2.8 Conclusion, discussion and further work 79

3 Waves Near Vertical Walls **84**

3.1 Introduction 84
3.2 Waves near coastal structures 87
3.3 Small amplitude theory for bed quantities 91
3.3.1 Parameters characterising shallow water waves 91
3.3.2 Bed velocity 93
3.3.3 Pressure 98
3.3.4 Pressure gradients 101
3.4 Standing waves on very shallow water 105
3.4.1 Bed parameters under reflecting solitary waves 105

3.5 Discussion and conclusion 107

4 Overtopping of Vertical Walls **110**

4.1 Introduction 110

4.2 Parameters affecting overtopping 113

4.3 Previous work on wave overtopping 116

4.4 Overtopping model 118

4.4.1 Limitations of simple model 123

4.5 Results with gravity waves. 125

4.5.1 Without berm 125

4.5.2 With berm 127

4.6 Comparison to existing experimental data 133

4.6.1 Franco 1994 133

4.6.2 Juhl (1995) 134

4.7 Overtopping with gravity-capillary waves 136

4.8 Run-up of solitary type waves with surface tension 139

4.8.1 Overtopping volumes with surface tension 141

4.9 Further work and conclusion 143

5 Conclusion **146**

Bibliography **150**

List of Figures

1.1 Waves generated by a wind of $6\,\mathrm{ms}^{-2}$ in a laboratory flume. *(Ebuchi, Kawamura & Toba. 1987).* 2

1.2 Phase velocity as a function of wavelength, linear theory. $T = 72\,\mathrm{dyn/cm}$. 5

1.3 Surface profiles for pure irrotational capillary waves up to the limiting profile. Calculated using equations of Crapper (1957). 12

2.1 Surface disturbance to a stream for $U > c_m$ 18

2.2 Domain for the periodic problem. 29

2.3 Surface tension parameter σ against characteristic length scale, $l\,\mathrm{cm}$ for g=980.6 cms^{-2}, $\rho_0 = 1\mathrm{g\ cm}^{-3}$ and $T' = 74\mathrm{g\ s}^{-2}$. 33

2.4 Kinetic (top) and potential (bottom) energy for a wave with initial Stokes wave profile $ak = 0.227$, $\lambda = 6.82\,\mathrm{cm}$. Non-dimensionalised against initial energies. 37

2.5 Non-dimensional kinetic energy (top), potential energy (middle) and surface energy (bottom) for a wave with initial Stokes wave profile $ak = 0.227$, $\lambda = 6.82\,\mathrm{cm}$. 38

2.6 ky against kx. Comparison of steady wave for 200 and 400 surface calculation points. $ak = 0.3$, $\lambda = 8\,\mathrm{cm}$. No regridding. (Wave propagation is in the $+x$ direction). 39

2.7 ky against kx. Comparison of steady wave for 200 and 400 surface calculation points (no regridding). Close up of trough region. $ak = 0.3$, $\lambda = 8\,\text{cm}$. The ripples calculated with 400 calculation points have a shorter wavelength. 40

2.8 Quasi-steady surface profiles with (below) and without (above) regridding the surface calculation points $ak = 0.315$, λ=8 cm. Propagation is in -x direction. 43

2.9 Surface slope of quasi-steady waves with (below) and without (above) regridding the surface calculation points $ak = 0.315$, λ=8 cm. Propagation is in -x direction. 43

2.10 Computation of the development of surface profile from an initial gravitational progressive Stokes wave, $ak = 0.32$. λ=8 cm. 46

2.11 Overplotting of ky against kx over 10 wave periods. $ak = 0.32$, $\lambda = 8\,\text{cm}$. (Wave propagation is in the $+x$ direction). 47

2.12 Surface profiles for $\lambda = 8\text{cm}$, $ak = 0.24, 0.26, 0.28, 0.30, 0.31, 0.315, 0.32$. (Wave propagation is in the $-x$ direction). 51

2.13 Surface slopes for $\lambda = 8\text{cm}$, $ak = 0.24, 0.26, 0.28, 0.30, 0.31, 0.315, 0.32$. (Wave propagation is in the $-x$ direction). 52

2.14 (a) Surface elevation and (b) slope for $\lambda = 8\text{cm}$, $ak = 0.24, 0.26, 0.28$ and 0.30 (subcritical). NB: For both (a) and (b), the profiles have been shifted for clarity. *Longuet-Higgins (1995)*. 53

2.15 (a) Surface elevation and (b) slope for $\lambda = 8\text{cm}$, $ak = 0.32, 0.34$ and 0.36 (supercritical). NB: For both (a) and (b), the profiles have been shifted for clarity. *Longuet-Higgins (1995)*. 54

2.16 ky against kx for a Stokes wave ak=0.315 (dashed) and a fully developed capillary gravity wave started from the Stokes wave profile (solid) for $\sigma = Tk^2/g = 0.0452$. The corresponding vertical lines delimit the region around the crest in which the stream velocity is less than the minimum linear wave speed. (Wave propagation is in the $+x$ direction). 56

2.17 dy/dx against kx for a Stokes wave ak=0.315 (dashed) and a fully developed capillary gravity wave started from the Stokes wave profile (solid) for $TK^2/g = 0.0452$. The corresponding vertical lines delimit the region in which the stream velocity is less than the minimum linear wave speed. (Wave propagation is in the $+x$ direction). 57

2.18 Numerically calculated drift velocity for a gravity-capillary waves of wavelength 8.25cm. 58

2.19 Development of the surface from $ak = 0.227$, $\lambda = 6.82\,\text{cm}$. 59

2.20 Development of surface from $ak = 0.227$, $\lambda = 6.82\,\text{cm}$ in frame of reference moving with gravity wave crest. (Wave propagation is in the $+x$ direction). 60

2.21 Comparison of (a) the measured 5.26Hz profile (chosen representative image) with (b) the theory of Longuet-Higgins (1963). The bold line is a wave of the correct steepness and the second line is the wave which gives the same predicted capillary amplitude as observed. (c) is the theory of Crapper (1970) and (d), (e) and (f) three possible numerical solutions determined using the Schwartz and Vanden-Broeck scheme (1979) *Perlin et al. (1993)*. 65

2.22 (a) The profile of a wave at 5.26Hz as recorded by Perlin *et al.* (1993). (b) The profile calculated by Longuet-Higgins (1995) for $ak = 0.227$, $\lambda = 6.82\,\text{cm}$. *Perlin et al. (1993)* 66

2.23 ky against kx. Numerical calculation of surface profile after 2 and 20 wave periods. $ak = 0.227$, $\lambda = 6.82\,\text{cm}$. (Wave propagation is in the $-x$ direction). 67

2.24 Comparison of (a) the measured 4.21Hz profile (chosen representative image) with (b) the theory of Longuet-Higgins (1963). The bold line is a wave of the correct steepness and the second line is the wave which gives the same predicted capillary amplitude as observed. (c) is the theory of Crapper (1970) and (d) numerical solution determined using the Schwartz and Vanden-Broeck scheme (1979). *Perlin et al. (1993)* 68

2.25 Wave calculated by Longuet-Higgins (1995) for $ak = 0.25$, $\lambda = 10.2\,\text{cm}$. *Longuet-Higgins (1995)* 68

2.26 dy/dx (top) and ky (bottom) against kx from our numerical code for $ak = 0.25$, $\lambda = 10.2\,\text{cm}$. Plots have been shifted (but not scaled) to fit on same graph. Direction of propagation is right to left. 69

2.27 Wave evolution until breaking for $ak = 0.44$, $\lambda = 50\text{cm}$. 70

2.28 Wave evolution until breaking for $ak = 0.42$, $\lambda = 50\text{cm}$. 71

2.29 Wave evolution for initial Stokes wave $ak = 0.24$, $\lambda = 4\,\text{cm}$ in a reference frame moving with the phase speed of the initial Stokes pure gravity wave. (Propagation is in the $+x$ direction). 73

2.30 Capillary gravity waves generated by a 12 and 16 knot wind respectively. The scale in the photograph is 2cm long. Schooley (1958). . . 74

2.31 Development of a capillary-gravity wave travelling in the $-x$ direction. Depth, $d = 1\text{cm}$. The initial surface profile is that of a pure gravity wave of $a/d = 0.7$. 76

2.32 Surface gradient of capillary-gravity wave at $t = 8$ for $d = 1\text{cm}$, initial $a/d = 0.7$. 77

2.33 Surface profiles of capillary gravity waves for $d = 1$cm (top), 2cm, 3cm, 4cm, 5cm and no surface tension (bottom). a/d=0.7 78

3.1 Bed velocities under standing waves with maximum crest acceleration $0.3\,g$. Calculated using numerical code of Dold & Peregrine (1986). . 94

3.2 Surface profiles for a near standing wave with maximum crest acceleration $0.5\,g$ for $U_r = 1.75$. Surface displacement has been scaled by 2. 96

3.3 (a) Contour plot of bed velocity under near standing wave on depth $kh = 0.5$. Maximum crest acceleration is $0.5g$. (b) Contour plot of bed velocity under reflecting solitary wave $a/kh = 0.15$ ($U_r = 3.75$). Calculation using numerical code of Dold & Peregrine (1986). (The small oscillations are due to the contouring program.) 97

3.4 Bed pressures under standing waves with maximum crest acceleration $0.3\,g$. Calculation using numerical code of Dold & Peregrine (1986). . 100

3.5 Bed pressure gradients under standing waves with maximum crest acceleration $0.3\,g$. (U_r 0.023, 0.14 and 0.41). 103

3.6 Contour plot of bed (a) over pressure (b) over pressure gradient, dp/dx under near standing wave on depth $0.5\,/k$. $U_r = 3.5$. Calculation using numerical code of Dold & Peregrine (1986). 104

3.7 Contour plot of bed (a) over pressure (b) over pressure gradient, dp/dx under reflecting solitary waves. ($U_r = 3.75$). Calculation using numerical code of Dold & Peregrine (1986). 104

3.8 Contour plot of bed velocity under solitary wave collision with a wall. $a = 0.5h$. Calculation using numerical code of Dold & Peregrine (1986).106

3.9 Contour plot of bed (a) over pressure (b) over pressure gradient, dp/dx under solitary wave collision with a wall. $a = 0.5h$. Calculation using numerical code of Cooker (1990). 107

3.10 Close up of contour plot of bed over pressure gradient under solitary wave collision with a wall. $a = 0.5h$. Calculation using numerical code of Cooker (1990). 108

4.1 Cross sections of a some typical harbour breakwater. 111

4.2 Schematic cross section of a harbour breakwater with definition of terms. 112

4.3 Overtopping of breakwaters presents many problems. (Warning sign, Alderney Harbour Breakwater, Channel Islands.) 114

4.4 Solitary wave collision with vertical wall. Wave height, $H = 0.75d$ . . 120

4.5 Solitary wave steepening over wide berm 126

4.6 Solitary wave overtopping on water of constant depth; different wave heights, H 127

4.7 Solitary wave overtopping; berm width = d, different berm heights. $H = 0.7d$ 128

4.8 Solitary wave overtopping; berm width = $2\,d$, different berm heights. $H = 0.7d$ 129

4.9 Solitary wave overtopping; berm width = $3\,d$, different berm heights. $H = 0.7d$ 130

4.10 Vertical wall with berm width $2\,d$, height $0.5\,d$. $H = 0.75d$ 130

4.11 Solitary wave overtopping; berm height = $0.1\,d$, $H = 0.7d$. 131

4.12 Solitary wave overtopping; berm height = $0.2\,d$, $H = 0.7d$. 131

4.13 Vertical wall with berm width $4\,d$, height $0.5\,d$, $H = 0.75d$. 132

4.14 Exceedence probabilities for our non-dimensional results. 134

4.15 Comparison of estimated overtopping rates with Juhl (1995) (wind speed= 0, angle of attack= 0^o) 135

4.16 Imbalance of cohesive and adhesive forces can lead to an elevation of the equilibrium contact point. 138

4.17 y/d against x/d at times up to maximum run-up for a solitary wave a=0.7 d, d=5cm, berm width=4 d, berm height=0.1 d. 140

4.18 y/d against x/d at time of maximum run-up for a solitary wave $a = 0.7d$, for d=2cm, 5cm, 10cm, 20cm, 50cm and ∞ i.e. no surface tension. Profiles have been shifted vertically for clarity. 141

4.19 Dimensionless overtopping volume against dimensionless free-board for a solitary wave $a = 0.7d$, d= 5cm, 10cm, 20cm, 50cm and ∞ i.e. no surface tension. 142

4.20 Dimensionless overtopping volume against dimensionless free-board on a berm of width $4d$ for a solitary wave $a = 0.7d$, for d=5cm with no surface tension. 143

List of Tables

3.1 Numerically calculated maximum absolute non-dimensional pressure gradient under reflecting solitary waves. 107

4.1 Thickness of the jet tip at the time of maximum run-up. 139

Chapter 1

Introduction

1.1 Capillary waves

On any fluid surface, there are two main restoring forces; gravity and surface pressure. For water, gravity is dominant for large scale surface disturbances (of order greater than 10cm). The pressure exerted on a surface by the atmosphere can for most applications be regarded as constant, i.e. the upper fluid is light enough to cause no significant variation in hydrostatic or dynamic pressure. At small scale however, this pressure force is modified by a interfacial wind stress or surface tension. Surface tension is the force that pulls water droplets into spheres and tends to flatten a surface. It arises from attractive forces between partially polarised water molecules. A fuller account is available in Batchelor (1967).

The study of fluid surfaces at small scale has been an area of increasing interest over recent years, although reports in the literature of such waves can be traced back to the last century. A look at the surface of any wind blown stretch of water will reveal many small-scale ripples or *capillary* waves.

Figure 1.1 shows a picture of such waves from experimental work by Ebuchi, Kawamura & Toba (1987). Observations of such waves are given by Russell (1844) (also quoted in Lamb (1932 §350). Capillary waves are typically of wavelength from a millimetre to several centimetres. This can be of the same order as the wavelength of the electromagnetic radiation used in radar remote sensing (see Jahne & Riemer

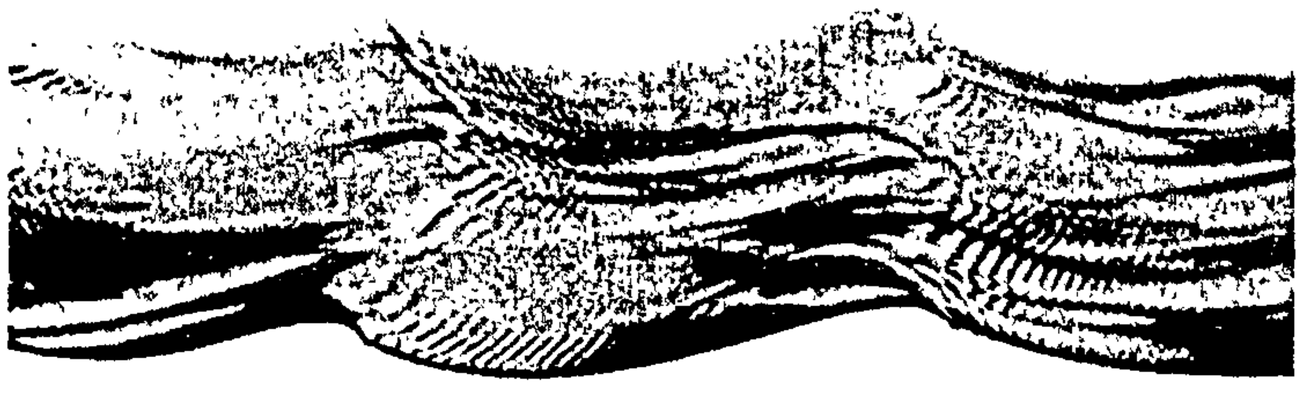

Figure 1.1: Waves generated by a wind of $6\,\mathrm{ms}^{-2}$ in a laboratory flume. *(Ebuchi, Kawamura & Toba. 1987).*

1995 for example). The waves make a significant contribution to the return signal in such cases.

Short waves, both capillary and 'capillary-gravity', where both restoring forces can be considered to be important, add 'roughness' to the ocean surface. Gravity waves generally have moderate slopes, but the slopes of capillary waves can be unlimited. The roughness increases the wind stress acting on the ocean surface, and affects the wind profile immediately above it. Although most air to sea energy and momentum transfer is by pressure, this stress can also play an important role.

Capillary wavelengths and the length scales associated with laminar diffusion of gases across the ocean-atmosphere interface are of the same order. It has been proposed that capillary effects play an important role in ocean-atmosphere gas transfer. Such transfer is would play an important role in any study of global climate.

Laboratory experiments, for example Schooley (1958) and Koga (1982), have provided some evidence that capillary waves break by pinching off bubbles of air. Further evidence for this has come from the study of the limiting form of pure irrotational capillary waves (Crapper 1957). Air entrainment is thus thought to occur as part of the 'micro-scale' breaking of capillary waves. This breaking also has important consequences for underwater acoustic background noise, which is of interest to sub-mariners.

Capillary waves also play a further role in transfer processes by influencing near-

breaking gravity waves. At the region of high curvature around the sharp crest of a steep gravity wave, surface tension is locally important. It has been proposed (Longuet-Higgins 1963 - see below) that the subsequent pressure distribution acts like a travelling disturbance to generate capillary waves ahead of the crest. Such capillary waves are frequently observed on the front of much larger gravity dominated waves.

As such they extract energy from the underlying wave and dissipate it through viscosity. They are also a source of near surface vorticity. Because of the high surface curvature of the capillary waves, they generate a vorticity much larger than the gravity wave alone. This vorticity may then contributes to the vortex roller sometimes seen at the crest of short gravity waves (see Longuet-Higgins 1992a).

Research in recent years been divided into two broad areas. One area is the study of the solution space for two-dimensional symmetric capillary-gravity waves. These correspond to the lengths scales where both surface tension and gravity are important. Solutions corresponding to families of travelling periodic waves, and solitary waves have been found.

The other area has been towards gaining an understanding of the mechanisms involved in the generation of capillary waves and their interaction with gravity waves. This deals with length scales where gravity is the dominant restoring force, but surface tension remains locally important at regions of high curvature.

1.2 Basic equations

The irrotational theory of water waves has proved highly successful since its first presentation by Laplace and Stokes. If we assume inviscid, incompressible motion, an expression for the phase velocity of surface waves can quickly be arrived at.

For a two dimensional surface given by

$$y - \zeta(x) = 0, \tag{1.1}$$

the modification of (dimensional)pressure at a point O on the surface is given by

$$P = P_o - T\kappa \tag{1.2}$$

where P_o is the pressure on the exterior side of the surface, T is the coefficient of surface tension and κ is the curvature of the surface given by

$$\kappa = \left(\frac{x_\zeta y_{\zeta\zeta} - y_\zeta x_{\zeta\zeta}}{\left(x_\zeta^2 + y_\zeta^2\right)^{3/2}} \right)_O \tag{1.3}$$

For the interface between pure water and air $T = 73.5$ dyn/cm at 15^o. Values of T decrease slowly with temperature. A table of T for different fluid boundaries, and temperatures for water is given in Batchelor (1967). Surface tension can also be significantly affected by any absorbed material or surfactant. The effect of such material is usually to decrease surface tension, by an amount which increases with the concentration of contaminant (see Batchelor 1967). Different values for the coefficient of surface tension are taken by different authors, depending on the conditions they wish to model. Values between 72 and 74 dyn/cm are often used for water under normal conditions.

The effect of surface tension is easily included in the linearised water wave equations. For a train of progressive waves, the phase velocity c satisfies

$$c^2 = \frac{1-s}{1+s}.\frac{g}{k} + T'k \tag{1.4}$$

where

$$s = \frac{\rho'}{\rho}\ ,\ T' = \frac{T}{\rho - \rho'}, \tag{1.5}$$

ρ' and ρ being the densities of the top and bottom fluid respectively. For applications to water waves, we usually take $\rho = 1$ and $\rho' = 0$, (i.e. $s = 0$). An important point to note is that the phase speed has a minimum value, c_m, given by

$$c_m^2 = \frac{1-s}{1+s}.2.\left(T'g\right)^{\frac{1}{2}}, \tag{1.6}$$

with corresponding wavelength

$$\lambda_m = \frac{1-s}{1+s}.\frac{2\pi}{k_m} = \frac{1-s}{1+s}.\left(\frac{T'}{g}\right)^{\frac{1}{2}}. \tag{1.7}$$

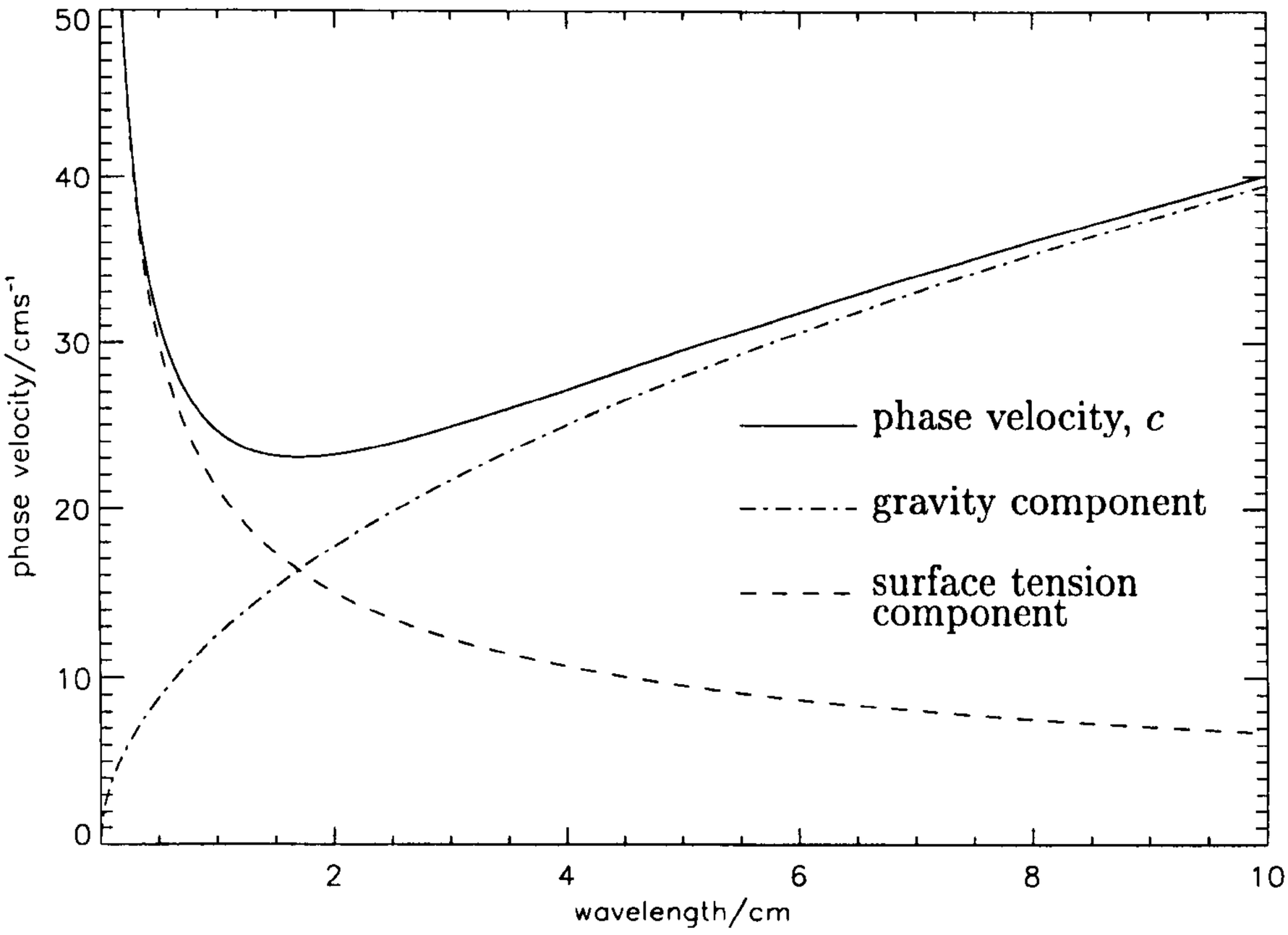

Figure 1.2: Phase velocity as a function of wavelength, linear theory. $T = 72\,\mathrm{dyn/cm}$.

Thus for any value of c greater than c_m, there are two possible wavelengths. A graph of c against wavelength λ is shown in figure 1.2. This is known as the dispersion relation, as it shows that waves of different wavelengths travel at different velocities.

We can see that for sufficiently large λ the first term dominates, so the motion is governed mainly by gravity. Such waves are called gravity waves. The term 'gravity-capillary wave' is often used for waves with parameters close to, but to the right of the minimum of the dispersion relation, i.e. where surface tension effects are important but smaller than gravitational effects. For sufficiently small λ the second term dominates. These waves are called ripples or capillary waves. If they are close to, but to the left of the minimum they are sometimes referred to as capillary-gravity waves. From here on, unless otherwise stated, it will assumed that $\rho = 1$ and $\rho' = 0$, and the dashes will be dropped from further equations. The ratio of

effects of surface tension to gravity for relatively deep water can be expressed by the dimensionless quantity

$$\sigma = \frac{Tk^2}{\rho g} \tag{1.8}$$

where g is gravitational acceleration, k the wavenumber and ρ the density (equal to 1 for water). Here

$\sigma \gg 1$ corresponds to capillary waves.

$\sigma \ll 1$ corresponds to gravity waves.

If we take $T = 72\,\mathrm{dyn/cm}$, this means that

$\sigma \leq 0.01$ for waves longer than $17\,\mathrm{cm}$.

$\sigma \geq 100$ for waves shorter than $0.17\,\mathrm{cm}$.

The nondimensionalisation assumes the wavelength is the characteristic length scale for the problem being considered. In between, both surface tension and gravity play a role. For wavelengths about 1.7cm, the forces are of roughly equal importance. These waves are known as Wilton's Ripples after Wilton (1915) in which a series representation for the steady state finite amplitude solution is first analysed in detail.

Other parameters commonly used to characterise capillary-gravity waves are the Bond number, defined as,

$$B = \frac{T}{\rho g h^2}, \tag{1.9}$$

where h is the undisturbed water depth and the Froude number,

$$F = \frac{c}{\sqrt{gh}} \tag{1.10}$$

These parameters are important for characterising flows on shallow depths. Most of the work within this thesis concerns deep water, at least on a scale compared to the capillary wavelength (i.e. a high Froude number). For relatively deep water, the wavelength, rather than the depth, becomes the important length scale. Thus (1.8) gives the more natural nondimensionalisation under such circumstances and is

used to nondimensionalise the surface tension effects in the numerical code presented later.

Previous work by other authors includes studies of capillary-gravity waves for Froude numbers near one. I shall briefly review this in the following sections.

1.2.1 Numerical and analytical studies of capillary-gravity waves

Most work on surface tension has been with waves in the capillary and capillary-gravity regime. That is, the region around and to the left of the minimum of the dispersion relation shown in figure 1.2. Previous authors have mainly considered steady two-dimensional waves for irrotational, incompressible, inviscid flow. The main work of this thesis will concentrate on the gravity-capillary regime. Here gravity is the dominant restoring force but surface tension makes an important contribution if there are regions of high surface curvature. As a background illustration some of the previous work with waves of smaller wavelength will be described first.

The first model for weakly nonlinear 'long' waves is Korteweg & de Vries (1895). Long here means in comparison to the water depth. Since the water depth, rather than the wavelength is the important lengthscale we might expect the Bond number to play a role in the behaviour of the solution. Following Rayleigh and Boussinesq (1872), they arrive at an approximate differential equation for governing the shape of the free surface, ξ for waves travelling in one direction:

$$\frac{\partial \xi}{\partial t} = \frac{3}{2}\sqrt{\frac{g}{h}}\left(\xi\frac{\partial \xi}{\partial x} + \frac{2}{3}\alpha\frac{\partial \xi}{\partial x} + \frac{1}{3}\gamma\frac{\partial^3 \xi}{\partial x^3}\right). \tag{1.11}$$

This is often known as the *KdV equation.* Here α is a small but otherwise arbitrary constant and

$$\gamma = \frac{1}{3}h^3 - Th/g\rho. \tag{1.12}$$

The importance of the Bond number, B, in characterising the shallow water solutions is immediately apparent. Whether B is greater or less than $1/3$ determines

the sign of the third order term γ. For $B \simeq 1/3$ the equation is no longer valid (see below).

The properties of capillary-gravity solitary waves are more complicated than pure gravity solitary waves. They can occur on both finite and infinite depth water and can have oscillatory tails. Solitary waves without surface tension have been shown to be symmetric (Craig & Sternberg 1988), whereas it is speculated that solitary waves with surface tension can be asymmetric.

There are also two types of small-amplitude capillary-gravity solitary wave, although it can be shown that one can go smoothly from one to the other via finite amplitude waves. These are a family of depression waves and a family of elevation waves. Depression waves (called *negative* waves by Korteweg & de Vries) are such that the level at the origin is lower than that at infinity, although this terminology is not appropriate for large amplitude waves. Elevation waves are the converse.

Korteweg & de Vries, taking capillarity into account, draw the conclusion that for sufficiently shallow water (explicitly, for $B > 1/3$), the solitary wave is one of depression. This approximate solution had for a long time since been overlooked however. As recently as 1981, it was concluded (Shinbrot 1981) that the solitary wave "is completely obliterated when surface tension is present and the depth is small enough" (see Benjamin 1982) as he found no elevation solitary wave solution for $B > 1/3$.

Recently extensions to the results of the Korteweg & de Vries have been made using numerical methods. Hunter & Vanden-Broeck (1983) and Vanden-Broeck (1991) for example, reformulate the exact nonlinear problem for the unknown shape of the free surface, and also carry out a perturbation expansion near $B > 1/3$. They show that for $0 < B < 1/3$ the KdV equations do not in general accurately describe periodic capillary-gravity waves. Their numerical calculations predict a number of families of solutions with local surface depressions or 'dimples' which are on a length scale smaller than considered in the derivation of the KdV equations.

In addition they find elevation solitary waves cannot be found as the continuous limit of periodic waves as the wavelength tends to infinity. Analytic work has since proved the existance of depression solitary waves for $B > 1/3$ and elevation solitary waves for $0 < B < 1/3$ (see Vanden-Broeck 1991 for references).

Elevation solitary waves

These elevation solitary waves generally approach a train of ripples in the far field and not a uniform stream. They are not, in general, accurately described by the KdV equations. However, the amplitude of these far field ripples varies along the solution branch, and for sufficiently small solitary waves can have zero amplitude. These particular solutions form a family that are accurately described by the KdV equations. Solitary waves with small amplitude oscillatory tails are ofter called *generalised* solitary waves.

Longuet-Higgins (1993) shows that the elevation solitary wave corresponds to stationary solutions of the nonlinear Schrödinger equation that governs slow modulations in space and time of capillary-gravity waves. In certain regions of parameter space it is well known that the nonlinear Schrödinger equations admit solutions in the form of wave packets characterised by two length scales; the length of the envelope and the wavelength of the oscillation inside the envelope. The envelope travels at the group velocity while the oscillations travel at the phase velocity. Steady wave packets are therefore obtained when the phase and group velocities are equal.

Depression solitary waves

The other type of wave is well approximated by the solitary wave solution of the KdV equation for Bond number greater than $1/3$. From a physical point of view, these waves are probably not relevant in the context of water waves. For a water/air interface at 20^oC, a Bond number, $B \simeq 1/3$ and Froude number, $F \simeq 1$, the solution corresponds to waves with a velocity 21.5cms^{-1} on water of depth 4.5mm.

For such waves the effect of viscosity should not be neglected.

Waves near the minimum of the dispersion relation.

For waves in the region around the minimum of the dispersion relation, (corresponding to Bond number, $B = 1/3$, and Froude number $F = 1$, the coefficient of the third-order derivative term becomes small and the KdV equation is no longer valid. In this case previous authors (see Hunter & Vanden-Broeck 1983 for example) have arrived at a higher order approximation with fifth-order derivative term. This modified system is sometimes referred to as the generalised KdV equation.

The first attempt to explicitly consider periodic capillary-gravity waves of finite amplitude in this vicinity is made by Harrison (1909). Here a third order solution for capillary-gravity waves is quoted, but not analysed in detail. Wilton (1915) is the first to study the solution, presenting a fifth order Stokes expansion of the surface profile. Both he, and Harrison before him, noticed that the perturbation expansion has zero radius of convergence at certain wavelengths. By reformulating the expansion, Wilton finds that two possible waves can exist at the shortest of these wavelengths. The wavelength given by the capillary branch (see figure 1.2) being an integral divisor of the wavelength given by the gravity branch. The perturbation method fails since the primary wave resonantly interacts with one of it's higher harmonics. It was thought that no solutions existed at these wavelengths, in real applications the effect being reduced by viscosity.

Much work has since concentrated on the failure of the perturbation expansion at these wavelengths (see Hogan 1979). Hogan (1981) however, shows that the irregularities in the traditional solution are merely consequences of the non-uniformity in the ordering of the Fourier coefficients. Further unexpected results for capillary-gravity waves were found, such as rapid decrease with increasing wave height of the gravitational potential energy. The decrease, after the expected increase, is connected with the extreme distortion of the profile. Hogan also finds that the crest

height above mean level is not a monotonic function of wave height.

The advent of sufficiently fast computers permits the numerical study of the full nonlinear problem. Several papers providing accurate numerical results have been published including those mentioned above by Hogan (1979, 1980, 1981), Schwartz & Vanden-Broeck (1979) and Chen & Saffman (1980).

Following existence theorems for symmetric solitary waves by Iooss & Kirchgässner (1990) and others, much numerical work has concentrated on exploring the solution space of the steady capillary-gravity problem for symmetric waves. Recent progress has been made in understanding the global periodic solutions of the capillary-gravity wave problem by Aston (1993), Dias (1994) and Dias, Menasce & Vanden-Broeck (1996). It is found that a given wave form is characterised by three dimensionless parameters, two of which are independent; a dimensionless capillary number, a wave speed parameter and a wave steepness parameter.

Analytical and numerical work (Hogan, Chen and Saffman, etc.) has shown that there is a multiplicity of solutions for any set of parameter values. In particular, many different families of capillary-gravity waves exist when the Bond number is in the interval $0 < B < 1/3$. Buffoni, Groves & Toland (1996) have recently shown that near the minimum of the dispersion relation there are infinitely many distinct solitary waves.

1.2.2 Pure capillary waves

The most famous result for waves with surface tension is that of Crapper (1957). Crapper's solution is an *exact* solution to a nonlinear problem; giving a finite amplitude pure capillary wave profile on infinite depth water. By applying a Stokes expansion technique to a wave in which surface tension is the only restoring force an exact, rather than a series, solution is found.

Figure 1.3 shows profiles up to the limiting case where the surface touches itself. Unlike gravity waves, these have broad flat crests and sharp troughs. It has previ-

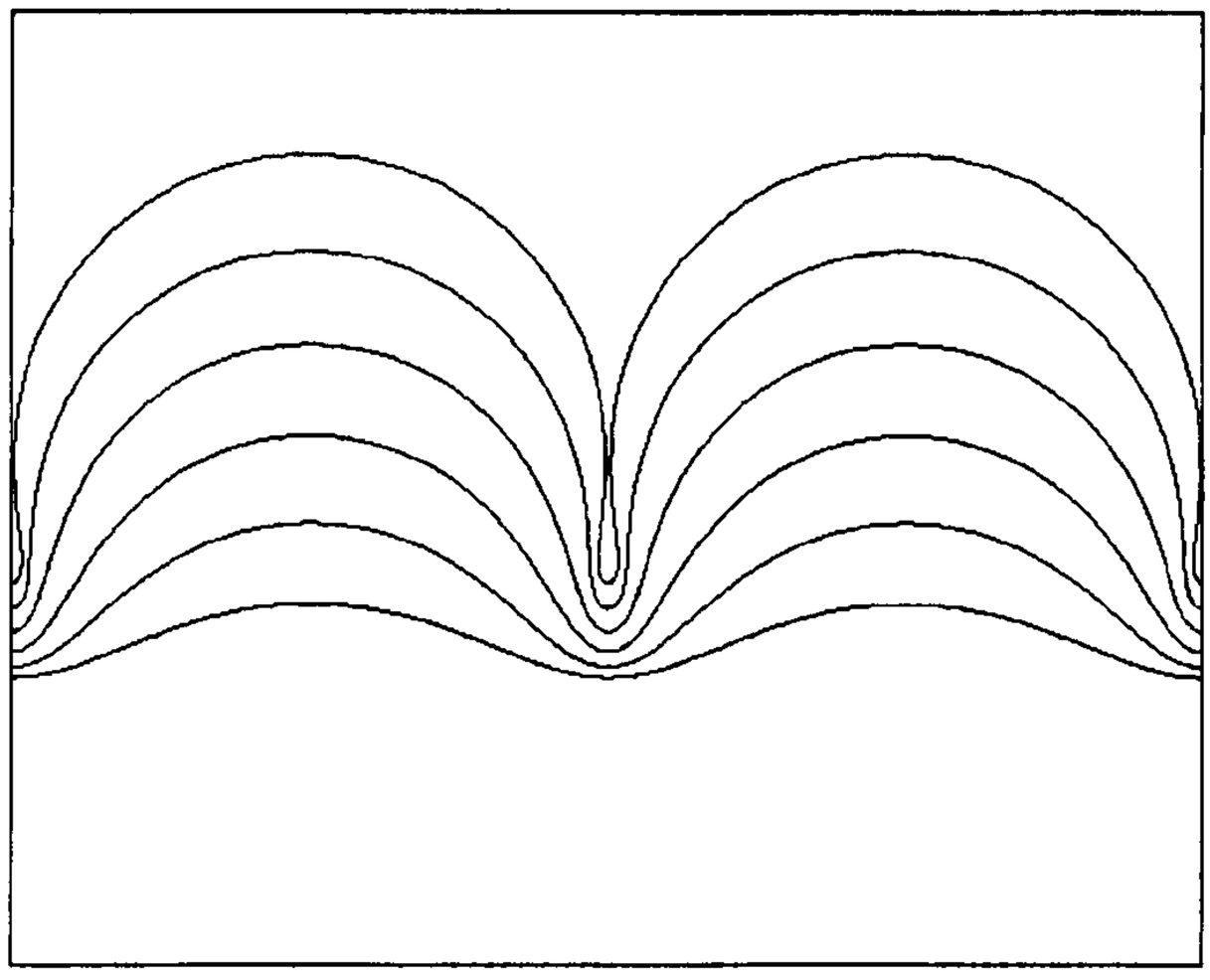

Figure 1.3: Surface profiles for pure irrotational capillary waves up to the limiting profile. Calculated using equations of Crapper (1957).

ously been proposed that the method for capillary wave breaking is shown in the behaviour of the Crapper solution in limit. That is, the troughs steepen to the point that the opposing sides touch, enclosing a bubble of air. This has been confirmed to some extent by experiment (Schooley 1958 for example) in which bubbles of air were observed beneath the water surface.

Crapper's solution is generalised by Kinnersley (1976) to waves on sheets of fluid. The analysis of small amplitude capillary waves on fluid sheets had previously been carried out by Taylor (1959). He found both symmetric and antisymmetric waves can exist, that is fluid sheets in which the wave train on one side is in phase with that on the other, and sheets in which the wave trains are π out of phase. He produced both experimentally. Kinnersley's waves are the finite amplitude version of Taylor's and are derived as a straightforward generalisation of Crapper's approach. Taylor's waves can be found again as the small amplitude limit of Kinnersley's solution.

1.3 Summary of chapter 2

Chapter 2 mainly concerns the effects of surface tension on wavelengths longer than mentioned above. On waves of between 5 to 50 centimetres, so-called 'parasitic capillaries' are observed. Several theories for the generation and propagation of these ripples have previously been proposed, along with experiments to analyse them. Surface tension has been added to an existing fully nonlinear potential flow solver. Chapter 2 presents comparisons of computational results with theory and experiment. Some calculations for waves not covered by present theories are also presented.

1.4 Summary of later chapters

The numerical code used for the studies in Chapter 2 can be employed for a wide variety of other free surface problems. One such situation is the flow above the bed boundary layer under standing or near standing waves. This problem is of interest to coastal engineers. Wave reflection at coastal structures means that standing or near-standing waves are often formed. In determining erosion from sediment transport in front of structures simple formulae are used. These vary according to the conditions the engineer wishes to account for, but are normally based on bed velocities. Experimental studies in this field have received much attention, and there is still some debate as to which dynamic flow properties most influence sediment transport. It is the aim of Chapter 3 to provide some guidance on when such models can be applied, in particular for case of near-standing waves on shallow water by highlighting the bed parameters under such waves.

The dynamics of shallow water standing waves are important to coastal engineers for other reasons than sediment transport. The run up of steep waves against the structure can cause a flow of water over it or 'overtopping'. The design of coastal structures such as harbour breakwaters has previously been such as to minimise the possible damage from high impact pressures. The increased recreational use

of breakwaters is one reason why design engineers have also recently been considering wave overtopping. The current method of assessing wave overtopping of a structure is to extrapolate from existing small scale experimental data. From such data empirical formulae for overtopping rates have been derived. These give the non-dimensional overtopping volume per unit width per second overtopping. However, more important as far as structural damage is concerned are the individual overtopping volumes which are much harder to obtain experimentally.

Our numerical code can calculate the run up of steep waves against vertical walls. A simple model is constructed to use these results to estimate overtopping volumes for the most common mode of overtopping. From work in Chapter 3 we can test this model with the largest waves likely to approach such structures. We see that individual overtopping volumes show the same qualitative behaviour as the overtopping rates found in experiments.

We can also consider the affect on overtopping volumes of changes in structural geometry. Vertical harbour breakwaters are constructed with foundation berms which extend from the foot of the wall. Previous work has highlighted the strong affect that changes in the geometry can have with impact pressures. Little work has been done in estimating the corresponding changes in overtopping. Our code permits the inclusion of smooth foundation berms, and their influence on overtopping is presented in Chapter 4.

The formulae used in estimating overtopping rates are assumed to be non-dimensional. Thus results from small scale experiments, where the wave height may be less than 10cm, are applied to estimating overtopping for full scale structures. Chapter 2 has shown that the effect of surface tension at such length scales is not necessarily negligible. The addition of surface tension to our numerical code allows accurate calculation of wave motion at such small scales. Work from preceding chapters is brought together at the end of Chapter 4. A comparison of predicted overtopping volumes at small scale with those calculated with pure gravity waves

(effectively very large scale) is presented. Results show that for scales at which experiments are often performed surface tension considerably affects the overtopping volume and nondimensional wave run up.

Chapter 2

Surface Tension Effects On Steady Gravity Waves

2.1 'Parasitic' capillary waves

Chapter 1 presented a resumé of previous work on capillary and capillary-gravity waves. For much longer waves than these, surface tension may still play a crucial role. Short capillary waves with wavelengths of several millimetres can often be seen near the crests of steep gravity waves with lengths 5 - 25cm.

Such waves were first investigated experimentally by Cox (1958), although they had been reported by Scott Russell as long ago as 1844. Cox's experiments aimed at understanding the effects of wind on waves. However, even in the absence of wind, high frequency capillary waves were reported near the crests of steep gravity waves; it was apparent that the gravity waves themselves were generating the capillary waves. Cox found that capillary waves were especially noticeable when the underlying gravity waves have wavelength between 5 and 50 centimetres.

Munk (1955) had suggested previously their origin might lie in some unknown disturbance near the gravity wave crest. The disturbance would produce capillary waves upstream of the crest (Lamb 1932, §271), i.e. on the forward face of the gravity wave as observed. A corresponding longer wave would also be produced on the leeward face of the gravity wave, although hard to detect experimentally.

2.1.1 A dynamical theory of parasitic capillary waves

The dynamical theory of the generation of these ripples is first presented by Longuet-Higgins (1963). A theoretical mechanism for the non-linear transfer of energy from gravity to capillary waves is given. In the analytic approach, the underlying wave is treated as a pure non-linear steady, irrotational gravity wave. Surface tension is introduced as a linear perturbation, so that contributions from different parts of the gravity wave surface can be simply added together.

Longuet-Higgins argues that surface tension is important locally at the crest due to the high surface curvature. A progressive, irrotational gravity wave had been shown by Stokes (see Kinsman 1965 for example) to have a limiting crest angle of 120^o. It then seem likely that just short of this limit the curvature would become very large, so that if surface tension were included, a significant surface stress would be produced.

It is proposed that the capillary waves are thus generated by the normal stresses associated with the effects of surface tension near the crest of the gravity wave. The crest acts like a travelling disturbance which produces a train of ripples ahead of it.

Surface disturbance of a stream

The work of Longuet-Higgins (1963,1995) rests on the linear theory of a point pressure disturbance of a steady stream presented by Lamb (1932) (§270,271). Lamb shows that there are several possible solutions to the problem depending upon whether the stream velocity is greater, less than or equal to the minimum wave velocity c_m, as given by the minimum of the dispersion relation (see fig. 1.2). If the stream velocity is greater than c_m, there are two possible waves, with wave numbers $k_1 > k_m$ and $k_2 < k_m$, which could remain stationary in space on the flowing stream (see fig. 2.1). Here k_m denotes the wave number of the wave with wave velocity c_m. k_1 lies to the left of the minimum on the dispersion relation graph and thus corresponds to a ripple or capillary wave. k_2 lies to the right and is dom-

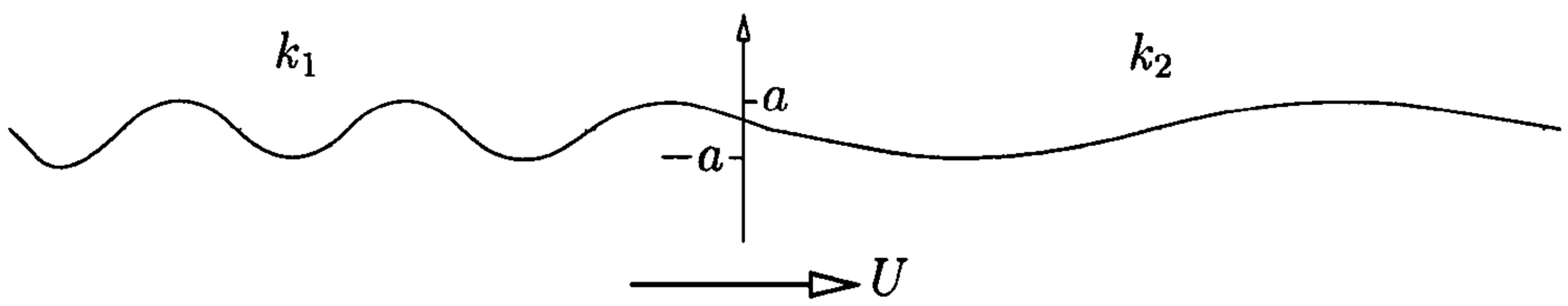

Figure 2.1: Surface disturbance to a stream for $U > c_m$.

inated by gravity. Lamb shows that apart from a correction term near the pressure source, the surface disturbance is made up of a system of the two waves, both with amplitude $a = 2P/(T(k_1 - k_2))$, where P is the applied force per unit transverse length. The shorter capillary waves remain upstream and the longer gravity waves down stream of the pressure disturbance. For k_1 the group velocity is greater than the stream velocity, whilst for k_2 it is less which explains why the two wave trains are respectively found ahead and to the rear of the disturbance.

We can see from the behaviour of the amplitude above that the linear theory breaks down as the stream velocity approaches c_m from above, since for this velocity $k_1 = k_2 = k_m$. For a stream velocity less than c_m , there is no wave that can remain stationary on the stream. The disturbance level is then confined to a region about the pressure source and decays rapidly to zero with distance from it. For the critical case, viscosity becomes important and it is found (see Lamb 1932 §271) that the amplitude of the surface disturbance is given by $P/T'\mu'^{\frac{1}{2}}$.

The above work is modified by Longuet-Higgins (1963) to that for a steady but non-uniform stream. This flow models that around the gravity wave crest in a frame of reference moving with the phase speed. Several corrections to this basic model are presented in Longuet-Higgins (1995). A non-uniform stream means that while the surface velocity can be less than c_m in the vicinity of the pressure disturbance, it can be greater than c_m some distance from it. The same problem of infinite amplitude occurs around this cross over point, or caustic.

To obtain the disturbance caused by a pressure distribution over a finite breadth, Longuet-Higgins integrates over the contribution from many point sources. The

assumption of linearity allows these contributions to be simply added.

The theory presented by Longuet-Higgins is not valid for regions where the amplitude of the predicted capillary waves becomes nonlinear, i.e. where the surface velocity, in a frame of reference moving with the gravity wave speed, is sufficiently close to the local minimum wave speed, c_m. The integral calculation of the surface profile is stopped some finite distance from these points. Viscosity is also not taken into account.

2.1.2 Energy of parasitic capillaries

The capillary waves take energy from the gravity wave in two ways: by the action of surface tension at the sharp crest, and by interaction of the capillary waves with the non-linear velocity field on the forward face of the gravity wave through *radiation stress*. (For a full treatment of radiation stresses see Longuet-Higgins & Stewart 1964, in particular §9). It has previously been shown (Lamb 1932 §250, for example) that surface waves possess momentum in the direction of propagation and proportional to the square of their amplitude. Radiation stress is defined as the excess flux of momentum due to the waves. The capillary waves on the forward face of the gravity wave propagate against the steady straining velocity field of the underlying wave. This straining flow does work against the radiation stress to provide a momentum balance. Energy is thus gained by the capillary waves at the expense of the gravity wave.

At the same time, the capillary waves lose energy through the action of viscosity. For pure capillary waves of energy density E and wavelength $2\pi/k$, the rate of energy dissipation by viscosity is given by $4\nu k^2 E$ (Lamb 1932, §348). The effectiveness of energy dissipation through viscosity by the capillaries compared to the gravity wave is inversely proportional to the underlying wavelength. For the range of wavelengths studied here the rate of energy dissipation by the gravity part of the wave remains less than that by its parasitic capillaries assuming the two have equal steepness.

Predictions of the theory of Longuet-Higgins (1963)

Some qualitative predictions from the theory compare favourably to experiment. such as capillary steepness near the crest of the gravity wave. The predicted waves on the front face of the gravity wave are stationary in a coordinate system moving with the gravity wave crest. At some distance from the crest the waves appear in the approximation to be free capillary waves with amplitude proportional to the underlying current.

Other quantitative predictions cannot be tested however due to their dependence on the undisturbed curvature at the crest, which is difficult to measure experimentally (see Chang, Wagner & Yuen 1978).

There are some discrepancies between predicted and observed phenomena however. One is that the theory predicts a decrease in the wavelengths of parasitic capillaries towards the trough of the underlying gravity wave. The slopes of these capillaries are predicted to first increase then decrease when moving away from the crest. This is in contradiction to the experimental results of Schooley (1958) and Ebuchi, Kawamura & Toba (1987), which report a dip in the measured slopes of the capillary waves near the underlying crest.

2.1.3 Generation of vorticity by parasitic capillaries

The existence of strong vortical region near the crest of a gravity wave had previously been reported in experiments. Longuet-Higgins (1992) accounts for the surface dip and the vortical crest region by calculating the vorticity that would be produced by steep capillary waves. If there is no tangential stress at a free surface, then there is a surface vorticity due to viscosity given by $\omega = -2\kappa q$, where κ is the curvature and q the tangential velocity. In surface water waves this produces a vorticity boundary layer, with some vorticity diffusing into the body of fluid.

Longuet-Higgins finds that vorticity generated by the parasitic capillaries and released below the boundary layer is much greater than that from the the original

gravity wave. It accumulates very rapidly (within the time taken by the gravity wave to travel one wavelength) near the crest of the gravity wave. This may contribute significantly to the sometimes observed crest vortex, which in turn may affect the dynamics of the parasitic capillaries. Our model presented later solves for potential flow and thus does not include viscosity or vorticity. We may therefore expect some differences between our numerical calculations and experiments.

2.1.4 Blocking of capillary waves

The theory of Longuet-Higgins (1963) is further improved upon by Longuet-Higgins (1995). Capillaries are again considered to be a linear perturbation to an otherwise steady, irrotational, non-linear gravity wave. A more accurate knowledge of the profile of the underlying Stokes wave is used. In particular, the incorrect hypothesis that the curvature at the gravity wave crest is proportional to the wave amplitude is discarded. Instead the asymptotic theory of Longuet-Higgins & Fox (1977,1978) for the 'almost highest wave' is used.

The effect of gravity on the capillary waves themselves is also taken into account. This follows a proposal of its importance by Ruvinsky & Friedman (1981). Further, the effect of particle acceleration in the Stokes wave is also included. This the replaces ordinary gravity, g, with an effective gravity, g^*, defined as

$$g^* = g\cos\alpha - \kappa U^2. \tag{2.1}$$

Here α is the inclination of the gravity wave surface and U the particle velocity at the free surface in a frame of reference moving with the phase speed, c. κU^2 is then the acceleration of a fluid particle normal to the fluid surface.

Following these improvements, a better agreement between predictions of surface slopes and those reported by Cox (1958) is reported. The theory is also compared to experiments by Perlin, Lin & Ting (1993) and appears in approximate agreement, despite the apparent unsteadiness of the waves reported by them (see Longuet-Higgins (1995) §11, paragraph 3).

The steadiness in the theory is only of course a first approximation. Complete steadiness would require a constant input of energy, by wind for example. Without this there would be a decay in the gravity wave amplitude as they propagate since energy is continuously lost through the action of viscosity. In many situations in the ocean, the wind provides energy to the capillaries at much the same rate as they are being dissipated with the result that they are in approximate equilibrium (Crapper 1984). Another reason why complete steadiness would not be achieved is the interaction of the capillary wavetrain with itself and with waves of different frequency.

2.1.5 Three- and four-wave interactions

When several dominant wave-modes are present there is a mutual interaction between them. In general this interaction is very weak which is partly why simple linear theories, which ignore nonlinear terms, have proved so successful. However interaction between wave modes can be significant, especially if a resonance between the modes exists.

The simplest case of such resonant interaction is between groups of three waves. Suppose the dominant linear modes have the form

$$\mathrm{Re}\{a_j(t)\exp\left[i(\mathbf{k}_j\cdot\mathbf{x}-\omega_j t)\right]\} \qquad (j=1,2,3), \tag{2.2}$$

with small amplitudes $a_j(t)$ where each amplitude is slowly varying in time. Then the interaction of any two modes, l and m say, gives $O(a^2)$ terms with periodicities

$$\exp\{i\left[(\mathbf{k}_l\cdot\mathbf{x}-\omega_l t)\,(\mathbf{k}_m\cdot\mathbf{x}-\omega_m t)\right]\}. \tag{2.3}$$

Three wave resonance occurs when any of these terms has the same period as that of the third wave mode, i.e. when

$$\begin{aligned}\mathbf{k}_1\pm\mathbf{k}_2\pm\mathbf{k}_3&=0,\\ \omega_1\pm\omega_2\pm\omega_3&=0,\end{aligned} \tag{2.4}$$

where the wavenumbers and the frequencies are also related through the dispersion relation. McGoldrick (1965) showed that three capillary-gravity waves may interact resonantly, and later investigated such resonant interactions experimentally (McGoldrick 1970). For some systems, deep water gravity waves for example, no three-wave resonance is possible and the strongest interactions occur between four waves. Again, this interaction is strongest, producing nonlinearities of $O(a^3)$, when the general conditions for four wave-resonance are met;

$$\begin{aligned} \mathbf{k}_1 \pm \mathbf{k}_2 \pm \mathbf{k}_3 \pm \mathbf{k}_4 &= 0, \\ \omega_1 \pm \omega_2 \pm \omega_3 \pm \omega_4 &= 0, \end{aligned} \tag{2.5}$$

with corresponding signs and $\mathbf{k}_i$ and ω_i satisfying the dispersion relation. Such four-wave and indeed higher number wave interactions can occur for capillary-gravity waves, although the order of nonlinearities in wave amplitude decrease with the number of waves involved (a^{n+1} for n th order interaction), so interactions between higher numbers of waves are considerably weaker.

Resonant interaction gives a exchange of energy between modes, the total energy being conserved. For three wave interaction, if at any instance the energy density of one component is decreasing, the energy density of the other two components is simultaneously increasing. These energy exchanges are periodic and involve a substantial fraction of the total energy.

Resonant interaction has important consequences for the stability of a single finite amplitude wave train. If in (2.2) a_1 is of finite amplitude and a_2 and a_3 infinitesimal, it is found that the infinitesimal modes can grow exponentially until comparable in amplitude to the initial wave. Thus a finite amplitude wave train can be unstable to infinitesimal disturbances.

A set of three modes that do not precisely satisfy (2.4), but the more general condition

$$\begin{aligned} \mathbf{k}_1 \pm \mathbf{k}_2 \pm \mathbf{k}_3 &= 0, \\ \omega_1 \pm \omega_2 \pm \omega_3 &= \Delta\omega, \end{aligned} \tag{2.6}$$

where $\Delta\omega$ is small, can also undergo resonant interaction. Resonant interactions can also occur for wavetrains that vary slowly in space as well as time. For three-wave interaction, 'slow' means such that derivatives of amplitude variation are at most $O(a^2)$. The equations governing the rate of energy exchange then have extra terms, but the qualitative behaviour remains the same.

In a wavefield consisting of many components any given wavenumber may be contained in a large number of resonant sets. Few analytic results have been obtained for such wave fields. However it has been shown that most of the energy transfer occurs amongst groups of almost equal wave number.

McGoldrick's series of experiments (1970a, 1970b, 1972) with capillary-gravity waves showed that certain wave numbers corresponding to waves near the minimum of the dispersion realtion can interact with their own higher harmonics. There is a continual energy exchange between the primary wave and its harmonics and steady state solutions are not found in such circumstances.

From the above we might therefore expect the parasitic capillary wavetrain that forms on the front of the steep gravity wave to undergo some interaction with itself, or to a lesser extent the underlying gravity wave or the longer gravity wave also formed by the pressure disturbance at the crest. Thus, if we observed the surface profile over a sufficiently long time period, we might expect to see a modulation of the capillary wave amplitudes due to this mechanism. For supercritical wave calculations, modulations of amplitude 1 or 2^o were noted in the surface slopes with periods several times that of the underlying wave. Such a variation is indistinguishable on the graphs of surface profiles presented later. For strongly subcritical waves, modulations involving significant changes in amplitudes were noted for all times. Both of these modulations could be caused by resonant interaction described above.

2.1.6 Breaking of parasitic capillary waves

If capillary waves can be generated by a sharp crested gravity waves, how does this effect the gravity wave itself? For short, steep gravity waves the energy dissipated

by the capillaries is much greater than that dissipated by the gravity wave alone. As stated above, Longuet-Higgins (1963) proposes that the capillaries take energy from the gravity wave. Thus capillaries may effect the stability of the underlying wave and play a crucial role in consequent wave breaking. Analytic work on energy transfer to non-linear parasitic capillaries is presented in Crapper (1970). An energy equation is formulated which gives the capillary steepness. Results show that sufficiently steep capillaries can form and break by enclosing a bubble of air, and as Crapper points out, this is what happens when gravity waves are seen to break. However the energy imparted to the ripples would be less than that predicted by Crapper's theory since he neglects the effect of the breadth of the pressure distribution at the crest. A pressure distribution that is wide compared to the capillary wavelength will not result in as large amplitude capillaries as may be expected due to an interference of waves from different parts of the pressure disturbance (see Lamb §271). Surface tension would however play an important role in the stability of the crest.

2.1.7 Origin of parasitic capillary waves

Parasitic capillaries on the forward face of gravity waves are initially generated by a 'travelling disturbance' at or near the gravity wave crest. Until recently the consensus of opinion had been that this disturbance was due to the action of surface tension at the sharp crest (see above). However, for short gravity waves, recent analytic and experimental work has suggested another source.

Duncan, Philomin, Behres & Kimmel (1994) present high speed photographs of mechanically generated gently spilling breaking waves. Formation of a bulge on the forward face of the waves is reported as they steepen. At the toe of the bulge is a region of sharp concave curvature simultaneously develops. Capillary waves are seen to form ahead of this. This feature does not last long however and the bulge rapidly moves down the forward face of the gravity wave, eventually becoming turbulent.

Longuet-Higgins (1996) investigates whether such a surface feature can exist in a steady state, assuming irrotational, inviscid flow. The feature is referred to as a

'capillary jump'. He shows that on a non-uniform current, such as is found on the front face of steep gravity waves, a quasi-steady wave may exist in which the wave height in the up-stream direction differs from that in the downstream. Furthermore Longuet-Higgins proposes that energy from the jump may be a source of parasitic capillary waves.

2.2 Current work on parasitic capillaries

The current work has focused on a general investigation of the parasitic capillaries produced on the forward face of steep gravity waves. In particular whether our fully non-linear numerical code predicts the same results as the linear perturbation method of Longuet-Higgins.

2.2.1 Numerical formulation

The program used during numerical calculations of unsteady flows is a version of the fully nonlinear potential flow solver of Dold & Peregrine (1986). A boundary integral method is employed which reduces the calculation of the fluid motion to evaluation of the surface alone. This approach had previously been employed by Longuet-Higgins and Cokelet (1976), Vinje and Brevig (1981), Baker, Merion and Orszag (1981) and Roberts (1983). The code has since been modified by Cooker (1990) to allow the study of flow over an irregular bed. Its numerical properties are described by Dold (1992).

2.2.2 Basic numerical model

For inviscid, irrotational and incompressible flow a velocity potential $\phi(\mathbf{r}, t)$ exists and satisfies Laplace's equation,

$$\nabla^2 \phi \;=\; 0. \tag{2.7}$$

Thus all the interior properties of the fluid are determined by its properties at the boundaries alone. The entire motion can thus be modelled by considering a point

discretisation of the surface.

If the fluid is contained above a fixed impermeable lower boundary δB, the component of velocity normal to the boundary is zero at the boundary, i.e.

$$\phi_n(\mathbf{r}, t) \equiv 0 \qquad \text{for } \mathbf{r} \in \delta B. \tag{2.8}$$

For a flat horizontal bed $y = -h$, this condition simplifies to

$$\phi_y(\mathbf{r}, t) \equiv 0 \qquad \text{for } y = -h. \tag{2.9}$$

In such cases the domain can be reflected in the bed and the symmetric flow solved, given large savings in the size of the required numerical calculation (see figure 2.2). The velocity of the fluid at the surface is determined using

$$\mathbf{u} \;=\; \nabla\phi \;=\; \phi_s\hat{\mathbf{s}} + \phi_n\hat{\mathbf{n}}, \tag{2.10}$$

where $\hat{\mathbf{s}}$ and $\hat{\mathbf{n}}$ are tangential and normal unit vectors respectively. The kinematic condition is that the fluid that starts as part of the surface remains as part of the surface. Thus the surface discretisation points move with the surface velocity;

$$\frac{D\mathbf{r}}{Dt} \;=\; \mathbf{u}. \tag{2.11}$$

The dynamic condition is given by Bernoulli's equation,

$$\frac{D\phi}{Dt} \;=\; \frac{1}{2}\mathbf{u}^2 - P/\rho - gy. \tag{2.12}$$

Here ρ is the fluid density and g is the acceleration due to gravity in a direction of decreasing y. Surface tension is included by defining P as

$$P = P_0 - \sigma\kappa, \tag{2.13}$$

where P_0 is the pressure on the exterior side of the surface. σ is the coefficient of surface tension defined in (1.8) for periodic deep water waves. For the infinite domain with shallow water, the depth becomes the dominant length scale and the Bond number given in (1.9) is used instead of σ in nondimensionalisation. Note, for

calculations of solitary waves on shallow water given later the results are presented in dimensional form. κ is the curvature of the surface given by

$$\kappa \hat{\mathbf{n}} = \mathbf{R}_{ss}, \tag{2.14}$$

or

$$\kappa = (x_\xi y_{\xi\xi} - y_\xi x_{\xi\xi}) \,/\, \left(x_\xi^2 + y_\xi^2\right)^{\frac{3}{2}} \tag{2.15}$$

where $\mathbf{R} = (x(\xi, t), y(\xi, t))$ is the fluid surface. ξ is a parametric variable that represents a particle following coordinate. It increases from 0 to n, where n is the number of discretisation points, with arclength along the surface. The surface is then discretised by considering only integer values of ξ. P_0 can be chosen to approximate the effects of wind or a localised pressure on the surface, though it is not used in the results described here.

Solution of Laplace's equation

If we take $r = x + iy$ as the complex equivalent of position vector $\mathbf{r} = (x, y)$, ϕ is an analytic funcion of r. It follows that the complex potential gradient, defined as $q(r) = \phi_x - i\phi_y$ is also an analytic function of r. Similarly taking $R(\xi, t)$ as the complex equivalent of the surface profile vector $\mathbf{R}$, q can be defined in terms of the tangential and normal gradients of ϕ at the surface by

$$q^* = \phi_x + i\phi_y = R_s(\phi_s - i\phi_n), \tag{2.16}$$

where $R_s = R_\xi/|R_\xi|$ is the arclength derivative of R along the surface and * denotes complex conjugate. If we assume that the surface contour is smooth, then applying Cauchy's integral theorem gives

$$\phi_s - i\phi_n = \frac{R_s}{i\pi} \oint \frac{\phi'_s - i\phi'_n}{R' - R} ds'. \tag{2.17}$$

ϕ_s can be found directly, so rearranging the above gives us an equation for the unknown, ϕ_n;

$$\pi\phi_n = \oint \mathrm{Im}\frac{R_s}{R' - R}\phi'_n ds' + \oint \mathrm{Re}\frac{R_s}{R' - R}\phi'_s ds', \tag{2.18}$$

where the arclength s' is a scalar variable which in the above equation increases in an anticlockwise sense around a closed contour. The primed variables are those that

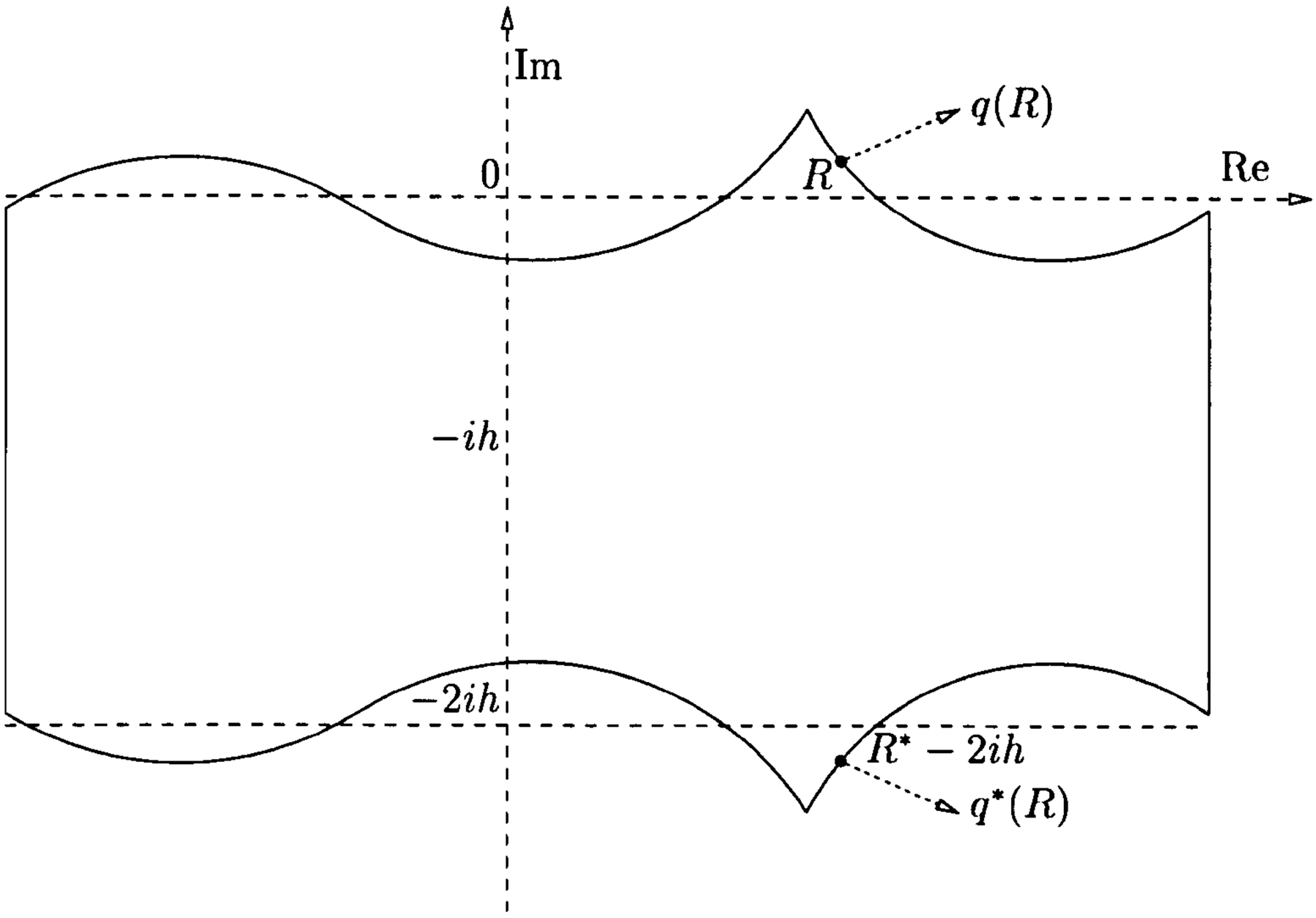

Figure 2.2: Domain for the periodic problem.

are evaluated at the surface. How this contour is formed depends on whether we are interested in solution in a periodic or infinite domain. In either case however the vertical parts of the contour make no contribution. In the periodic case the two ends cancel as the values are the same, but are integrated in opposing directions. For the unbounded domain, it is assumed that all variables tends to zero at large positive and negative x, such that the contribution from each end is zero. In both cases for finite depth, the horizontal bottom condition is taken into account by assuming the fluid region extends continuously to a reflection of the surface in the bottom. In this way a large saving in the required total number of calculation points is made. For infinite depth, the bottom condition is replaced by $\nabla\phi \to 0$ as $y \to -\infty$.

The motion of the reflected surface mirrors that of the real surface such that the condition

$$q(R^* - 2ih) = q^*(R) \tag{2.19}$$

IY
BRISTOL
LIBRARY

holds. Thus (2.13) can be rewritten

$$\begin{aligned} \pi\phi_n &= \oint \mathrm{Im}\left(\frac{R_s}{R'-R}+\frac{R_s}{R'^*-R-2ih}\right)\phi'_n ds' + \\ &+ \oint \mathrm{Re}\left(\frac{R_s}{R'-R}-\frac{R_s}{R'^*-R-2ih}\right)\phi'_s ds', \end{aligned} \tag{2.20}$$

where s' now increases from right to left along the surface only. This is then used as the basis of an iterative scheme to solve for ϕ_n numerically.

Time stepping of the surface

Time stepping of the surface has previously been described in Cooker (1990) and Dold (1992). ϕ_t and ϕ_{tt} are also analytic functions satisfying Laplace's equation in the domain and the bottom boundary condition. Thus similar equations to (2.15) can be set up for ϕ_{tn} and ϕ_{ttn}. Once the kernels of the integrals in (2.15) have been calculated they can also be used to obtain time derivatives of the surface motion. From these, Lagrangian time derivatives of $\mathbf{R}$ and ϕ are found. A truncated Taylor series is then used to march the surface values of $\mathbf{R}$ and ϕ forward in time. An analysis of the errors involved in this procedure is given in Dold (1992).

Previous work with this numerical code has been under the assumption of a constant surface pressure, i.e. with no surface tension. Surface tension is now included using (2.13). To time step the surface time derivatives of the pressure are needed. However, pressure given by (2.12) is only defined on the surface. Thus a switch to Lagrangian derivatives is required. Equations for this are given in Appendix A of Dold (1992). It remains to find DP/Dt and D^2P/Dt^2, which are given by

$$\begin{aligned} \frac{DP}{Dt} = &- \sigma.\left[\left(x_\xi^2+y_\xi^2\right)^{\frac{3}{2}}\left(u_\xi.y_{\xi\xi}+x_\xi.v_{\xi\xi}-v_\xi.x_{\xi\xi}-y_\xi.u_{\xi\xi}\right)\right. \\ &- \left. 3.\left(x_\xi.y_{\xi\xi}-y_\xi.x_{\xi\xi}\right)\left(x_\xi^2+y_\xi^2\right)^{\frac{1}{2}}\left(x_\xi.u_\xi+y_\xi.v_\xi\right)\right] \\ &/ \left(x_\xi^2+y_\xi^2\right)^3 \end{aligned} \tag{2.21}$$

and

$$
\begin{aligned}
\frac{D^2P}{Dt^2} = \; - \;\; & \sigma.\Big[\Big[\left(x_\xi^2+y_\xi^2\right)^{\frac{3}{2}}. \\
& \left(\frac{Du_\xi}{Dt}.y_{\xi\xi}+2.u_\xi.v_{\xi\xi}+\frac{Dv_{\xi\xi}}{Dt}.x_\xi-\frac{Dv_\xi}{Dt}.x_{\xi\xi}-2.v_\xi.u_{\xi\xi}-\frac{Du_{\xi\xi}}{Dt}.y_\xi\right) \\
- \;\; & 3\left(u_\xi.y_{\xi\xi}+x_\xi.v_{\xi\xi}-v_\xi.x_{\xi\xi}-y_\xi.u_{\xi\xi}\right)\left(x_\xi^2+y_\xi^2\right)^{\frac{1}{2}}\left(x_\xi.u_\xi+y_\xi.v_\xi\right)\Big] \\
/ \;\; & \left(x_\xi^2+y_\xi^2\right)^3 \\
+ \;\; & 3\left(\frac{DP}{Dt}/\sigma\right)\left(x_\xi.u_\xi+y_\xi.v_\xi\right)/\left(x_\xi^2+y_\xi^2\right) \\
+ \;\; & 3P\left[\left(x_\xi^2+y_\xi^2\right)\left(u_\xi^2+x_\xi.\frac{Du_\xi}{Dt}+v_\xi^2+y_\xi.\frac{Dv_\xi}{Dt}\right)\right. \\
- \;\; & \left.2.\left(x_\xi.u_\xi+y_\xi.v_\xi\right)^2\Big]/\left(x_\xi^2+y_\xi^2\right)^2\Big]
\end{aligned}
\tag{2.22}
$$

Many of the calculations, including those immediately above, involve obtaining derivatives with respect to point number. The accuracy of the numerical scheme as a whole depends on that of this process. A spectral technique can be used, however any local inaccuracy about one point would immediately affect results at all other points due to the global nature of the method. Instead, estimates of first and second order derivative at a point are found using 10th order polynomials centred on the point in question. The relative error arising from such formulae is of the order of $|\delta\mathbf{r}/2|^{10}$ (Dold 1992).

2.2.3 Length scales and the choice of σ

All quantities calculated by the code are usually taken to be dimensionless. When running the code, the data is set up so that the length scale of the gravity wave is 2π in the periodic version, or depth 1 for shallow water problems. To regain dimensional quantities (dashed) from the non-dimensional calculated values for the periodic domain, they are scaled as follows;

$$x' = x/k \tag{2.13a}$$

$$t' = \frac{t}{\sqrt{gk}} \tag{2.13b}$$

$$v' = \sqrt{\frac{g}{k}}v \tag{2.13c}$$

where k the wave number. For shallow water problems we use the length scale d, the water depth. Thus

$$x' = dx \tag{2.13d}$$

$$t' = \sqrt{\frac{d}{g}}.t \tag{2.13e}$$

$$v' = \sqrt{gd}v \tag{2.13f}$$

By choosing σ we set a ratio of surface tension to gravity effects which effectively determines a length scale for the motion. If we take $g = 980.6\text{cm s}^{-2}$, $\rho_0 = 1\text{g cm}^{-3}$ and $T' = 74\text{g s}^{-2}$, (the value used by Longuet-Higgins 1995) then from (1.8) we have approximately, using c.g.s. units,

$$0.0754k^2 = \sigma \tag{2.14}$$

for periodic waves with wave number k (used in the periodic version of our numerical code), and

$$\frac{0.0754}{d^2} = \sigma, \tag{2.15}$$

using c.g.s. units, for shallow water (as used in the unbounded version for solitary wave calculations). We can see then that an increase of surface tension of a factor of n^2 is equivalent to reducing the spatial scale of the numerical calculation by a factor of n. This of course does not take into account possible viscous effects. The relationship between the two is shown in fig. 2.3

This then gives us that a non-dimensional length of 2π will scale to dimensional lengths of 18.0cm, 1.8cm and 0.18cm if we use values for the surface tension parameter σ of approximately 0.01, 1 and 100 respectively. These correspond to regimes where surface tension effects are 100 times less than, equal to, and 100 times greater than those due to gravity.

2.2.4 Numerical instabilities and smoothing

The numerical scheme proves to be occasionally susceptible to numerical instabilities. These manifest themselves as saw-tooth modes that appear in the surface

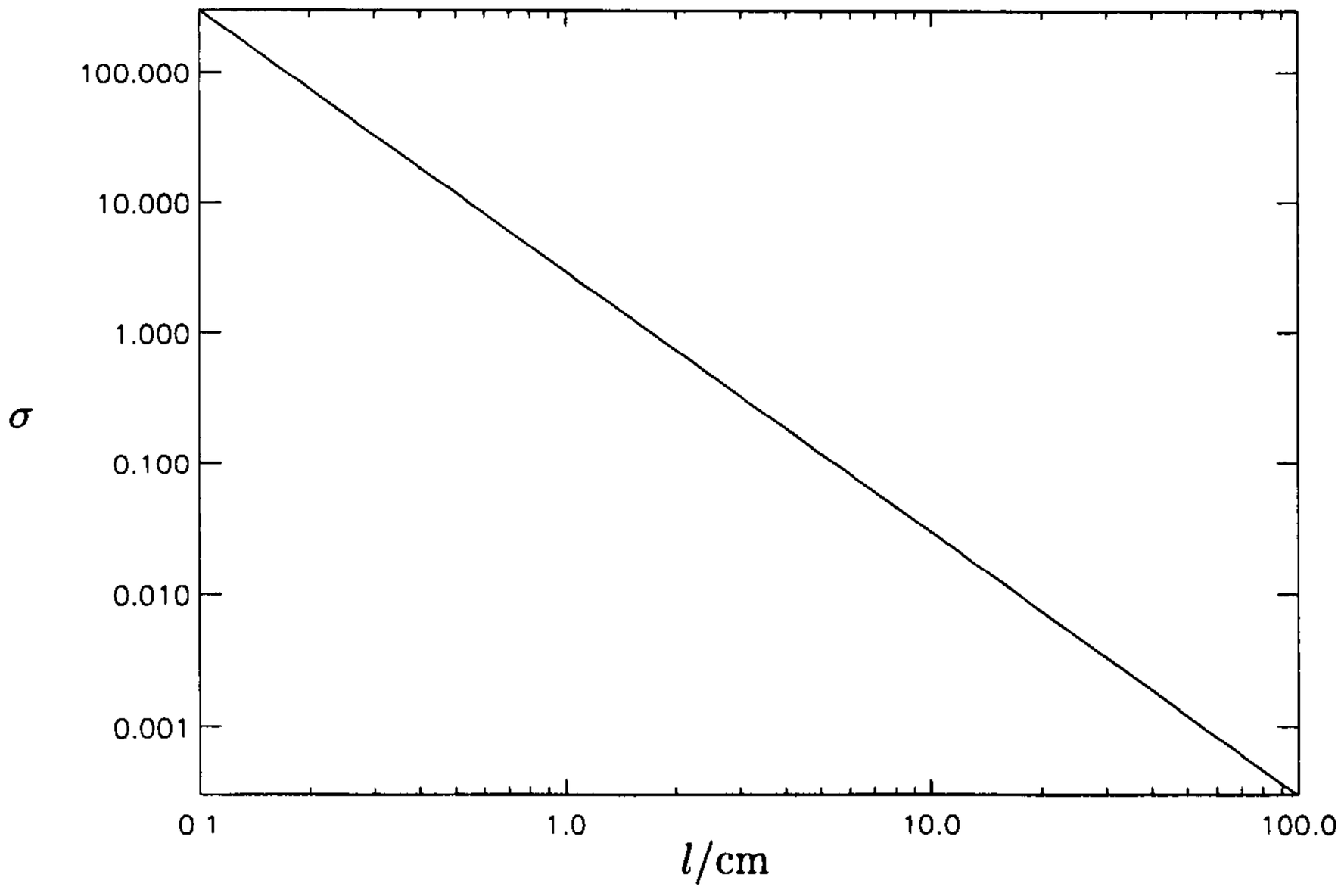

Figure 2.3: Surface tension parameter σ against characteristic length scale, l cm for g=980.6 cms^{-2}, $\rho_0 = 1$g cm^{-3} and $T' = 74$g s^{-2}.

variables. These saw-tooth modes are generally of length two surface calculation points. If left unchecked they lead to the eventual breakdown of the calculation. Such sawtooth modes arise in most existing numerical schemes for following the motion of surface waves. They were first encountered by Longuet-Higgins & Cokelet (1976) who developed smoothing techniques to control them. In the code used here saw-tooth modes are effectively removed by using the smoothing formula given by Dold (1992).

As with the estimation of arclength derivatives, the smoothing formulae are based on the fitting of high order polynomials to the surface data. We suppose that the data values at $M = 2m + 1$ consecutive points $-m \leq \zeta \leq m$ consists of a polynomial of order $M - 2$ and a displacement δ_M which is positive at even points and negative at odd points. This represents a two point saw-tooth disturbance to an otherwise smooth surface,

$$f(\xi + \zeta) \approx f_{(M-2)}(\zeta) + \begin{cases} \delta_M \text{ for } \zeta \text{ even} \\ -\delta_M \text{ for } \zeta \text{ odd.} \end{cases} \tag{2.16}$$

A similar equation for a three point saw-tooth disturbance can also be found. Fitting

the polynomial approximation leads to a solution for δ_M. M-point smoothing of a function f then achieved by subtracting the values of $\delta_M(\xi)$ from $f(\xi)$ at each value of ξ. Thus waves of wavelength two and three grid points can be selectively removed. The effect on the smoothing formula on longer waves lengths is very small, so that smoothing can be used repeatedly. With gravity as the only restoring force, such waves arise only as a result of numerical instabilities. However with the inclusion of surface tension such waves can arise as real phenomena. Smoothing now has more direct consequences for modelling very small wavelength capillaries and the total energy of the system.

2.2.5 Surface energy

In addition to kinetic and gravitational energy, the inclusion of surface tension introduces a surface energy. This surface energy is simply the product of the surface tension coefficient and the surface extension:

$$E_s = \sigma \left[\int_{x=0}^{x=\lambda} ds \; - \; \lambda \right], \tag{2.17}$$

where s is arc length. This is the total excess energy per unit length normal to the plane of motion for one wave cycle. It represents the work done in extending the surface against the restoring force of surface tension.

2.2.6 Effect of smoothing on energy

The equations for the pressure and its Lagrangian derivatives shows a numerical instability. To counteract this they are smoothed used a 15 degree polynomial formula as given in Dold (1992). The smoothing acts to selectively remove waves of wavelength two or three grid points.

These short surface modes increase the surface extension and thus a have an associated small energy. The inclusion of surface tension means that the energy involved with these small surface displacements is increased from that with gravity alone. That is, a sawtooth mode in the surface will act to increase the surface length

and thus the superficial energy. In removing the short waves, energy is taken from the system. Smoothing the surface without any form of imposed energy conservation thus leads to an slightly increased rate of energy loss compared to the original gravity only program. Without some form of imposed energy conservation the total energy of the system is then slowly reduced. Energy and mean level are conserved by the method given in Dold (1992). This scales the surface displacements from the mean level and the potential function. The scaling assumes an equal contribution from kinetic and potential energy and scales both potential and surface displacements by an equal amount to bring the total energy back to the initial value. It is not clear that this is the the best system for ensuring energy conservation with the inclusion of surface tension. However, some restoration of energy is desirable, even if done in a non-physical way since the study of Hamiltonian systems shows that it is essential to maintain the values of conserved quantities. Calculations with pure capillary waves show that using this method of energy conservation, Crapper's analytic solution for a steepness of 0.7 was maintained for over 50 wave periods. Very steep solutions developed superharmonic instabilities after a shorter period of time. Further calculations with such waves are not presented due to exhaustive coverage by previous authors.

Sawtooth modes are found to occur more frequently with the inclusion of surface tension. This is a least partly to do with the rapid variation in surface quantities with calculation point number in the presence of short ripples. Thus is the shorter scale oscillations in surface variables associated with the capillary waves that now provides much of the source of the unstable modes. The energy that drives these modes must then come predominantly from the surface energy.

The effect of smoothing was tested on a number of cases. For normal point distribution, smoothing with a lower order formula gave fewer parasitic capillaries on the forward face of the gravity wave, although of slightly larger maximum steepness, for the same number of points. Small short waves at the leading edge of the parasitic wave train are reduced, while having little effect on the parasitic capillaries near the

crest. The energy lost by removing capillaries is replaced by scaling the velocity potential and the surface displacement, hence a smaller number of slightly steeper capillaries. With more calculation points the possible effects of smoothing on the shortest ripples is reduced since each wave is specified by a greater number of points. They are also much reduced by changing the point distribution, either to one with is uniform with arclength or based on local surface curvature.

If too few points are used the very short capillaries generated naturally by the surface will be only a few calculation points in length. They are then significantly reduced in amplitude by the smoothing along with any possible numerically generated saw-tooth modes. It is important therefore to use sufficient surface calculation points to resolve any real capillary waves. The capillaries will not then be smoothed away. No smoothing leads to poor calculation of the higher Lagrangian derivatives of pressure and eventual breakdown in the program. Smoothing is then required to run the program over many wave periods. If we stipulate that each wave should be represented by at least 5 calculation points to limit any effects of smoothing, we limit the size of capillary wave we can accurately predict. For instance in the case of an 8 centimetre wavelength with 400 points we are approximately limited to accurately resolving capillary waves with wavelengths above 1 millimetre. For the calculations presented 400 surface calculation points were used and the use of smoothing minimised as far as possible.

In the energy conservation method described above the lost energy is made up by increasing the kinetic energy and the surface displacement which increases the gravitational and superficial energy. In real situations, energy would be lost through the capillary waves by viscosity (see Lamb 1932). On water surfaces such as lakes and oceans, a steady wave can be maintained by a input of energy via a wind stress, which acts to steepen the wave as reported in Crapper (1984). This process of maintaining total energy while some is lost through the capillary waves is reflected well in the present program, although not explicitly modelled.

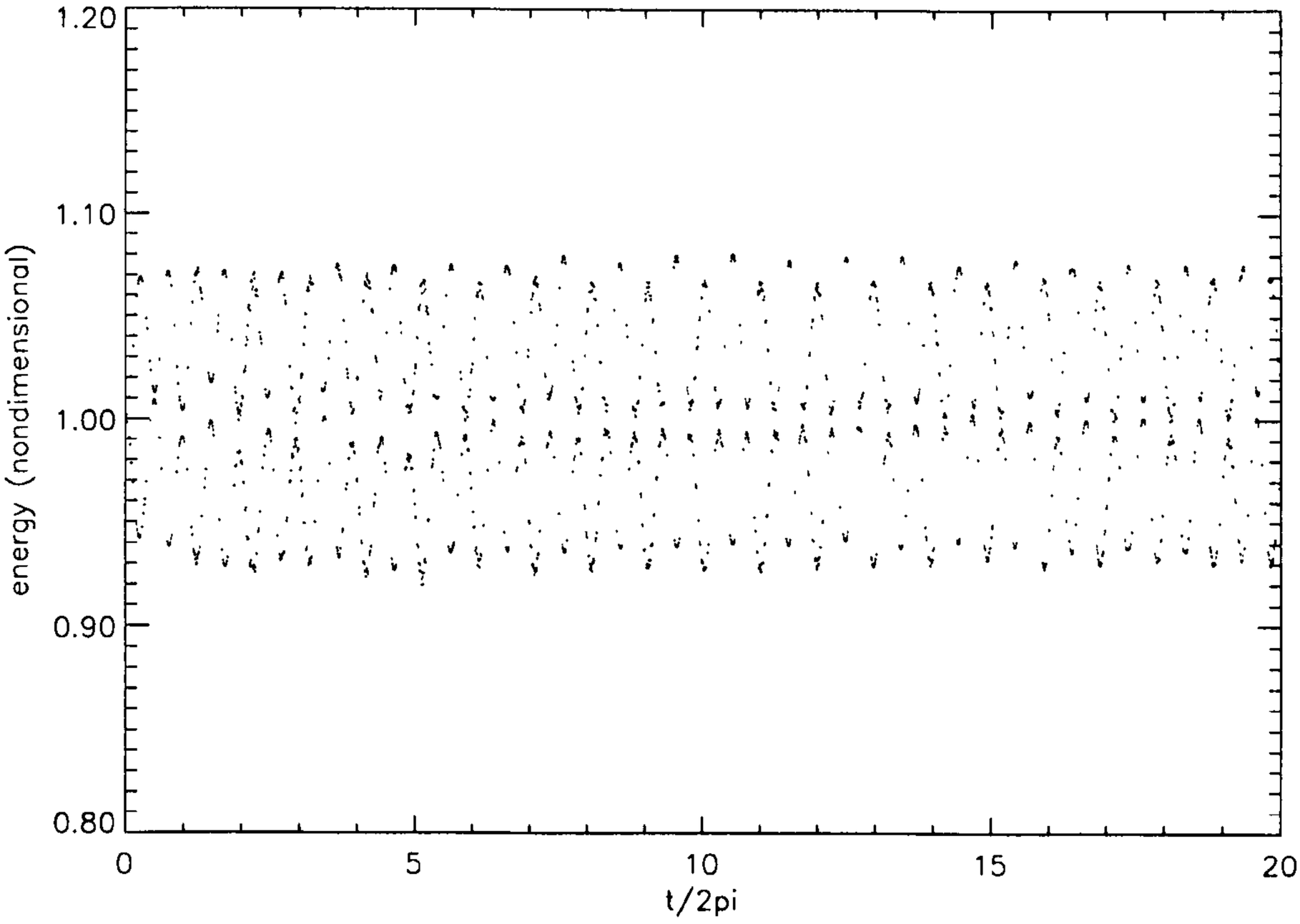

Figure 2.4: Kinetic (top) and potential (bottom) energy for a wave with initial Stokes wave profile $ak = 0.227$, $\lambda = 6.82\,\mathrm{cm}$. Non-dimensionalised against initial energies.

Fig 2.4 shows the development of non-dimensional kinetic energy and gravitational potential energy with time for a typical run with parasitic capillaries developing on a Stokes wave profile. Energies have been non-dimensionalised with those for the initial starting profile. Similarly, figure 2.5 shows non-dimensional kinetic, potential and surface energy. The initial value problem will in general give waves propagating in both directions. The energy variations observed correspond to small waves traveling in the opposite direction to that of the gravity wave. Such waves are seen in the calculations started with solitary waves with sufficiently high surface tension parameter. It may be possible to selectively absorb these waves and thus remove their effect from the calculation. Although the energy fluctuations persisted, the variation in the surface profile in most cases becomes smaller than graphical accuracy. The cases where the oscillation in amplitude of the capillaries remained noticeable were those where the underlying wave was strongly subcritical. It is noted

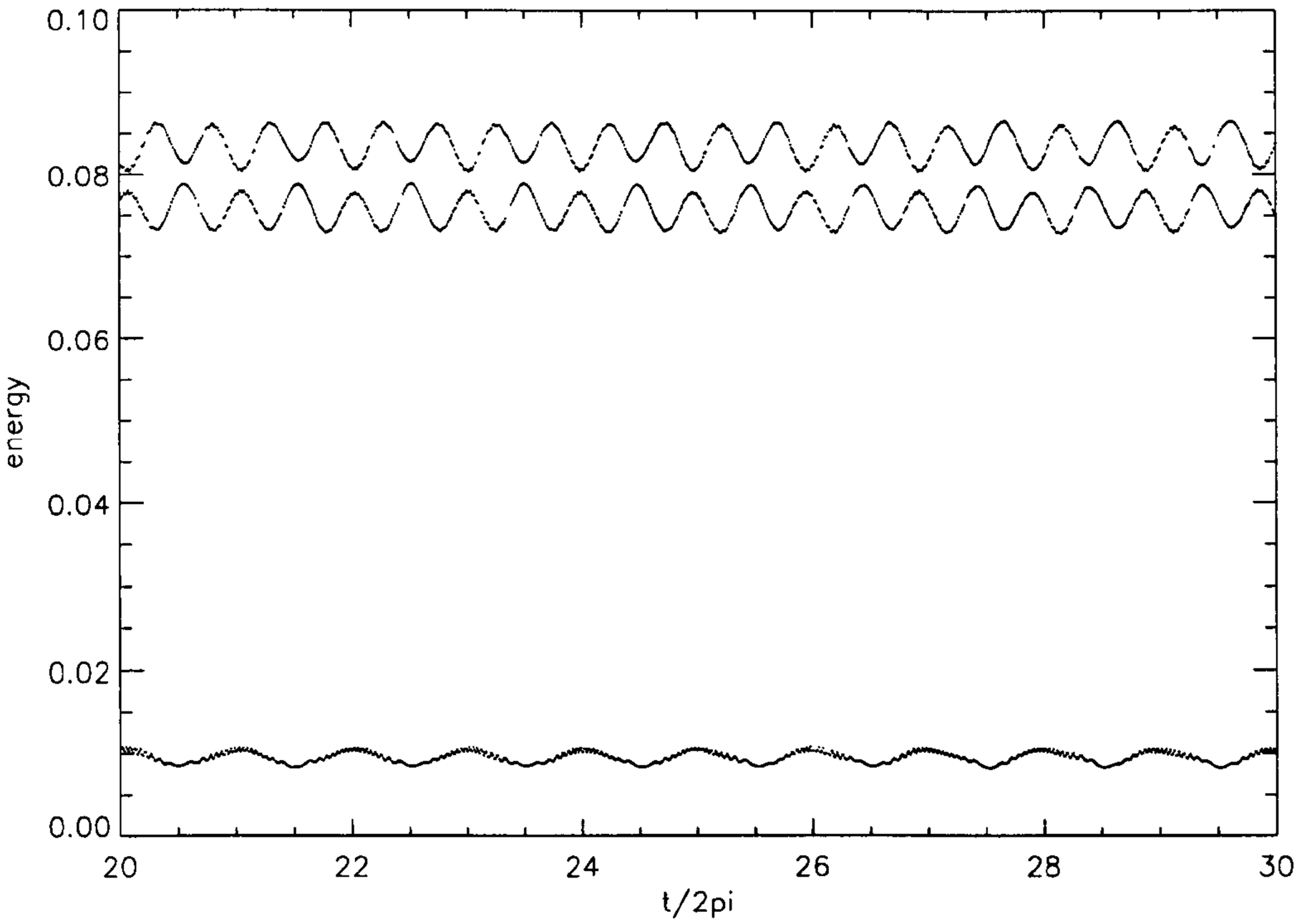

Figure 2.5: Non-dimensional kinetic energy (top), potential energy (middle) and surface energy (bottom) for a wave with initial Stokes wave profile $ak = 0.227$, $\lambda = 6.82\,\mathrm{cm}$.

that the oscillation in ripple amplitude generally had a different period to the energy oscillations reported above. For supercritical waves the surface but not energy oscillations decay. It is likely that the modulations in capillary wave amplitude and the exchanges in energy have a different causes. The possible contributary mechanisms for the observed modulations in parasitic capillary amplitude are discussed in §2.1.5 and §2.3.1.

2.2.7 Other effects of point number

One problem inherent in nonlinear boundary integral methods is that of numerical dispersion. This has previously been discussed, with particular reference to the program used here with zero surface tension, in Dold (1992). With N surface points uniformly spaced between 0 and 2π up to N/2 independent wave-numbers can be described. The shortest of these waves with wavenumber $k = N/2$ would have a

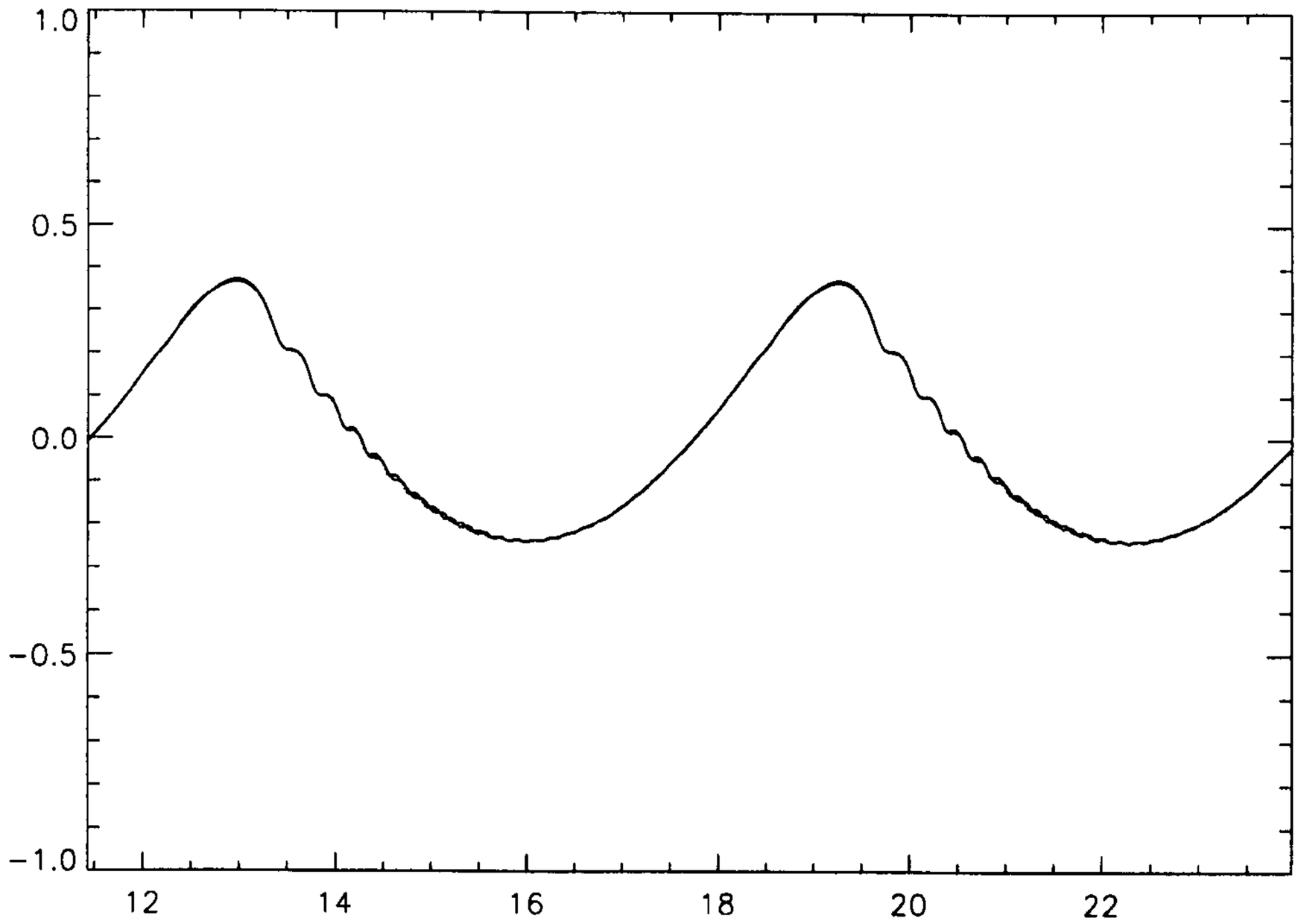

Figure 2.6: ky against kx. Comparison of steady wave for 200 and 400 surface calculation points. $ak = 0.3$, $\lambda = 8\,\mathrm{cm}$. No regridding. (Wave propagation is in the $+x$ direction).

wavelength of two points. It is found (see Dold 1992) that for waves described by only a few surface points, frequency and phase velocity are underpredicted. The percentage error decreases rapidly the more points that describe each wavelength.

Thus if we try to model the same surface with different numbers of points we would expect slightly different surface profiles for regions which contain very short waves on currents. In the case where we let the surface reach a quasi-steady state after a long period of time, small errors eventually make a small but noticeable difference. Figures 2.6 and 2.7 show the steady (to within graphical accuracy) profiles obtained from the same starting conditions using 200 and 400 calculation points per wavelength. The difference is most noticeable in the small capillaries on the bottom of the forward face of the underlying wave. With 200 points they are slightly longer and have amplitudes that decay quicker with distance from the crest. The decrease in amplitude can be explained by the effects of smoothing on waves

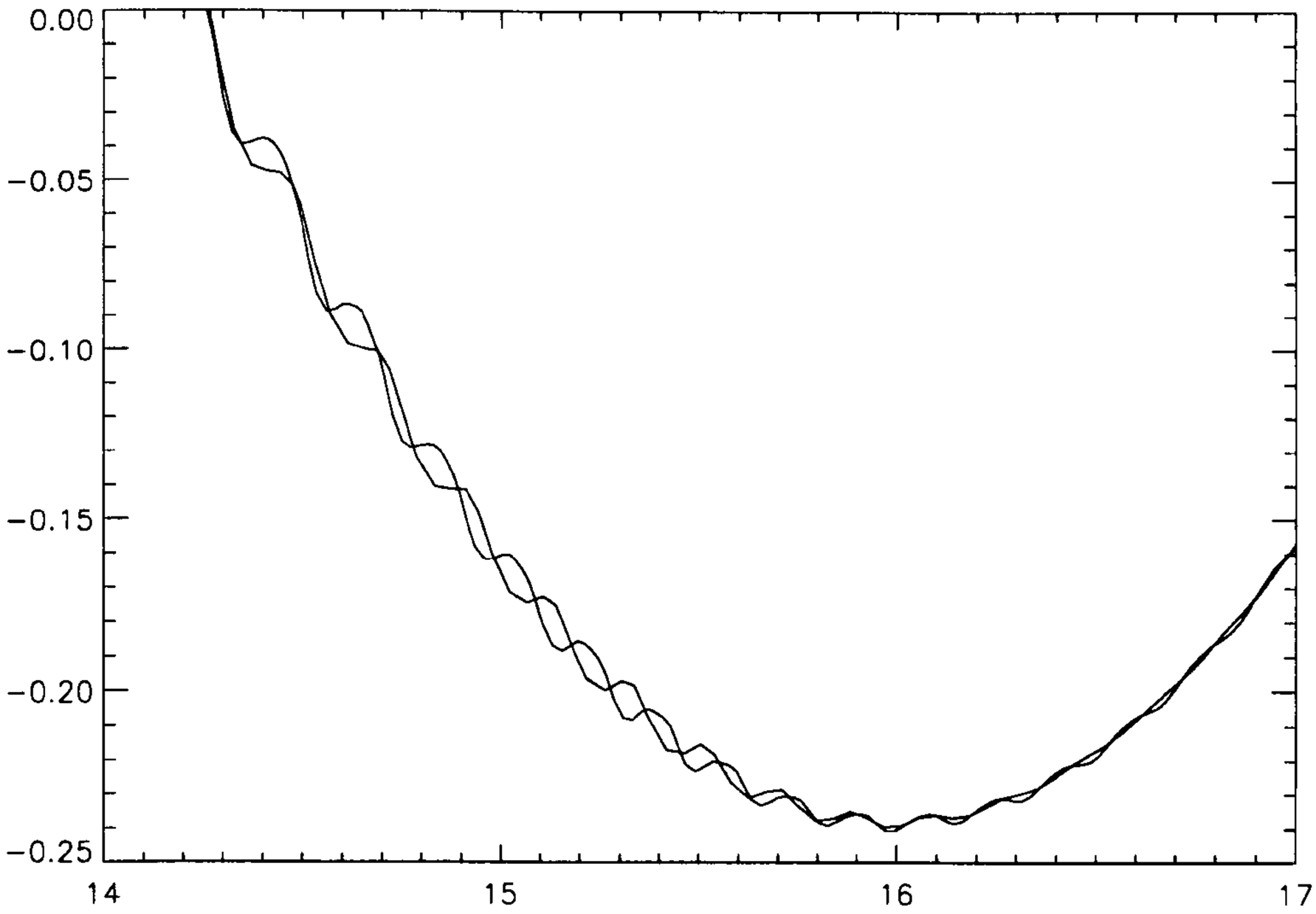

Figure 2.7: ky against kx. Comparison of steady wave for 200 and 400 surface calculation points (no regridding). Close up of trough region. $ak = 0.3$, $\lambda = 8\,\mathrm{cm}$. The ripples calculated with 400 calculation points have a shorter wavelength.

with few points per wavelength as described above.

The capillary waves are stationary in a frame of reference moving with the underlying wave. The phase speed of each capillary wave balances the underlying nonlinear velocity field; i.e. the wavelengths of the calculated stationary capillary waves must have numerical phase speed equal to the underlying velocity. In the case where we have less points describing that part of the surface, we see that the wavelengths are longer. As these waves are well within the capillary branch of the dispersion relation (fig 1.2), their phase speed increases with decreasing wavelength. For linear capillary waves we have the relation that

$$c = \left(\frac{2\pi T}{\rho}\right)^{\frac{1}{2}} .\lambda^{-\frac{1}{2}}. \tag{2.18}$$

This leads to the conclusion that numerical phase speeds for capillary waves of very few surface points are over-estimated, rather than under-estimated. A full investigation along the lines of Dold (1992) is needed to determine the full numerical

dispersion relation in the capillary regime.

2.2.8 Resolution of capillary waves

In the calculation of surface waves by the above scheme, it is important that surface variables are sufficiently slowly varying. This is required to ensure the accuracy of calculated surface derivatives for example. Where the surface variables vary rapidly with distance along the surface, sufficient number of calculation points have to be used so that the variation with calculation point number remains small. Steep gravity waves have smooth troughs and sharp crests, so require a higher point density at the crests where surface quantities vary more rapidly with arclength. It does not matter (apart from in terms of efficiency) if there are more points in the troughs, so long as there are a sufficient number of points around the crest.

With a scheme which follows the calculation points as surface particles, the points become denser in regions where the stream velocity is smallest. For surface waves this is at the wave crests. Thus when calculating steep gravity waves we can get away with a relatively small total number of calculation points as they will naturally be distributed in greater numbers around the sharp crests where they are most needed.

Steep capillary-gravity waves have an appearance more like the Crapper solution (figure 1.3), i.e. sharp troughs and broad, rounded crests. Thus to ensure a smooth variation of surface variables with point number, we need to take care that there are sufficiently many points at the wave troughs.

One way to do this is just to use many points. This is inefficient for calculating a surface consisting of purely capillary waves, but less so when the surface is a perturbation to a gravity wave, as in most of the solutions presented here. Another way is to regrid the surface, or change the calculation scheme such that the points no longer move as fluid particles but have position along the surface as some function of the surface variables such as curvature or arclength. By regridded the surface it can be specified by a smaller number of points. However, further calculations have

to be performed and the time-stepping process becomes considerably slower.

2.2.9 Regridding the surface

A regridding algorithm was included in the program that placed calculation points equi-distant along the length of the surface. The option for a point distribution proportional to local curvature was also included. The arclength of the surface is calculated using the current point distribution. From this the distance along the surface of each point in the new distribution is found. A 10th order polynomial centred on the nearest point in the current distribution is used to interpolate each surface variable and find its value at the new position along the surface. The surface is then stepped forward in time as normal. The interpolation can introduce errors on its own if too few points are used, so calculations presented here are for 400 points.

It is found that the natural point distribution is not sufficient. An equi-distant or curvature based point distribution is required to ensure that small capillary waves, particularly their troughs, are adequately resolved. Without regridding the sharp troughs of capillary waves can be subject to smoothing if they are only defined by a few calculation points, even if there are a relatively large number of points in each capillary wavelength. In such cases the smoothing algorithm reduces a sharp trough in the same way as a sawtooth instability. By placing more points around the troughs, the rate of change of surface variables with calculation point number is reduced along with any possible effects of smoothing.

The difference is seen in figures 2.8 and 2.9 which show surface profile and slope for an initial Stokes wave of steepness $ak = 0.315$ and length 8cm. Looking at the wave profile, the capillary waves are of larger amplitude, particularly in the underlying wave trough. Capillary wave troughs themselves are sharper, and certainly non-linear. The capillary ripples are also found to be slightly longer, by approximately 4% for the case shown here.

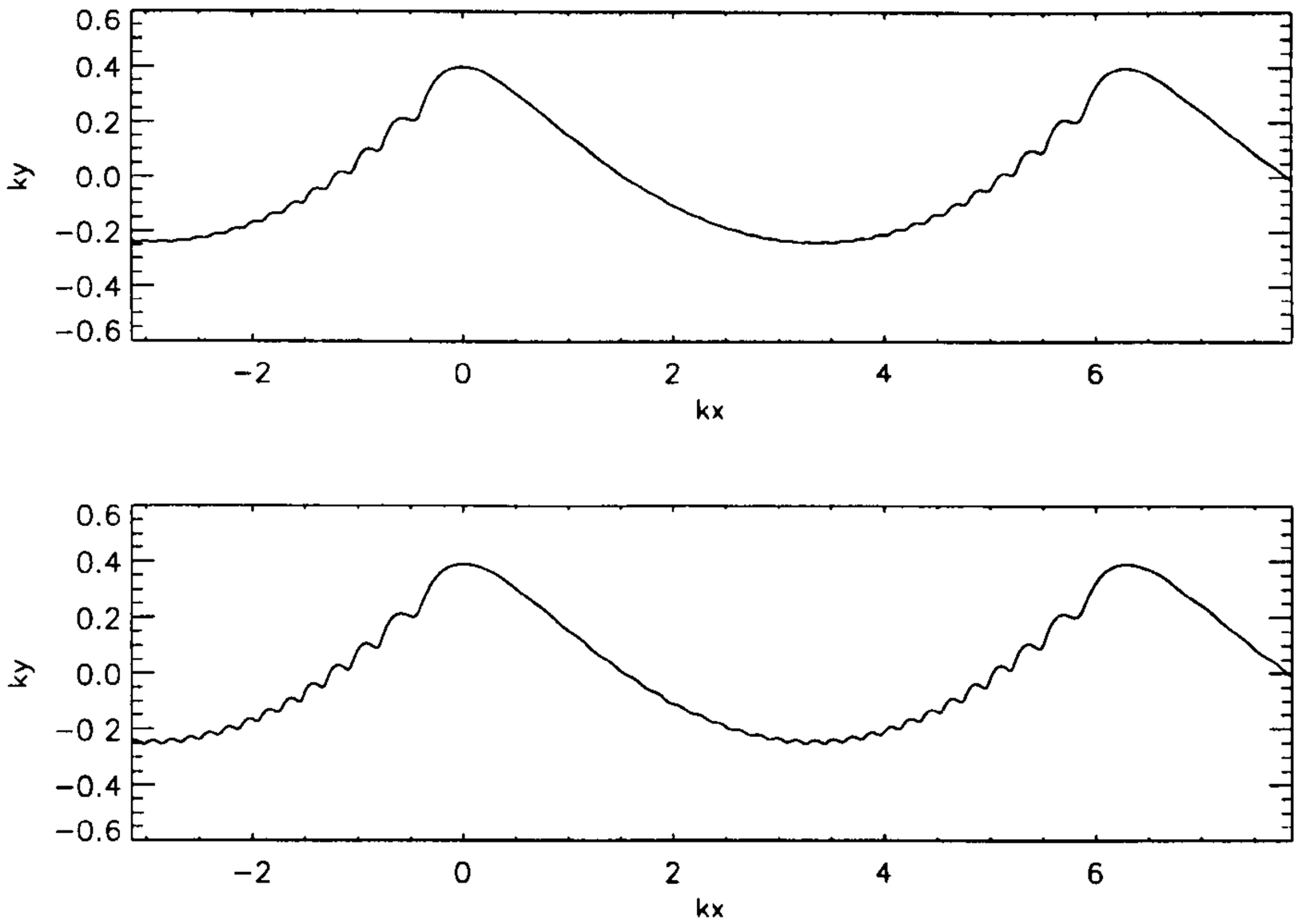

Figure 2.8: Quasi-steady surface profiles with (below) and without (above) regridding the surface calculation points $ak = 0.315$, λ=8 cm. Propagation is in -x direction.

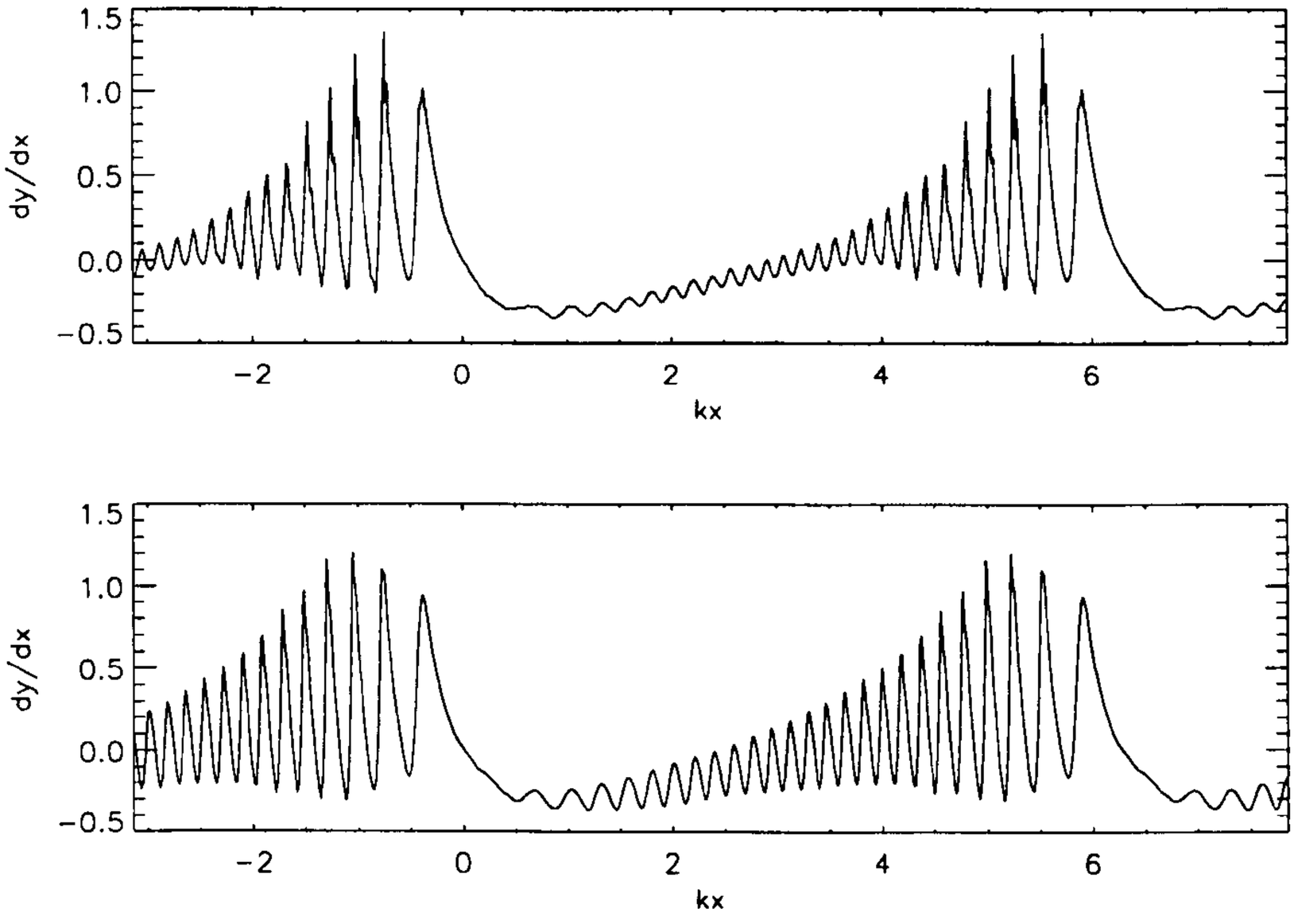

Figure 2.9: Surface slope of quasi-steady waves with (below) and without (above) regridding the surface calculation points $ak = 0.315$, λ=8 cm. Propagation is in -x direction.

2.3 Numerical calculations

The work presented here is for the generation of parasitic capillary waves by steep gravity waves. Calculations for steadily propagating pure capillary waves have also been performed, and are not presented due to the extensive amount of work on these by previous authors (see Chapter 1).

2.3.1 Quasi-steady capillary gravity waves

For the investigation of parasitic capillaries, pure progressive Stokes waves are used as initial starting profiles. These are calculated by the method of Teles de Silva & Peregrine (1988), which for zero vorticity is that of Tanaka (1983). It is then as if surface tension is switched on at $t = 0$. The result for a Stokes wave of length 8cm and steepness $ak = 0.3$ can be seen in figure 2.10. The wave soon develops ripples on its forward face. The ripples emerge from the smooth face of the wave. The capillary wave train grows forward from in front of the crest.

This is what we would expect at least for part of the profile which has surface velocity greater than the minimum possible wave speed. The energy associated with the pressure disturbance travels against the underlying surface velocity at the group velocity, c_g. If we take a frame of reference moving with the gravity wave crest, the surface velocity appears as a non-uniform current in a direction opposite to the direction of gravity wave propagation. Note that the of the value c_g will then vary along the profile. For capillary waves we have the approximate relation $c_g \simeq 3c/2$. For nonlinear capillaries, the actual group velocity would be slightly less than this. So if we look at the profiles in a moving frame of reference we would expect to see the spread of capillaries at a speed slightly less than half the surface velocity at that point.

The amplitude of the surface oscillation decays until a quasi-steady profile is obtained (see fig 2.11 below). It can be seen (figure 2.10) that there is a maximum in the capillary wave steepness shortly after the initial time. For this particular wave

the maximum occurs after the gravity wave have travelled a distance of approximately 2.25 wavelengths. This then coincides with the time taken for the energy associated with ripples generated at one crest to reach the next. The variation in capillary amplitude persists, as can be seen from their subsequent reduction and re-emergence in the figure. The ripple amplitude oscillates about a mean with maxima occurring each time the wave train travels another 2.25 wavelengths. However, the amplitude of this surface oscillation decays until a quasi-steady profile is obtained (see fig 2.11 above).

The discernible variation in surface profile decays with time to an extent dependent on the steepness of the underlying wave. For supercritical wave steepnesses the time taken to reach a profile that appears steady to graphical accuracy is of the order of ten wave periods. Figure 2.11 shows surfaces overplotted every wave period for ten periods For subcritical waves modulations in capillary wave amplitudes persist. Figure 2.4 earlier showed a plot of the kinetic and potential energies against time for a typical wave (shorter and less steep than the one shown in figure (figure 2.10). An oscillation in potential and kinetic energy can clearly be seen which does not decay in time. The kinetic energy remains above, and the potential energy below that of the initial Stokes wave for most later times. This has been found to a greater or lesser extent for all waves calculated. Figure 2.5 shows non-dimensional kinetic, potential and superficial energies against time for the same wave (this time not divided by the non-dimensionalised initial energy). It can be seen that the superficial energy also undergoes oscillations, but of twice the period. The possible source of these oscillations has been addressed earlier. The surface oscillations remained noticeable on the strongly subcritical waves. Such modulations could also be due to resonant wave interactions of the type discussed earlier. For most calculations shown here a quasi-steady profile was reached and in such cases it is these surface profiles that are shown. For the calculations in which significant modulations persisted (for example ak =0.24 and ak =0.26 for the 8cm wave), a representative profile is shown.

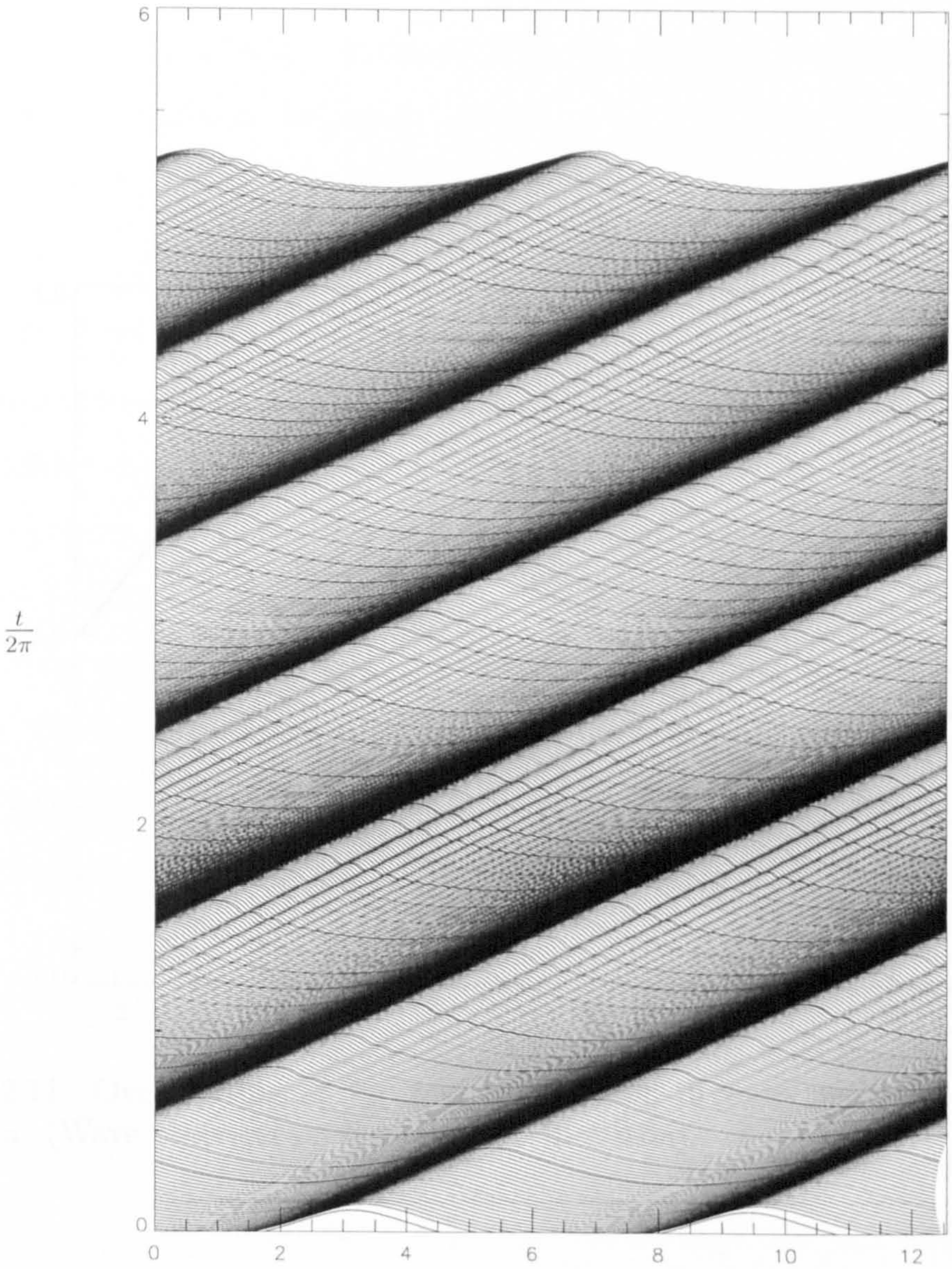

Figure 2.10: Computation of the development of surface profile from an initial gravitational progressive Stokes wave, $ak = 0.32$. λ=8 cm.

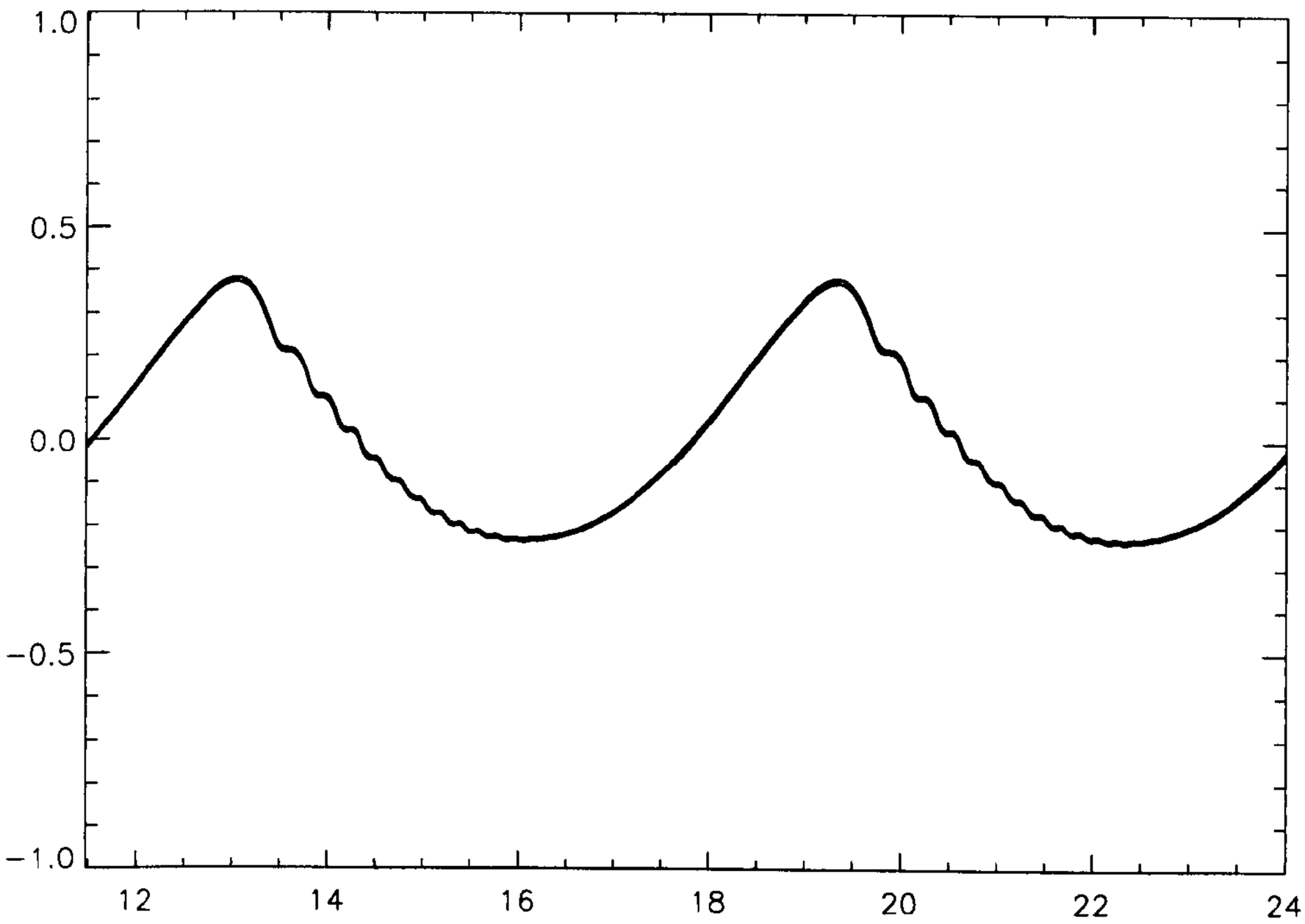

Figure 2.11: Overplotting of ky against kx over 10 wave periods. $ak = 0.32$, $\lambda = 8\,\text{cm}$. (Wave propagation is in the $+x$ direction).

OF BRISTOL
LIBRARY

2.4 Comparison with other numerical calculations

2.4.1 Longuet-Higgins (1995)

Numerical calculations of steady parasitic capillary waves are presented by Longuet-Higgins (1995). This further improves upon the theory of Longuet-Higgins (1963) (see above). Capillaries are again considered to be a linear perturbation to an otherwise steady, irrotational, non-linear gravity wave. A more accurate knowledge of the profile of underlying Stokes wave is used.

The inclusion of gravity in the capillaries has another important result. A critical steepness parameter $(ak)_c$ is introduced at which the surface velocity (in a frame of reference moving with the phase speed) equals the minimum (local) speed of capillary-gravity waves. For subcritical gravity waves, with steepness $(ak) < (ak)_c$, the surface velocity is everywhere larger than the minimum capillary-gravity wave speed. Thus capillary waves may theoretically be generated at all points on the surface. For supercritical waves, with $(ak) > (ak)_c$, the surface velocity in the vicinity of the crest is smaller than the minimum. Hence capillary waves can only be generated in the wave troughs and are bounded away from the crests.

Surface profiles

Quasi-steady waves have been calculated starting from Stokes waves with length 8 centimetres and steepnesses $ak = 0.24, 0.26, 0.28, 0.30, 0.31, 0.31.5$ and 0.32. Surface profiles are shown in figure 2.12, and the corresponding surface slopes in figure 2.13. Comparable calculations presented in Longuet-Higgins (1995) are reproduced in figures 2.14 and 2.15, which have a greater vertical exaggeration. Note that the profiles have been shifted, but not scaled, for clarity. For 2.14 mean ky should be zero and for 2.15 mean dy/dx should be zero for each profile.

The sudden end of the capillary waves in the trough of the supercritical waves

in figure 2.15 (most noticeable in the plots of surface slope) may not be a physical phenomenon. The equations used by Longuet-Higgins have singularities at the caustics that limit the 'blocked' region, so the integral calculation is stopped a finite distance from these points. The singularity arises from the $1/(k_1 - k_2)$) dependence of the wave amplitude from Lamb (1932) §271 mentioned earlier. It can be seen that there is good agreement between the profiles calculated and those presented by Longuet-Higgins up to steepness 0.3. A marked increase is seen in ripple amplitude as the critical steepness is approached. In addition the capillary wave steepness is seen to first increase than decrease away from the crest. In general our method predicts a slightly shorter wavelength for the parasitic capillaries than that from Longuet-Higgins by up to 4%. Another difference is the decay in capillary wave steepness with distance from the crest. Our calculations show the same maximum slope, but a slightly quicker decay in slope away from the crest. This may be an effect of numerical smoothing.

A maximum amplitude for parasitic capillaries in the trough is found around $ak = 0.31$ for the wave of 8cm. More calculations are required to find the exact critical steepness for this particular wavelength. This is partly consistent with the calculations of Longuet-Higgins (1995), and is to be expected from the disturbance to a stream work of Lamb. We do however find that capillary amplitude near the underlying wave crest remains the same to within the small modulations observed beyond the critical steepness for the cases studied; i.e. the disturbance becomes more localised around the wave crest. We cannot at present accurately calculate parasitic capillaries on much steeper Stokes waves due to the very steep capillaries that from shortly after the initial time, before a quasi-steady profile is reached. Thus we cannot check whether this feature continues far beyond the critical steepness.

Longuet-Higgins gives the wave profiles assuming the capillary waves generated are small linear perturbations to the underlying Stokes wave profile. It can be seen that the capillaries generated are certainly nonlinear, having sharper troughs and rounded crests. For supercritical waves the linear capillary perturbation is only

calculated by away from the caustics. This may lead to the double bump in the profile near the crest that can be seen in figure 2.15, particularly fo ak =0.32. Our calculations show a single large bulge continues at the crest as the steepness is increased above the critical value. This may be the source of the inconsistency between our continued large amplitude, but increasingly localised capillaries on supercritical waves, and the uniform amplitude reduction given by the theory presented by Longuet-Higgins (1995).

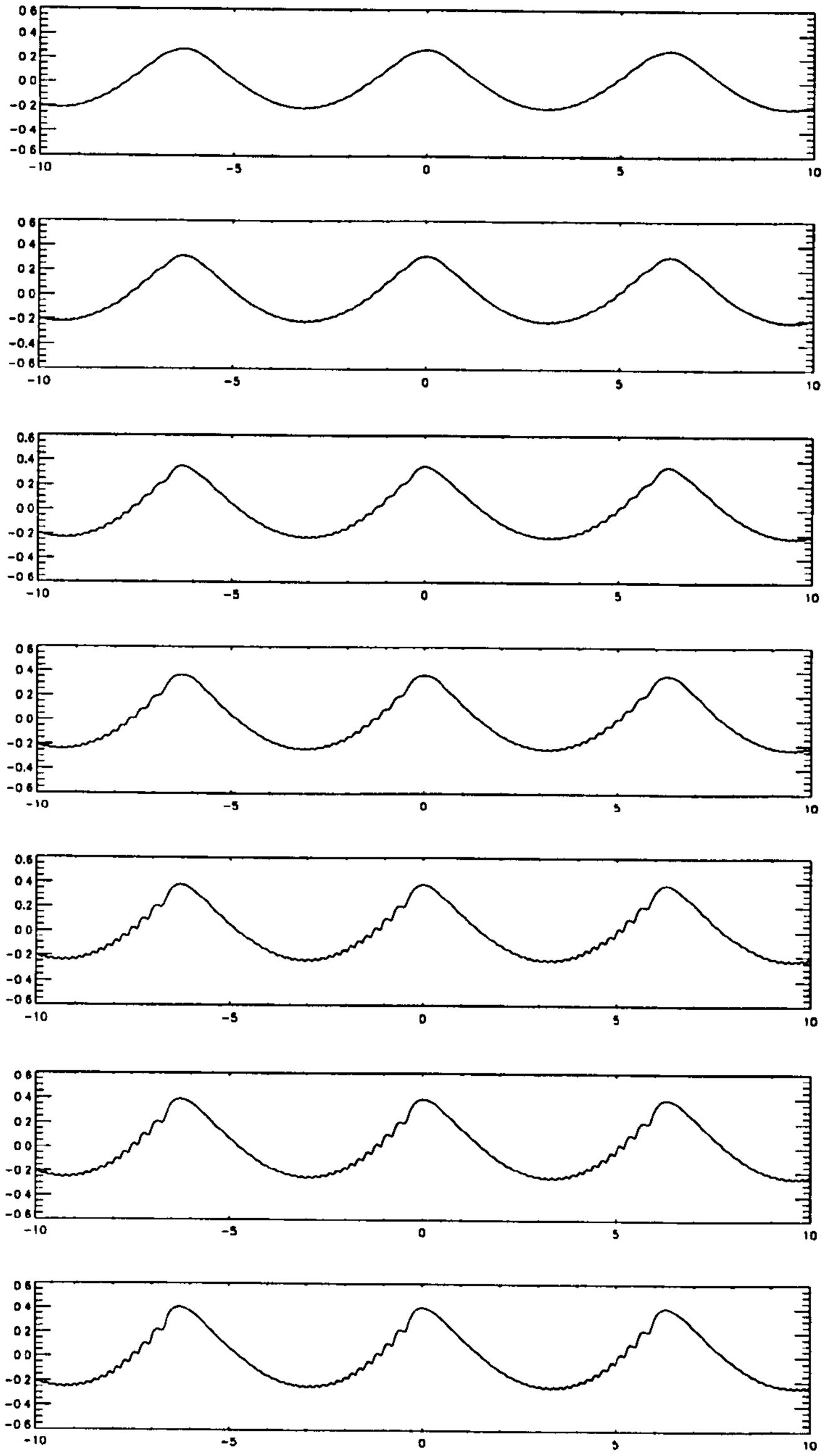

Figure 2.12: Surface profiles for $\lambda = 8\text{cm}$, $ak = 0.24$, 0.26, 0.28, 0.30, 0.31, 0.315, 0.32. (Wave propagation is in the $-x$ direction).

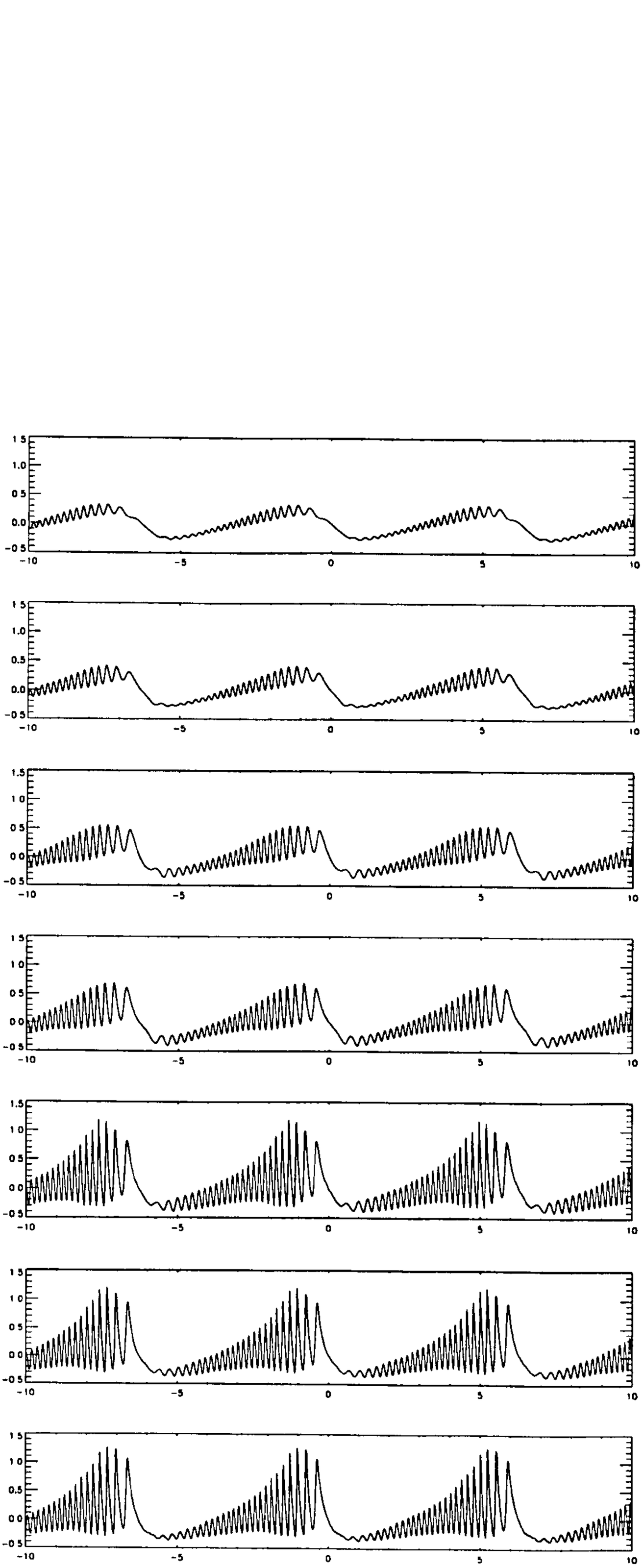

Figure 2.13: Surface slopes for $\lambda = 8$cm, $ak = 0.24$, 0.26, 0.28, 0.30, 0.31, 0.315, 0.32. (Wave propagation is in the $-x$ direction).

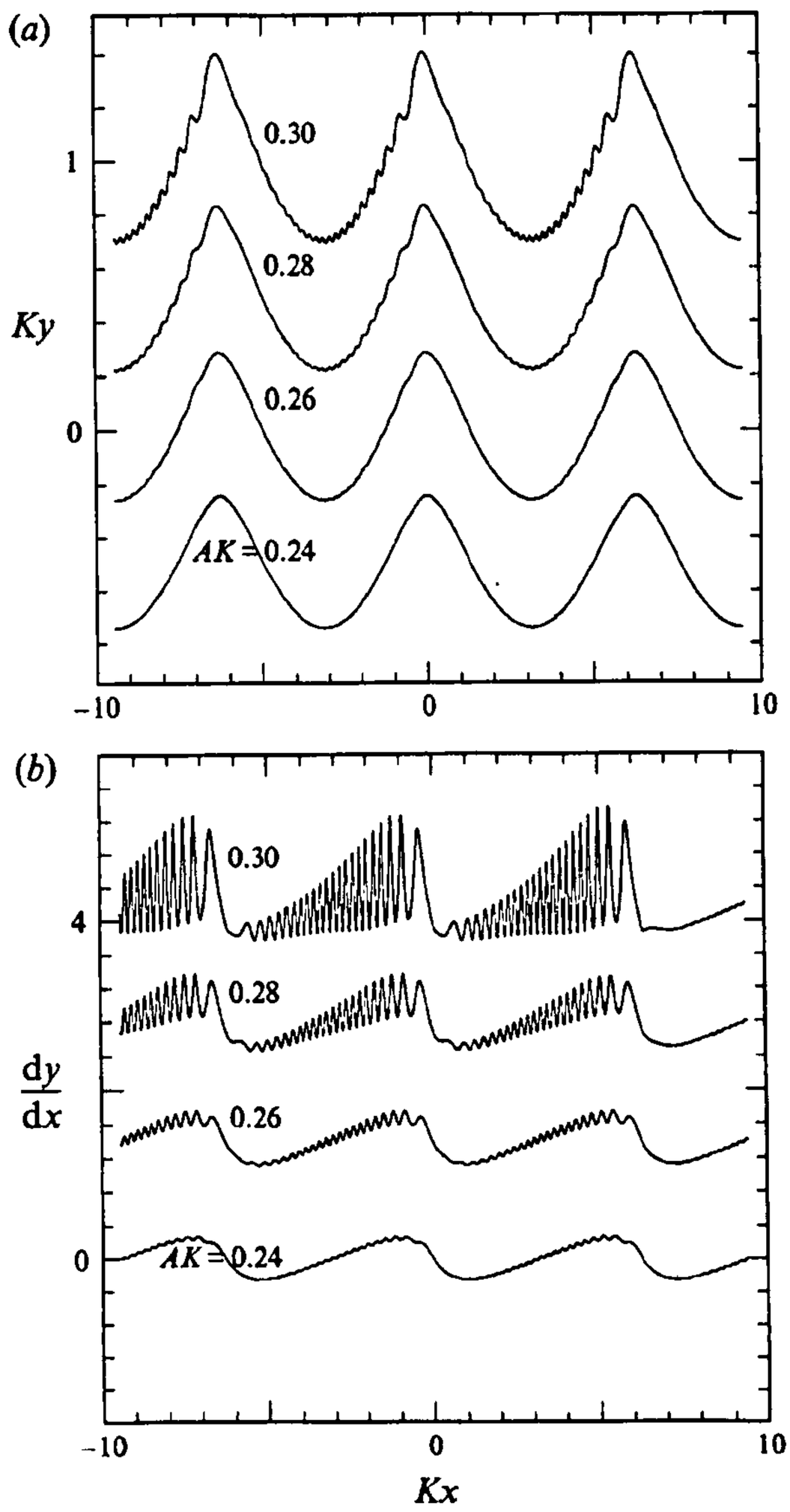

Figure 2.14: (a) Surface elevation and (b) slope for $\lambda = 8$cm, $ak = 0.24$, 0.26, 0.28 and 0.30 (subcritical). NB: For both (a) and (b), the profiles have been shifted for clarity. *Longuet-Higgins (1995)*.

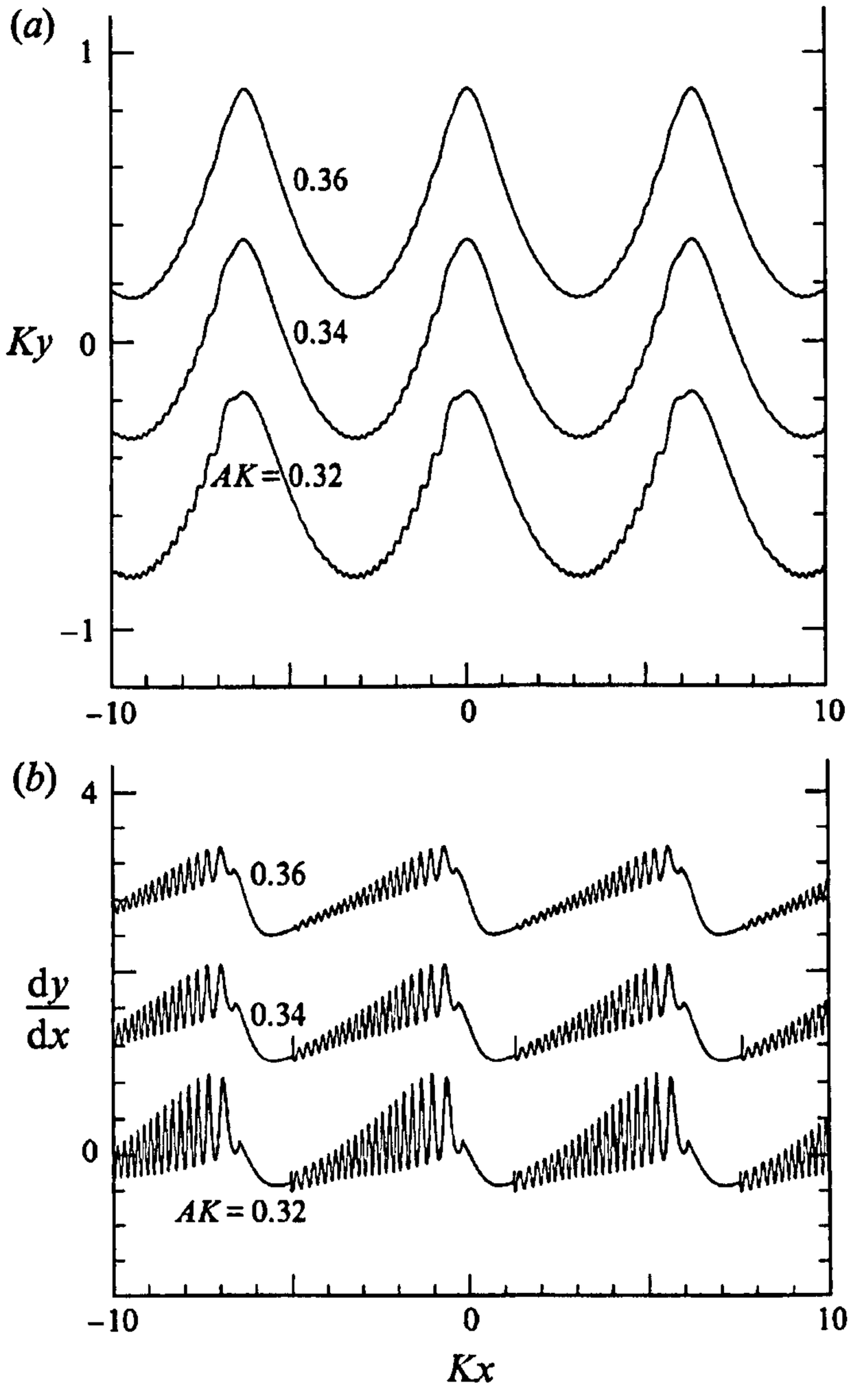

Figure 2.15: (a) Surface elevation and (b) slope for $\lambda = 8$cm, $ak = 0.32$, 0.34 and 0.36 (supercritical). NB: For both (a) and (b), the profiles have been shifted for clarity. *Longuet-Higgins (1995).*

Blocking

Our calculations show the presence of a 'blocked' region in agreement with the linear perturbation theory of Longuet-Higgins. The blocked region calculated by Longuet-Higgins is that in which the local velocity in a frame of reference moving with the wave is less than the minimum wave velocity as given by linear theory. Thus linear waves that are stationary in the moving reference frame cannot exist here.

Figure 2.16 shows the surfaces profile and region in which capillary waves are excluded for a Stokes wave and the corresponding capillary-gravity wave for a supercritical steepness. The limits of this region in the Longuet-Higgins (1995) are calculated on the Stokes wave profile (dashed vertical lines on figure 2.16). The effect of the capillaries on the underlying flow is not taken into account. The solid vertical lines on figure 2.16 show the corresponding blocked region for the fully developed capillary-gravity wave. It can be seen that the blocked region is shifted forward, corresponding to the forward shift of the crest capillary-gravity wave crest. The blocked region is also wider. The effect of the parasitic capillaries is to reduce the orbital velocity at the crest compared to the pure gravity Stokes wave.

According to the theory developed by Longuet-Higgins, there should be no capillary waves within this region. Close inspection of the slope of the supercritical capillary-gravity wave calculation within this region reveals ripples of very small amplitude. However, these are considerably smaller than the waves found outside the 'blocked' region as can be seen in the graph of surface slope in figure 2.17. Since the surface quantities outside this region are rapidly varying, some very small variation inside might be expected as a numerical artifact.

The extent of the blocked region is calculated using linear wave theory. For nonlinear ripples, the phase velocity decreases with steepness from the linear value. Thus in practice nonlinear waves with slower phase velocities could exist within the limits of this region.

Also, the theory presented by Longuet-Higgins does not well represent the neigh-

bourhood close to the 'blocking points', due to the singularity in the expression for capillary amplitude there, similar to that in Lamb's surface disturbance to a stream given earlier. Longuet-Higgins states that "there may be some detectable capillary gravity activity there".

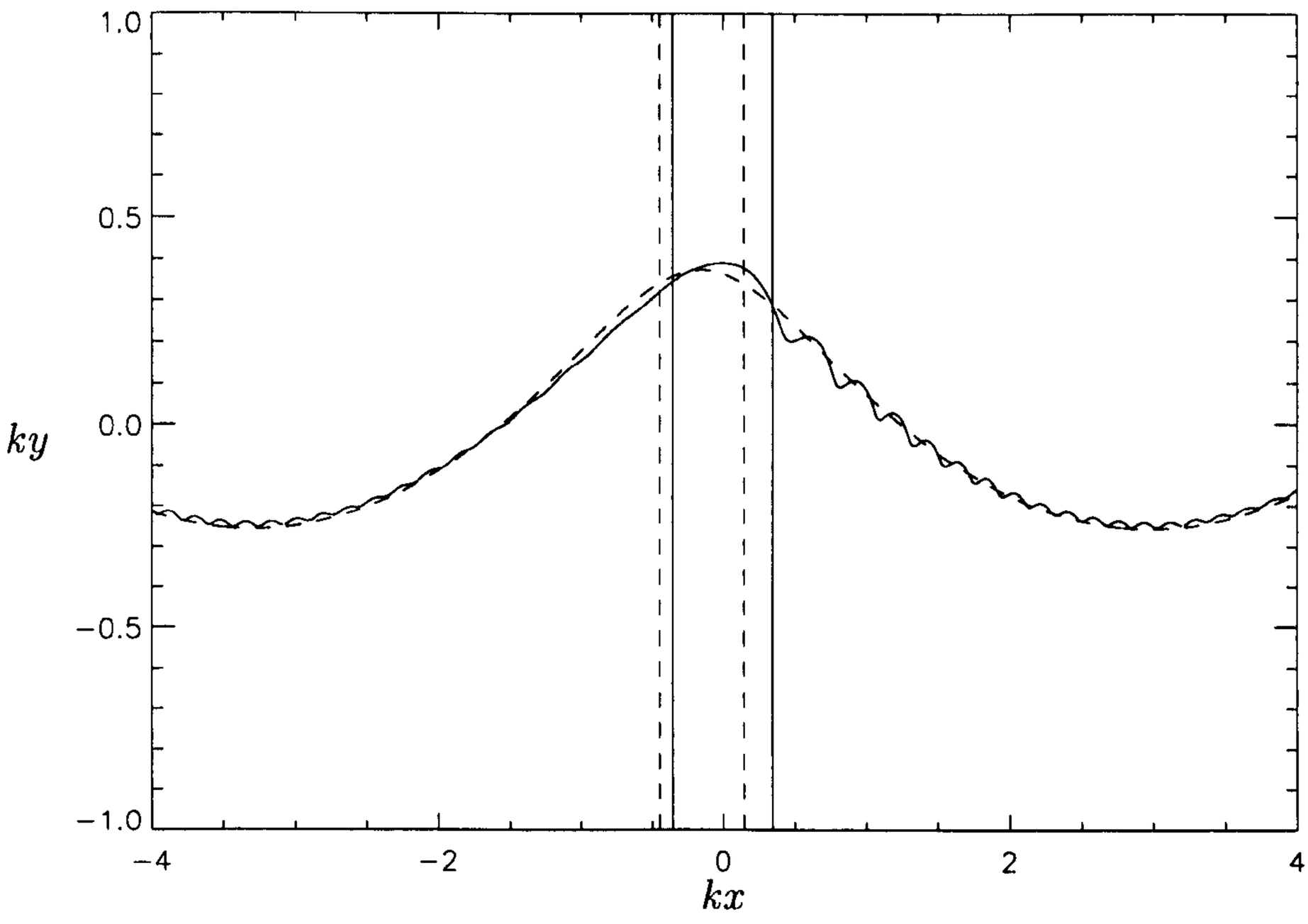

Figure 2.16: ky against kx for a Stokes wave ak=0.315 (dashed) and a fully developed capillary gravity wave started from the Stokes wave profile (solid) for $\sigma = Tk^2/g = 0.0452$. The corresponding vertical lines delimit the region around the crest in which the stream velocity is less than the minimum linear wave speed. (Wave propagation is in the $+x$ direction).

Although important for waves produced in laboratory flumes, blocking is not important for waves longer than 1 m, such as found on the ocean surface. The effect of the velocity field of the gravity wave on the steepness, wavelength and dissipation of capillaries has received further attention in Longuet-Higgins (1987). One small but noticeable difference between sub- and supercritical waves is in the averaged Stokes drift velocity. Figure 2.18 shows the averaged drift velocity against wave steepness for a wave of length 8.25cm. The points have been joined with

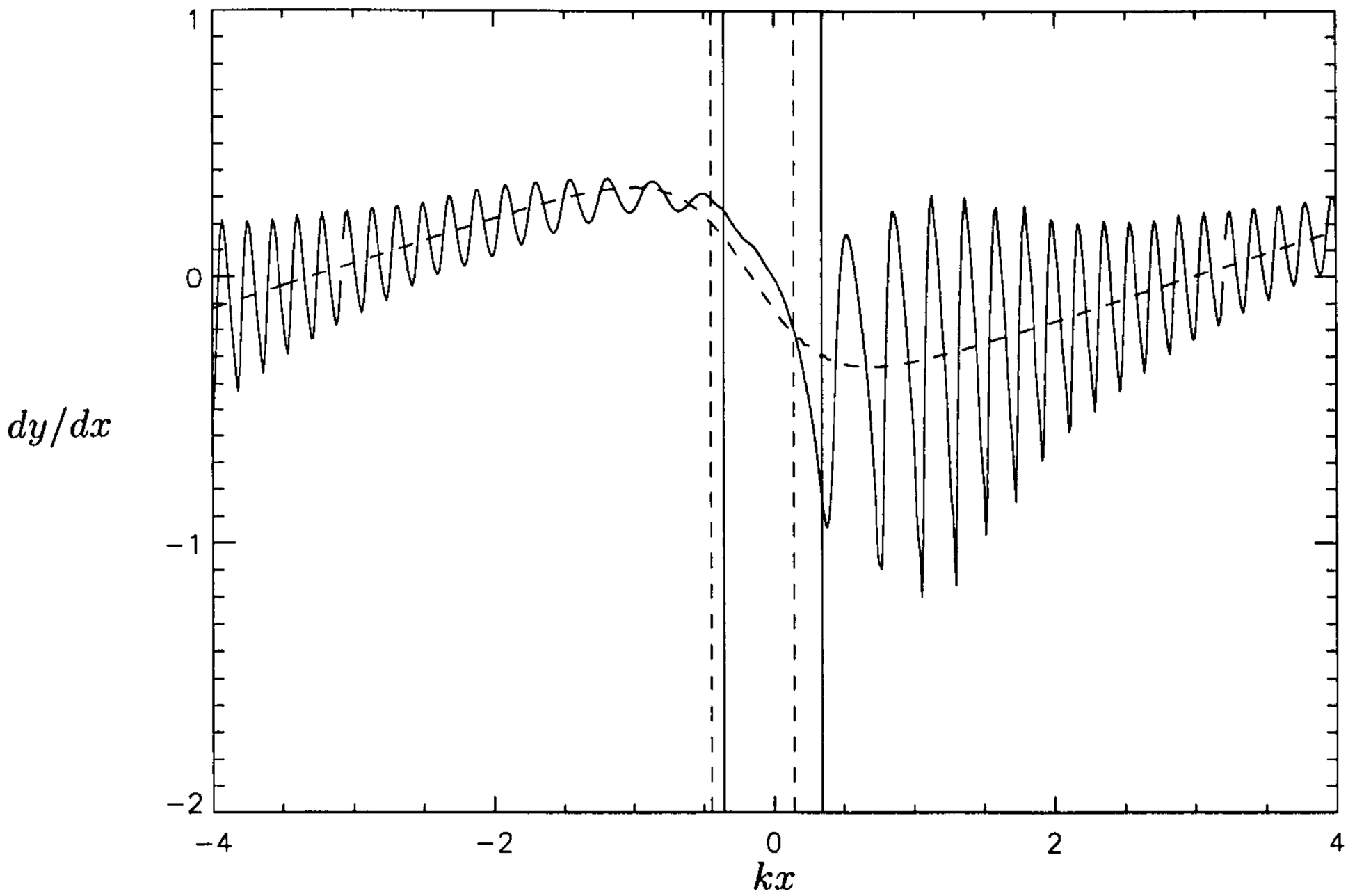

Figure 2.17: dy/dx against kx for a Stokes wave ak=0.315 (dashed) and a fully developed capillary gravity wave started from the Stokes wave profile (solid) for $TK^2/g = 0.0452$. The corresponding vertical lines delimit the region in which the stream velocity is less than the minimum linear wave speed. (Wave propagation is in the $+x$ direction).

straight lines to highlight the step in the otherwise linear plot between $ak = 0.315$ and 0.32. The critical steepness for this wave lies within this interval. Surface calculation points move as surface particles, so calculating the average drift is a simple matter. In performing the calculations previously presented, it was noted that the calculation points were carried further at the crest of the waves with increasing steepness, particularly for supercritical waves. From figure 2.18 we see there is a small jump in drift velocity which coincides with the critical steepness. Over the small steepness range shown it appears that for both sub- and supercritical waves Stoke's drift increases linearly with steepness. For supercritical waves the rate of increase with steepness is slightly greater (the straight lines for sub- and supercritical waves are respectively $u_{drift} = 71.1(ak) - 14.6$ and $u_{drift} = 93.8(ak) - 21.3$).

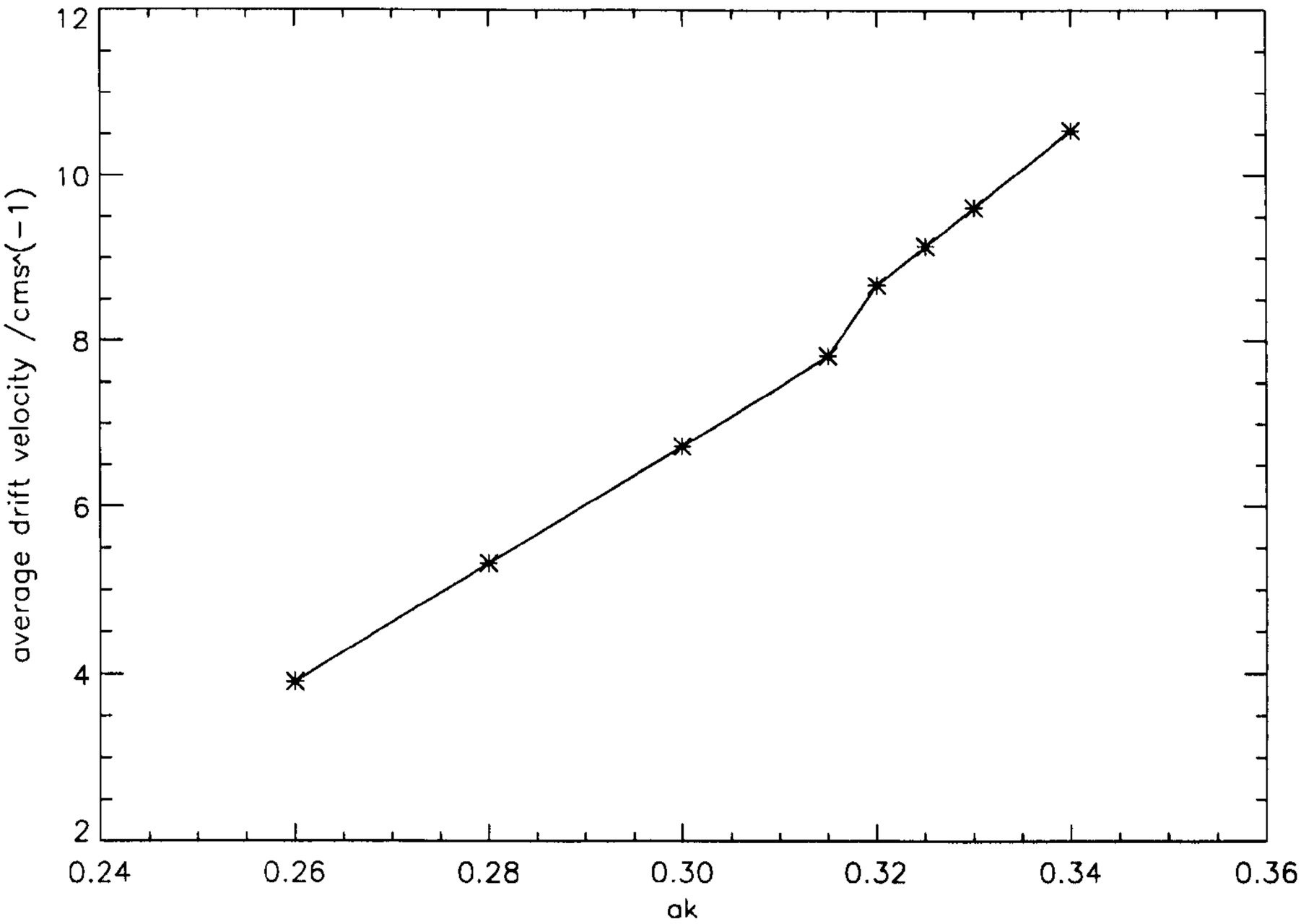

Figure 2.18: Numerically calculated drift velocity for a gravity-capillary waves of wavelength 8.25cm.

2.4.2 Comparisons with Perlin, Lin & Ting (1993)

The observations made by Perlin *et al.* (1993) are of plunger- generated waves at two frequencies: 5.26 and 4.21 Hz. For the 5.26 Hz wave, a comparable profile is given by a Stokes wave of length 6.82 cm and $ak = 0.227$. Figure 2.19 shows the development of the capillary waves from an initial Stokes gravity wave of wavelength 6.82cm and steepness $ak = 0.227$. This is a strongly subcritical wave, where we might expect capillaries generated by one crest to catch up with the next. It is not easily seen that there is an appreciable overlap of capillary-gravity waves generated on one crest with those from the next. Capillary ripples quickly form on the forward face of the initially pure gravity wave. The start from the sharp crested wave leads to oscillations in the amplitude and steepness of the parasitic capillaries. These can be best seen in figure 2.20 which follows a wave crest.

Figure 2.19: Development of the surface from $ak = 0.227\,,\ \lambda = 6.82\,\mathrm{cm}$.

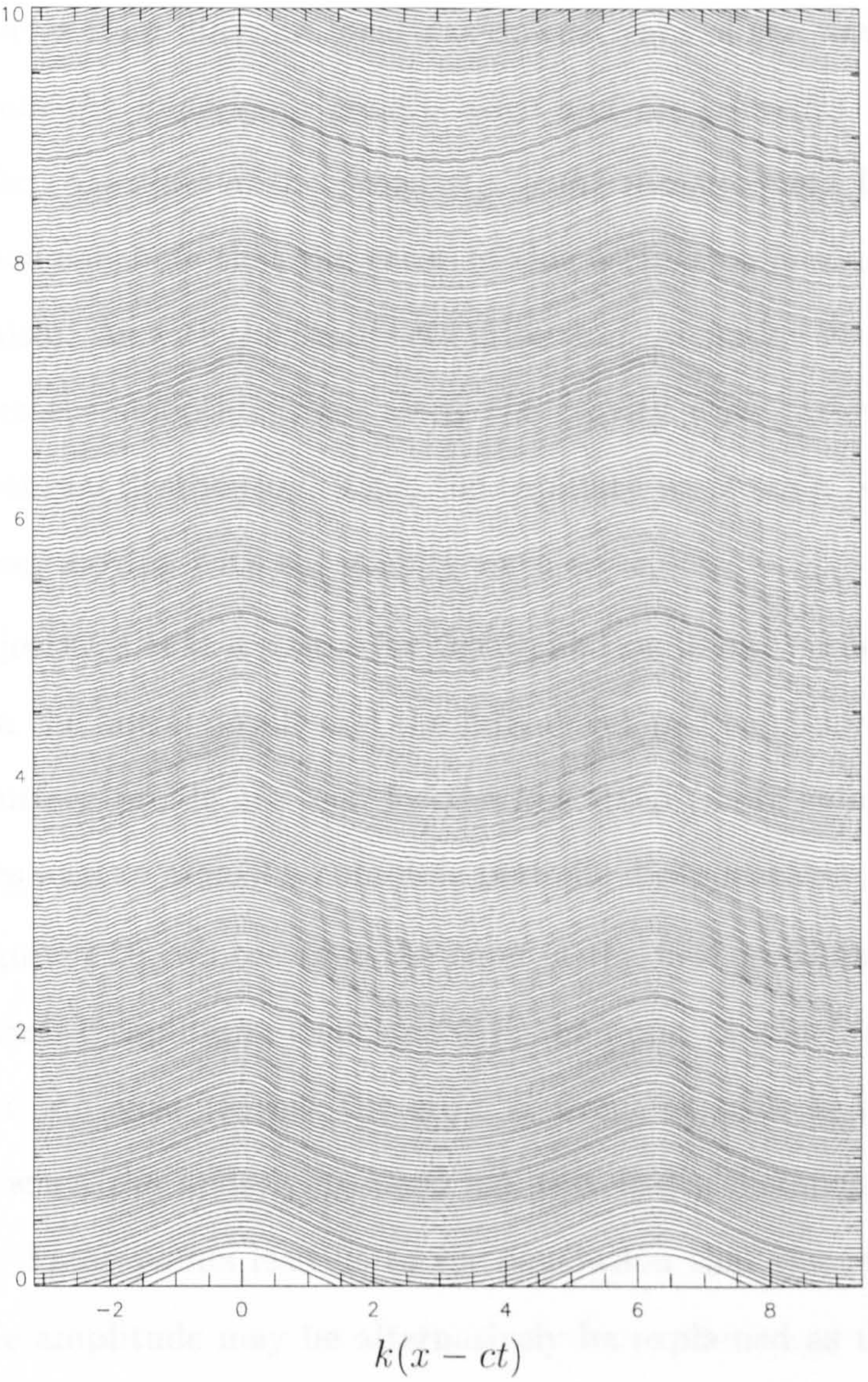

Figure 2.20: Development of surface from $ak = 0.227\,,\ \lambda = 6.82\,\text{cm}$ in frame of reference moving with gravity wave crest. (Wave propagation is in the $+x$ direction).

The total energy of the system remains constant as in previous runs. Although there was an oscillation between kinetic and potential energy in the calculations previously shown, the effect on the surface profile remained small, to the extent that surfaces had to be overplotted before such oscillations were apparent (at least for later times). With this shorter wave however, the modulation of the parasitic capillaries in both space and time is clearly visible, and is still apparent at later times.

This recurrence-like phenomenon is reported in the experiments of Perlin *et al.*. By comparing images from different locations downstream of the wave-maker they conclude that *"both the underlying gravity wave and the parasitic capillaries are temporally periodic regardless of the proximity of the measurement location to the wave-maker"*. They conclude that the cause of this oscillation is some (undefined) resonance mechanism. As with the results of Perlin *et al.* we notice that the capillary waves emerge from the smooth surface along the gravity wave rather than propagating to their eventual destination. Thus the capillary wave train is stationary in a coordinate system moving with the gravity wave crest.

It may be conjectured that a source for the oscillation in our model is the initial difference between the initial profile and the fully developed capillary gravity wave. Modulations in surface profile are seen for the less steep (more subcritical) waves and for such waves lead to almost a complete periodic disappearance of the ripples.

Looking at figure 2.20, we see that the time of the first maximum in the amplitude of the parasitic capillaries coincides with the point at which capillary wave development from one crest reaches the crest in front, as with figure 2.10. This occurs at a time when the underlying wave has travelled a distance of more than two wavelengths. These points lead us to the conclusion that the recurrence phenomenon in ripple amplitude may be alternatively be explained as the interaction of capillaries formed in front of one crest with those in front of the next.

Suppose then that a wave with a sharp crest is quickly formed, such as by a wave-maker. Parasitic ripples will develop in front of the crest due to the pressure disturbance from the action of surface tension at the region of high curvature. The energy is propagated from the crest at a velocity of slightly less than $c/2$ in a frame of reference moving with the crest. Capillary development will then reach the next crest in front after the underlying wave has travelled a distance of slightly more than two wavelengths. The ripples modify the curvature and in turn affect the parasitic capillaries generated at that crest. This process is then repeated at

equal time intervals as the energy associated with the initial disturbance propagates over the wave profile. After a sufficiently long period this energy would be dispersed over a wider region, thus the magnitude of the oscillation in the parasitic capillaries reduced to an extent, as observed. Since for subcritical waves the capillary waves can exist at all points on the surface, the continuation of the amplitude modulation is likely to be due to a resonant self interaction as descibed earlier. On supercritical waves the short capillary wavetrains on each Stokes wave are blocked from eachother, so the possibility of resonant interaction is reduced.

In the numerical experiments carried out here the initial wave is unlikely to be identical to that produced at the wave-maker. However, both start with a wave profile different to the final steady wave and show that form an initial non-steady profile a quasi-steady profile is eventually formed.

Perlin *et al.* choose an arbitrary image from their data set to compare to the predictions made by theories from Longuet-Higgins (1963), Crapper (1970) and Schwartz & Vanden-Broeck (1979). The theory presented by Crapper (1970) is similar to that of Longuet-Higgins (1963) in calculating the parasitic capillary waves as perturbations to an underlying Stokes wave profile. Crapper (1970) uses the exact pure capillary wave solution of Crapper (1957) (see chapter 1) at first order however, and a nonlinear ordinary differential equation for capillary wavelength and amplitude is derived from energy considerations. Schwartz & Vanden-Broeck (1979) calculate symmetric waves of permanent form for an inviscid, irrotational, incompressible flow. This method is not limited to perturbations from a Stokes wave profile. It permits a steady wave formed by a train of capillary waves travelling against the non-uniform surface velocity of an underlying longer wave, and it is found that a number of possible such solutions can exist for the chosen parameters of nondimensional surface tension wave speed and wave steepness.

The image is from a time series in which the surface profile is quasi-stationary and nearly symmetric. Thus, according to Perlin *et al.*, *"comparison between theory and*

experiment should be favourable". The comparison of the measured 5.26Hz profile with these theories is reproduced from Perlin *et al.* in figure 2.21, and further with the improved theory of Longuet-Higgins (1995) in figure 2.22.

The Longuet-Higgins (1963) theory severely underpredicts the amplitude of the capillary waves for an underlying wave of the correct amplitude (2.21 (b), bold line). The second line on 2.21(b) shows the surface profile from the theory of Longuet-Higgins (1963) that gives the same capillary wave amplitude as observed in the experiment. It can be seen that according to this theory a much steeper gravity wave is required to produce parasitic capillaries of the observed amplitude. The improved (1995) theory (fig.2.22) does much better, although there is still an underprediction. A possible explanation for this is given in Longuet-Higgins (1995). Perlin *et al.* reported that the amplitude of the parasitic capillaries decayed with distance from the plunger such that for the 5.26Hz wave they were 'almost non-existant by 2.5 wavelengths downstream'.

One reason for this is energy dissipation through viscosity. Longuet-Higgins also points out that wave-makers itself might generate freely propagating capillary waves. In this case the capillaries that are generated purely by the progressive wave cannot be isolated. These transient effects mean that larger amplitude capillaries should be expected soon after the generation of the underlying wave. By the time the wave has settled down to an almost steadily propagating profile the parasitic capillaries would be smaller. At a greater distance from the wave-maker the surface would still be very slowly varying due to energy loss by viscosity. The theories against which the experiments of Perlin *et al.* are compared all assume energy conservation, thus would only be expected to accurately model the experimental results further down stream. This said, the theory of Longuet-Higgins (1963) only produces a wave with comparable amplitude parasitic capillaries for a underlying wave with an amplitude half as large again (2.21 (b), thin line). The theory of Crapper (1970) predicts the correct amplitude waves on the forward face of the wave, but overpredicts amplitude on the leeward face. The three possible solutions from the Schwartz

& Vanden-Broeck scheme either completely underpredict capillary wave amplitudes, or overpredict them in the trough and on the leeward face. All these solutions are symmetric.

Figure 2.23 shows the development of the surface profile calculated by our numerical code after 2 (bottom) and 20 (top) wave periods. At 2 wave periods the surface is still developing. By 20 wave periods the oscillations in capillary wave amplitude and length have reduced, but are still visible. It can immediately be seen that the profile after 2 wave periods is close match to the experimental data. However the eventual steady surface has small capillaries over the entire surface, although their amplitude remains greatest on the forward face of the wave. The steady profile predicted is a close match to that predicted by the improved method of Longuet-Higgins. It is also noticeably more symmetric than the calculations with steeper, slightly longer waves shown previously.

Perlin *et al.* also present experiments for a steep wave generated at 4.21Hz. Figure 2.24 reproduced from that paper again compares a 'characteristic' wave with the steady theories of Longuet-Higgins (1963), Crapper (1970) and Schwartz & Vanden-Broeck (1979). However as with the 5.26Hz wave, the capillary amplitude is reducing quickly with time (as can be seen from figures 10 and 12 from that paper). The authors of the paper note that by 2 to 2.5 wavelengths downstream the surface on the forward face of the underlying wave is nearly smooth.

This quick decay is most likely due to the effects explained in Longuet-Higgins (1995) as noted above. Again it is unlikely therefore that the steady theories would predict comparable parasitic capillary amplitudes. Figure 2.25 shows the wave profile predicted by the improved theory of Longuet-Higgins (1995), and figure 2.26 the profile and surface slope predicted by our time-stepping model. Both profiles show no discernible parasitic capillaries, although some can be clearly seen in the plot of surface slope.

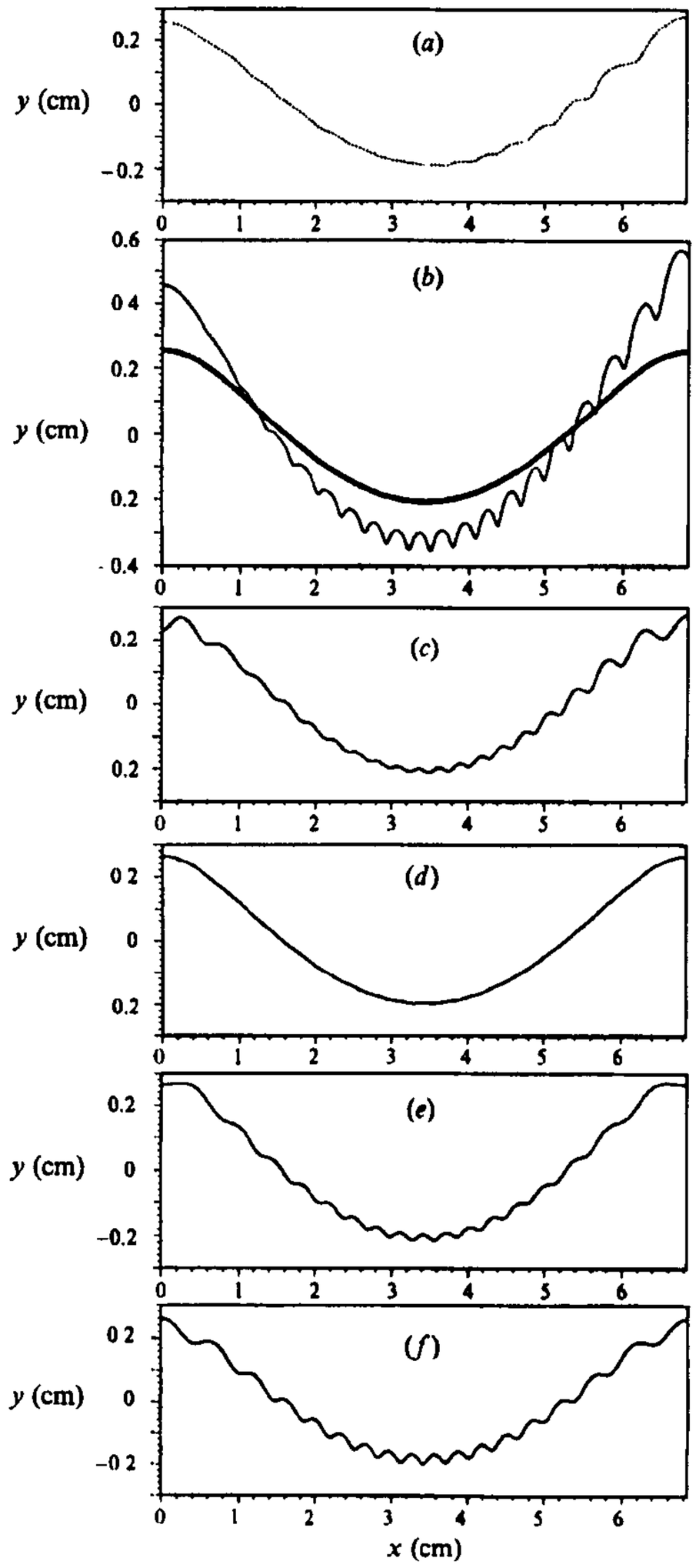

Figure 2.21: Comparison of (a) the measured 5.26Hz profile (chosen representative image) with (b) the theory of Longuet-Higgins (1963). The bold line is a wave of the correct steepness and the second line is the wave which gives the same predicted capillary amplitude as observed. (c) is the theory of Crapper (1970) and (d), (e) and (f) three possible numerical solutions determined using the Schwartz and Vanden-Broeck scheme (1979) *Perlin et al. (1993).*

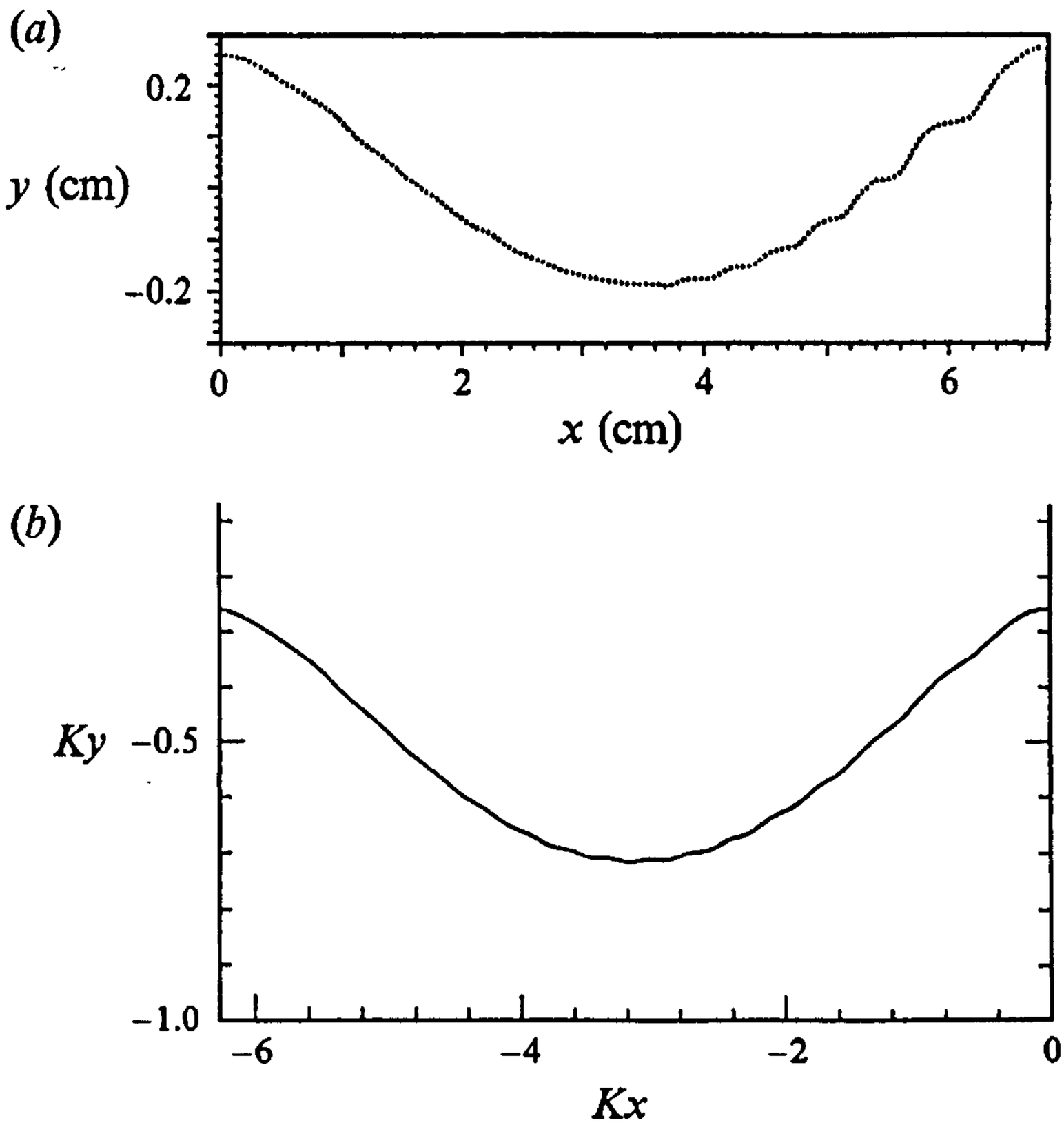

Figure 2.22: (a) The profile of a wave at 5.26Hz as recorded by Perlin *et al.* (1993). (b) The profile calculated by Longuet-Higgins (1995) for $ak = 0.227$, $\lambda = 6.82\,\mathrm{cm}$. *Perlin et al. (1993)*

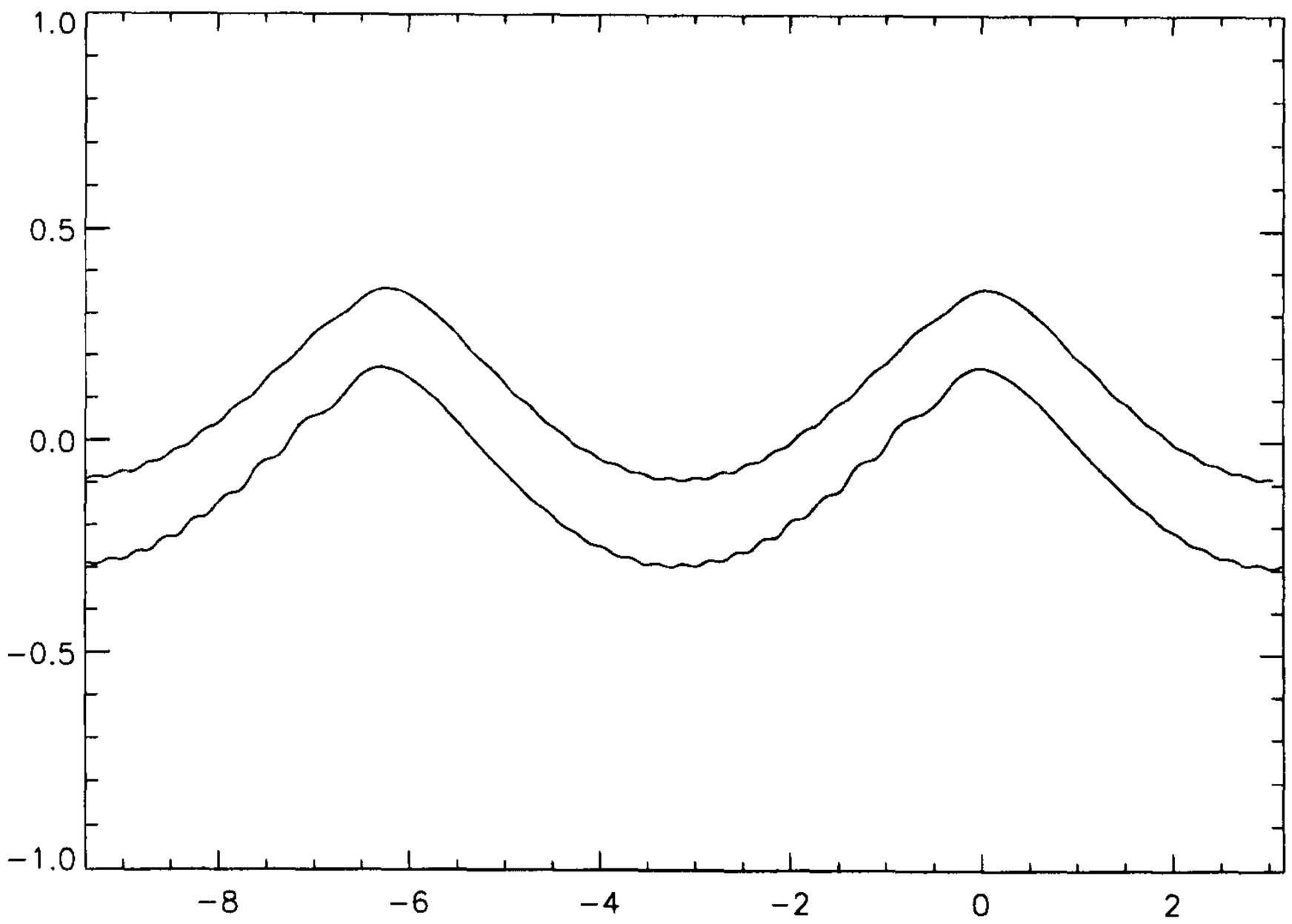

Figure 2.23: ky against kx. Numerical calculation of surface profile after 2 and 20 wave periods. $ak = 0.227$, $\lambda = 6.82\,\mathrm{cm}$. (Wave propagation is in the $-x$ direction).

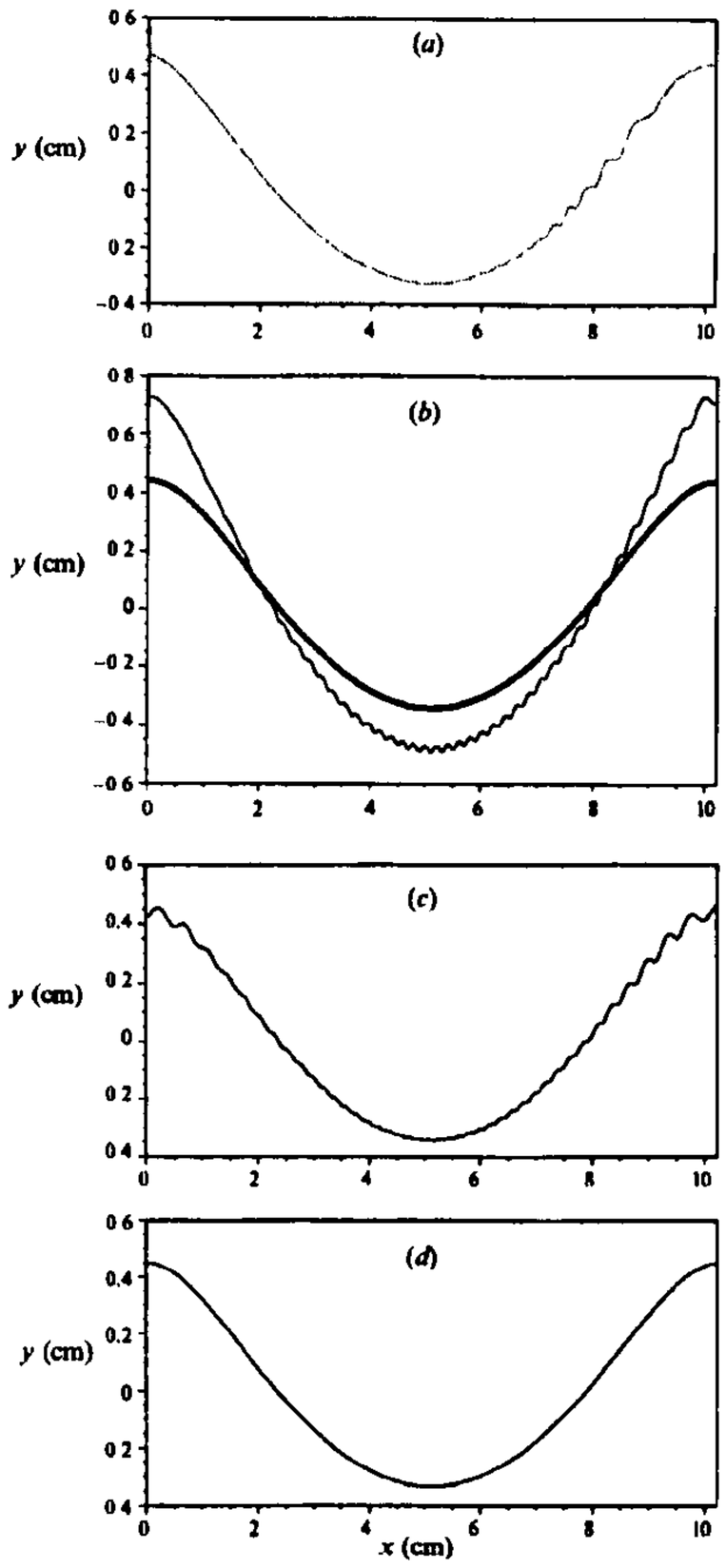

Figure 2.24: Comparison of (a) the measured 4.21Hz profile (chosen representative image) with (b) the theory of Longuet-Higgins (1963). The bold line is a wave of the correct steepness and the second line is the wave which gives the same predicted capillary amplitude as observed. (c) is the theory of Crapper (1970) and (d) numerical solution determined using the Schwartz and Vanden-Broeck scheme (1979). *Perlin et al. (1993)*

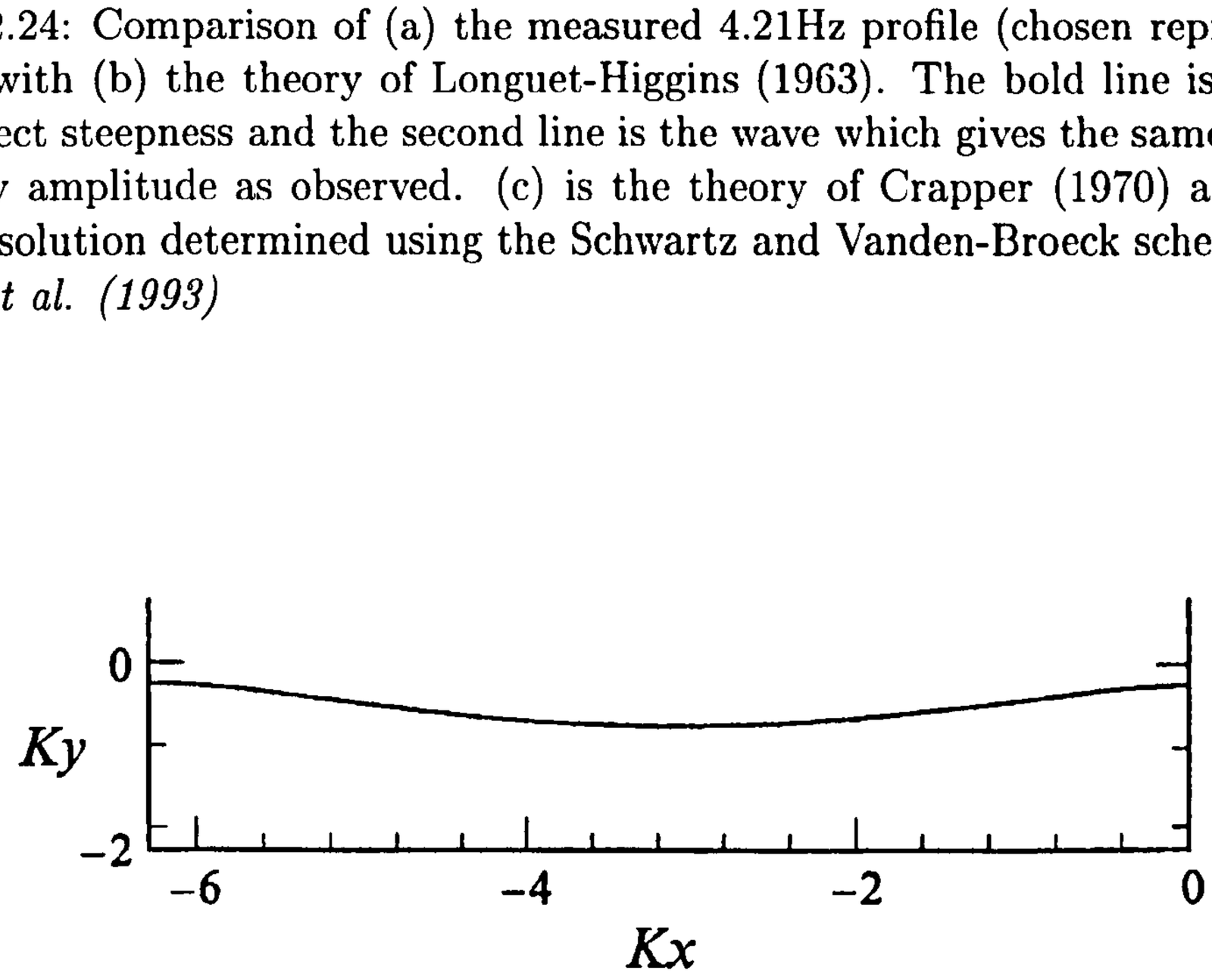

Figure 2.25: Wave calculated by Longuet-Higgins (1995) for $ak = 0.25$, $\lambda = 10.2\,\mathrm{cm}$. *Longuet-Higgins (1995)*

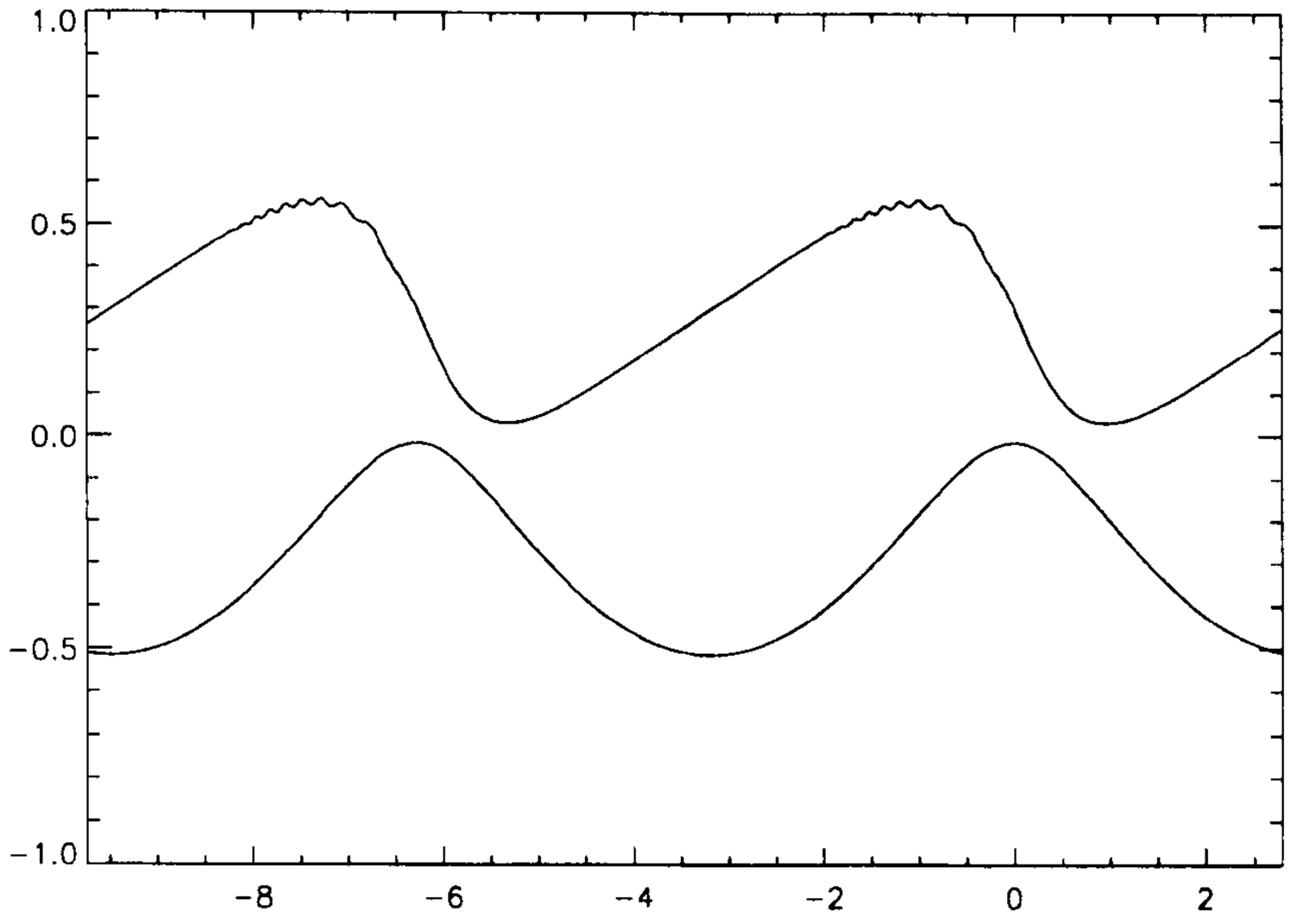

Figure 2.26: dy/dx (top) and ky (bottom) against kx from our numerical code for $ak = 0.25$, $\lambda = 10.2\,\mathrm{cm}$. Plots have been shifted (but not scaled) to fit on same graph. Direction of propagation is right to left.

Both our method and those of Longuet-Higgins underpredict the capillary wave amplitude in comparison to the experimental results. The Crapper (1970) solution has considerably shorter capillaries as well as larger capillaries on the leeward face of the underlying wave. From the plot of surface slope we see that our method also predicts shorter capillary waves. The symmetric Schwartz & Vanden-Broeck (1979) solution shows no noticeable ripples and closely matches that of Longuet-Higgins and our own calculations.

2.5 Very steep gravity waves

Longuet-Higgins & Cleaver (1994) show that, considered in isolation, the crest of a steep, irrotational gravity wave is unstable. The instability is presented as a limiting form of the instability previously found (Tanaka 1983 , Longuet-Higgins 1986) for steepnesses around $ak = 0.4292$ corresponding to the lowest energy maximum. This instability has the effect of shifting a volume of water near the crest towards the forward face. The resulting bulge of water has a region of sharp positive curvature

at its 'toe' for a sufficiently large initial perturbation. In such cases, it is argued that this could then be that this region of positive curvature is the disturbance causing the capillary waves.

Some experimental evidence for this has come from Duncan, Philomin, Behres & Kimmel (1994). They present high speed photographs of mechanically generated gently spilling breaking waves. Formation of a bulge on the forward face of the waves is reported as they steepen. At the toe of the bulge is a region of sharp concave curvature simultaneously develops. Capillary waves are seen to form ahead of this. This feature does not last long however and the bulge rapidly moves down the forward face of the gravity wave, eventually becoming turbulent.

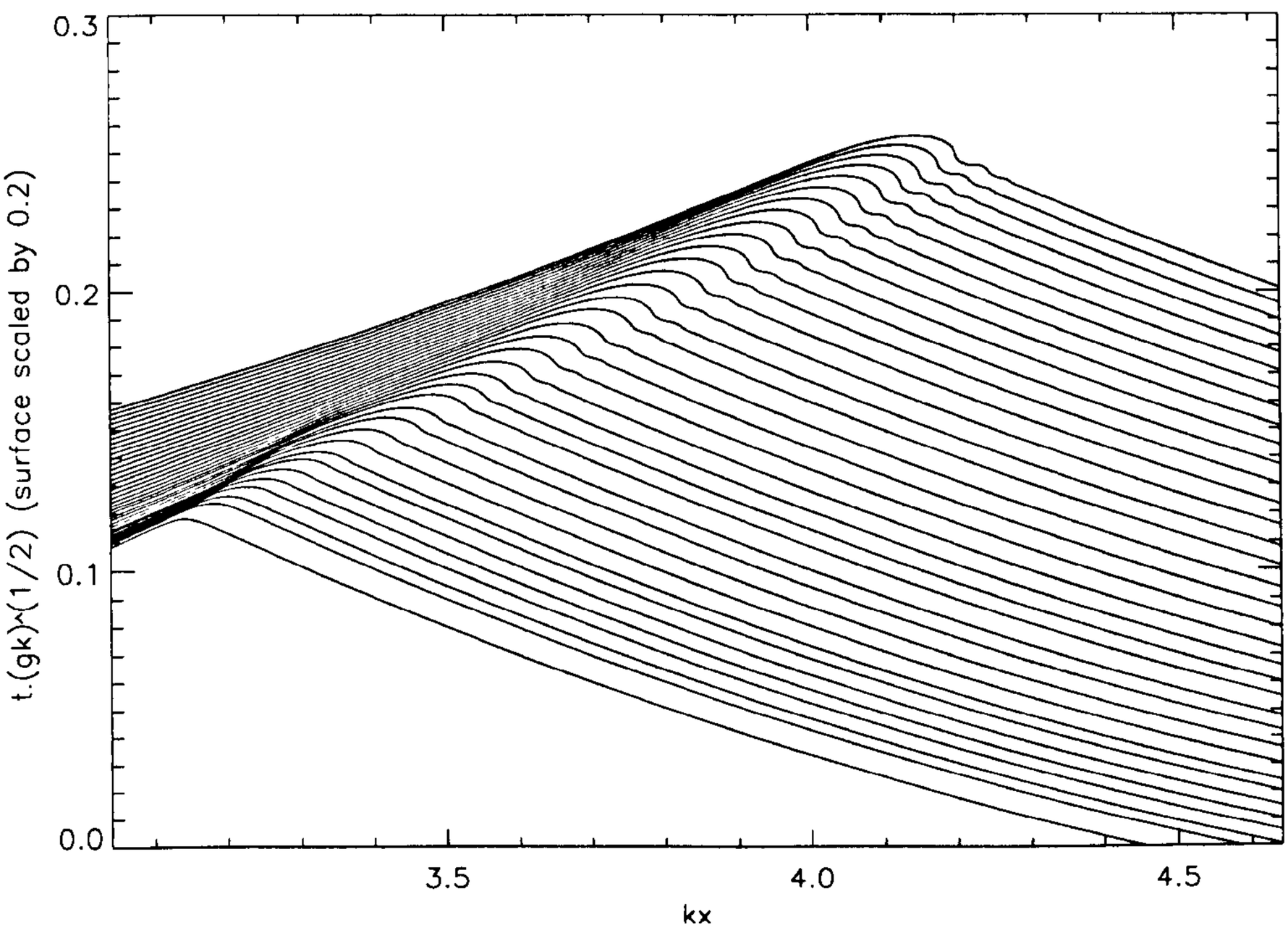

Figure 2.27: Wave evolution until breaking for $ak = 0.44$, $\lambda = 50$cm.

Figure 2.27 shows the results of a numerical calculation until breakdown for a wave of length 50cm and steepness $ak = 0.44$. The initial profile is that of a pure gravity Stokes wave. We also see a shift of a volume of water at the crest towards

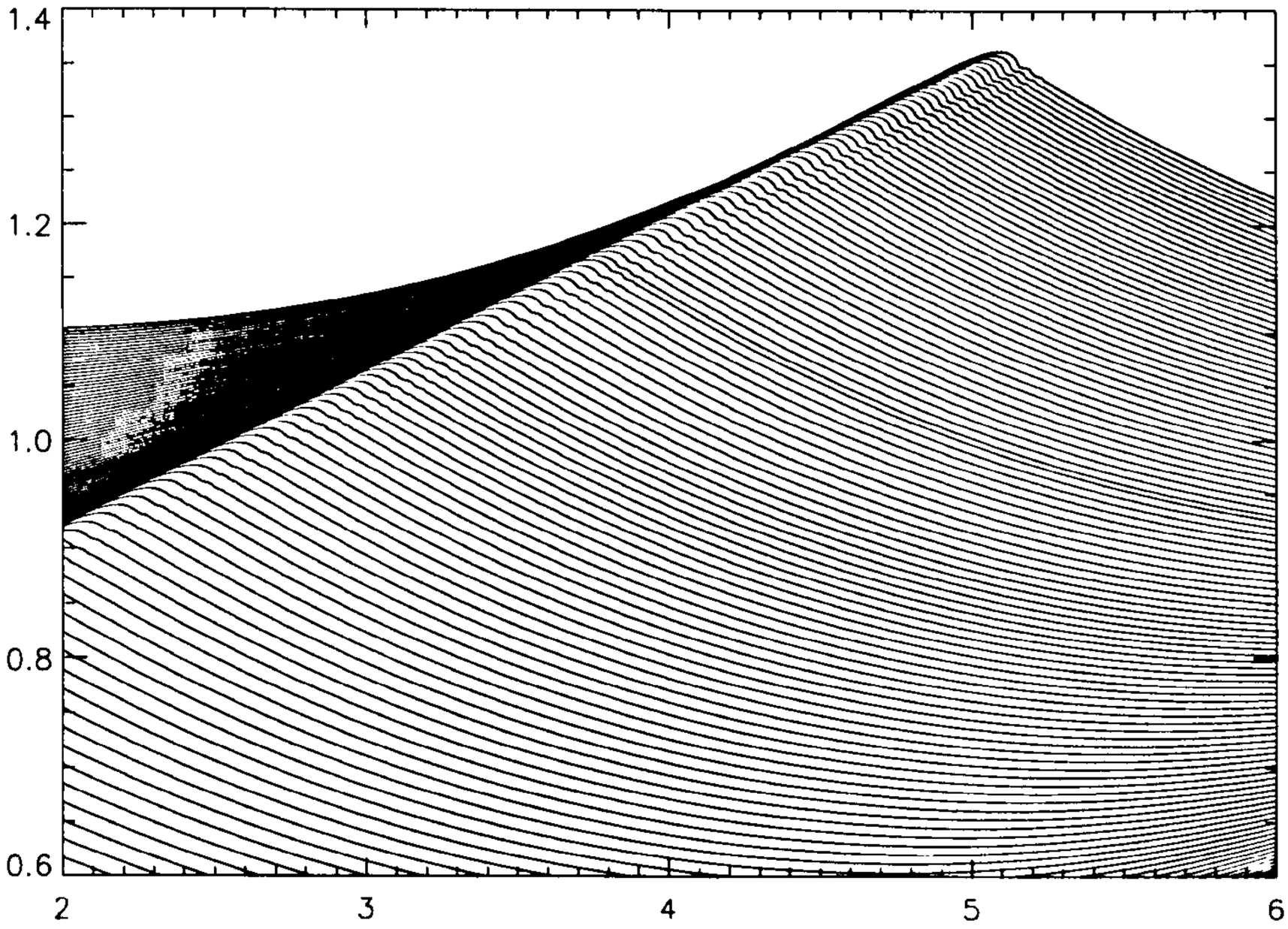

Figure 2.28: Wave evolution until breaking for $ak = 0.42$, $\lambda = 50$cm.

the forward face. However, from similar calculations with other less steep waves, (for example $ak = 0.42$ in figure 2.28) this appears to be no more than the extension of the mechanism previously described. The crest instability only occurs above a certain wave steepness, about $ak = 0.4292$. We might expect to find a corresponding difference in the behaviour of calculated crest evolution for steepnesses above and below this instability limit. Instead the same behaviour occurs to a correspondingly lesser extent for waves of lower steepness, with no sudden change as steepness is increased.

The crest of the initial Stokes wave becomes much sharper with increasing steepness. The corresponding breadth of the initial pressure distribution caused by the action of surface tension is thus considerably narrower than in calculations previously shown. The result is the large surface displacement just in front of this in accordance with the theory presented in Lamb (1932, §271). In such calculations the displacement begins to break and computation cannot be continued. Since this behaviour occurs for waves less steep than the threshold of the instability described

by Longuet-Higgins & Cleaver (1994), we conclude that in the calculations presented here it arises from the action of surface tension at the sharp crest. It is likely that such a feature would also be seen with the development of jets in breaking waves under the influence of surface tension and give better comparisons with the experimental work of Duncan *et al* (1994).

2.6 Short capillary-gravity waves

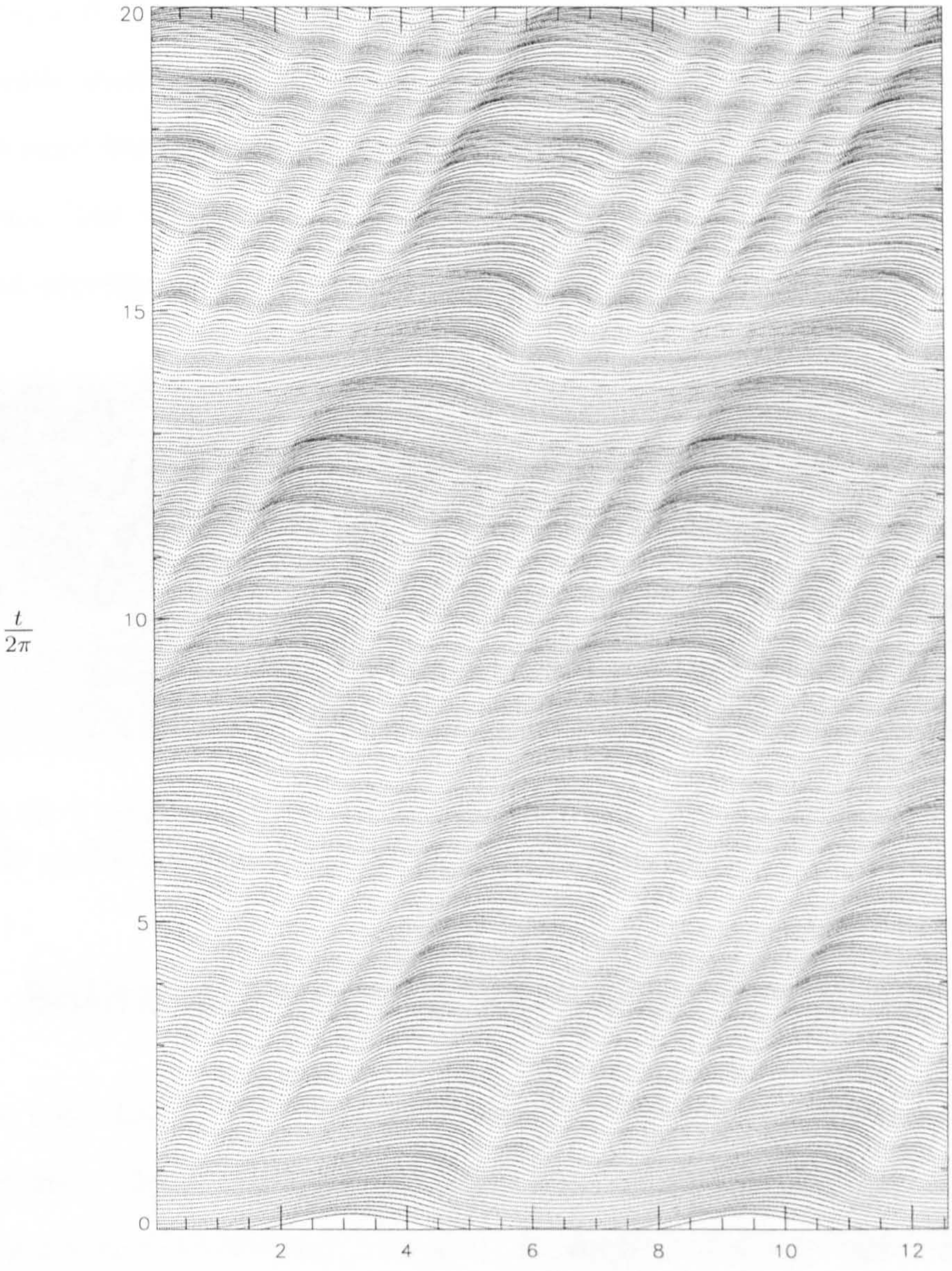

Figure 2.29: Wave evolution for initial Stokes wave $ak = 0.24$, $\lambda = 4\,\text{cm}$ in a reference frame moving with the phase speed of the initial Stokes pure gravity wave. (Propagation is in the $+x$ direction).

Some calculations were also performed using considerably shorter wavelengths. Figure 2.29 shows the surface evolution starting from an initial Stokes wave profile of $ak = 0.24$, $\lambda = 4\text{cm}$. A current equal to that phase speed of the pure gravity Stokes wave has been imposed to attempt to bring the waves to rest. It can thus

be immediately seen that these capillary-gravity waves travel faster. Unlike the corresponding 8 centimetre length waves presented earlier, we see that capillary waves soon form and dominate the flow. Strong modulations persist so that no steady or quasi-steady wave profile is formed. This is not of course to say that such a profile does not exist for this wavelength, merely that it does not arise from these starting conditions. The appearance of these waves is similar to the wind generated waves produced experimentally by Schooley (1958), reproduced in figure 2.30.

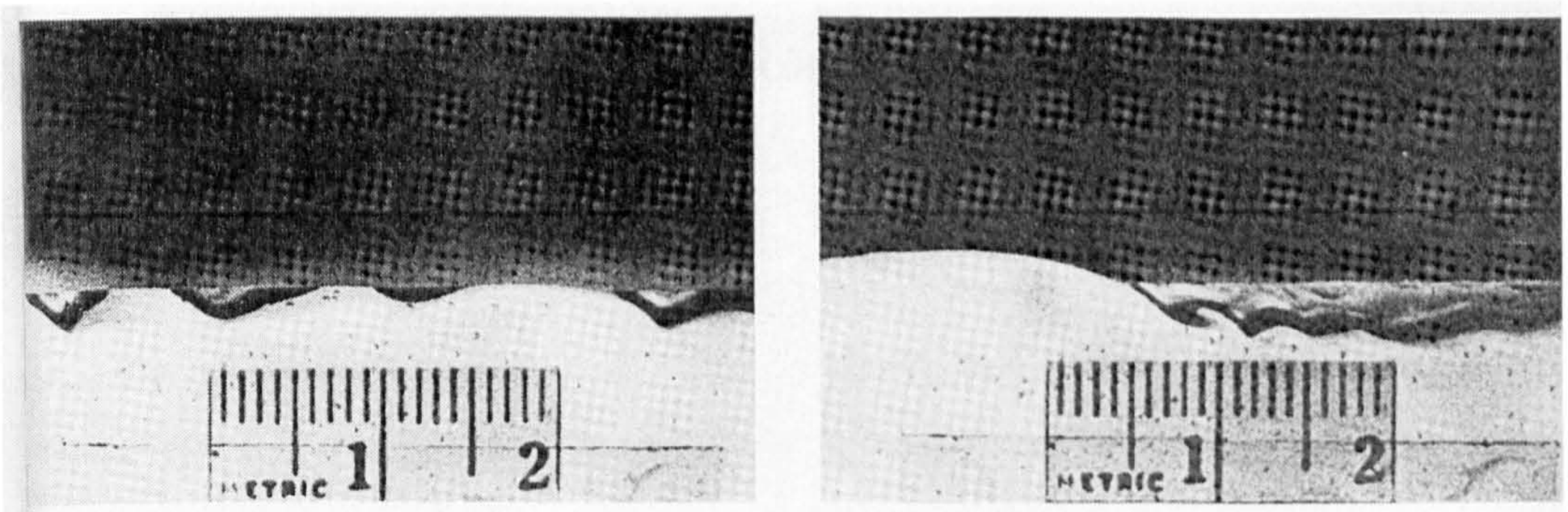

Figure 2.30: Capillary gravity waves generated by a 12 and 16 knot wind respectively. The scale in the photograph is 2cm long. Schooley (1958).

2.7 Solitary-type capillary-gravity waves

Chapter 1 mentioned the existence of capillary-gravity solitary waves on both infinite and finite depth. The investigation of gravity-capillary waves has received less attention due to the intractable nature of the analytic problem. Using the numerical code described above we are able to compute the unsteady surface profiles starting from pure gravity solitary waves and adding surface tension. For sufficiently steep solitary waves the pressure disturbance at the sharp crest will be such as to cause the development of ripple on the forward face of the wave in manner similar to that caused by a pressure disturbance on a steady stream given in Lamb (1932) §271.

Calculations similar to those with Stokes waves, as above, have been carried out in a non-periodic domain with the initial profile is being a solitary wave, calculated by Tanaka's method (1986). This is the profile for a pure gravity wave, so in running

the program it is as if surface tension were suddenly added at $t = 0$. The result is that again there is a period of time over which parasitic capillaries develop on the forward face of the wave. We now also see a train of small amplitude capillaries shed by the wave at $t = 0$ which continue to travel in the opposite direction to that of the main wave. These may also be occurring for the calculations started with periodic waves giving the energy fluctuations noted earlier. An example of the development of the profile of the main wave is given in figure 2.31. The profile is shown from a frame of reference moving with the wave speed, which in this case is in the $-x$-direction, and the conditions correspond to that for water of 1cm depth.

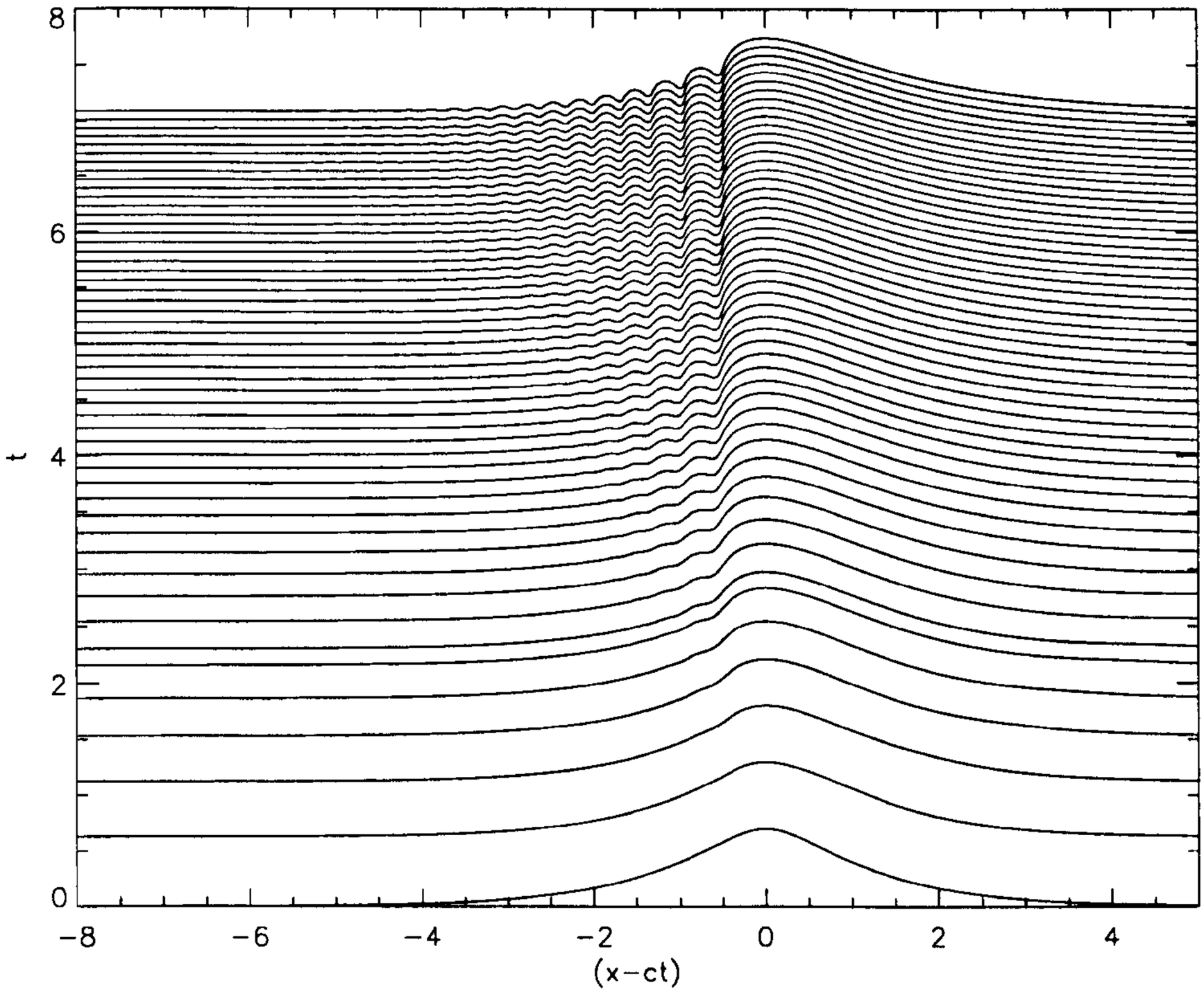

Figure 2.31: Development of a capillary-gravity wave travelling in the $-x$ direction. Depth, $d = 1$cm. The initial surface profile is that of a pure gravity wave of $a/d = 0.7$.

As with the periodic waves, we see that initially the crest steepens. A small bulge begins to appear in front of this. As this bulge and the crest behind it continue to steepen a second bulge develops in front of the first. This process continues with each new capillary forming forward of the last. Thus the train of parasitic capillaries is slowly built up, appearing to emerge from the smooth surface of the underlying wave as reported in the periodic wave experiments of Perlin *et al.* earlier.

The speed of the spread of the capillaries against the non-uniform velocity field of the underlying wave is given by the local group velocity, c_g, i.e. the rate at which the wave energy is propagated. For capillary waves we have that $c_g \simeq 3c/2$, so that the energy propagates faster than the capillary waves themselves.

For the case of the wave on a depth of one centimetre we find the main wave crest moves at a speed of 44.8 cm/s. Far ahead of the crest the ripples that are

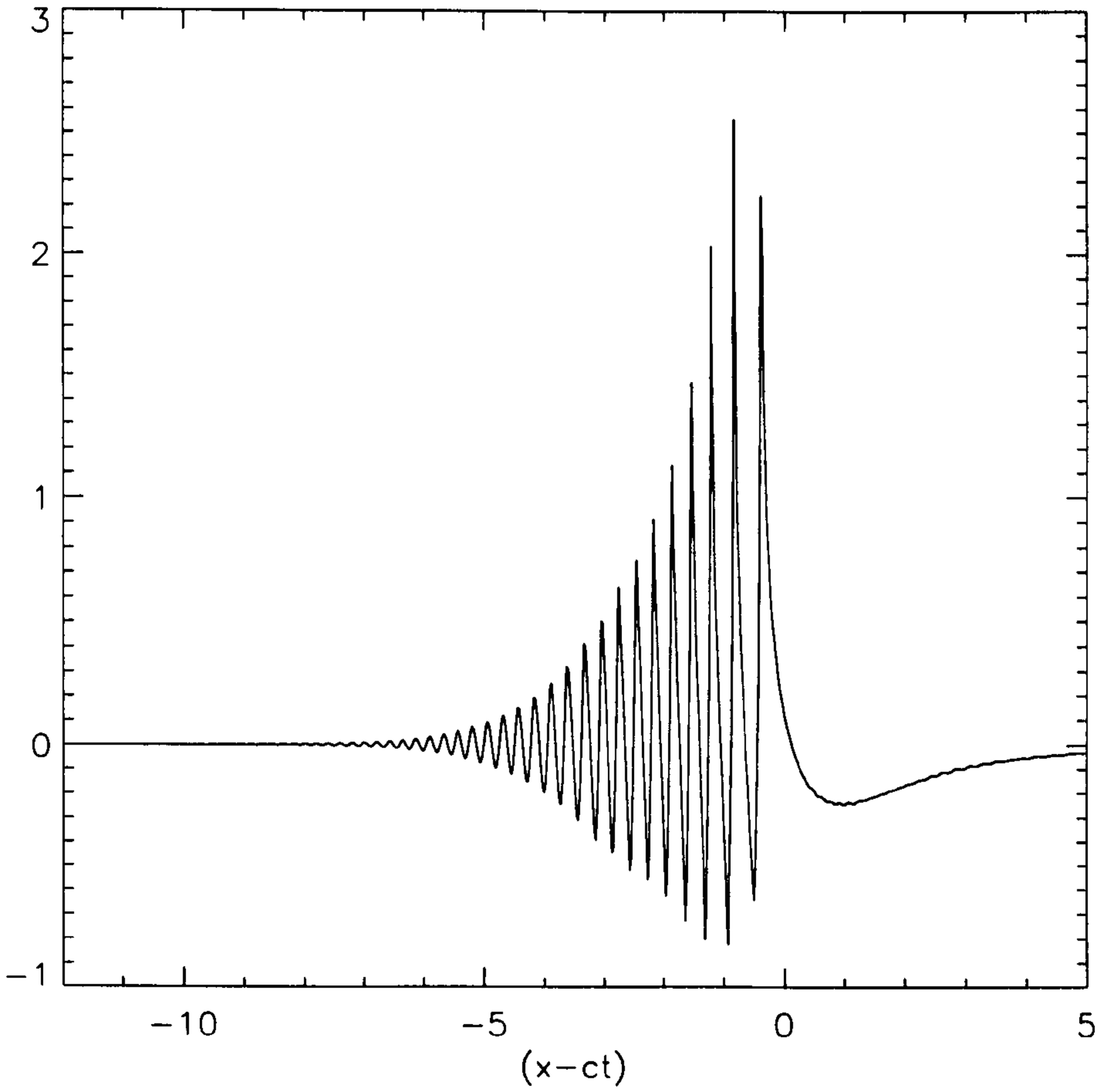

Figure 2.32: Surface gradient of capillary-gravity wave at $t=8$ for $d=1$cm, initial $a/d=0.7$.

stationary in frame moving with it are than also moving at this speed. If we assume that sufficiently far in front of the crest they are moving across an initially flat, undisturbed surface then their speed is also 44.8 cm/s. Using (1.4), this gives us a capillary wavelength of $2\pi/26.6 = 2.4\,\text{mm}$. Looking at the plot of surface slope in figure 2.33 we calculate a wavelength of 2.2mm at a horizontal distance 15cm in front of the wave crest and 2.6mm at a distance 10cm in front. Then to a rough estimate it appears that we within 10% of the correct phase speed even for these small wavelength ripples.

For solitary waves of the same a/d on deeper water, the parasitic capillaries are less prominent, or completely absent. It has previously been proposed that the

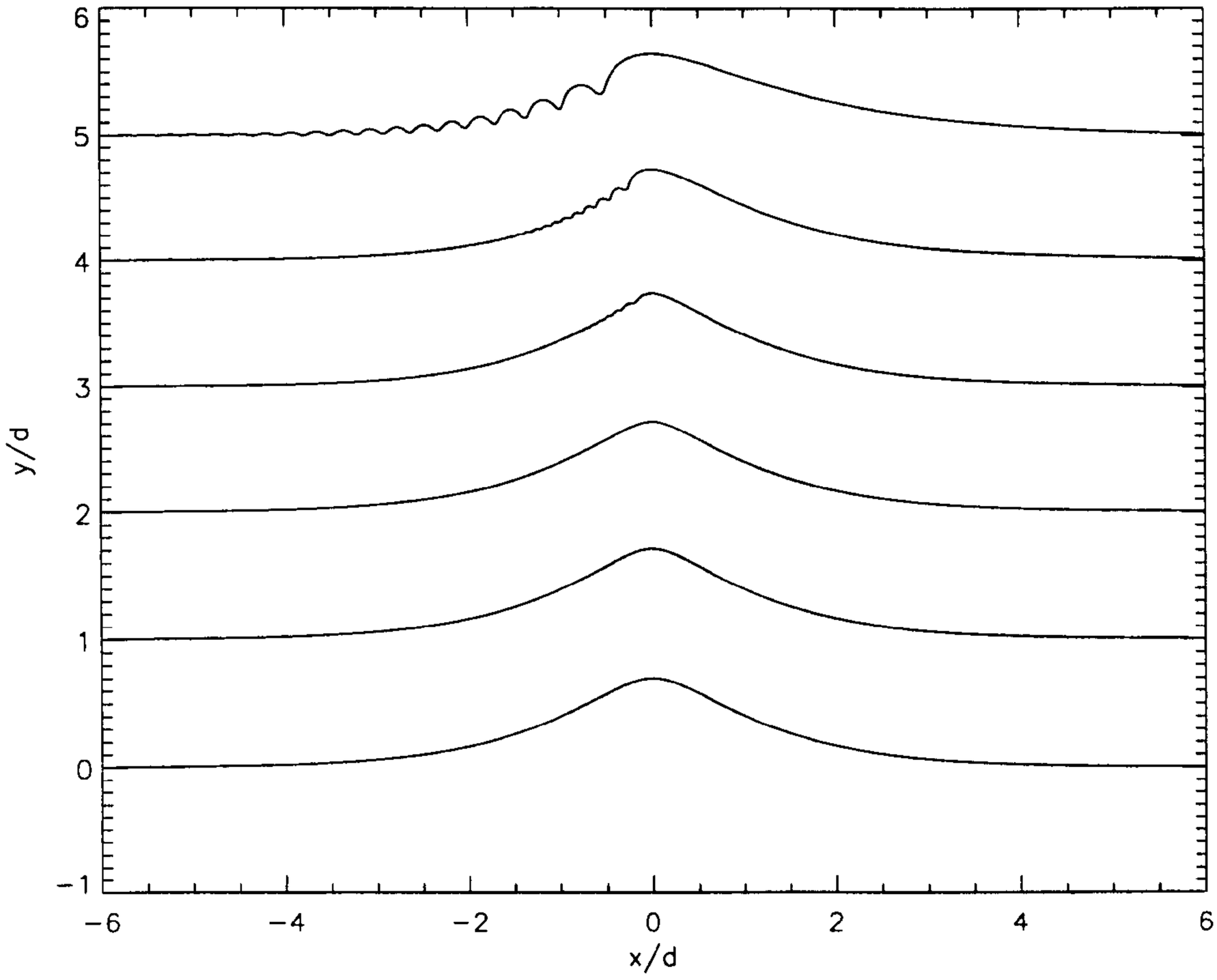

Figure 2.33: Surface profiles of capillary gravity waves for $d = 1$cm (top), 2cm, 3cm, 4cm, 5cm and no surface tension (bottom). a/d=0.7

source for the parasitic capillaries is the pressure caused by the effect of surface tension at the high curvature at the crest. With the solitary waves on a larger scale, the curvature at the crest is less and the corresponding breadth of the resultant pressure source greater. The result is that capillaries are not produced and the solitary wave propagates almost unchanged from its non-dimensional pure gravity profile. We thus have that solitary waves with sufficiently small a/d propagate unchanged even at scales down to depths of several centimetres. This is to be expected from the analytic work with pressure distributions on steady streams presented in Lamb (§271).

However, we can find a solitary wave sufficiently near the limiting a/d ratio such that the crest region is sharp enough to produce an initial pressure distribution of

breadth smaller than the capillary wavelength. Parasitic capillaries will always form ahead of this region in such cases.

2.7.1 Blocking on solitary waves

The 'blocking' of capillary waves by short steep non-breaking gravity waves was first suggested by Philips (1981), and treated in depth in Shyu & Philips (1990). Capillary wave blocking is an important feature of periodic gravity-capillary waves since the ripples in one wave trough are isolated from those in the next. With a solitary wave 'blocking' has no such significance, since one crest travels in isolation.

2.8 Conclusion, discussion and further work

Surface tension as been added to a fully non-linear potential flow solver. This has been used to compute surface profiles for gravity capillary waves. It is found that the surface point distribution must be regridded to resolve the sharp wave troughs of the small capillary waves. In accordance with previous experimental and analytic work we find that ripples form on the forward face of steep propagating Stokes waves. Lower frequency steep gravity waves generate capillaries with higher wave numbers. In general the predicted profiles are found to be in agreement with previous experimental work. For subcritical steepnesses, these profiles are also found to be in broad agreement with those predicted by the linear perturbation theory of Longuet-Higgins (1995). This theory is based on the idea that the capillary waves are a result of the action of surface tension at the sharp gravity wave crest causing a pressure disturbance. In accordance with the theory of Longuet-Higgins (1995) we find 'blocked' regions on waves above a critical steepness. In this region we do find some detectable oscillation in surface slope, especially towards the leeward face, but a level considerably lower than that just outside. The 'blocked' region is calculated considering the linear minimum phase velocity, so nonlinear waves with lower minimum phase velocities could exist within the limits of this region.

The limits of the 'blocked' region calculated from the possible capillary wave speed along the surface coincide with points were capillary wave amplitude is seen to be reduced. We also note that there is a small jump in the calculated Stoke's drift velocity between sub- and supercritical waves.

We find, in accordance with Longuet-Higgins (1995), that a critical steepness exists corresponding to the formation of a blocked region. At this steepness the amplitude of the parasitic capillary waves in the underlying wave trough is a maximum. Above this we find capillary amplitudes in the trough decrease but the amplitude at the crest remains approximately the same. It appears that the disturbance begins to become more localised around the Stokes wave crest. A comparison of point distributions was made to ensure this was not a numerical feature.

Longuet-Higgins considers the parasitic capillaries to be linear and have no effect on the underlying flow. The equations used to calculate the linear capillary wave perturbation have a singularity at the caustics that limit the blocked region, so the capillary wave perturbation is only calculated away from this. This the likely reason why our nonlinear method gives a single large bulge at the crest rather the two smaller waves at and just in front of the crest as calculated by Longuet-Higgins (1995) for just supercritical waves. It may also be the cause of the difference in the decay of capillary wave amplitudes above the critical wave steepness given by our numerical code and Longuet-Higgins.

Apart from the non-linearity of the ripples themselves and their effect on the underlying gravity wave, there is another possible reason for differences between profiles computed here and those by Longuet-Higgins (1995). The linear theory presented by Lamb (1932) (§271) also gives long gravity waves behind downstream of the pressure disturbance. Although these are the same amplitude as the ripples on the forward face, the length of the gravity wave means that it has a much less noticeable affect on the surface slope, so is hard to detect experimentally. This long wave is neglected in the theory presented by Longuet-Higgins (1995).

Perlin *et al* (1993) calls for numerical calculations in order to test whether the asymmetry seen in experiments is a viscous or inviscid phenomenon. As with Longuet-Higgins (1995) we find asymmetric profiles that closely match those found experimentally. In addition our numerical results also exhibit the same temporal behaviour as those found in the wave-maker produced waves of Perlin *et al.* In attempting to calculate steadily propagating gravity-capillary waves we find modulations in the parasitic capillary amplitudes and also in the proportions of kinetic, superficial and potential energy. The solution never settles to a completely steady profile over the time periods calculated. The location of the capillary waves is quasi-stationary in a coordinate system moving with the underlying wave. Energy oscillations persist in all cases,although changes in the surface profile become small for supercritical waves. Modulations in parasitic capillary amplitude are reported in the experiments of Perlin *et al* (1993). In the same paper the authors call for numerical time-marching calculations to see whether the 'resonance' seen in experiments can be predicted. Here then we predict such modulations although their source is not clear. The modulations can be most clearly seen on subcritical waves. The first maximum of the capillaries coincides with the moment that the system of ripples from one crest reaches the next. From then on the period of the oscillations in capillary amplitude continue at this frequency - i.e. at a period given by the time taken for a particle travelling with the capillary group velocity to travel from one crest to the next. This suggests that the disappearance and re-emergence of the ripples is due to an interaction of capillary waves from different crests starting from a profile slightly different to the final steadily propagating state. A contributing factor could be a resonant self interaction in the wavetrain, as decribed in section 2.1.5.

It was not possible to compute quasi-steady surface profiles starting with very steep Stokes waves. For such waves the rate of change of curvature in front of the crest became too great to continue accurate computation. All calculations in the first part of the chapter were started with a Stokes wave profile. It is possible that other

solutions exist for the same wave steepness and length. A different profile would have a different initial pressure distribution over the surface and hence possibly lead to a different eventual quasi-steady profile. Other numerical methods that specifically look for steady waves, notably Schwartz & Vanden-Broeck (1979), have found a multiplicity of solutions for the same dimensionless surface tension and steepness parameters.

We note that for less steep waves, still within the range of validity of the analysis of Longuet-Higgins (1995), the profile is more symmetric. Some further calculations have been performed with short gravity waves, with wavelength less than the region of validity of the theory of Longuet-Higgins (1995), and with solitary waves. We note that starting with initial Stokes wave profiles quasi-steady solutions were not found for such waves. Instead modulations persisted. This is not to say that steady solutions do not exist at such wavelengths, merely that they are not found from similar starting conditions to those used to generate the gravity-capillary wave profiles above. The profiles calculated compare qualitatively to those produced by a wind stress in the experiments of Schooley (1958).

Other calculations were performed with solitary waves. It is shown that the profiles of such waves are well approximated by the normal pure gravity solitary wave profile for depths greater than 5 centimetres or so, depending on the non-dimensional amplitude a/d. Parasitic ripples are always formed if the pressure disturbance at the crest is sufficiently narrow. This is in accordance with the theory of a pressure disturbance on a steady stream presented in Lamb (1932).

Further work might include looking at the affects of surface tension in wave breaking at very small scales. Some recent work has been done modelling free surface flows as a line vortex approaches the surface from below (Barnes, Brocchini, Peregrine & Stansby 1996). This gives rise to surface 'scars', features that are often seen at the edges of an area of vorticity on free surfaces. These features are at a scale within the gravity-capillary regime, but studies so far have neglected surface tension.

The formation of jets under the influence of surface tension is also of interest and may provide a better insight into the experimental results of Duncan *et al.* (1994).

Chapter 3

Waves Near Vertical Walls

3.1 Introduction

Scouring and the transport of suspended particles are of interest to the coastal engineer because they affect the distribution of sediments and shore line evolution. Changes in the bed profile near the shoreline can also have consequences for navigation. Particle transport is also important to pollutant disposal in the sea, and to the transport of nutrients needed for the sustaining of marine life.

Breakwaters and sea walls are now a common feature along many coastlines. The function of these walls is to protect the area behind from waves and the resulting flows and erosion. The main purpose is not to protect the sea bed beach in front. Such coastal structures have been blamed for the disappearance of beaches in front as well as adjacent to them. Scour in front of some the long breakwaters in Japan has developed up to 6 metres deep and almost 100 metre in length. Such scouring threatens the stability of the breakwater. An increase in the water depth immediately in front of the breakwater may increase the design wave height. It can also directly scatter or remove armour blocks leading to an increase in impact pressures on the structure.

The successful description and prediction of sea bed changes is thus an important part of planning coastal defence, and assessing the stability of structures such as sea-bed pipelines and breakwaters. In the construction of coastal structures, the bed

in front is often replaced with stone or a more stable material in order to reduce scouring. The stability of this material depends on the hydrodynamic forces, which can be estimated if the the near bed velocity is known.

Although scouring is important at coastal structures, the complexity of the problem means that solutions are usually estimated using simple approximation formulae. Sediment transport formulae are often used in solving practical engineering problems. Many different formulae have previously been proposed. Different formulae stress the importance of different aspects of the possible flow so the correct selection has to be made when solving a particular problem. Transport formulae based on time-averaged velocity distributions and time averaged sediment concentration distributions are often used. Much sediment transport takes place under waves rather than steady currents however.

Recent experimental studies have shown that water waves can sometimes fluidise silty soil beds. Total fluidisation is where a block of soil particles becomes almost effectively in complete suspension, with its weight supported almost entirely by the intervening fluid. Laboratory wave flume experiments by Clukey *et al* (1983) show that states of total or partial fluidisation can be achieved in a soil trench below shallow water waves. Packwood & Peregrine (1980) showed analytically that fluidisation can also occur under sufficiently steep bores. This is based on the work of Madsen (1974), who showed that a sufficiently large pressure gradient alone is enough to cause fluidisation of the bed under certain conditions.

The oscillatory nature of flows above sea beds has also recently attracted much interest. This is due to the large amount of sediment observed to be transported by oscillatory sheet flows.

Most of the existing transport models, even ones specifically designed to incorporate unsteady flow, do not explicitly consider pressure gradient. (Note that pressure is related to the acceleration by $Du/Dt = 1/\rho.\nabla p$). Instead, fluid velocity is the dominant independent variable, for example King and Seymour (1982). Although

velocity is the important parameter in transportation of sediment in suspension, how the sediment first becomes suspended or under which conditions it first moves may crucially depend on other parameters.

The force fluid particles is often included indirectly in simple models by assuming a sinusoidal wave profile or a 'wave friction factor' (see Madsen & Grant 1976 for example). These models still assume that the acceleration during the orbital oscillation is of minor importance. This view is not supported by the results of Davies (1980) for example. Davies (1980) presents experimental results of near-bed velocity and observed sediment movement. The lack of strong correlation between the two illustrates that orbital velocity may not be a good determinant of the threshold of movement. Instead bed shear stress gives a much better indication, so would need to be explicitly considered in an accurate sediment transport model.

Hallermeier (1982) also discussed the dependence of bed load transport on acceleration and concluded that the fluid accelerations play a "direct role" in sediment transport. The importance of acceleration in the near bed kinematics is also highlighted by Soulsby & Dyer (1981). Here accelerations due to variations in tidal current over a time scale of order 10 minutes are initially considered. Even though the departure from the velocity profile without acceleration is small, it is found to be important for the calculation of shear stress.

An understanding of the near-bed velocity and pressure field generated by random waves interacting with a coastal structure is crucial for understanding and predicting movement of fronting material. This applies regardless of the particular model used. Research in this area has been largely based on long wave flume experiments. These show the importance of near bed kinematics in beach response. Little work has been done on direct measurement of near-bed kinematics in front of coastal structures however, due to the difficulties and subsequent cost involved.

3.2 Waves near coastal structures

The strong reflection of incident waves by a vertical structure means that the waves directly in front of it structure are well modelled by standing or near-standing waves if no breaking occurs. Perfect reflection of progressive waves at a vertical wall will produce such a standing wave, resulting in surface oscillation antinode at the wall and a node distance $L/4$ from it, where L is the wave length. Such waves are the topic of this chapter.

Two dimensional standing waves were first studied by Rayleigh (1915), who calculated a perturbation series of the surface profile to 3rd order for deep water. This work has been progressively extended both to include much higher order terms and to include surface tension and arbitrary depths. Numerical models have also been developed, in particular by Mercer & Roberts (1992) and (1994), which enable the calculation of limiting standing waves on water of arbitrary depth. Their calculations show that appearance of the standing waves becomes more like a reflecting solitary wave as depth is decreased. The largest waves that can approach any sea or harbour wall are shallow water waves whose crests are very similar to solitary waves.

Solitary waves are commonly used to represent shoaling waves on mild beaches and as a model for tsunami waves. Thus solitary waves continue to be of interest to the coastal engineering community. The fact that the shallow water limit of a standing wave is a reflecting solitary wave gives a further reason for interest.

Standing Waves

Two dimensional standing waves were first studied by Rayleigh (1915) who calculated a perturbation series to 3rd order for deep water. This work has been progressively extended. Penny and Price (1952) increased the series to 5th order on deep water and 2nd order on finite depth. For the case of infinite depth, the series has been extended to 25th order by Schwartz & Whitney (1981) using conformal

mappings. Mercer & Roberts (1992) used a numerical method to calculate the motion and stability of near limiting form standing waves. Wave steepness was found to have a maximum short of the most extreme profile, thus it is unsuitable for parameterising near limiting waves. Instead, Mercer & Roberts used non-dimensional maximum crest acceleration, $a^* = a/g$, as determining parameter, the theoretical (although still contested) limit being a standing wave with $a^* = 1$.

For finite depth, Tadjbakhsh & Keller (1960) calculated a 3rd order series for surface profile, potential function, pressure and frequency in terms of amplitude/wavelength. They noted that at certain depths the linear theory did not give a unique solution to the problem. This is due to resonance between the fundamental wave and its higher harmonics. The strength of the resonances between the higher order harmonics decay rapidly with the order of harmonic, so this did not affect their numerical scheme. Tadjbakhsh & Keller (1960) also found that there is a critical depth, $kh = 1.07$, (later refined by Marchant & Roberts (1987) to 1.058), such that for depths greater than kh the fluid free oscillation frequency decreases with amplitude and for depths shallower than kh its free oscillation increases with amplitude.

Concus (1962,1964) extended this work to include surface tension. He also showed that the depths at which the linear theory does not have a unique solution are everywhere dense. However, he argued that resonances between the higher order harmonics would be damped by viscous forces, hence the agreement between the experiments of Fultz (1963) and work of Tadjbakhsh and Keller (1960). Vanden-Broeck & Schwartz (1981) used a numerical scheme using truncated infinite series. This proved unsuitable for extreme waves due to the slow decay of series coefficients.

Recently Mercer and Roberts (1994) extended their numerical method of (1992) to finite depth to study near extreme standing waves. Particular attention was paid to harmonic resonances and multiple solutions found near resonant depths. They found an appreciable difference between the extreme profiles on infinite depth and deep water.

As the depth is decreased, calculations show that appearance of the standing waves becomes more like a solitary crest reflecting between two walls. In the limit as the depth tends to zero this can be interpreted as a reflecting solitary wave.

Bed Velocities

The phenomenon of standing waves in front of vertical structures and associated bed evolution has previously been described, by Oumeraci (1994) for example. Here experimental results of scour development for standing waves in front of vertical breakwaters is presented. Attention is paid to the influence of wave period, wave height and sediment size. A recent area of research has also been to investigate the possibilities of using a Boussinesq model coupled to a description of the sediment transport in the simulation of scour.

Some success has been achieved in providing guidance formulae to estimate velocity parameters for arbitrarily defined incident wave spectrum. This success has to an extent been limited to relatively deep water. Hughes (1992) for example outlines a linear method for the prediction of velocities in front of a vertical wall. The surface elevation is generated by the straight superposition of a unidirectional incident wave and the partially reflected wave from the structure. The horizontal water particle velocity at any depth below the surface is assumed to be given by linear wave theory. This provides the basis for a simple method of determining the spectrum of horizontal water particle velocities for the case of random waves interaction with a coastal structure. The simple linear theory is compared with a series of irregular wave experiments. The results show a tendency to overpredict velocities at low relative depth ($h/gT_p^2 < 0.01$, where T_p is the period associated with the peak spectral frequency) by as much as 11%.

O'Donoghue & Goldsworthy (1995) have extended this model to include waves in front of sloping as well as vertical walls. They were concerned with the root mean square of velocity, a variable often used in bed response equations. They found that

80% of u_{rms} measurements were within 10% of predicted values. A general trend towards poorer agreement between predicted and measured u_{rms} as relative depth is decreased was found. The authors state that this may be due to a combination of effects including enhancement of wave non-linearities by shallow water conditions, and less accurate phase and reflection coefficient data. The tendency was towards overprediction of velocities at low relative depths, as by found Hughes.

Reflection or partial reflection at the wall will lead to the formation of near standing waves. As the depth is decreased a standing wave becomes more like a reflecting solitary wave. The surface profile of a train of solitary waves has broader flatter troughs and steeper narrower crests. Here linear theory is no longer appropriate.

The pressure and velocity history on a wall due to standing waves has previously been reported by many authors, for example see Nagai (1969). Nagai found that although higher order solutions considerably extend the range of validity in comparison to linear theory, considerable discrepancies were still present particularly under severe wave conditions.

The run up of steep waves has also been studied numerically and experimentally. Sen (1992) compares numerical calculations of standing waves at a wall to the experiments of Nagai (1969) and to linear and third order theory using a boundary integral potential flow solver. Near standing waves were generated by reflection of an incident wave group at the wall. He showed that such a numerical scheme produces results that generally compare better to experiment than the linear or third order solution.

The pressure and velocity profile on the bed under standing and near standing waves has received rather less attention and is the subject of this chapter. I first look at standing waves on relatively deep water. Bed quantities other than pressure here are well modelled by linear theory. On shallow depths however linear theory begins to break down, as found by previous authors in modelling experimental work mentioned above. On extremely shallow depths, linear theory is completely inap-

propriate. On such depths a solitary wave is a good model for the moving crest of a standing wave and some computations are presented for solitary wave collision at a wall.

3.3 Small amplitude theory for bed quantities

Assuming the fluid is both incompressible and irrotational, the velocity potential in the fluid region satisfies Laplace's equation. It can be easily verified, see Lamb (1932) for example, that the surface profile

$$\eta = a \sin(kx) \cos(\omega t + \epsilon) \tag{3.1}$$

,where ω and k are the radian frequency and the wavenumber respectively, satisfies the linear boundary conditions for small amplitude, a. This represents a standing sinusoidal wave. The corresponding velocity potential is given by;

$$\phi = \frac{ga}{\omega} \frac{\cosh(kz + kh)}{\cosh(kh)} \cos(kx) \cos(\omega t + \epsilon) \tag{3.2}$$

3.3.1 Parameters characterising shallow water waves

There are three length scales that need to be considered in the characterisation of shallow water waves. These are the maximum wave amplitude, a defined as half the maximum crest to trough distance, the still water depth h, and the wavelength $l = 2\pi/k$. A commonly used method for finding approximate irrotational, incompressible and inviscid water wave solutions is to linearise the free surface boundary conditions and apply them at the undisturbed position of the surface. This approximation assumes all the variables can be expanded in a Taylor series. The above equations are a solution to such a linearisation for a standing wave formed by the superposition of two periodic wavetrains travelling in opposing directions. To see when such an approximation is valid the order of the neglected terms, compared to those retained needs to be considered. It is found (see Peregrine 1972 for example)

that for the above, the conditions

$$ak \ll 1, \tanh(kh), \text{ and } \coth(kh) \tag{3.3}$$

must hold. If kh is not small these conditions are satisfied by

$$ak \ll 1, \tag{3.4}$$

implying the wave slope must be small. If kh is also small, then it is required that

$$a \ll h, \tag{3.5}$$

i.e., the amplitude must be much less than the water depth for depth much less than a wavelength. A further condition was first mentioned by Stokes (1849). In expanding the potential of a regular wavetrain in powers of a/h he found that the second order term is small compared to the leading term only when

$$al^2/h^3 \ll 1. \tag{3.6}$$

This parameter was not discussed in further papers by Stokes, and it's importance not recognised until a paper by Ursell (1953) in reference to the so-called 'long wave paradox' in the theory of gravity waves. One aspect of this paradox concerns the apparent contradictory theories of Airy (1845) and Rayleigh (1876). Airy concluded that the progressive long waves cannot propagate without change of form. In the derivation of this theory, Airy assumed that the pressure at any point in the fluid is exactly equal to the hydrostatic head of water above the point, the 'long wave hydrostatic assumption'. The resulting equation includes terms quadratic in wave amplitude. However, from what appeared to be a similar set of assumptions, Rayleigh (1876) developed the theory of a solitary wave, a long wave of small amplitude that travelled without change of form.

Analysing the assumptions made by these authors and in the simple linear approximation, Ursell found that the conditions for their validity were best given in terms of the dimensionless parameter al^2/h^3. The similar parameter a/k^2h^3 has

since been referred to as the Ursell parameter, U_r, by later authors. The usual criterion for the validity of linear theory, $ak \ll 1$ (see Lamb 1932 §250 for example) is shown to be insufficient. In reference to the Boussinesq equations (1872), nonlinear terms are only neglible if the condition $U_r \ll 1$ holds, when dispersion is more important than nonlinear effects. Conversely, the Airy theory assumes that nonlinearity is more important than dispersion, and is valid only for $U_r \gg 1$. Thus in characterising the flow we consider the Ursell parameter.

3.3.2 Bed velocity

Note that the velocity potential decreases exponentially with depth, and with wavenumber. If we describe a general fluid surface as the Fourier sum of waves of the form (2.14), we can immediately see from (2.15) that the motion produced by the higher harmonics, with correspondingly larger wavenumbers, decays with depth at a much higher rate. Thus if we want to consider motion on the bed for depths greater than the wavelength, linear theory gives a very good approximation. For shallower water, higher harmonics begin to affect the magnitude and appearance of the bed velocity. For a standing wave with $ak = 0.6$, the contribution to the magnitude of bed velocity from 2nd and higher harmonics compared to linear is approximately 2% for a depth, $kh = \frac{2\pi}{2}$ and only 10% for $kh = \frac{2\pi}{6}$. For less steep standing waves, these non-linear contributions are correspondingly less.

Figure 3.1 shows how the profile of non-dimensional velocity on the bed changes with depth for a standing wave with maximum crest acceleration $0.3\,g$ (U_r 0.002 to 0.41).

The calculations were performed using the fully nonlinear potential flow of Dold (1992). The initial standing wave profiles were calculated by the numerical method of Mercer & Roberts (1994). The initial surface profile is with crests at $kx = 0$ and 2π. Half way through the motion, the crest is at $kx = \pi$ before returning to 0 and 2π after one wave period. The figure shows contour plots of the velocity on the bed with axes x (nondimensionalised with k) and time (nondimensionalised with

$\sqrt{gk}$) for one wave period. Bed velocities for a standing wave with same maximum crest acceleration on four depths are shown.

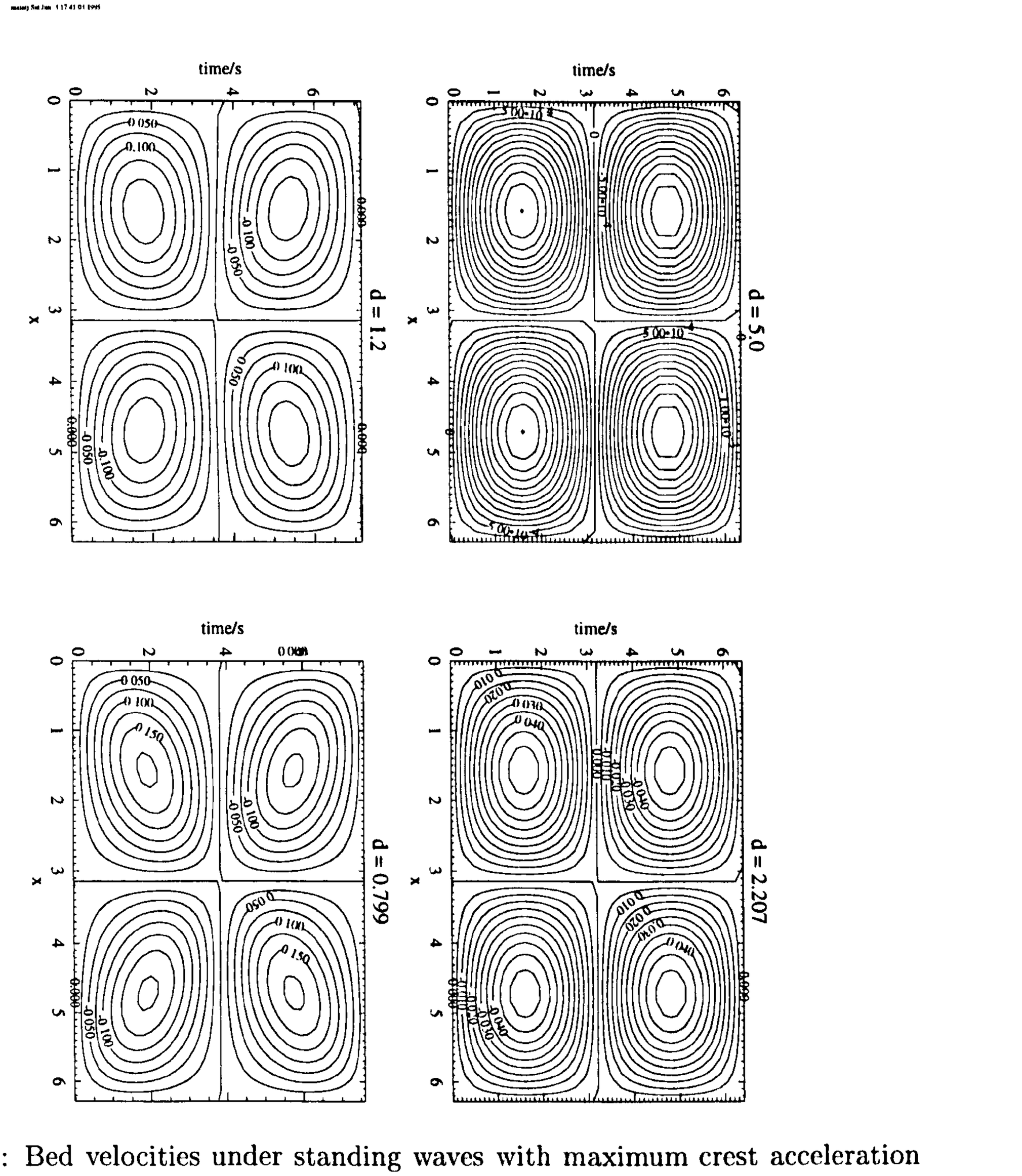

Figure 3.1: Bed velocities under standing waves with maximum crest acceleration $0.3\,g$. Calculated using numerical code of Dold & Peregrine (1986).

There are two important trends to note. The first is an increase in the magnitude of the velocities as depth is decreased. The innermost contour on the first graph, for $kh = 5$, $ak = 0.25$ ($U_r = 0.002$) corresponds to a nondimensional velocity of 0.006, while that on the last, for $kh = 0.799$, $ak = 0.2$ ($U_r = 0.41$) shows a nondi-

mensional velocity of 0.2. The exponential decay in velocity with depth means that compared to an equivalent standing wave on deep water, a standing wave in shallow water causes significantly greater velocities on the bed. The maximum velocities are over-estimated if we attempt to use small amplitude theory for finite waves, the over-estimation increasing as depth decreases. This is due to poor representation of the shape of the standing waves, which on shallower water have broad flat troughs and narrow crests and thus produce less disturbance on the bottom than a corresponding sinusoid.

The next trend to note is the slight distortion in the shape of the velocity contours as the depth is decreased. The small amplitude, linear theory gives a profile consisting of four concentric ring systems of symmetric elliptical shape contours. This is clearly visible for the case $U_r = 0.002$. A small amplitude approximation still provides a good approximation to the velocity profile on the bed for the shallower depths, i.e. a symmetric elliptical shape. However, note as the depth is decreased that the elliptic shape becomes increasingly 'squashed'. The full symmetry is lost and instead the contours are drawn towards a X pattern. This trend is also seen for increasing steepness on the same depth.

Figure 3.2 shows the sequence of numerically calculated surface profiles of a near standing wave with maximum crest acceleration $0.5\,g$ It can be seen the surface has broad flat troughs and narrow crests. A reflecting solitary wave would give a similar surface profile and bed velocity contours concentrated under the travelling crests, i.e. an X shape indicated by the trend highlighted above. Figure 3.3 shows the bed velocity under near standing wave with maximum crest acceleration $0.5g$ for $U_r = 1.75$, and for a reflecting solitary waves of amplitude $0.3\,kh$ $(U_r = 3.75)$ Comparing these profiles to figure 3.1 shows a continuation of the trends previously highlighted. The nonlinear bed velocity profile leads to the start of regions of high acceleration each side of the crest as the extreme profile is reached (see the equivalent plot of pressure gradient in figure 3.7). Linear theory gives a profile the same shape as that for the $kh = 5$ case on figure 3.1, so this feature is not captured.

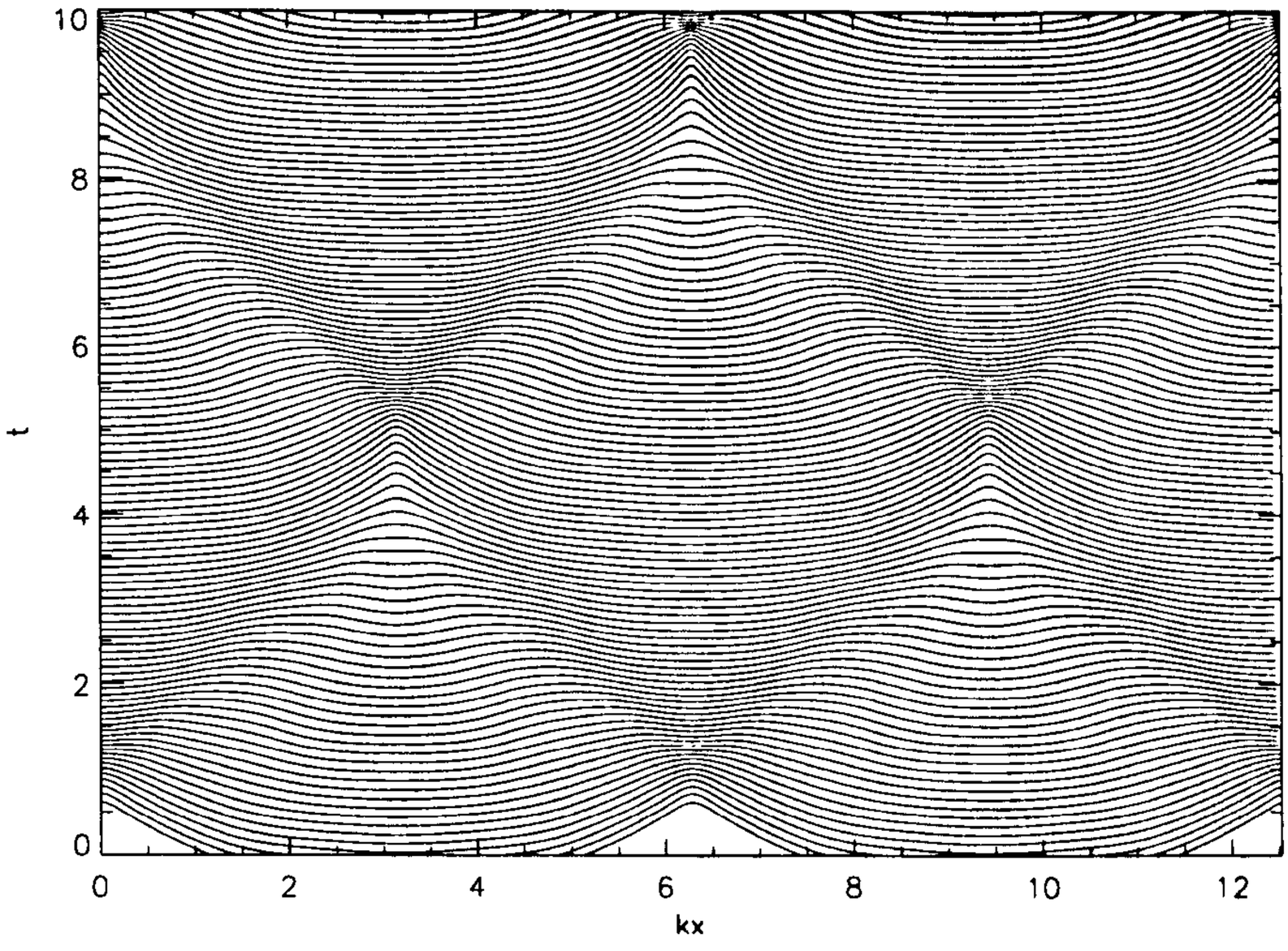

Figure 3.2: Surface profiles for a near standing wave with maximum crest acceleration $0.5\,g$ for $U_r = 1.75$. Surface displacement has been scaled by 2.

In defining formulae to estimate bed parameters under standing waves, linear theory is often employed. In all cases (see Hughes 1992 or O'Donoghue and Goldsworthy 1995 for example), this leads to an over- prediction in bed velocity, often by as much as 20% for simple standing waves for the parameter range studied.

An explanation for the failure of small amplitude linear theory (as used by O'Donoghue and Goldsworthy 1995 for example) at small relative depths can be seen by looking at the wave profiles for the standing waves. Although we would not expect first order approximations to give accurate results for all but $U_r \ll 1$, they are still used in models of sea bed hydrodynamics under standing or near standing waves, so it is useful to highlight the differences that can be expected.

As noted by Mercer and Roberts (1994), for shallower depths the standing waves increasingly take on more of the characteristics of a solitary wave reflecting between two walls one wavelength apart. As the Ursell parameter is increased, the trough becomes broader and the crest narrower compared to the more sinusoidal looking profile of deep water standing waves. The poor representation of this profile by a

sinusoid then leads to an overprediction in velocity magnitude if using small amplitude theory, since an initial sinusoidal profile of the same amplitude has a greater potential energy.

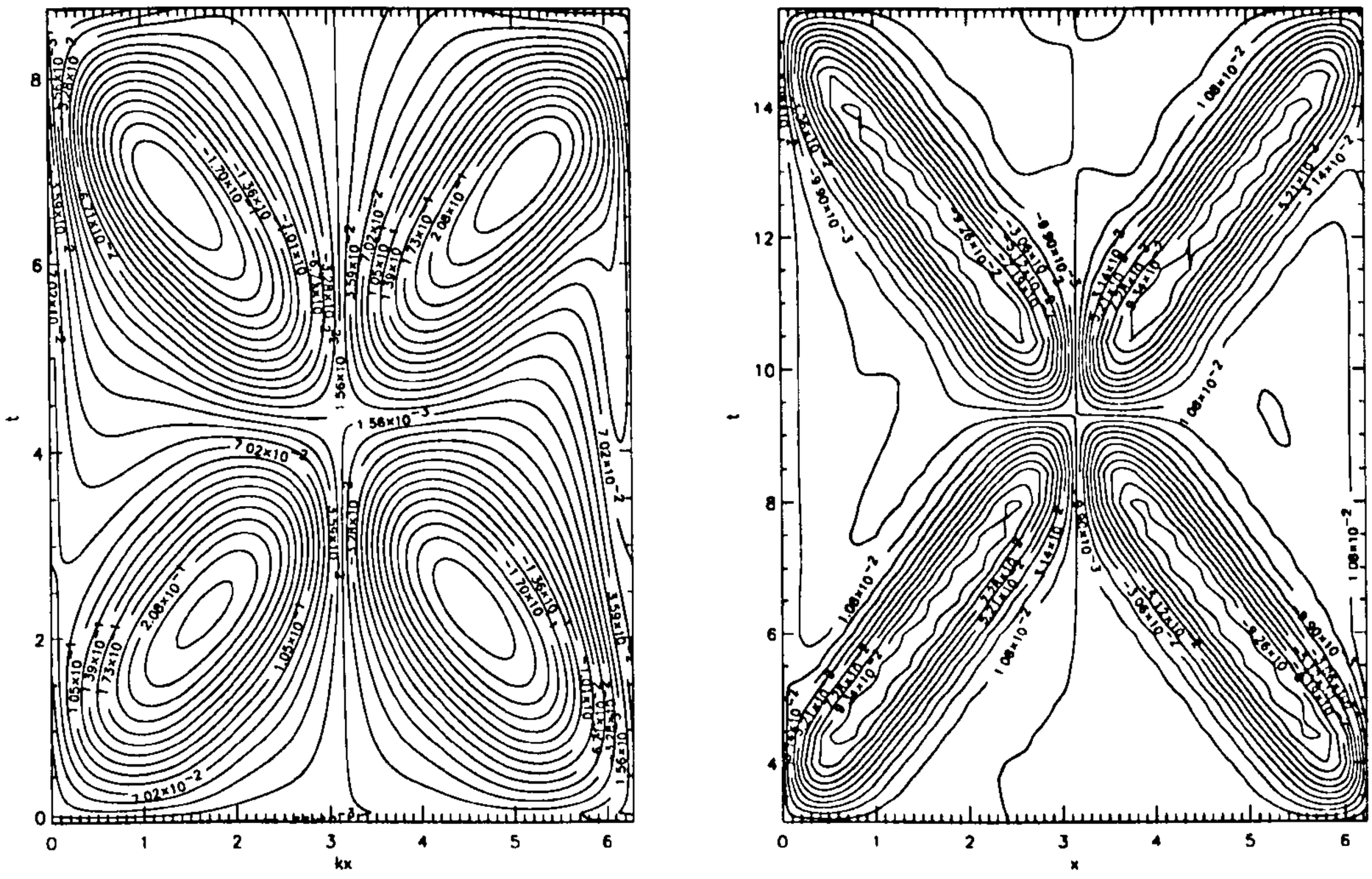

Figure 3.3: (a) Contour plot of bed velocity under near standing wave on depth $kh = 0.5$. Maximum crest acceleration is $0.5g$. (b) Contour plot of bed velocity under reflecting solitary wave $a/kh = 0.15$ ($U_r = 3.75$). Calculation using numerical code of Dold & Peregrine (1986). (The small oscillations are due to the contouring program.)

3.3.3 Pressure

The pressure at depth $-z$ beneath the mean surface is given by,

$$\frac{p}{\rho} = -gz - \frac{1}{2}\left(\phi_x^2 + \phi_z^2\right) - \phi_t + B(t), \tag{3.7}$$

where $B(t)$ is a function of time only. Since we have $p = p_o$ at the surface, and an equation for ϕ we can find expressions for $B(t)$ and $(\phi_x^2 + \phi_z^2)$. We obtain

$$\frac{p}{\rho g} = -z - \frac{1}{2}\omega.a^2.\frac{\cosh^2(kz+kh)}{\cosh^2(kh)}\sin^2(\omega t) +$$

$$a.\frac{\cosh(kz+kh)}{\cosh(kh)}\sin(kx)\cos(\omega t+\epsilon) - \frac{1}{2}\omega.a^2\cos(2\omega t) \tag{3.8}$$

to second order in wave steepness, where ω is the radian frequency and ϵ a phase shift.. It can be seen that first order theory predicts an oscillatory pressure field that decays exponentially with depth. An unattenuated pressure component which oscillates at twice the frequency of the surface is revealed by considering 2nd order terms. Figure 3.4 shows contour plots of non-dimensional bed over-pressure over one period for standing waves with a maximum crest acceleration of $0.3\,g$ on four different depths as in figure 3.1. (The axes have been nondimensionalised as in figure 3.1). Calculations are again using the nonlinear potential flow solver.

It can be seen how the 2nd harmonic becomes less dominant as depth decreases. For the case $kh = 5$ $(U_r = 0.002)$ we can see that the over-pressure undergoes two oscillations in one surface wave period. If we follow the pressure at $kx = \pi$ for one wave period, T, we see that it is initially negative under the wave trough. As the trough of the standing wave rises to become the crest we see that the pressure increases to a maximum before $T/2$. The pressure then reduces slightly, then increases to another maximum after $T/2$ before decreasing again as the crest moves away from $kx = \pi$. This 'double-hump' profile in pressure history under standing waves crests has been well reported by previous authors, for example Nagai (1969). The linear component which decays exponentially with depth is dominated by the unattenuated second order harmonic on such deep water.

As depth is decreased, conversely to with velocity profile, we see an improvement in the qualitative behaviour predicted by a first order approximation. The double hump in over pressure underneath the crest is still present for $kh = 2.207$ ($U_r = 0.02$) but not captured on the resolution of contours given for $kh = 1.2$ ($U_r = 0.14$). For $kh = 0.799$ ($U_r = 0.41$) there is just a single, although elongated maximum under the crest. The increasing relative importance of the first harmonic of shallower depths is clearly visible. For $kh = 0.799$ we see an over pressure profile similar to what we would expect from a first order approximation for this particular standing wave. Quantitatively, small amplitude theory gives over-estimates for bed over pressure on shallow water, again due to the failure to model the shape of the surface profile. For the case $kh = 0.799$ ($U_r = 0.41$) this overprediction is of the order of 10%, and for the case $kh = 0.5$ ($U_r = 1.75$) shown in figure 3.6 approximately 27%. In relation to the Ursell parameter, we would expect a first or second order approximation to give a poor prediction of the standing wave motion for all but very small U_r. We find that, for both a quantitative and qualitative description of motions on the bed, a second order approximation gives fairly good results for $U_r < 1$.

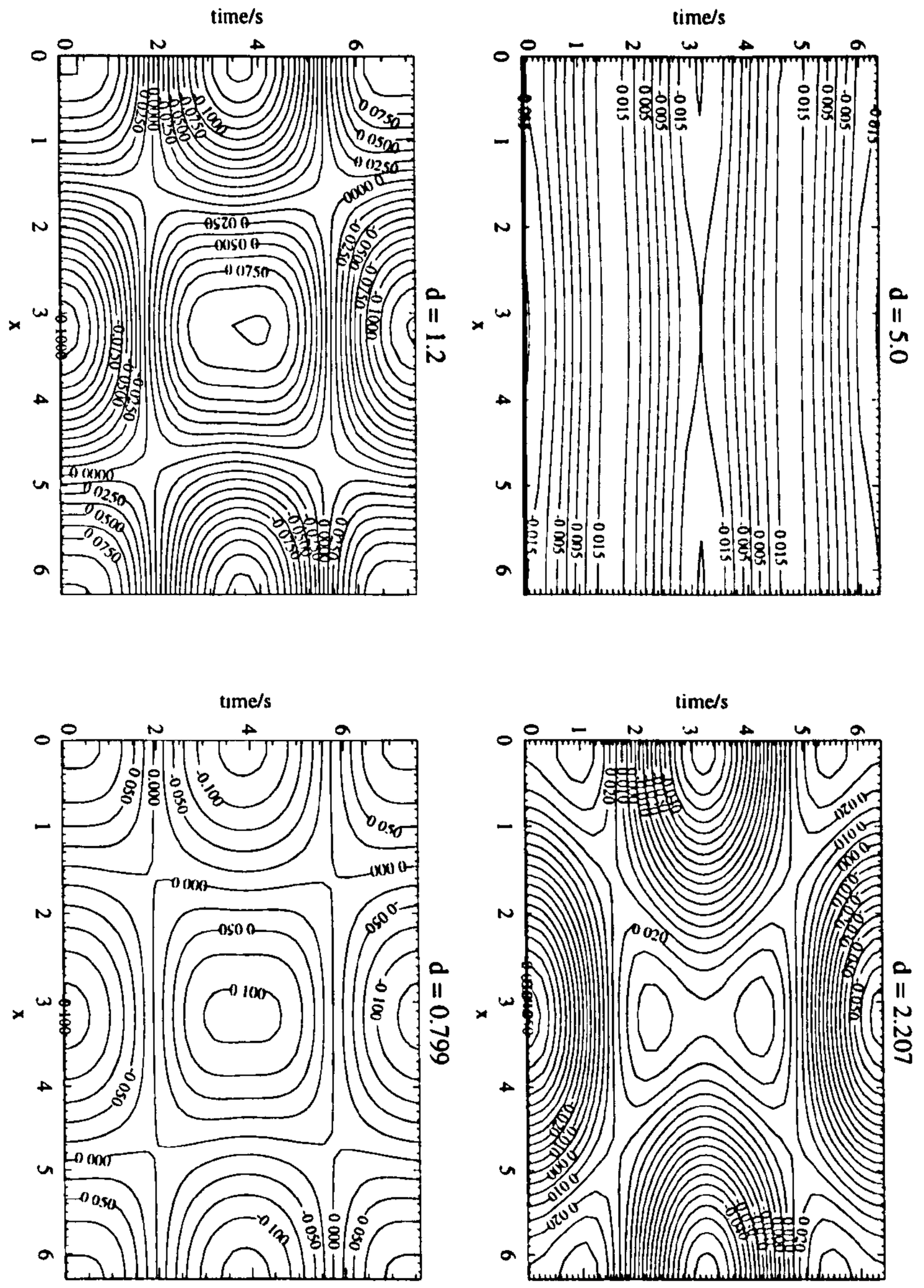

Figure 3.4: Bed pressures under standing waves with maximum crest acceleration $0.3\,g$. Calculation using numerical code of Dold & Peregrine (1986).

3.3.4 Pressure gradients

Pressure gradients are important to sediment transport. The pressure gradient alone can cause a saturated bed to fail. The particles in the bed become fluidised when the net vertical force on them is zero. When exactly this occurs depends on the bed material. Madsen (1974) suggests that the critical pressure gradient for fluidisation is given by

$$\frac{-1}{\rho g}\left(\frac{\partial p}{\partial x}\right)_{crit} \simeq \frac{\gamma^*}{\gamma_f}\tan\theta \simeq 0.5 \quad \text{for } \theta = 35^o, \tag{3.9}$$

where γ^* is the specific submerged weight of the solid, γ_f is the specific weight of the fluid, and θ is a parameter depending on the characteristics of the sand which varies slightly under different load conditions. Generally $\gamma^*/\gamma_f \simeq 0.7$, $0 \leq \theta \leq 20^o$ for clays and $0 \leq \theta \leq 35^o$ for saturated sands. The value of $\theta = 35^o$ chosen by Madsen may give an overestimate of the pressure gradient needed for fluidisation. A value of $\theta = 20^o$, as for clays, gives the non-dimension pressure gradient of $\simeq$ 0.25.

Figure 3.5 shows contour plots of nondimensional pressure gradient, $\frac{dp}{dx}$ on the bed under a standing wave with maximum crest acceleration $0.3\,g$, calculate as above. We see that none of the pressure gradients produced by these standing waves would give bed fluidisation for saturated sands or clays. The profiles show little qualitative difference as the depth is reduced, but an increase in the magnitude of the gradients. Figures 3.6 and 3.7 show the bed overpressure and presure gradient for a near standing wave for amplitude $ak = 0.25$ ($U_r = 3.5$), and for reflecting solitary waves of amplitude $ak = 0.045$ ($U_r = 3.75$). A trend towards localised pressure gradients at the time the extreme profile is reached is seen. Rather than occurring approximately half way between the crest and trough as is seen in 1st and second order linear theory, the pressure gradient maxima occur close to the crest for shallow depths. This is consistent with the narrow crest and broad trough structure of the standing wave profile. As well as the poor prediction of pressure gradient profile, a second order approximation (as given by 2.4) significantly overpredicts the

the maximum pressure gradient; by 25% for the case $U_r = 0.41$ in figure 3.5 and 60% for the case $U_r = 1.75$ in figure 3.6.

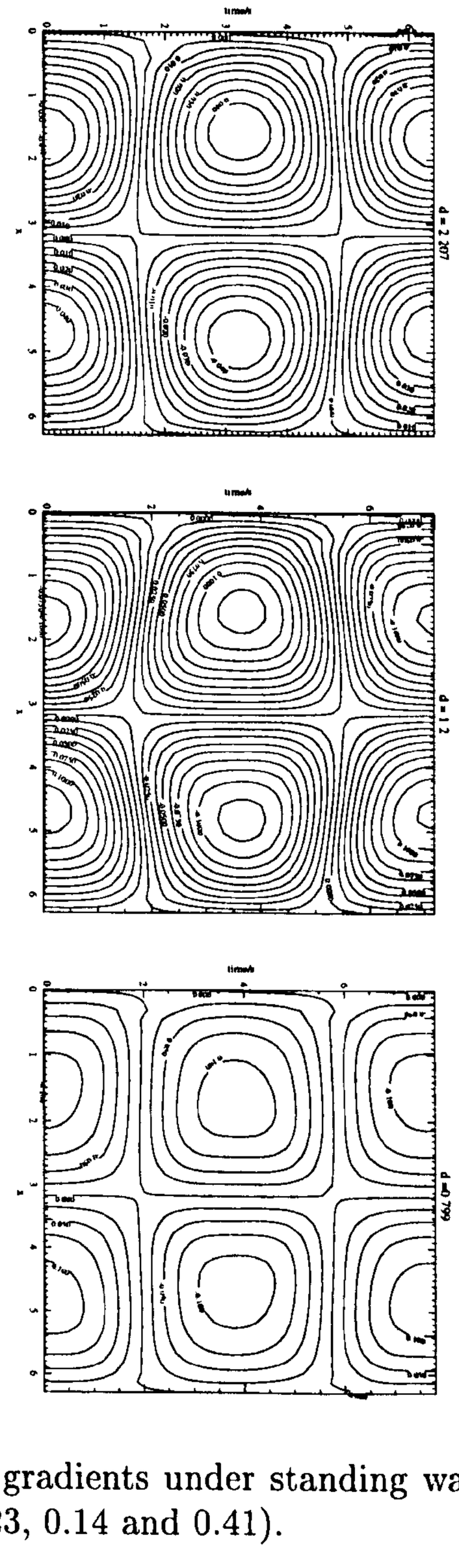

Figure 3.5: Bed pressure gradients under standing waves with maximum crest acceleration $0.3\,g$. (U_r 0.023, 0.14 and 0.41).

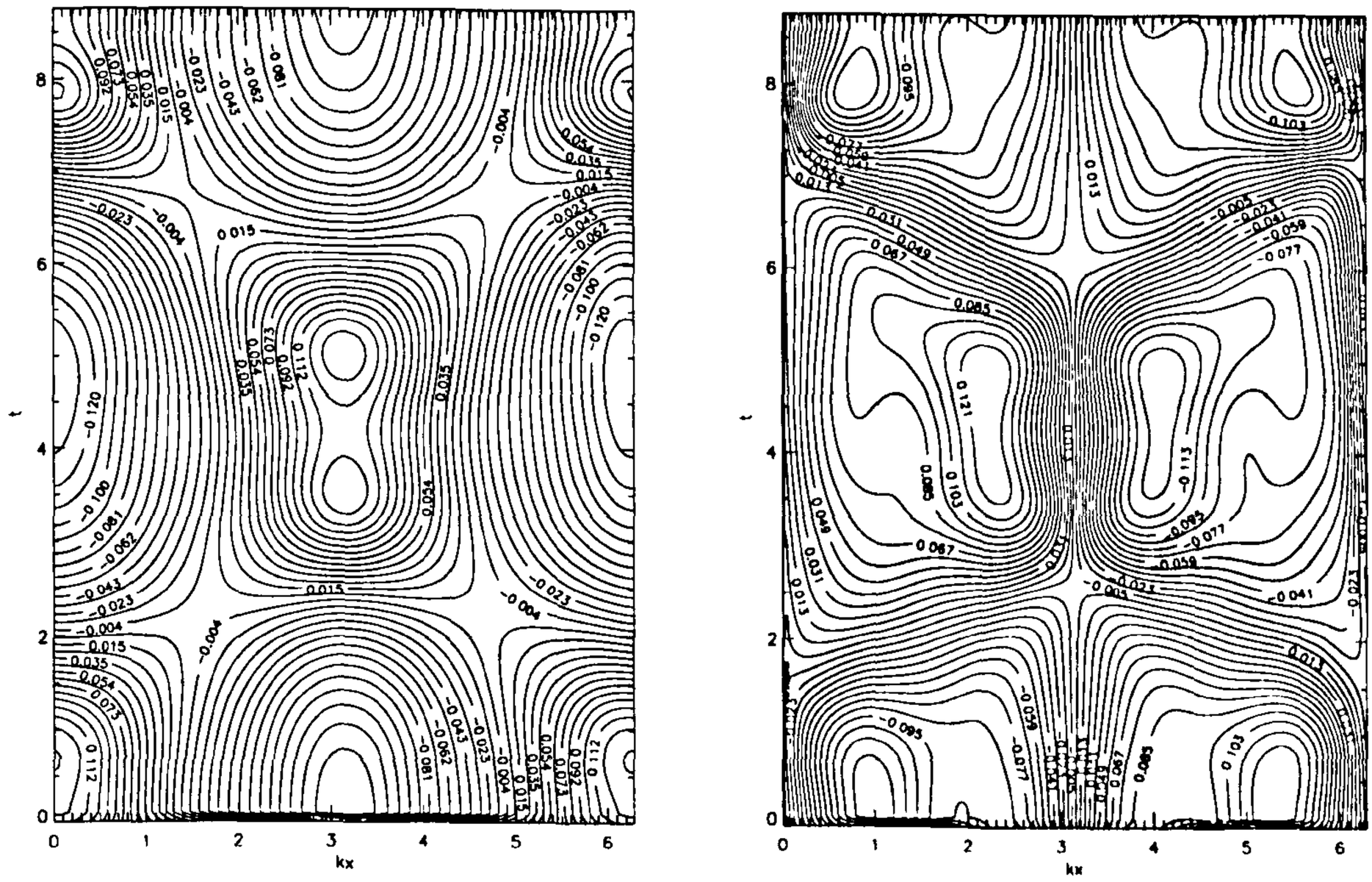

Figure 3.6: Contour plot of bed (a) over pressure (b) over pressure gradient, dp/dx under near standing wave on depth $0.5/k$. $U_r = 3.5$. Calculation using numerical code of Dold & Peregrine (1986).

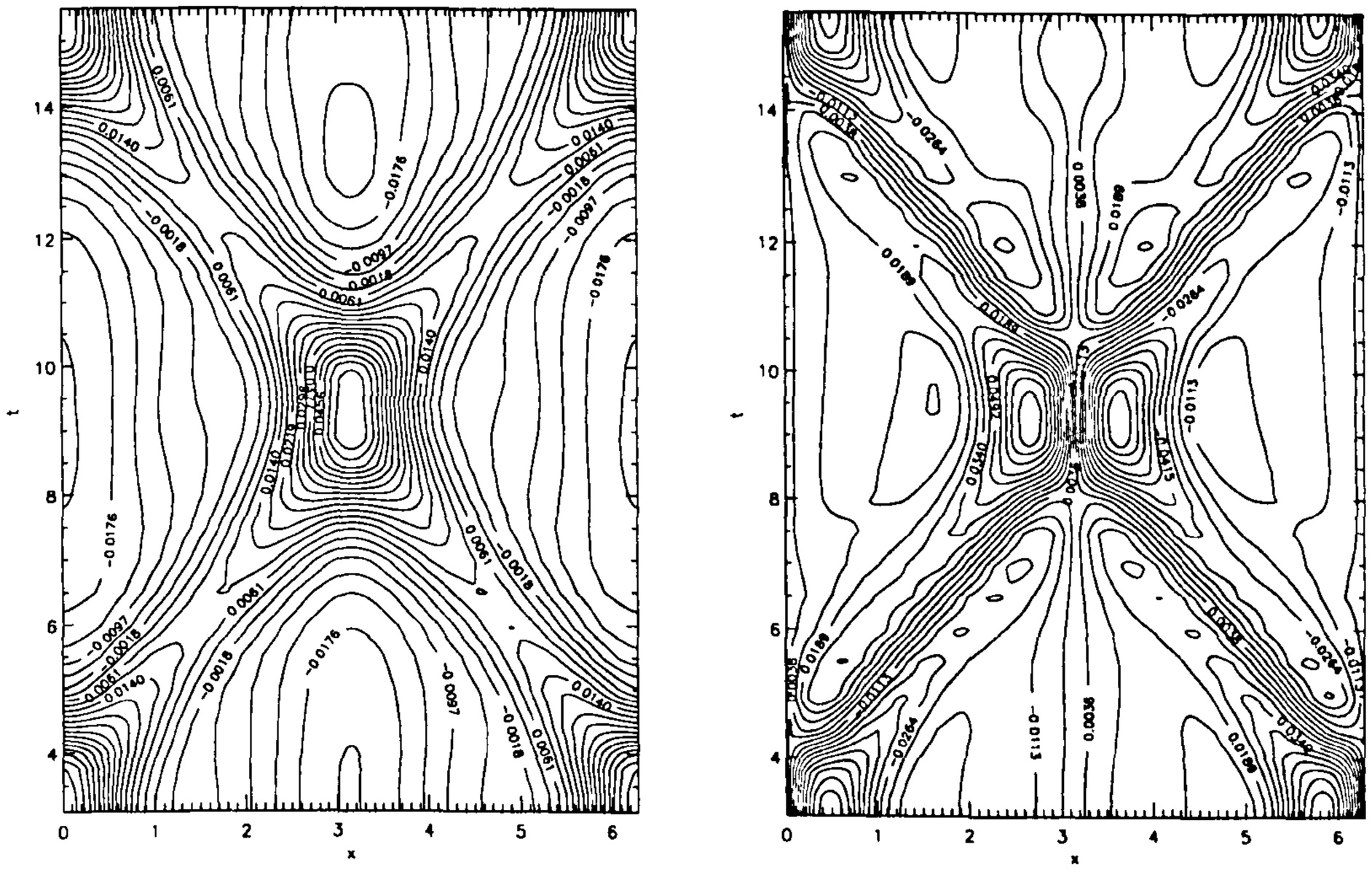

Figure 3.7: Contour plot of bed (a) over pressure (b) over pressure gradient, dp/dx under reflecting solitary waves. ($U_r = 3.75$). Calculation using numerical code of Dold & Peregrine (1986).

3.4 Standing waves on very shallow water

For very shallow water, $kh \ll 1$, wave tank experiments and analytic work has been carried out by Chester & Bones (1968) and Chester (1968) respectively. They looked at near resonant oscillations of liquid in a tank and compared them to long wave theory. It was found that when dispersion was significant, the surface profile could be likened to a series of reflecting cnoidal waves. As expected, small amplitude theory give very poor predictions for all but the smallest of waves. High bed velocities, over-pressures and pressure gradients are localised under the travelling crest, and are underestimated by the linear theory.

3.4.1 Bed parameters under reflecting solitary waves

For very shallow water in front of a vertical breakwater, the above work has indicated that the most extreme non-breaking wave likely to meet the structure can be modelled by a solitary wave. The interaction of solitary waves with walls can be accurately calculated using the previously mentioned potential flow solver of Cooker (1990). The wall is modelled by the collision of two identical solitary waves placed symmetrically about $x = 0$ and initially far enough apart that there is no interaction between them. Our model is for inviscid, incompressible flow so we do not take into account possible effects of viscous damping or compressibility at the wall and energy is conserved. Calculations of the maximum pressure on the wall using this code have previously been presented in Cooker (1990) and are in good agreement with the numerical results of Fenton & Rienecker (1982).

Figure 3.8 shows calculations of bed velocity, u for a solitary wave of amplitude $0.5\,h$. Here the amplitude refers to the full height of the solitary wave, from crest to still water level. The figure shows how velocity is localised under the solitary wave crest and in the direction of propagation for both the incident and reflected wave. As the wave collides with the wall there is a brief period of almost zero bed velocity.

Figure 3.9 shows the corresponding calculations for non-dimensional over pres-

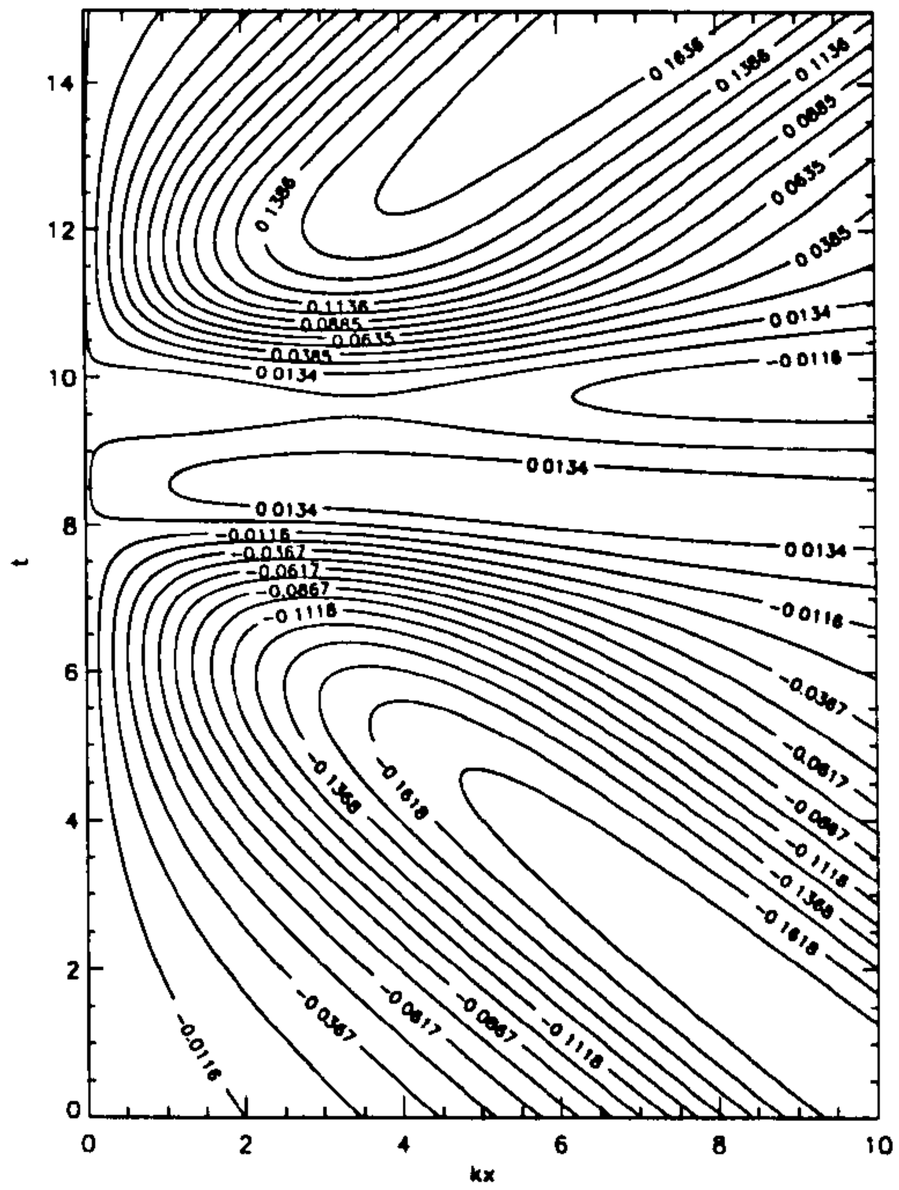

Figure 3.8: Contour plot of bed velocity under solitary wave collision with a wall. $a = 0.5h$. Calculation using numerical code of Dold & Peregrine (1986).

sure and pressure gradient. For this amplitude wave we note that the pressure maximum occurs at the foot of the wall after the moment of maximum run up. The pressure history along the bottom of the wall shows a double hump of two almost equal maxima. Looking at the non-dimensional pressure gradient (equivalent to the bed acceleration Du/Dt), we see that a maximum value of approximately 0.2 (see 3.10) is reached which occurs before the moment of maximum run-up at some distance, approximately $2\,h$, from the wall. Note that the maximum non-dimensional pressure gradient for the standing waves considered earlier (figures 3.5) and 3.6) reached only 0.12, and considerable less for greater depths. We find that the maximum pressure gradient is greater, but more localised than predicted by linear theory on very shallow depths.

Table 3.1 shows the maximum non-dimensional pressure gradient under reflecting solitary waves of different amplitude to depth rations. Even for the nearly steepest solitary wave we find that the pressure gradient alone is not enough to cause bed fluidisation on saturated sands using the formula of Madsen (1974). However, local

a/h	$\lvert dp/dx \rvert_{max}$
0.50	0.199
0.60	0.209
0.70	0.278
0.75	0.292
0.80	0.302

Table 3.1: Numerically calculated maximum absolute non-dimensional pressure gradient under reflecting solitary waves.

fluidisation could occur for clays under reflecting steep solitary waves.

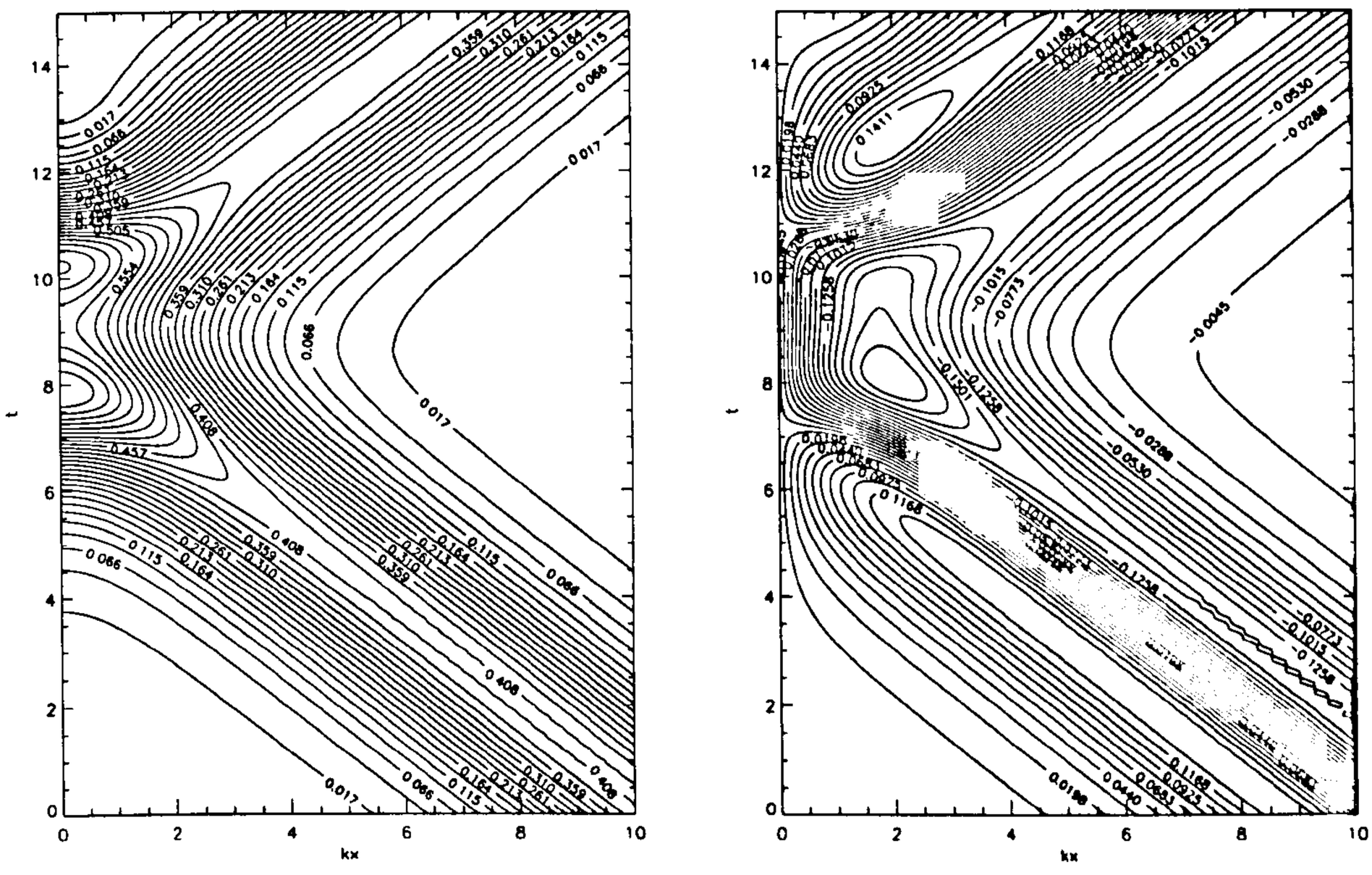

Figure 3.9: Contour plot of bed (a) over pressure (b) over pressure gradient, dp/dx under solitary wave collision with a wall. $a = 0.5h$. Calculation using numerical code of Cooker (1990).

3.5 Discussion and conclusion

Ursell (1953) shows how we can only expect a first order approximation to be valid for $U_r \ll 1$. Despite this, first order approximations are often used in modelling bed parameters under waves with U_r $O(1)$ and greater. This chapter has highlighted some of the differences that can be expected if such an approximation is made.

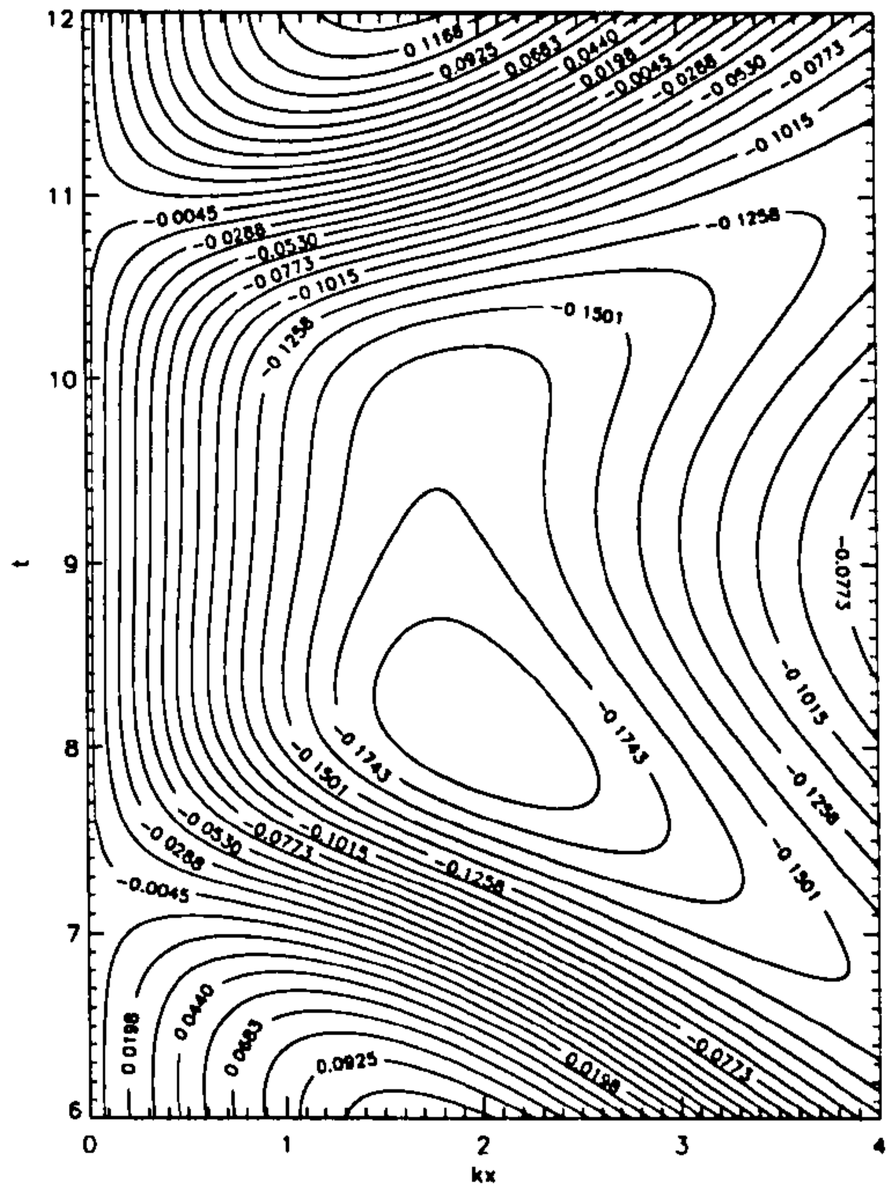

Figure 3.10: Close up of contour plot of bed over pressure gradient under solitary wave collision with a wall. $a = 0.5h$. Calculation using numerical code of Cooker (1990).

Previous work by Nagai (1969) has indicated the range of applicability of first and third order approximations in estimating pressures under a standing wave crest. For large U_r, the behaviour becomes increasingly similar to that of a reflecting solitary wave.

A first order increasingly overpredicts bed velocity with increasing Ursell parameter. Similarly, and second order approximation, required to find the 'double hump' behaviour in bed overpressure, also overpredicts bed values and does not capture the areas of localised pressure gradient and acceleration found under such waves. Solitary waves are typical of the largest waves that could meet a shallow water structure. Although linear first and second order theory is often used, we have seen that is not applicable to such waves, so would give erroneous results.

The reflection of a solitary waves at a wall produces a highly localised region of strong bed acceleration and pressure gradient. For large amplitude solitary waves however, the pressure gradient is alone great enough to cause localised fluidisation

of clay beds according to the simple rule of Madsen (1974).

Chapter 4

Overtopping of Vertical Walls

4.1 Introduction

Vertical breakwaters are now found all round the world. Their traditional home is Italy, where they have been used since Roman times, but they can now be found in increasing numbers along Britain's coastlines and especially in the Far East. The total length of Japanese vertical breakwaters for instance exceeds several hundred kilometres. Some typical breakwater cross-sections are reproduced from Goda (1985) in figure 4.1

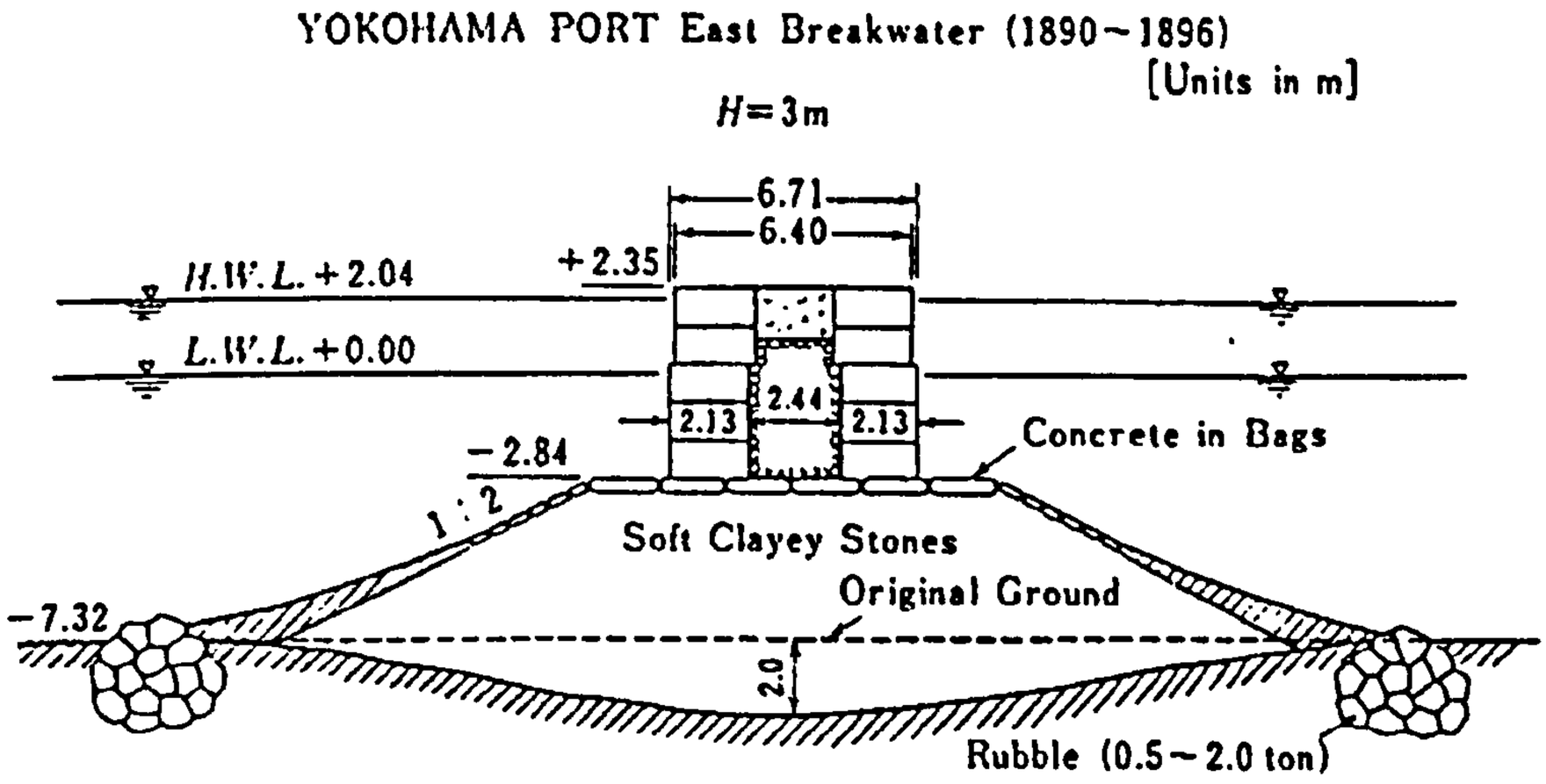

The salient features of a vertical breakwater that play a role in determining it's interaction with sea waves, at least in terms of overtopping rates and forces, are

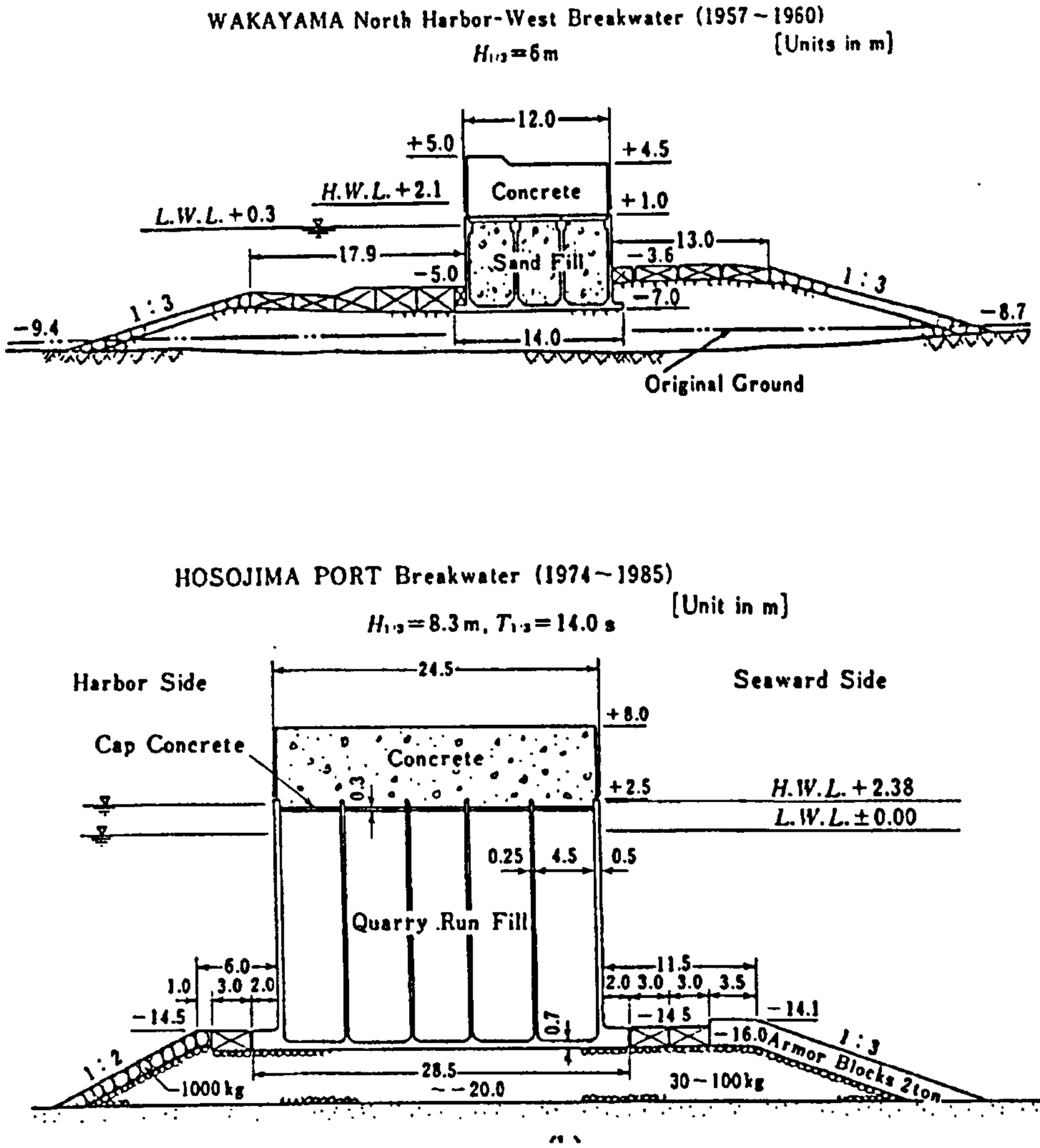

Figure 4.1: Cross sections of a some typical harbour breakwater.

the shape and size of it's foundation berm, the crest free-board or height above still water level, and the depth of water in which it is built (see fig. 4.2). Here, still water depth is labelled d to avoid confusion with the normal choice of H for the wave height. It is fairly obvious that less water will overtop the structure the higher out the water it is, but less obvious what influence the shape of the foundation can have.

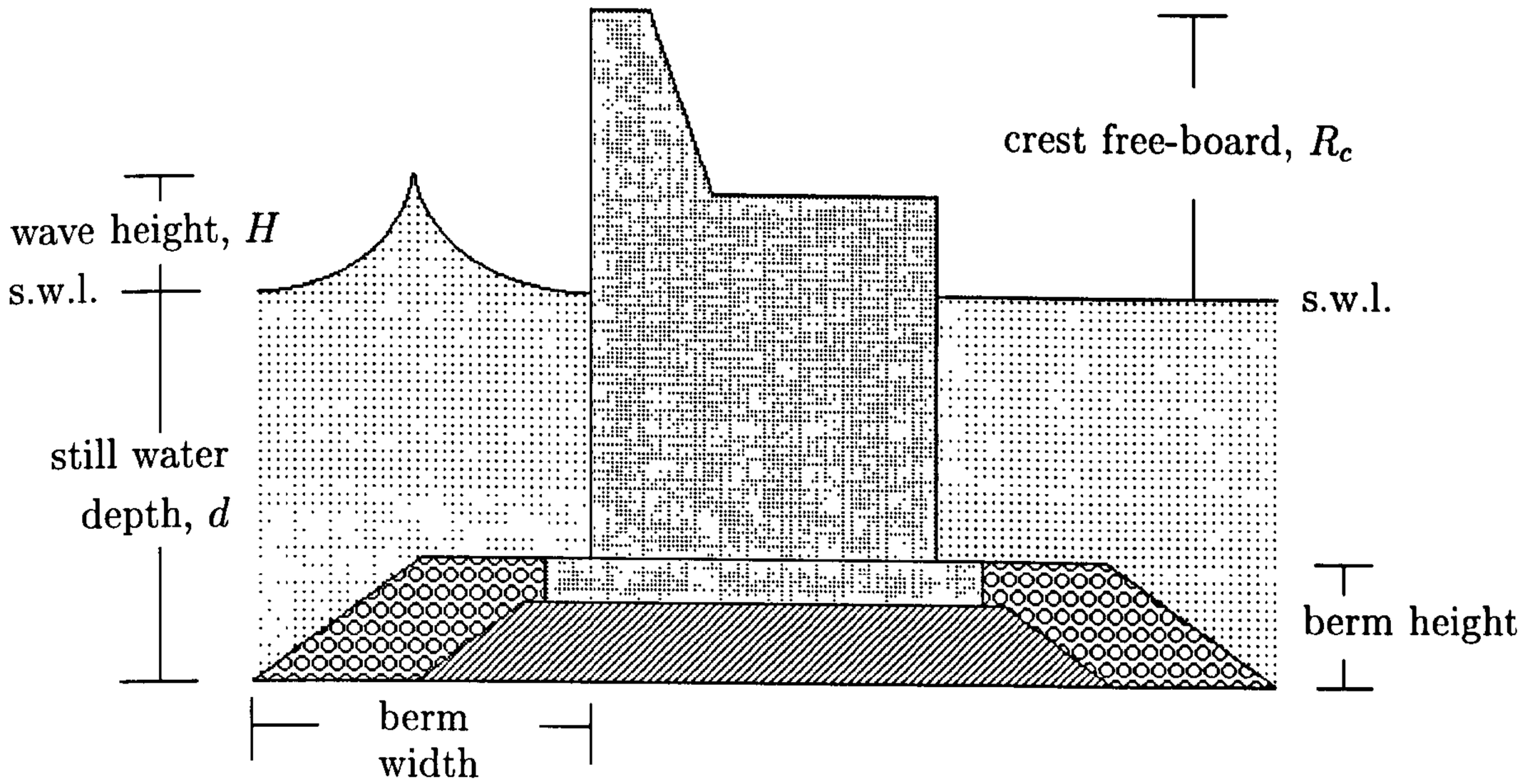

Figure 4.2: Schematic cross section of a harbour breakwater with definition of terms.

Advantages of vertical breakwaters

The alternative, where a harbour wall or breakwater is required, is to build a rubble mound. However, vertical breakwaters are now increasingly used for a number of reasons. Due partly to the long history of vertical breakwaters, engineers are familiar with the main problems involved. Vertical breakwaters take up less room, so can allow bigger harbours. Also vertical caisson breakwaters, particularly those of recent construction, have proved less prone to failure than rubble mound design of breakwater. This is due to recent improvements in construction technologies which also allow rapid installation and comparatively low maintenance costs.

Drawbacks of vertical breakwaters

An immediate disadvantage to a vertical, rather than a sloping structure, is the strong reflection of incoming waves. As discussed in the previous chapter, reflection of a group of waves can lead to the formation of standing waves, themselves much steeper than the incident waves. These waves are hazardous to vessels in front of

the structure. As well, the formation of standing waves has some important consequences for erosion of the local sea bed. This has also been discussed in the previous chapter. Despite these apparent drawbacks, vertical breakwaters are sometimes designed to maximise the chance of standing wave formation (see Franco 1992). In this way the chances of waves breaking in front of the structure and the resulting large impact pressures are reduced.

Another important disadvantage of such vertical structures is the resultant overtopping of water waves, even on fairly calm days. On rougher days, it is not uncommon for 'sediment' of the order of 10 centimetres diameter to be brought over the structure by the overtopping waves. Such overtopping can itself cause damage to the structure. The offshore breakwater of Gela, on the south coast of Scicily is built in a depth of 12m. In 1991 it was hit by a storm with an estimated peak significant wave height of 6m. Although the caisson structure remained stable, heavy wave overtopping resulted in damage to pipelines running along the structure and breaching of the crown wall. Wave overtopping was also the main cause of damage to the breakwater at Bagnara in Southern Italy also in 1991.

The safety against wave overtopping in particular has gained importance with increased recreational use of breakwaters, which are commonly easily accessible to the public. For the structure itself the resulting flow of water can be important because of consequent erosion and potential for flooding.

Harbour breakwaters are meant to protect vessels and harbour installations from the effects of waves but if too much overtopping occurs it can interfere with harbour activities, and cause damage to the structure, and vessels moored on the rear side.

4.2 Parameters affecting overtopping

There are clearly many parameters that influence the mean rate of overtopping of a structure. A list of such is given by de Waal (1994) for example. These can be divided into those that specify the wave conditions and those that specify the structure.

Figure 4.3: Overtopping of breakwaters presents many problems. (Warning sign, Alderney Harbour Breakwater, Channel Islands.)

The wave parameters are usually taken to refer to the incident, undisturbed waves. They include the significant wave height (or some measure of mean wave height) and the distribution of wave heights (or a probability distribution for wave height exceedence), the peak period and spectrum shape and the mean angle of attack. Those that are important in defining the structure are the shape below the still water level including water depth at the toe of the wall, slope of foreshore and shape of berm, the shape above the still water level including crest height and the structure shape between still water level and crest height, and the roughness and permeability of the wall and berm. Parameters like crest height are well defined and quantifiable, whereas others, such as berm shape are not.

Overtopping is also influenced by the action of wind, both in affecting wave shape and in carrying spray over the structure. Thus wind velocity parameters can also be included in this list. Here gravity is a fixed parameter, at least for real applications. Surface tension is ignored as for prototype scale overtopping its effect

would be small. We can also think of other secondary parameters that would play a role, air entrainment and salinity for example.

Due to the large number of relevant parameters and the very complex water motion at the structure a purely theoretical approach to the wave overtopping problem is not practical. In previous work, a restriction to the number of variables is made by choosing certain simple wave and structure parameters. Attention is focussed on those that are likely to play major role, and which are easily quantifiable. Common choices for the specification of the incident waves are;

- perpendicular wave attack.
- long crested waves (no directional spreading)
- JONSWAP (Joint North Sea Wave Project) empirical wave spectrum.
- Rayleigh distribution of wave height exceedence probabilities.

Similarly, a simple structure is often chosen, i.e. straight, vertical, smooth and impermeable. Experimental work has shown that the most important factor affecting overtopping discharge is the relative crest freeboard, R_c/H_s, where R_c is the wall crest height above the still water level and H_s the significant wave height (see Franco 1993). Experimental results are thus usually presented as graphs of overtopping against relative crest freeboard, even if it is some other parameter that is being changed.

In general the above parameters all play a role in influencing the water motion at the structure. The behaviour of a non-breaking wave at a vertical wall however is almost completely determined by its own dimensions and does not depend on the characteristics of the preceding waves. For such waves, only the characteristics at the wave crest are relevant to overtopping. The details of motion however are still determined by a complex relationship between most of the above mentioned parameters.

In the calculations presented later, we have chosen a single wave representative of the steepest waves likely to approach such a structure. This is a steep solitary wave. Thus the ratio a/d is also fixed for our calculations, although we would expect the variation of these two parameters independently to have affect overtopping rates. The idea then is to firstly see if a simple model can predict the same relationship as observed experimentally. We can then go on to see the effect changing other parameters, such as the shape of the foundation berm and the scale of the motion. There are two types of behaviour characteristic of extreme standing waves, or waves reflecting (Thais & Peregrine, in preparation). One is a thin sheet like jet that we see in figure 4.4, but a berm can also give the other almost "table-like" elevation as in figure 4.10, or wave breaking before the wall.

4.3 Previous work on wave overtopping

Work done so far consists largely of small scale wave basin experiments, for example Prud'homme and Perez (1992). This has concentrated on the relationship between dimensionless overtopping discharge or rate and relative crest free-board. In the rubble mound experiments of Juhl and Sloth (1994) for example a water depths between 0.4m and 0.35m, crest free-boards between 0.05m and 0.1m and significant wave heights between 0.05m and 0.11m are used. Thus the corresponding Ursell parameter for the steepest wave near the breakwater itself is likely to be $O(1)$ and thus fairly well represented by solitary waves.

Such experimental work has been carried out with both pure vertical walls and with rubble mounds for both normal and oblique wave attack. By far the majority of work has been done for rubble mounds however, for example de Waal and van der Meer (1992), Yamamoto and Horikawa (1992)

In Franco(1994) an empirical formula is established for the mean overtopping discharge for vertical breakwaters exposed to normal wave attack, based on a series of random wave wave basin experiments. For vertical breakwaters dimensionless

overtopping discharge, Q, related to relative crest free-board through the relation

$$Q = A.\exp\left(B.\frac{R_c}{H_s}\right) \tag{4.1}$$

for constants A and B.

Work with rubble mounds has also found that for dimensionless free-boards less than about 1.5 overtopping discharge is also well described by an exponential function of R_c/H. Here different parameters were found for plunging (breaking) and surging (non-breaking) waves, which may also be important in interpreting the results presented later.

A set of safety criteria is proposed in Franco (1992) based on statistical analysis of failures for structural damage. The safety criteria for people, cars and the structure itself have been arrived at by comparison of test results using ballasted scale models with those from full scale objects and volunteers.

A crucial factor in the design of a breakwater is the crest free-board. This must be a compromise between providing a protection against overtopping (requiring larger free-board heights) and construction costs.

All the above mentioned work considers rates of overtopping rather than individual overtopping volumes. Overtopping rates are easier to measure as they just involve weighing the collected overtopping water after a certain period of time. However, maximum overtopping volumes are better indicators of the damage likely to occur. An estimate of individual overtopping volumes can be arrived at using statistical methods although a more accurate method would be desirable.

An empirical prediction formula for distribution of individual overtopping volumes is presented in Franco (1994) based on wave basin experiments with random waves. Details of the experimental set up were not given, so our model cannot be directly compared. However we can compare trends. Results in Franco (1994) show that typically a pure vertical face produces a smaller percentage of overtopping waves, but with larger maximum volumes and thus a greater probability for damage to the structure. Rock protection in front of the caisson was found to increase the

overtopping discharge.

Very few full scale in-situ measurements have been taken, due to the difficulty and cost of such operations. However the importance of obtaining full scale measurements has been recognised for validating experimental data, in particular for overtopping results. The topic of whether small scale experiments can accurately be extrapolated to full-scale is addressed in the second part of this chapter.

The main direction in the design of recent breakwaters however has been to engineer towards smaller overtopping volumes, in particular by varying the front geometry of the wall and the foundation berm. Initial analysis conducted at Hydaulics Research Ltd. at Wallingford indicated strong effects of local changes to the structure/sea bed geometry close to the wall on impact pressures. This section also shows how the local foundation geometry can also effect overtopping. No previous theoretical work so far has been carried out to test the direct influence of relative berm dimensions on overtopping.

Computational modelling of steep unsteady waves now permits calculation of waves meeting a vertical wall and causing a significant vertical jet of water. Such jets are an important element in many overtopping situations. The object of the work here is to present a simple theoretical model to calculate overtopping volumes per wave from such computations.

4.4 Overtopping model

The program used is that of Cooker, Peregrine, Vidal & Dold(1990) which is based on the accurate irrotational flow solver of Dold & Peregrine(1986) as described in Chapter 2. The version used here is for an unbounded, rather than periodic domain. The computation assumes inviscid, irrotational and incompressible flow, solving Laplace's equation with a boundary-integral method, and using the fully nonlinear boundary conditions to time step the computation. High-order numerical approximations are used. It is required that all surface variables tend to zero at

both ends so that the vertical contributions in the Cauchy integral of the surface contour can be neglected.

The reflection of waves by a vertical structure such as a breakwater means that the waves in front of the structure are well modelled by standing or near-standing waves if no breaking occurs. Breakwaters are sometimes designed so as to guarantee the formation of standing waves in front of the structure. In this way the chances of the occasional very high impact pressures which might lead to structural failure are reduced. An extensive series of model tests were carried out by Nagai (1973) to determine the effect of berm dimensions on ensuring total reflection of waves. He concluded that total reflection will occur for a wave height H if,

$$\text{depth at toe of foundation berm} \ \geq \ 1.8H$$

and

$$\text{depth at toe of wall} \ \geq \ 0.75(\text{depth at toe of foundation berm}).$$

Experimental observations (such as de Waal 1995) report that the most common modes of overtopping occurs when the crest of a standing wave reaches higher than the crest of the structure, or a steep wave collides with it. The previous chapter described how the appearance of the standing waves becomes more like a reflecting solitary wave as water depth is decreased. The largest H waves that can approach any structure are shallow water waves whose crests are very similar to solitary waves. Thus we use solitary waves as incident waves for the examples here.

Impact on a vertical wall is modelled by considering the symmetrical collision of two steep solitary waves. That is, the initial condition in the computation corresponds to two accurate solitary waves heading towards each other, but sufficiently far apart that there is no initial interaction between them. An initial solitary wave of any height can be accurately modelled using Tanaka's (1986) method. The program can include simple deformations to a flat bed, such as beaches and half ellipses. A berm of quarter-elliptical shape in front of the wall is modelled by placing a semi-ellipse on the bottom directly below the line of symmetry of the surface, where the

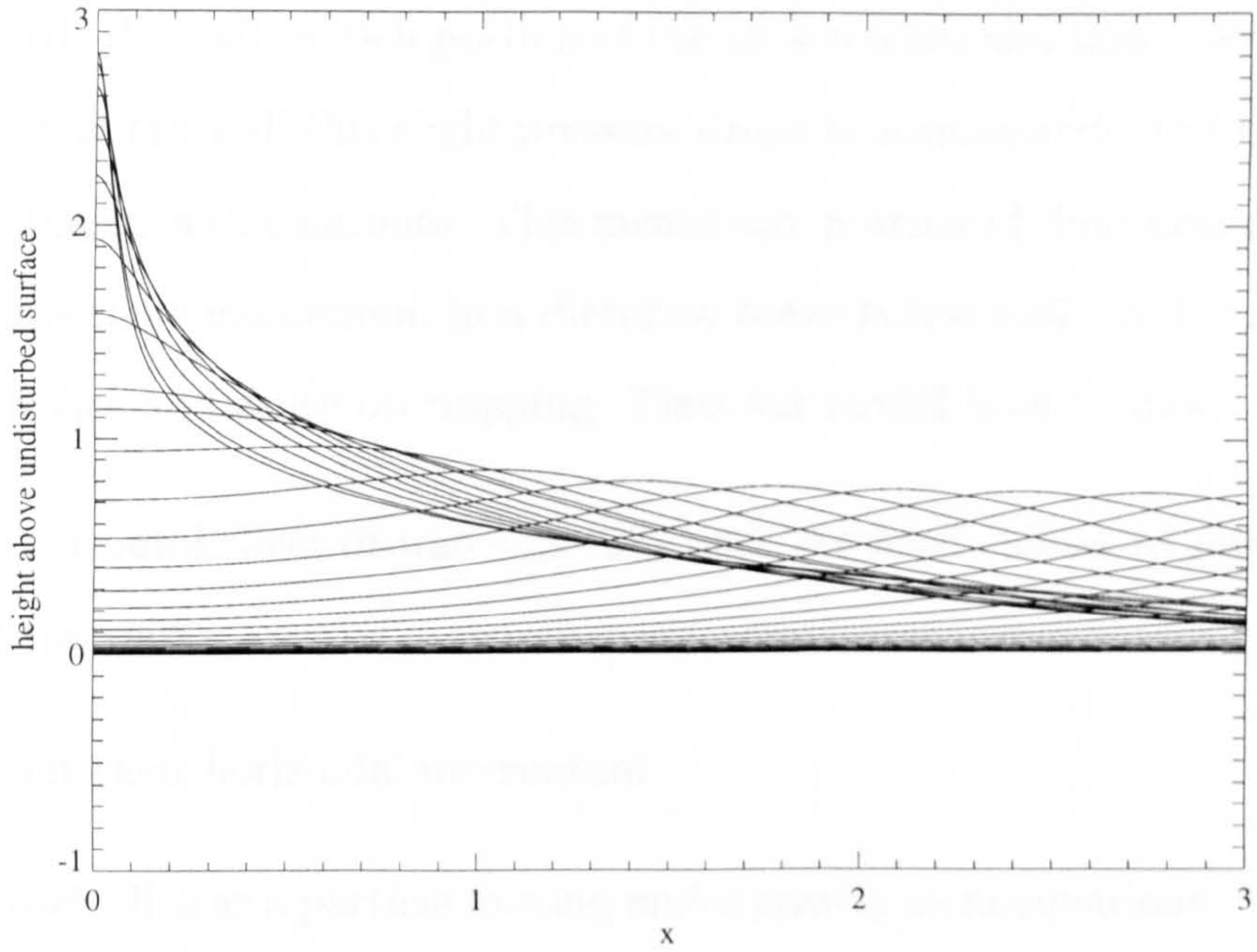

Figure 4.4: Solitary wave collision with vertical wall. Wave height, $H = 0.75d$

two solitary waves collide. Results for such cases are also reported. For sufficiently steep waves a vertical jet forms at the wall (see figure 4.4).

We are not able to explicitly model a wall of finite height using the present code. Substantial changes to the code along the lines of Grilli & Svendsen (1990) would be needed to do this. However, we make use of a feature of common to all jets arising from unsteady waves. That is once the jet forms the pressure field within the jet is very weak. This means that almost all the motion of water in the jet is close to purely inertial. Thus we assume that once the jet has formed, the motion of any fluid particle in the jet is governed by its initial momentum and gravity. Portions of fluid are modelled by considering their motion once above the crest of the wall as if they are a free particles moving under gravity, that is

$$y(t) = y_0 + v_0(t - T_0) - \frac{gt^2}{2} \tag{4.2}$$

$$x(t) = x_0 + u_0(t - T_0) \tag{4.3}$$

where the fluid particle has position (x_0, y_0) and velocity (u_0, v_0) at a time T_0 when it passes the crest of the wall.

As a jet ascends a wall there is some slight pressure against it. This is due to motion towards the wall as each portion of the jet stretches and thins. As the water passes the top of the wall this slight pressure drops to atmospheric, but the motion towards the line of wall continues. This means any portion of fluid passing the top of the wall has some momentum in a direction towards the wall which can carry it over the wall face and cause overtopping. Thus our model is as follows:

- Take horizontal slices of water as they pass the level chosen to represent the top of the wall.
- Work out their horizontal momentum.
- Treat each slice as a particle moving under gravity as in equations (1) and (2).
- Consider each slice as it returns to the level of the top of the wall. Use the position of its centre of mass to decide how much, if any, of the water has moved horizontally past the face of the wall and hence counts as overtopping.
- Add the contribution from all the slices that flow past the top of the wall to give an estimate of the total volume of water overtopping due to that wave.

This calculation could be further refined by allowing for the contraction of each slice under its initial velocity field. However, such contraction is influenced by the slight pressures exerted by adjacent slices, so that to try and include it would mean going beyond the simple modelling we wish to present here.

The velocity field in representative jets was examined in detail. It was found, as expected, that the vertical velocity is close to uniform across the jet at any one level. The horizontal velocity varies almost linearly from zero at the wall, so that although some initial computations used velocities from several points to assess the horizontal momentum, just one or two points are sufficient to evaluate the momentum of a slice in most cases. More points are used for the computations in which the jet shape is significantly altered by interaction with the berm.

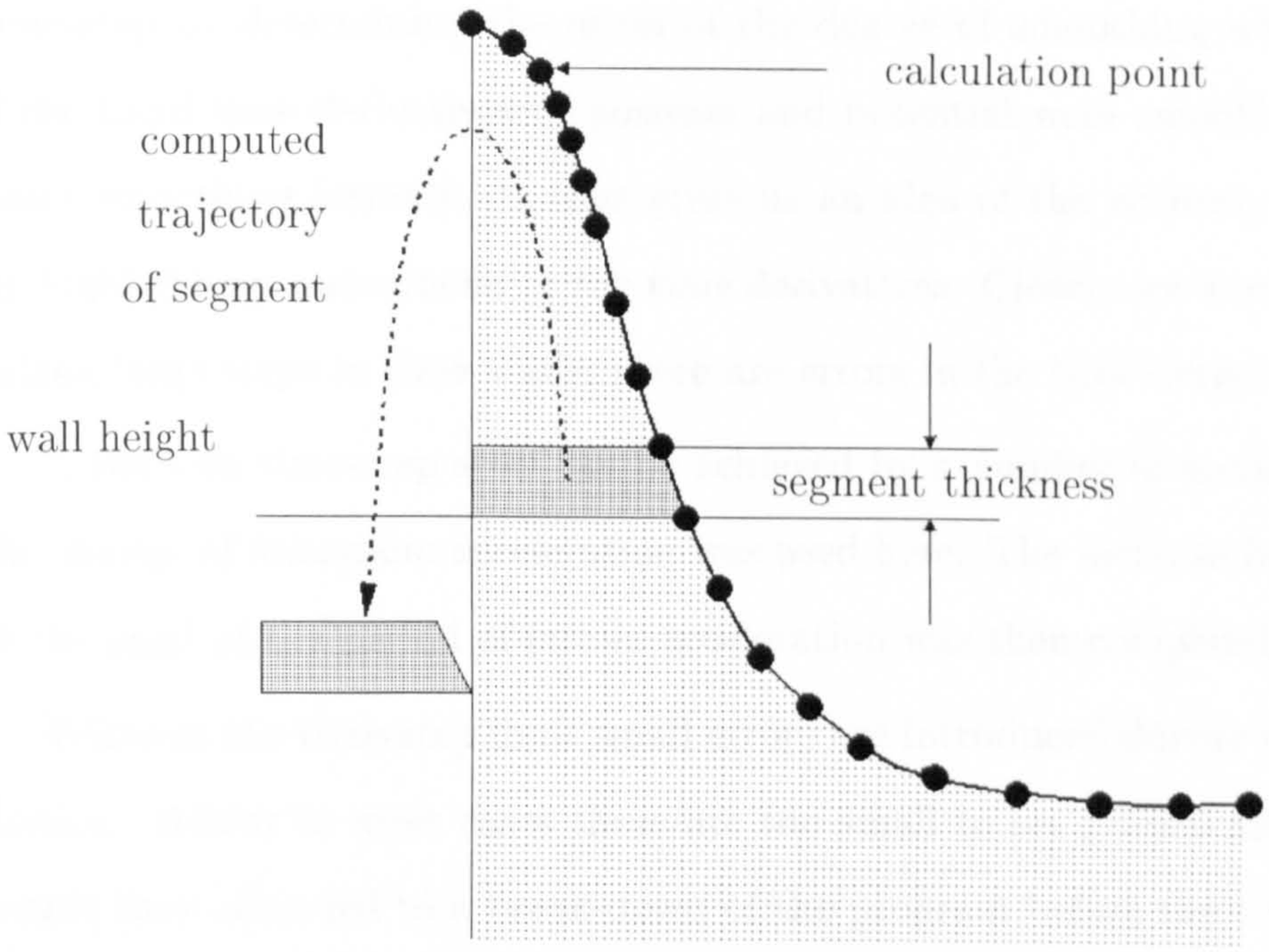

Slices were identified by stepping in time. The length of each time step and the vertical velocity together determining the thickness of each slice. Too short a time-step means good resolution but long computation times, too long a time step gives poor resolution. A time step size was chosen such that the thickness was always less than $10^{-4}d$, here d is the undisturbed water depth.

As the wave approaches the wall there is a period of rapid vertical acceleration of the surface at the wall. The acceleration of surface particles can reach several g even in milder wall collisions. For steeper waves this acceleration can be much greater. In such collisions, rather than the wave directly impacting on the wall it appears as though the surface at the wall suddenly flips through creating a strong vertical jet. This type of collision has been explored in detail in Cooker & Peregrine (1990).

The time-stepping size though the phase of rapid acceleration has to be sufficiently small. Although normal time-stepping here does not appear to cause any problems in program it does lead to a sudden temporary increase in the 'roughness'

of the solution. An estimate of the 'roughness' of the calculations is made at each time-step by determining the norm of the degree of smoothing which would arise if the third time derivatives of position and potential were smoothed using an 11-point smoothing formula. It thus gives us an idea of the accuracy of the solution by highlighting inaccuracies in the time derivatives. Clearly we would wish to avoid taking large steps in time whilst there are errors in the time derivatives.

A limit on time-step sizes can be achieved by a number of methods. A limit on the change of maximum acceleration was used here. The increase in roughness seen at the start of the period of strong acceleration was then completely avoided.

Without the time-step limit small errors are introduced during this phase of the motion. Whilst in most cases these are too small to see graphically in the surface profile they often led to a break-down of the program before the time of maximum run-up was reached. In some cases, a small difference in using a reduced time-step was the shape of the jet produced. This in turn led to small differences in the overtopping estimate.

4.4.1 Limitations of simple model

In these calculations it is assumed that solitary waves are an accurate representation of the likely steepest incoming waves (see previous chapter). For the collision of solitary waves only the case of no surface tension and constant depth has been previously studied (Cooker 1990 for example). When the waves are steepened by interaction with the berm a range of motions can develop, including flip-through motions as described by Cooker & Peregrine(1990). Flip-through motion is very sensitive to wave shape and can produce very violent jets. The present model is only applied to situations in which free surface calculated by the potential flow solver has reached or passed the time of maximum run-up before breaking down. Thus we cannot model overtopping from breaking waves such as seen in figure 4.5, or the strong 'flip-through' impacts described by Cooker & Peregrine since in such cases we cannot compute up to the time of maximum elevation. Experiments (Juhl 1990) have

shown that of the thin, high jets resulting from 'flip-through' type motions, about one half of the water falls back without overtopping. If the wave breaks directly against the wall, the water spurts moderately high and in a variety of directions. If the wave has already broken any resulting jet is small and mostly fails to overtop the structure. Thus the cases to which our model is restricted are those which happen to be responsible for most overtopping.

Since we do not include waves that produce the violent high jets, we might expect our model to underpredict overtopping volumes at high crest free-boards. Experiments would include some events which produce very high jets, and thus some overtopping at heights not reached by our non-breaking approximation. We would expect our model results to reach lower crest free-boards than found experimentally for waves of a particular steepness on certain berms. For wall heights near the limit of the jet, it is essential that the jet tip is fully resolved using a sufficiently large number of surface calculation points. Since the jet stretches and thins, the calculations points which follow particles paths on the surface become spread out along the sides of the jet. Regridding can be used to ensure there is a sufficient number of points around the jet to accurately resolve its surface and velocity. In experiments dimensionless free-boards between 0.5 and 5 are often used. Clearly, our model is inaccurate for wall heights below the height of jet formation, or for waves where no significant jet is formed, i.e. where the force due to internal pressure on a fluid particle is not negligible compared to gravity. Thus for example it does not apply to surging over low walls. In practice this means that only solitary waves of steepness greater than $0.5\,d$ were used, and the results are restricted to the higher end of the dimensionless freeboard range (approximately to above $R_c/H = 1.8$ in the calculations presented here).

4.5 Results with gravity waves.

Since these calculations assume two-dimensional waves the overtopping volumes calculated are volume per unit length of the wall, q. The undisturbed water depth, d, is used as the unit of length in computations, so for example the wave height, H, is a dimensionless ratio of wave height to that water depth. Following the presentation of results in previous papers on overtopping rates, the quantities presented in the following section are in terms of the overtopping volume q/H^2, and dimensionless wall crest free board R_c/H, where R_c is the height of the top of the wall above the undisturbed water level. Note, for these solitary wave computations the undisturbed level corresponds to trough level in a periodic or irregular wave train.

The primary computations are for a solitary wave travelling over constant water depth to meet a vertical wall. The flow is relatively simple since no breaking is involved. However, a more relevant configuration is obtained by considering a berm giving shallower water in front of the wall. By using a conformal mapping in the solution of Laplace's equation, see Cooker *et al* (1990), an elliptical berm can be placed on the otherwise horizontal bed. In each case the profile of the berm is one quarter of an ellipse; the given width refers to the horizontal semi-axis and the height to the vertical semi-axis. Berms wider than $4d$ were not used as this led to a breakdown of the program due to wave breaking or formation of extremely thin jets before the maximum water height was reached. Such steepening of the wave profile over a wide berm is shown in figure 4.5.

These berms are also outside the realistic range of berm dimensions currently used in vertical breakwaters.

4.5.1 Without berm

Figure 4.6 shows the results of dimensionless overtopping against dimensionless crest free board for the case of a horizontal bed. The dimensionless overtopping volume is plotted on a logarithmic scale. For solitary waves of amplitude 0.5 or less, no

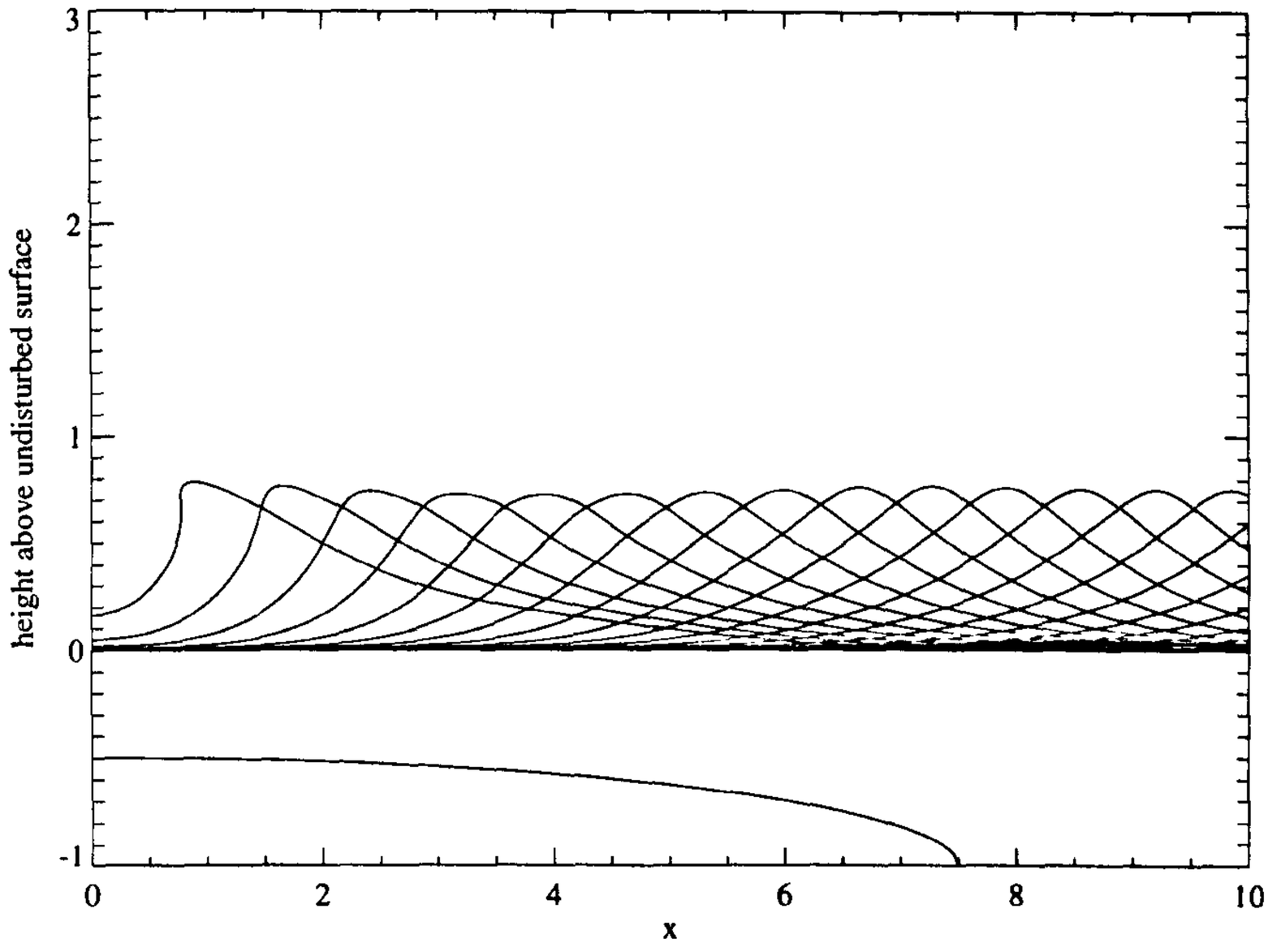

Figure 4.5: Solitary wave steepening over wide berm

significant jet is formed at the wall. Thus our model is not accurate for the wave of lower amplitude shown here for which it is only likely to give a rough indication of overtopping volumes. For most of the parameter range where we expect reasonable accuracy there is a roughly linear plot which indicates an exponential relation between wall height and overtopping volume. The variation with wave height reflects the greater height of run-up at wall for the highest waves. This is described in Cooker, Weidman & Bale (1997). Dimensionless overtopping volume increases with wave height.

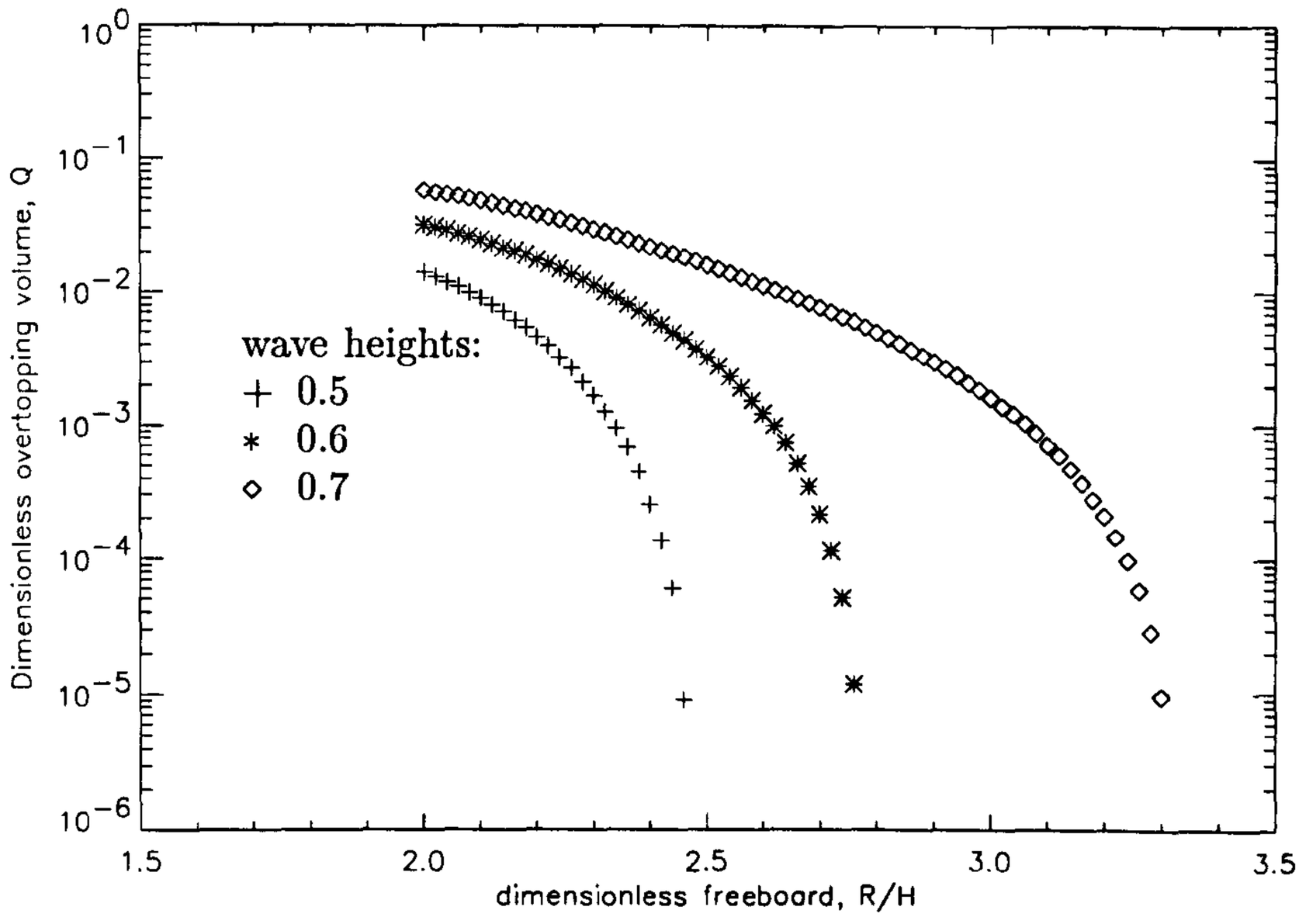

Figure 4.6: Solitary wave overtopping on water of constant depth; different wave heights, H

4.5.2 With berm

For cases with a berm a wave with $a/d = 0.7$ was used. From above this is likely to give us a good approximation to the type of motions found experimentally. It is also near the maximum inshore significant wave height which is found experimentally to produce maximum overtopping discharges (see Allsop *et al* 1995). For the case of a berm in front of the wall figures 4.7 and 4.8 show the results of dimensionless overtopping volume against dimensionless crest free board for a solitary wave with amplitude $0.7d$ for berm widths d and $2\,d$. These include a range of results for berms of different heights. Rather surprisingly, for berms of width d, $2d$, the overtopping decreases with increasing berm height. For these short berm widths, the higher berm interferes with the water motion near the wall. The influence on the shape of the resultant jet shape is small in the case of length d, but strong for the berm of length $2\,d$ (see figure 4.10 for example), making it increasingly wide and short. Such "table-like" elevations are one of the characteristic extreme standing or reflecting wave behaviours seen experimentally (Thais & Peregrine, in preparation).

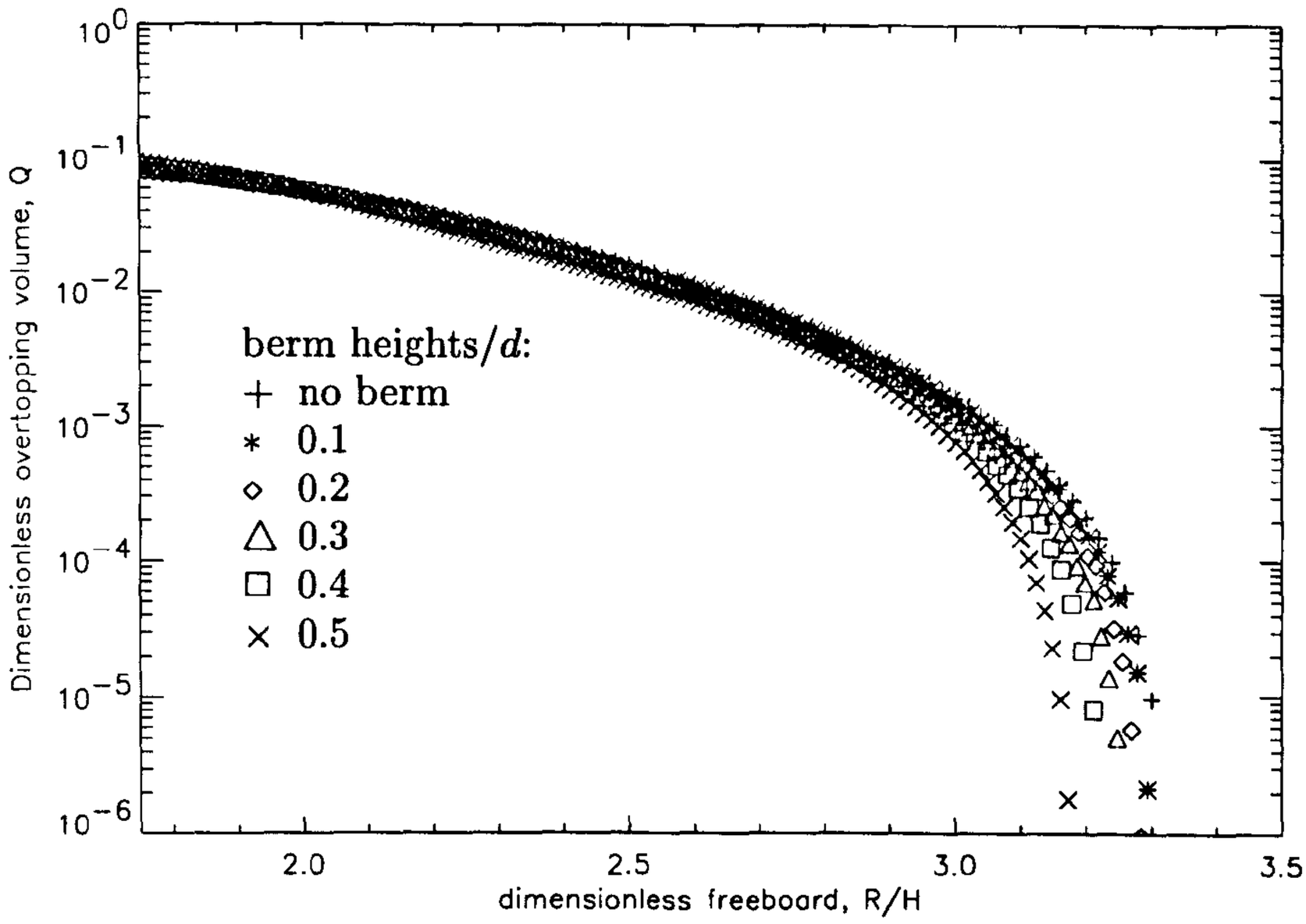

Figure 4.7: Solitary wave overtopping; berm width = d, different berm heights. $H = 0.7d$

It was noted in the introduction that previous work with impact pressures has highlighted the effects of local changes to the structure close to the wall. The above calculations show that the local geometry can equally strongly affect overtopping volumes. It can be seen in figure 4.10 that the berm forces the water level at the wall up earlier than in the case with no berm. The result is that the strong accelerations normally seen at this time are reduced and the water just sloshes smoothly against the wall. In this case the reduction in the violence of the collision also corresponds to a reduced impact pressure at the wall. However, since the motion of the water is directed up by the berm at the wall this may give larger overtopping volumes at low crest free-boards. This is beyond the scope of our current model. For berms of width $3\,d$ (figure 4.9) the effect seen with the $2\,d$ berm and that of wave steepening appear to cancel each other. The overtopping predicted is close to that with no berm. For wider berms still, wave steepening is the dominant effect, which increases the violence of the impact and the corresponding overtopping volume.

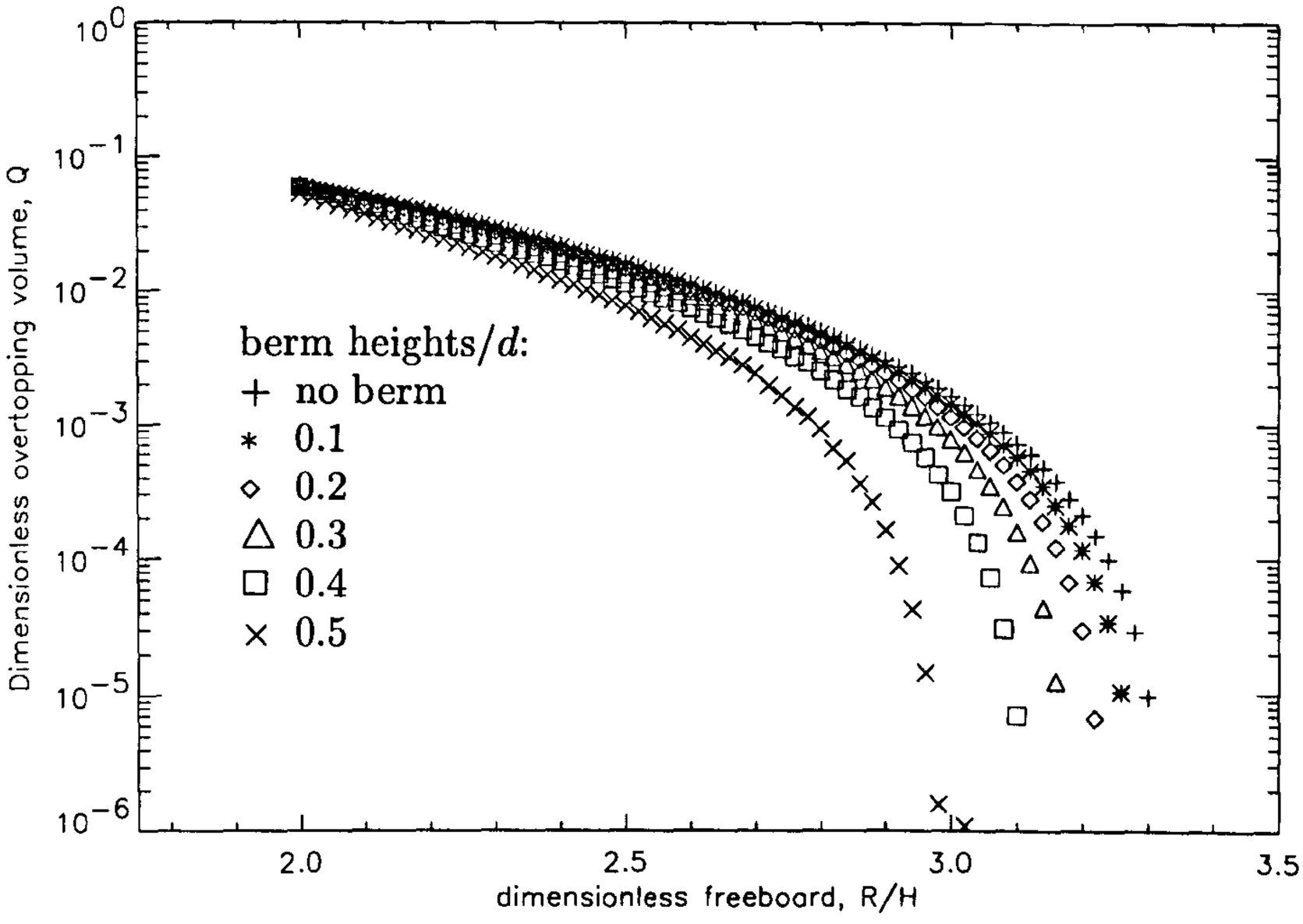

Figure 4.8: Solitary wave overtopping; berm width $= 2d$, different berm heights. $H = 0.7d$

Similar data is plotted in figures 4.11 and 4.12 which show the dimensionless overtopping volume against dimensionless crest free board for berms of fixed height but different width. For dimensionless free-boards up to 2.5 there is little difference; it is only in the free-boards near the maximum run-up height that the influence of the berms can be clearly seen. Results show that a berm of width less than $3d$ decreases q, compared to the no berm case. Over wider berms, the wave steepens giving a stronger jet on impact. (see figure 4.13). A clear exponential relation between individual dimensionless overtopping volume and dimensionless free-board (i.e. a straight line on the graph) can be see over much of the valid range.

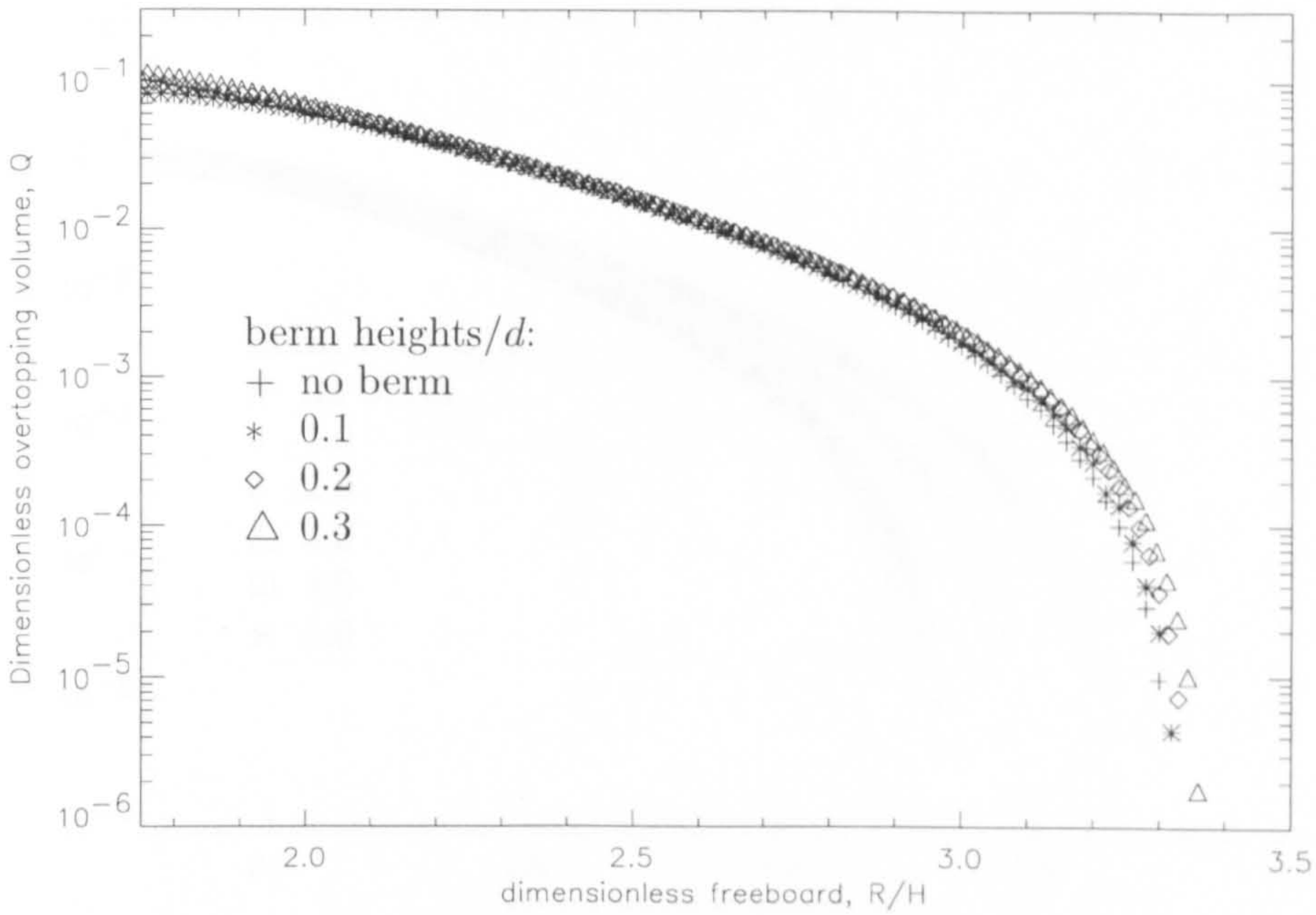

Figure 4.9: Solitary wave overtopping; berm width $= 3\,d$, different berm heights. $H = 0.7d$

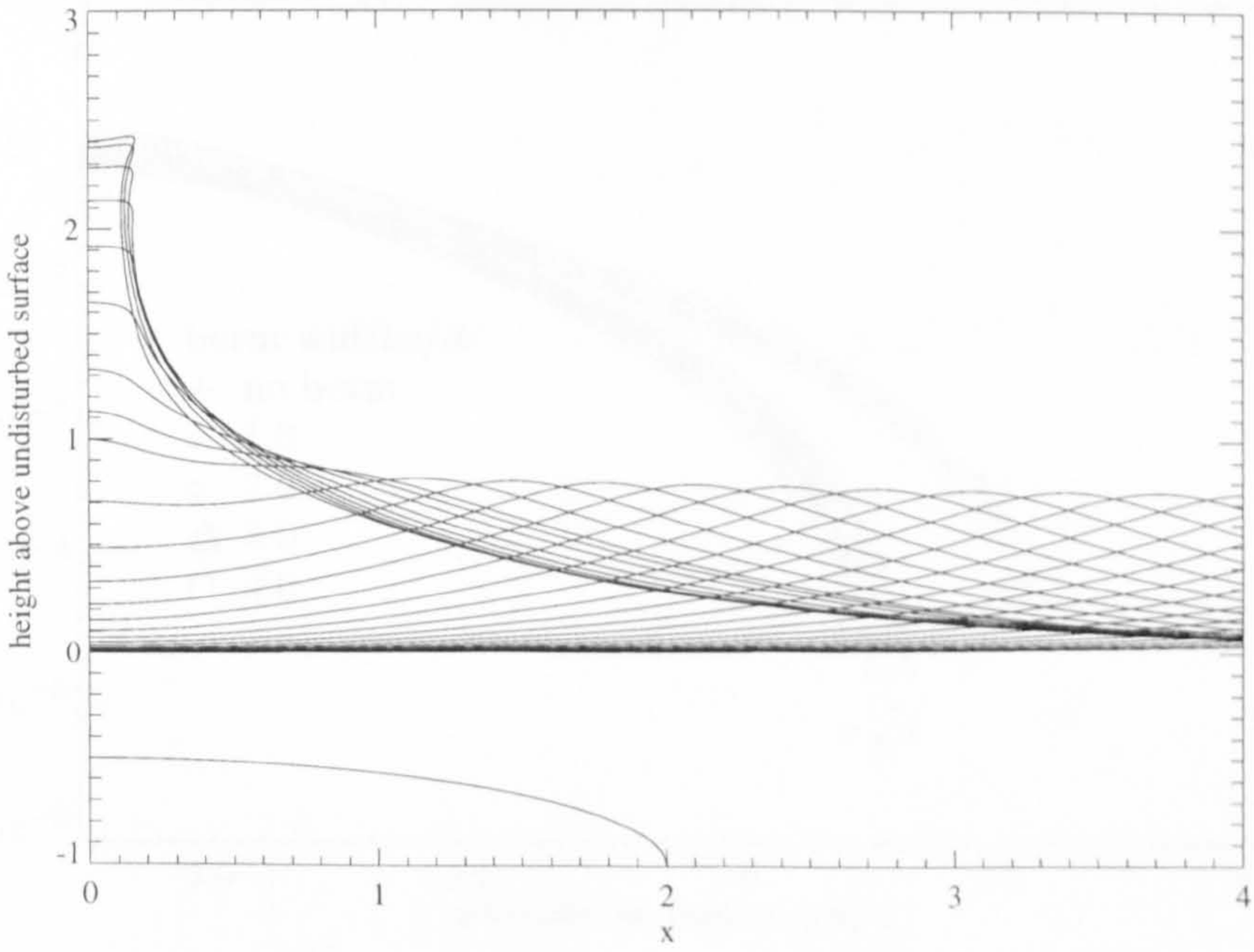

Figure 4.10: Vertical wall with berm width $2\,d$, height $0.5\,d$. $H = 0.75d$

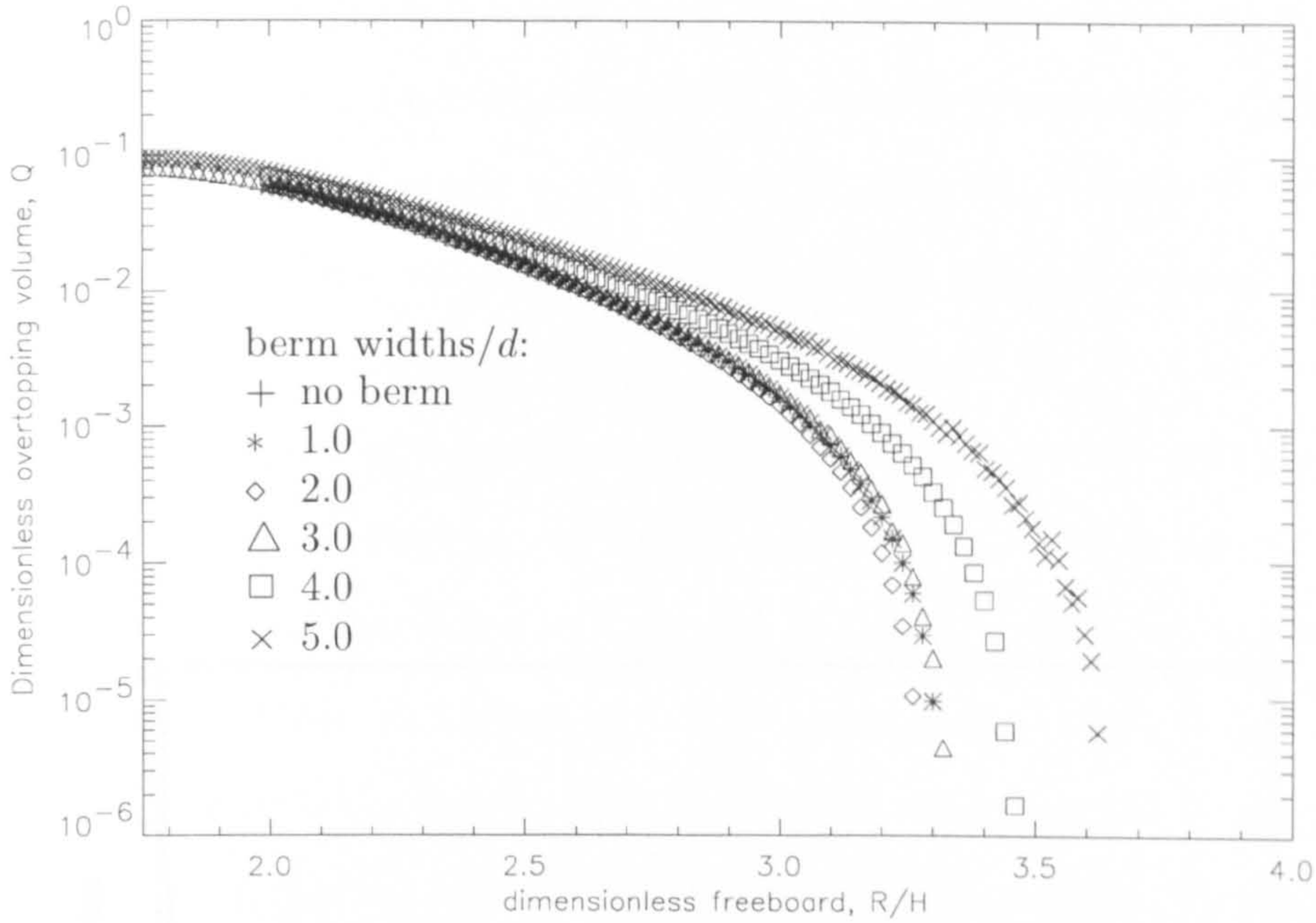

Figure 4.11: Solitary wave overtopping; berm height $= 0.1\,d$, $H = 0.7d$.

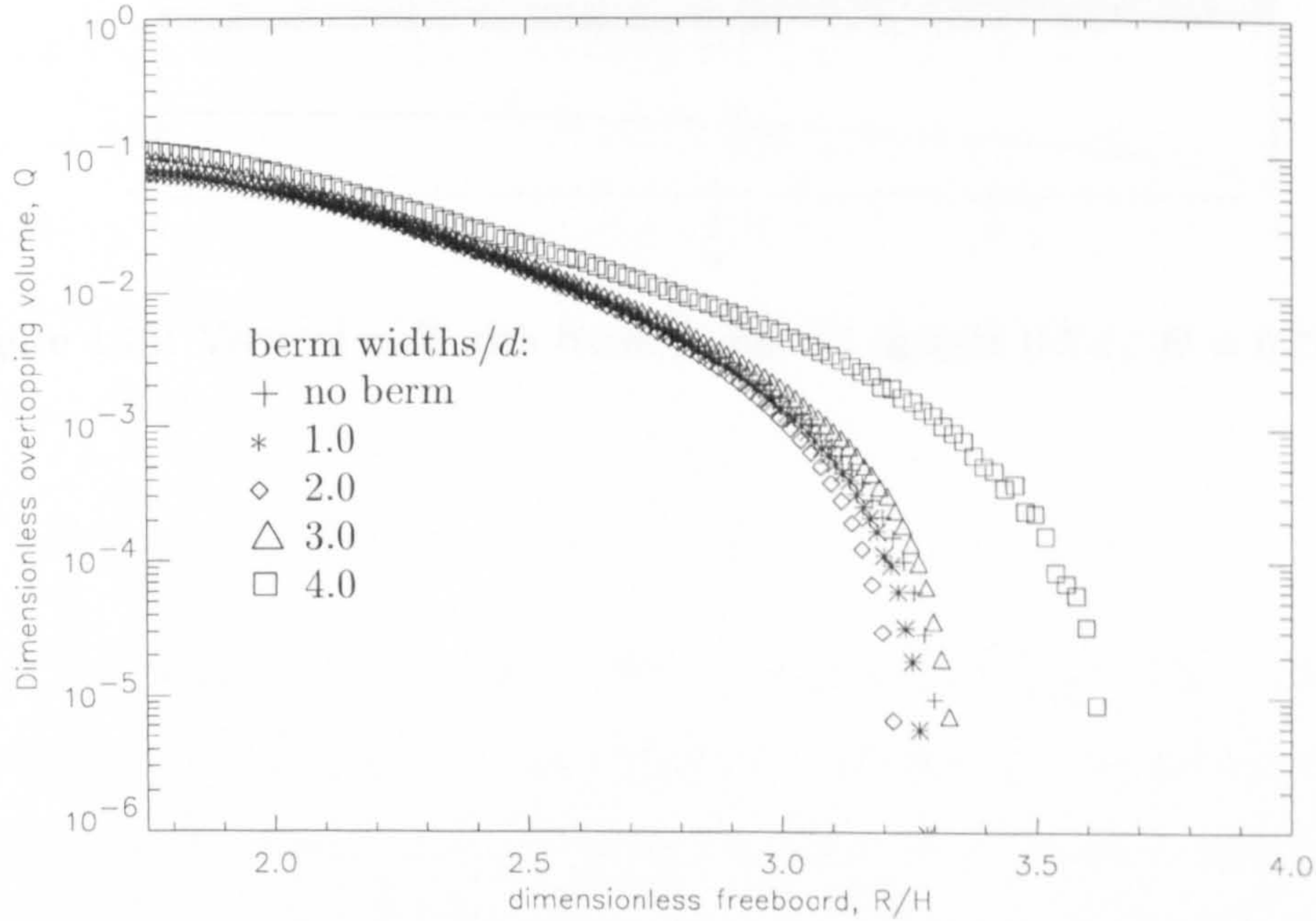

Figure 4.12: Solitary wave overtopping; berm height $= 0.2\,d$, $H = 0.7d$.

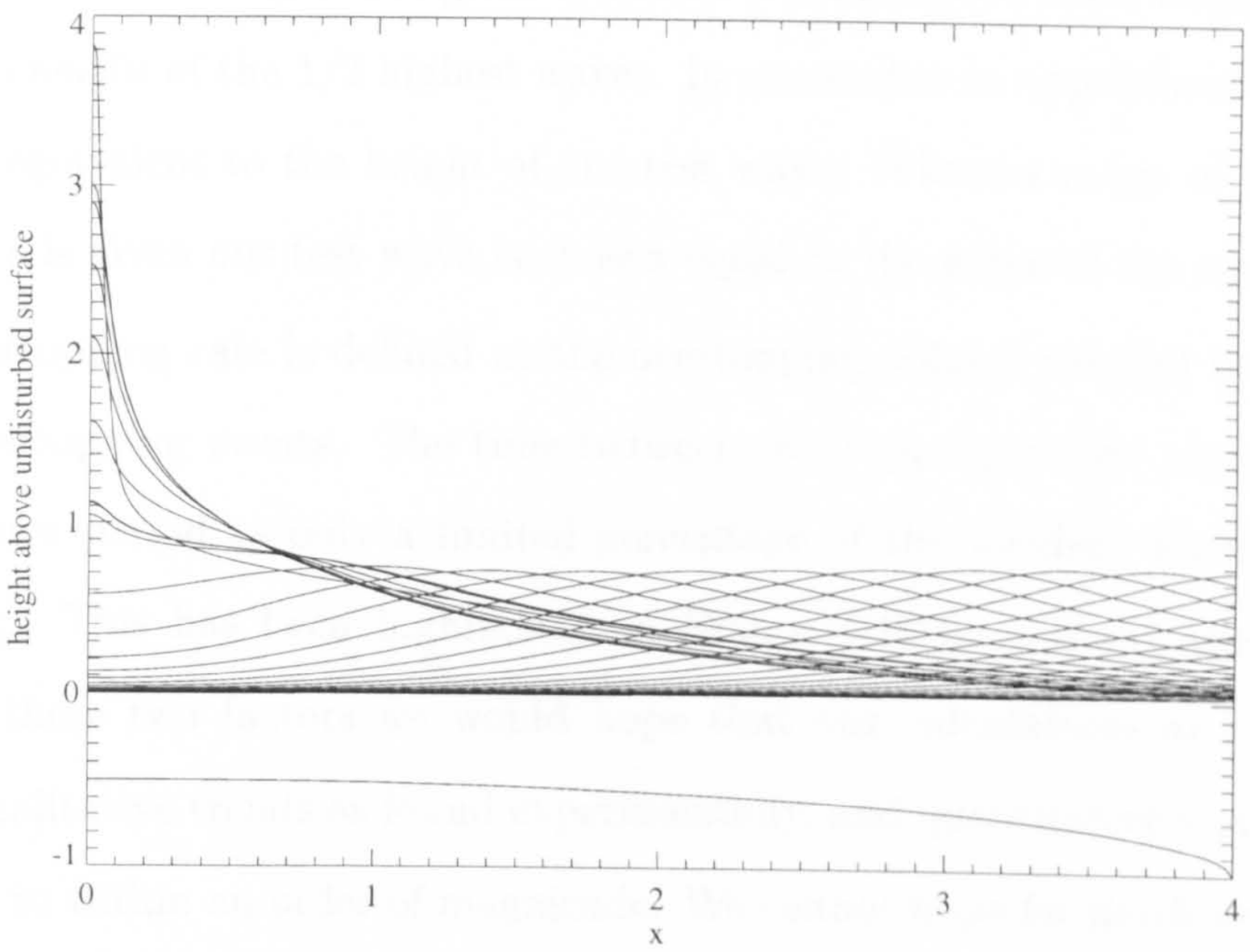

Figure 4.13: Vertical wall with berm width $4\,d$, height $0.5\,d$, $H = 0.75d$.

4.6 Comparison to existing experimental data

To the author's knowledge there are no experimental results for individual overtopping volumes for a vertical breakwater in which the required geometric and hydraulic characteristics are all given. Indeed, the purpose of this study is partly to fill that gap. We can however draw some parallels between the calculations presented here and some existing experimental results. From the knowledge of wave steepnesses (defined in related experimental work as wave height/distance between crests) and the nondimensional wave speed in our model, we can work out a rough overtopping rate. Values for wave heights are given in terms of a significant wave height, defined as the mean height of the 1/3 highest waves. In conversion to approximate rates we use this as equivalent to the height of our test wave. Where a range of significant wave heights is given our test wave is chosen equal to the mean of the range.

The overtopping rate is defined as the overtopping volume divided by the time between overtopping events. The time between overtopping events usually differs from the wave period as only a limited percentage of the incident waves produce overtopping. This has been highlighted in Franco (1994). Finally then, taking account of these two factors we would hope that our calculations at least show the same qualitative trends as found experimentally, and quantitatively give results comparable to within an order of magnitude. We cannot hope for much better than this due problems of converting individual overtopping volumes to random wave overtopping rates.

4.6.1 Franco 1994

Franco (1994) conducted 50 model tests at a scale of 1:30 on a plain vertical wall breakwater. The main purpose of the study was to determine the influence of wave period and spectral shape on overtopping volumes. A probability distribution of overtopping volumes per wave is presented. From the experimental results a global formula is derived which directly gives the overtopping volume per wave as a function

of the crest free-board, significant wave height and mean wave period. We can test our dimensionless overtopping volumes against the global empirical formula derived by Franco by calculating the exceedence probabilities. We would hope that it would follow the same trend, and predict realistic probabilities. A more accurate comparison is not possible since formula is for a wide range of wave conditions, only a small percentage of which produce overtopping. A time between overtopping events for our waves is estimated by using the wave speed and calculating a rough distance between waves using the steepness limits used in experiments. From figure

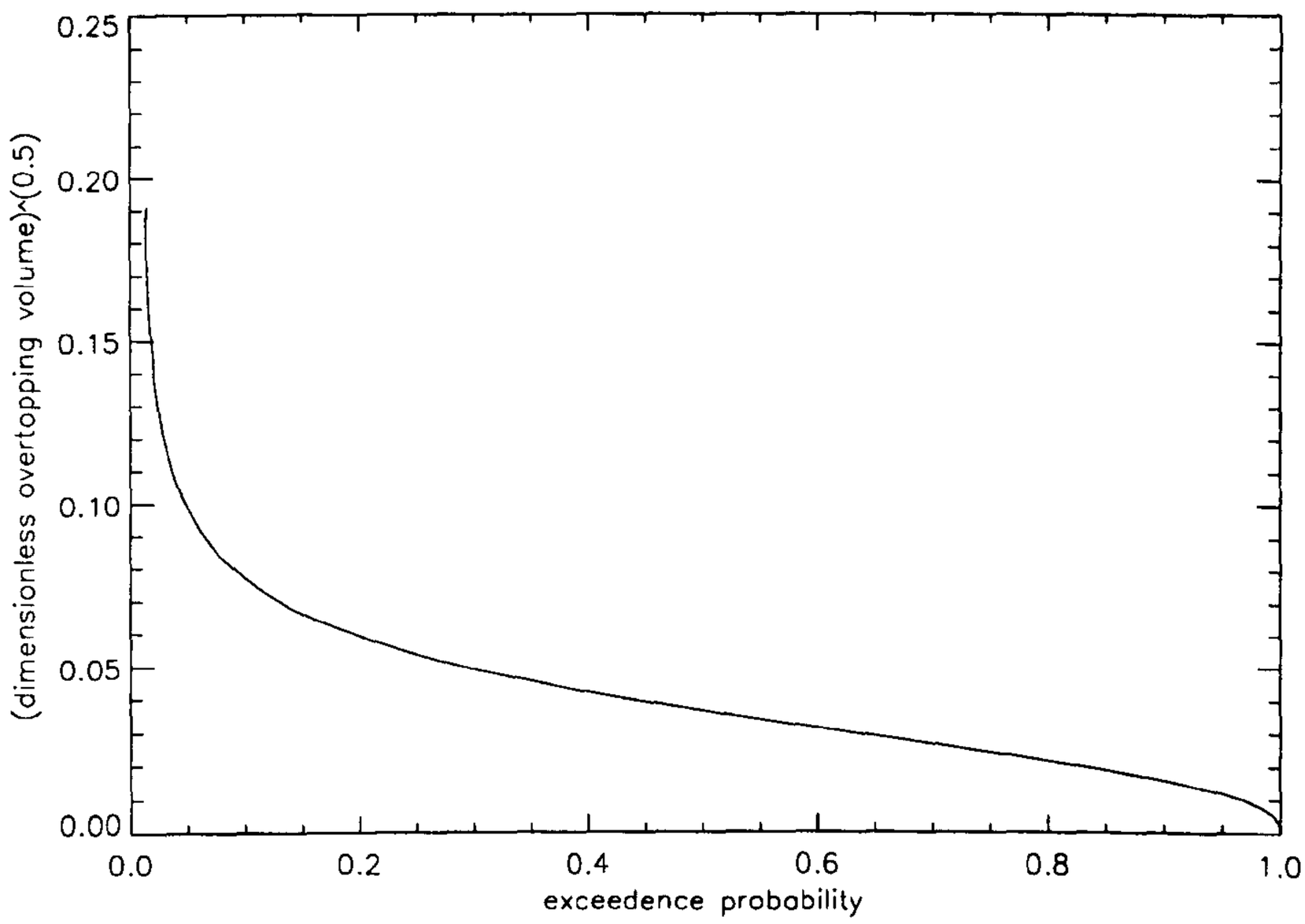

Figure 4.14: Exceedence probabilities for our non-dimensional results.

4.14 we can see that there is a sharp rise near the zero probability but for most of the probability range the graph approximates a straight line which mirrors the trend found in Franco (1994).

4.6.2 Juhl (1995)

A series of model test are carried out by Juhl (1995). Results for dimensionless overtopping rates are presented for differing angles of wave attack and wind velocities. Our model is only applicable to the results with zero wind velocity and normal wave

attack. Again, we have to be careful when comparing our model to results with overtopping rates. Suppose we assume that only 10% of waves produce overtopping, a likely figure from various experimental results. Our model thus only gives a rough approximation to the experimental data.

Figure 4.15 compares the rate of overtopping found with zero wind velocity and 0^o angle of wave attack to that predicted by our simple model over its range of validity. The period between overtopping events used to find the rate is derived by assuming the a periodic train of solitary waves which give a steepness equal to the average used in the tests, multiplied by the probability. We see that our model produces results that are of the same order of magnitude over most of the range. However there is a tendency for under-prediction at higher dimensionless free boards. This is explained earlier. The non-dimensional overtopping rate compares well to

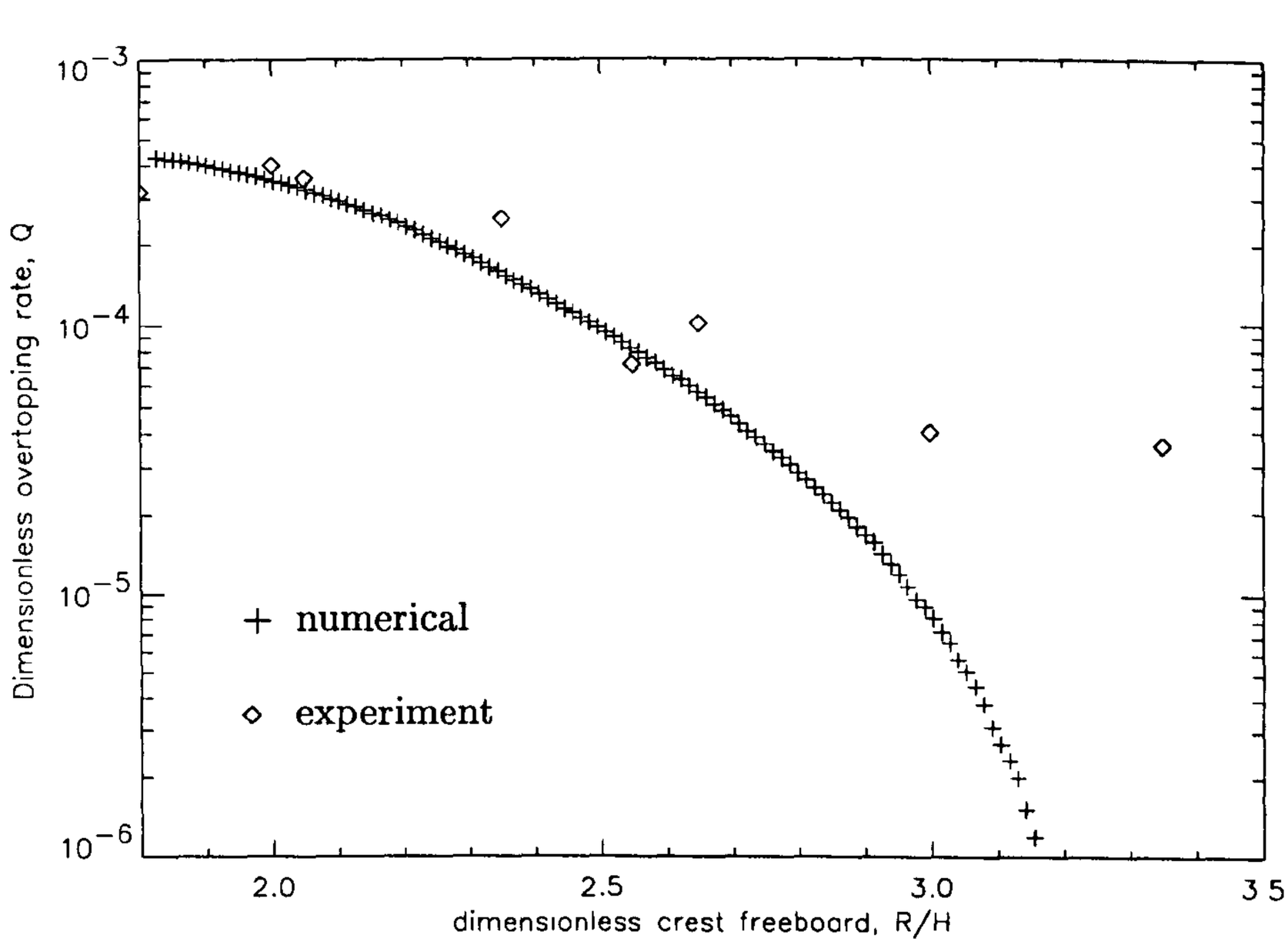

Figure 4.15: Comparison of estimated overtopping rates with Juhl (1995) (wind speed$=0$, angle of attack$=0^o$)

that of Juhl for dimensionless free boards in the range 2 to 3.

4.7 Overtopping with gravity-capillary waves

It has been noted in past experiments and analytic calculations that parasitic capillary waves are especially noticeable when the underlying gravity wave has wavelength between 5-50cm. Surface tension plays an important local role where-ever the surface curvature is sufficiently high. In the calculations above, extremely thin jets are often produced which have a region of very high curvature at the tip. Surface tension can have a significant effect on the shape of the jet at this tip. This in turn might effect the predicted overtopping volumes. There are two ways in which surface tension is likely to effect overtopping - by affecting the profile of the incident wave, and by affecting the resulting jet shape. We ask, at what scale would surface tension become significant in overtopping experiments?

In the rubble mound experiments of Juhl and Sloth (1994) for example, a water depths between 0.4m and 0.35m, crest free-boards between 0.05m and 0.1m and significant wave heights between 0.05m and 0.11m are used. A wave of height 5 to 10cm is certainly within the length scales over which we might expect surface tension to play an important role. This shown by the profiles of such waves (both periodic and solitary) which have been presented in chapter 2.

The lack of data on scale correction factors to date has been reported as substantially hindering the application of research results to practical engineering analysis or design (Oumeraci *et al* 1996). Using previous work in the laboratory and field, initial scale correction factors to be used for wave impact pressures / forces have previously been derived, but there exist no such correction data for overtopping events or indeed whether such a correction is necessary.

Our model permits the inclusion of surface tension in the evolution of the surface. There are, of course, other scale effects not included in our model. These include the break up of jets into water drops and the effects of any wind. There may also be problems including any air entrainment effects. We can however see if the action of surface tension on the wave and jet profile for the scale of wave flume experiments

makes a difference in overtopping volumes. As previously mentioned, in experiments ordinary overtopping occurs when the crest of a standing wave reaches higher than the crest of the structure. This normal mode for overtopping would then be well modelled here as there is little break up of the jet.

The two different starting conditions were tested. One is two solitary waves, sufficiently far apart so the that there is no initial interaction between them. Parasitic capillaries quickly become established on the forward face of the wave only for very small depths for the main test wave (a/d=0.7) used. Profiles at the time of collision are reported in the last chapter. Due to the unsteady nature of the surface, the full train of parasitic capillary waves may not have time to develop for the small scale waves if they are started close together. To investigate the effect of parasitic capillaries we can alternatively include surface tension just for the wave collision by restarting calculations from pure gravity wave runs to find the effect on the jet. The two different approaches were found to make very little difference to the final overtopping volumes predicted in all case except for the very shallow 1 centimetre depth. Here the parasitic capillary train became too steep to continue accurate computation shortly before collision of the main wave crest. The results are described in terms of the properties of clean water, and hence the description of water depth is used to specify the strength of surface tension.

Capillarity

Liquids display properties of both cohesion and adhesion. Both of these are forms of molecular attraction. Surface tension is due to cohesion of particles at the surface of the liquid, while adhesion enables a liquid to adhere to another body. Both cohesion and adhesion are important when considering the forces at a contact point between three media in equilibrium. Consider a liquid in contact with a vertical solid in equilibrium. Whether the point of contact is raised or depressed at the solid depends on whether adhesion of the liquid to the solid is more or less effective than

the self cohesion of the liquid.

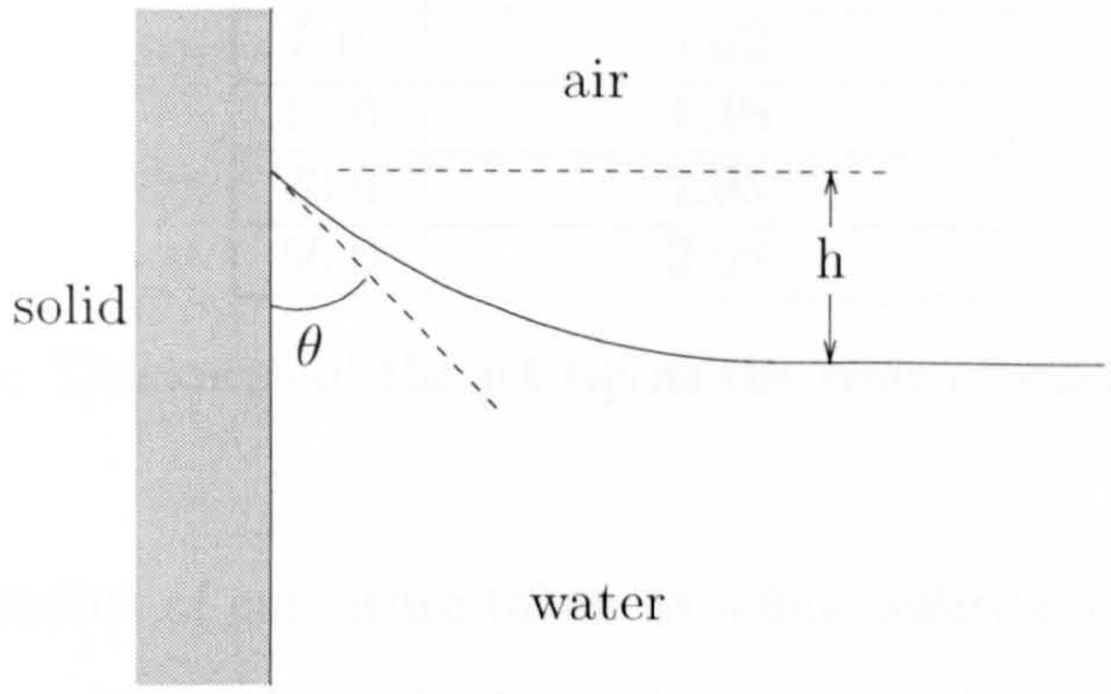

Figure 4.16: Imbalance of cohesive and adhesive forces can lead to an elevation of the equilibrium contact point.

The adhesive force depends on the nature of the solid and the liquid. It is affected by small scale roughness of the solid and on its absorption of both impurities and the liquid. The symmetric collision of two solitary waves is used to here model the impact of a single solitary wave against a vertical wall. Thus we ignore the difference between adhesive and cohesive effects. To include this difference would mean explicitly including the wall with possible values of the adhesive force for differing wall materials and roughnesses. In our symmetric approximation we implicitly assume a contact angle $\theta = 90^o$. In practice the contact angle may differ from this, and the water is not usually clean. For most solid materials the equilibrium contact angle will be $< 90^o$, i.e. a stronger adhesive force, with the water level at the wall raised. However, the contact angle will be greater, thus nearer to 90^o, for a liquid moving past a solid unless it is perfectly smooth and clean.

We can perform a dimensional analysis to see at what scale this approximation would affect the results presented here. For an air/water interface we assume the pressure may be regarded as constant in the air, whilst the liquid is of uniform density, ρ, and has pressure variation with height y due to gravity. The condition for equilibrium at any point of the two dimensional surface is then

$$\rho g y - T\left(\frac{1}{R}\right) = \text{const.}, \tag{4.4}$$

d/cm	(width of jet tip)/cm
2.0	0.66
5.0	1.02
10.0	1.49
20.0	2.05
50.0	2.56

Table 4.1: Thickness of the jet tip at the time of maximum run-up.

where R is the radius of curvature taken as being positive when the center lies on the air side of the surface. From this it can be calculated that the equilibrium height of the capillary rise h (see fig. 4.16) from an otherwise flat surface is given in terms of the contact angle by

$$h^2 = 2\frac{T}{\rho g}(1 - \sin\theta). \tag{4.5}$$

Thus the relevant length scale is $(T/\rho g)^{1/2}$. For the parameters chosen here this is approximately 0.27cm. This gives us a scale over which adhesive forces are important. We can compare this to the thickness of the jet tip at the time of maximum run-up (see table 4.1). For the smaller scales, the capillary length $(T/\rho g)^{1/2}$ represents a significant proportion of the jet thickness. Thus we can expect the results presented here to differ from experimental results by a small amount depending on the properties of the wall. The 90^o contact angle however will be a fairly good approximation as the water level at the wall rapidly rises.

4.8 Run-up of solitary type waves with surface tension

Chapter 2 shows how surface tension modified the shape of small scale gravity waves by producing a train of parasitic capillary ripples on the forward face for solitary waves with sufficiently sharp crests. Figure 4.17 shows the jet at the time of maximum run-up for a solitary waves with $a/d = 0.7$ and $d = 5$cm. A similar calculation for $d = 1$ cm did not reach the height of maximum run-up as the parasitic

capillaries broke against the wall before it was reached by the main wave. Further,

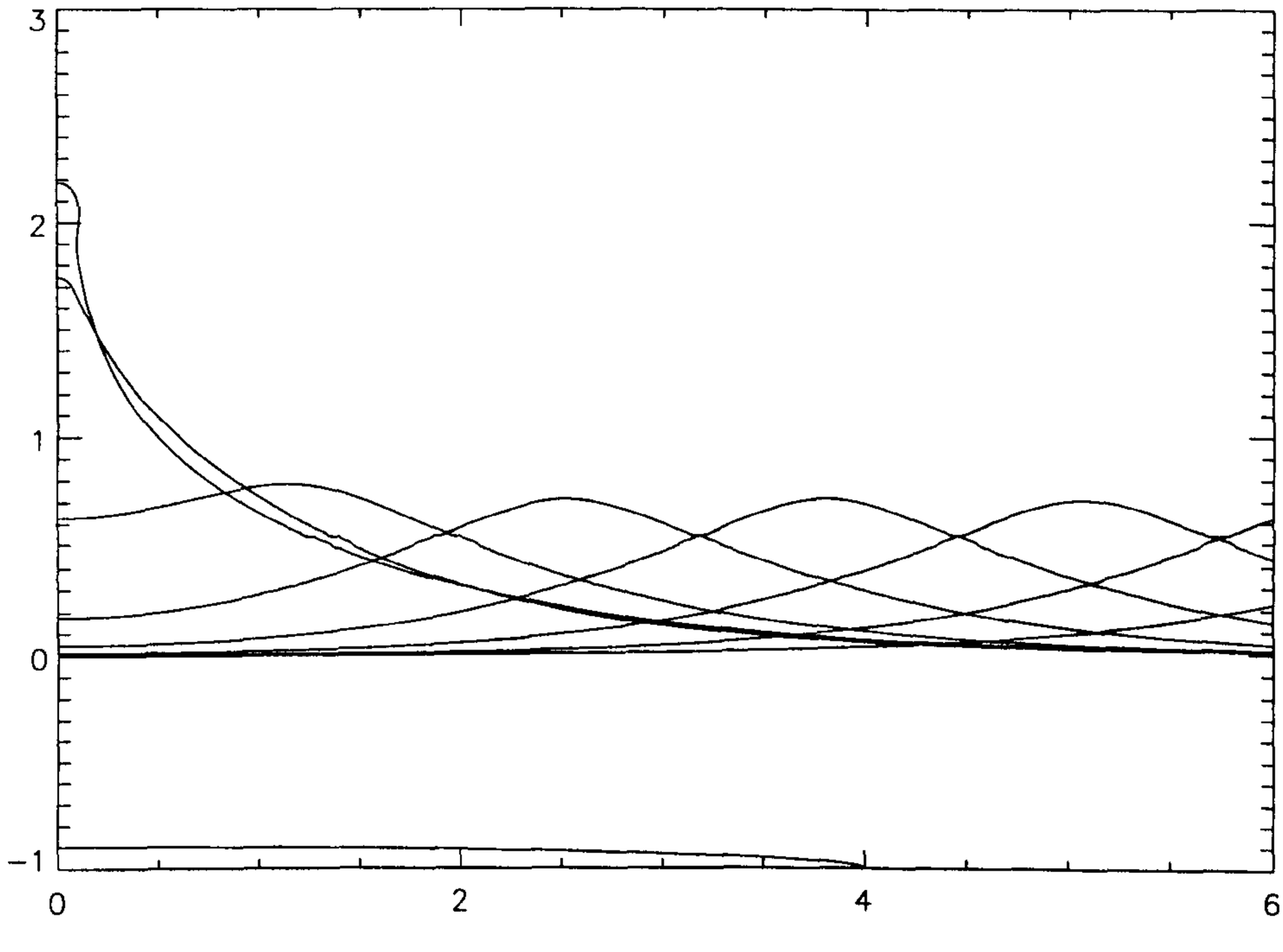

Figure 4.17: y/d against x/d at times up to maximum run-up for a solitary wave a=0.7 d, d=5cm, berm width=4 d, berm height=0.1 d.

figure 4.18 shows the jet profiles at the time of maximum run-up for solitary waves $a = 0.7d$, for d=2cm, 5cm, 10cm, 20cm, 50cm and ∞ (i.e. no surface tension). It can be seen that the jets have an increasingly rounded tip due to the action of surface tension over the time of run-up as the scale is reduced. Ripples down the sides of the surface can also be seen in the 2 and 5 centimetre cases. In the previous chapter it was seen that for the particular case of a solitary wave with $a/d = 0.7$ propagating on depths 5 centimetres and larger no noticeable capillary waves formed. Experimenters might then expect surface tension to play no measurable role in experiments. The main effect of the inclusion of surface tension is to modify the shape of the jet produced in the solitary wave collision. The jet is generally broader and shorter due to surface tension. A decreasing non-dimensional run-up height with increasing surface tension (i.e. decreasing scale) is found. For the $d = 5\,\mathrm{cm}$ case for example, the decrease in non-dimensional run-up height is approximately

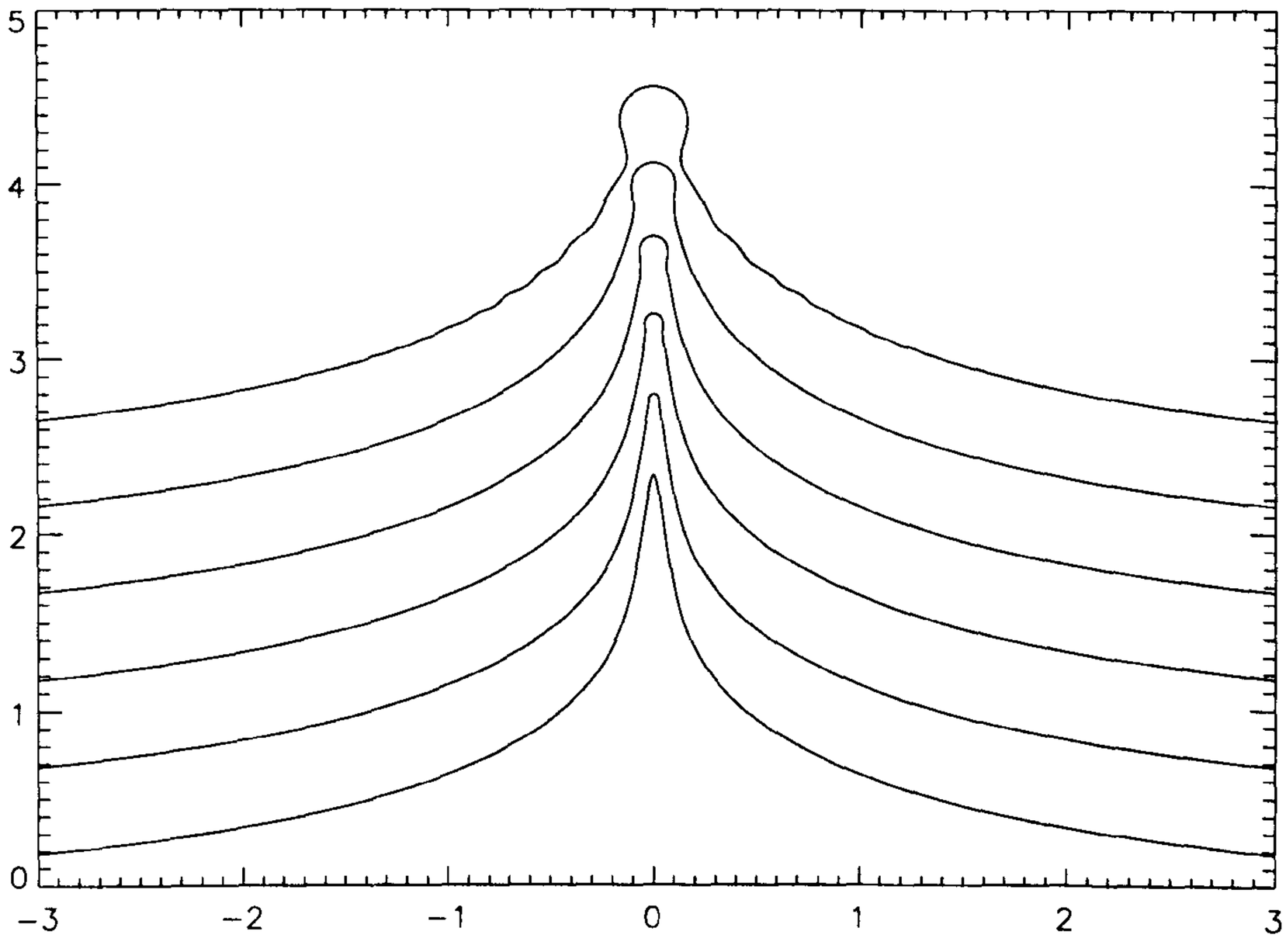

Figure 4.18: y/d against x/d at time of maximum run-up for a solitary wave $a = 0.7d$, for d=2cm, 5cm, 10cm, 20cm, 50cm and ∞ i.e. no surface tension. Profiles have been shifted vertically for clarity.

10%.

4.8.1 Overtopping volumes with surface tension

Figure 4.19 shows the dimensionless overtopping predicted by our model for a solitary wave of amplitude $a = 0.7d$. Results for depths of 5cm, 10cm, 20cm and 50cm are shown alongside the result for no surface tension. Results for depth 2cm are not shown: at this scale surface tension restricted the formation of a jet too much for our overtopping model to be valid. For small dimensionless free-boards we see that the results coincide. At higher dimensionless free-boards the difference in jet shape shown in figure 4.18 is affecting overtopping volumes. At smaller scale (higher nondimensional surface tension values) the run-up height is less, and the average velocity towards the wall is reduced. Even for the calculation for d=50cm there is a noticeable underprediction. Our neglection of the difference between cohesive

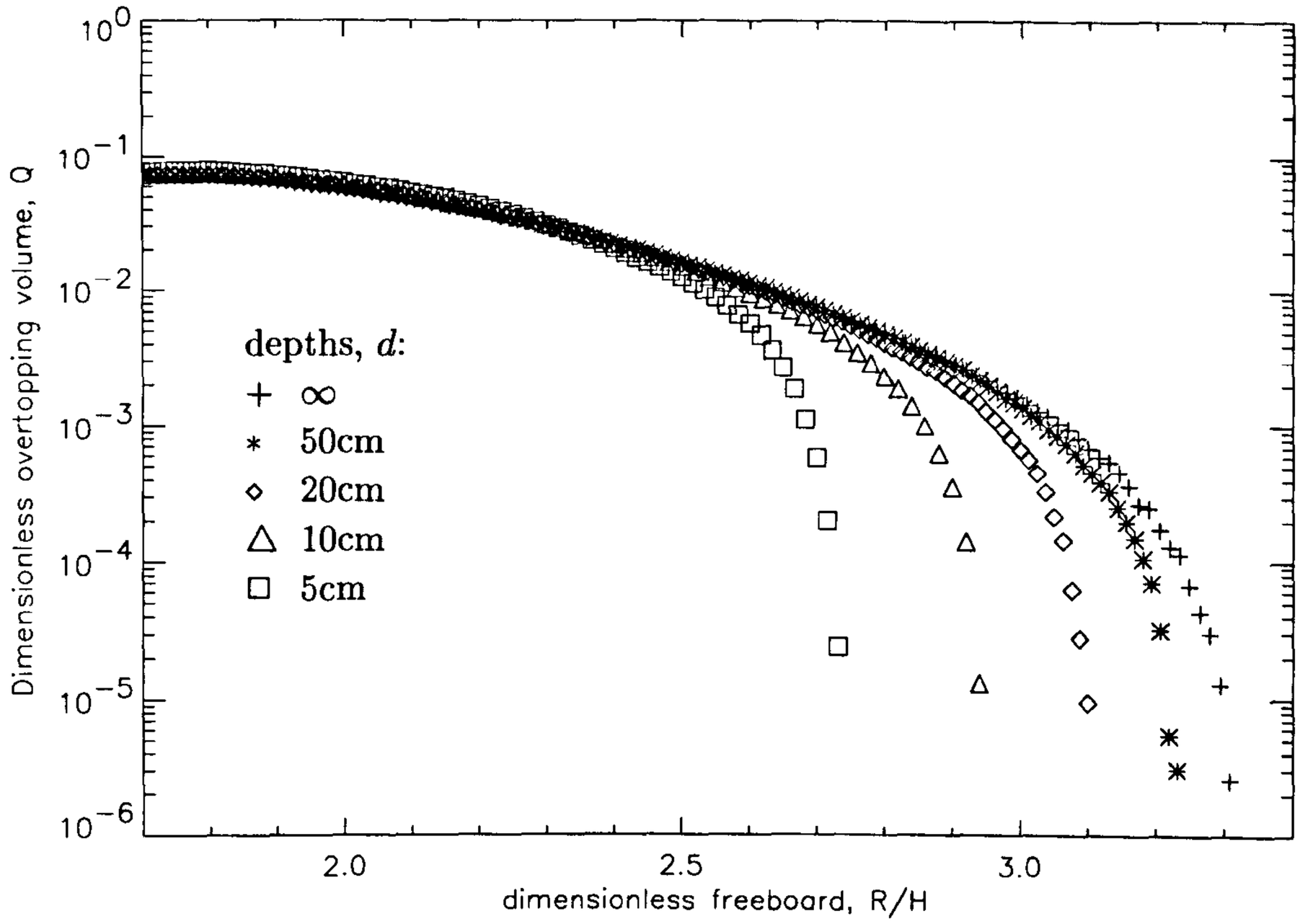

Figure 4.19: Dimensionless overtopping volume against dimensionless free-board for a solitary wave $a = 0.7d$, $d=$ 5cm, 10cm, 20cm, 50cm and ∞ i.e. no surface tension.

and adhesive forces at the wall by the assumption of a 90^o contact angle may affect the details of the results to a small extent, as would other the approximations made here. However, this would certainly not increase overtopping to the extent of the reductions shown here.

We can then see that even experiments carried out on depths of the order 20 to 50cm there is an underprediction at the upper limits of dimensionless free-board. For experiments where the incident wave is only 5-10cm relatively large underpredictions of overtopping volume and wave run-up can occur when scaling results back to full scale for use in breakwater design for $R_c/H > 2.6$. Of course here we are modelling only the non-breaking waves. More violent impacts produce jets beyond the scope of this simple model.

Figure 4.20 shows dimensionless overtopping for a wave on 5cm depth where the wave is steepened by a berm of width $4d$. As with no surface tension, wave steepening increases the strength of the jet produced. This can be seen in the

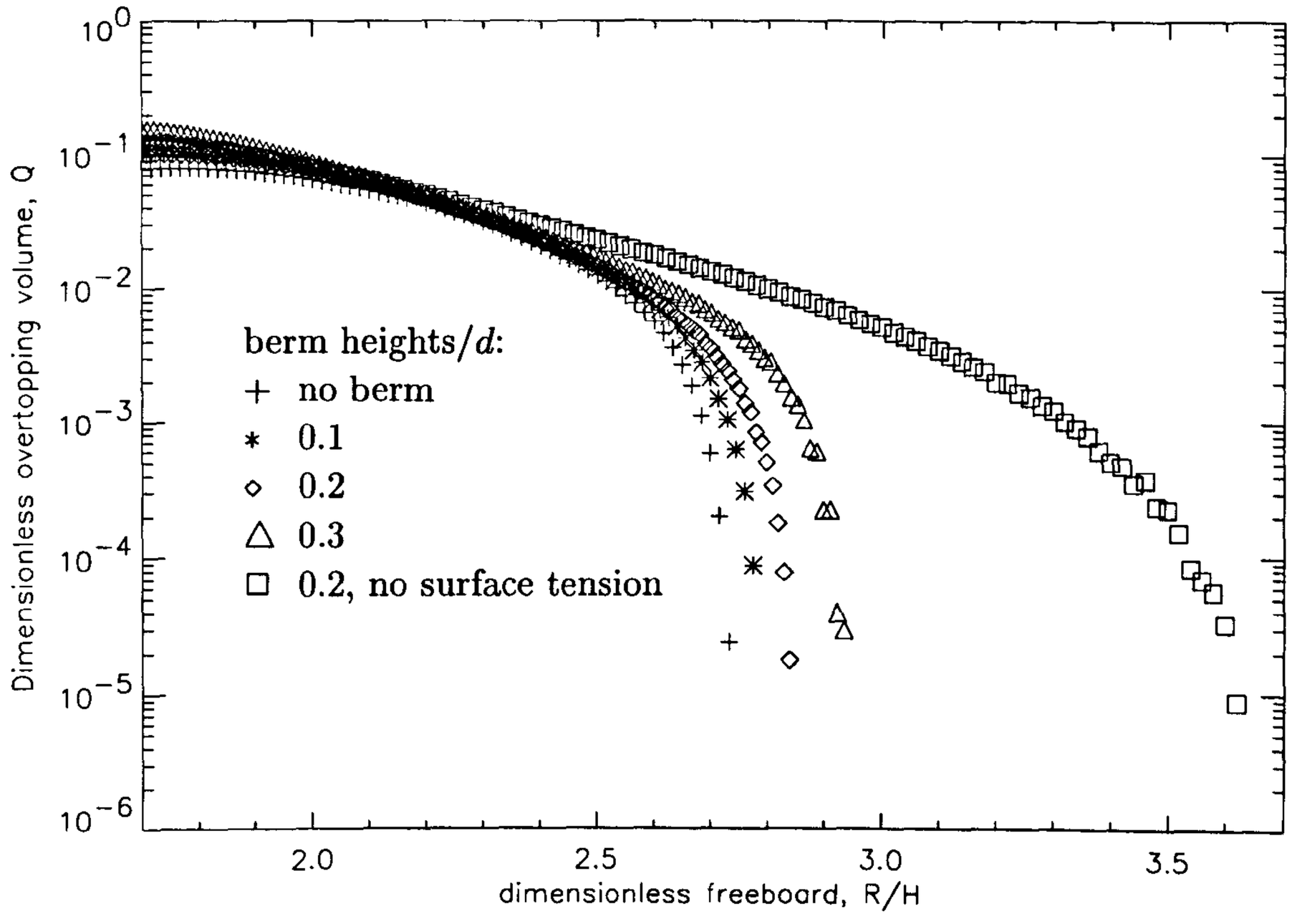

Figure 4.20: Dimensionless overtopping volume against dimensionless free-board on a berm of width $4\,d$ for a solitary wave $a = 0.7d$, for d=5cm with no surface tension.

trend towards a straight line for much of the range on figure 4.20 for higher berms. Without surface tension, overtopping is recorded for dimensionless crest free-boards of over 3.6, compared to only 2.85 with the corresponding 5cm calculation. It is clear then that extrapolating experimental results from such a small scale can give misleading values at high relative crest free-boards.

4.9 Further work and conclusion

It appears that this simple theoretical approach gives plausible results for overtopping volumes per wave for non-breaking solitary waves. When strong jets are formed, particularly in calculations were the wave is steepened by interaction with a long berm, it is found that the overtopping volumes have an exponential dependence on run-up for waves of a given height. Such an exponential relationship is similar to experimental results on overtopping rates (Franco, 1994, Juhl and Sloth, 1994, for

example). The method predicts the same trends as previously reported in measurement of overtopping rates. A comparison of the results to measured overtopping volumes per wave is needed to validate the method however. Quantitatively, overtopping rates compare well with experimental results of Juhl (1995), allowing for the expected underprediction at high relative crest free boards.

From the results it appears that for the parameter range studied the short high berms decrease overtopping, producing "table-like" elevations rather than thin jets. Wider berms steepen the incoming wave making its encounter with the wall more violent. In cases where the flow could be calculated up to the maximum run-up, wide berms tended to increase overtopping volume. Cases where the flow could not be computed up to the time of maximum run-up involved significant wave steepening, often to the point of breaking before impact with the wall.

Wind can also play a role in overtopping. A wind force would accelerates spray above wall height. It can thus act to significantly increase or decrease overtopping. Such a wind force could easily be incorporated into the simple mathematics of this overtopping model.

Most experiments are carried out at scales where surface tension plays a role in the jet dynamics. The effect of surface tension is generally not taken into account when extrapolating experimental results to full scale. Results here show that for overtopping rates that the effect of surface tension cannot be ignored for high crest free-boards. The action of surface tension on the tip of the jet leads to a considerable reduction in overtopping volume at relative crest free-boards greater than 2.6 for wave on depths up to the order of 20cm, and a corresponding reduction in non-dimensional run-up height. Since our model fits the most common mode of overtopping, we expect experimental results to be affected also, even though they generally include other modes of overtopping not covered here.

Since surface tension has a considerable affect on the wave run-up at small scale we might then expect other experiments in which this is a factor to be similarly af-

fected. For instance experiments to measure impact pressures typically scale results obtained from waves as small as 5 centimetres high. We can expect surface tension to have an affect at such scales and further work could investigate such problems.

Chapter 5

Conclusion

Surface tension as been added to versions of the non-linear potential flow solver of Dold & Peregrine (1986) for both periodic and unbounded domains. The point distribution in the program is changed so that sharp capillary wave troughs are accurately resolved. This has been used to investigate the formation of 'parasitic' capillary waves on steep gravity waves. Such waves are observed on gravity waves of length between 5 to 50 centimetres and have previously been studied experimentally and analytically. In particular our numerical results are compared with the theoretical predictions of Longuet-Higgins (1963, 1995) and experiments of Perlin, Ting & Lin (1993). We find that for most gravity wave steepnesses there is agreement with Longuet-Higgins (1963, 1995).

Consistent with the theory proposed by Longuet-Higgins (1995) we find that there exists a critical steepness above which stationary capillary waves in a frame of reference moving with the gravity wave crest are bounded away from the crest. The breadth of this 'blocked' region is wider than predicted by Longuet-Higgins as the capillaries modify the underlying flow to reduce the orbital velocity at the crest. However, we do find some small variation inside the blocked region as given by linear theory. A possible explanation is the nonlinearity of the capillary waves, which would travel at a lower phase speed.

We also find that the critical steepness coincides with a maximum in the amplitude of parasitic capillaries away from the Stokes wave crest. For the steepness

range studied we found that the near the crest the ripples remain large and do not decrease with steepnesses beyond critical. We also found that our calculated profiles for supercritical waves differ from that given by Longuet-Higgins in that single large bulge at the crest seen for subcritical waves remains. The theory presented by Longuet-Higgins gives the capillary wave disturbance only at a distance from the blocked region, so does not well represent the underlying crest for supercritical waves. This is a possible reason for these two differences.

A previously unreported jump in averaged Stoke's drift velocity is also found at the critical steepness. The apparent modulation phenomenon reported in the unsteady experiments of Perlin, Ting & Lin (1993) is found by our numerical method and possible mechanisms for its origin proposed. Significant modulations are only found for subcritical waves where waves generated by one crest can interact with those from the next. Further calculations show the generation of parasitic capillary waves on solitary waves.

In chapter 3 we consider surface gravity waves that are the usual waves in front of coastal structures. Scouring and the transport of suspended particles are of interest to the coastal engineer because they affect the distribution of sediments and shore line evolution. The reflection of waves by a vertical structure such as a breakwater means that the waves in front of the structure are well modelled by standing or near-standing waves if no breaking occurs.

Oscillatory flows above sea beds attract interest due to the large amount of sediment observed to be transported by such flows. Although hydrodynamic parameters on vertical walls under standing waves have been investigated experimentally and analytically by many previous authors, their profile on the bed under standing and near standing waves has received rather less attention. For standing waves on relatively deep water ($U_r \ll 1$), bed quantities other than pressure are well modelled by linear theory. For larger U_r however linear theory begins to break down, as found by previous authors in modelling experimental data. Trends in the behaviour

of hydrodynamic parameters as depth is decreased or wave steepness increased are identified.

On extremely shallow depths, ($U_r > 1$) linear theory is inappropriate. On such depths a solitary wave is a good model for the moving crest of a standing wave and some computations are presented for solitary wave collision at a vertical wall. It is found that under certain conditions pressure gradients resulting from the reflection of solitary waves may alone cause bed fluidisation.

Chapter 4 concerns another problem of interest to coastal engineers. The flow of water due to the overtopping of a vertical wall by waves is modelled. The waves are computed with the accurate irrotational flow solver of Dold & Peregrine (1986). The case where a jet of water is projected up the face of the wall is considered. A simple estimation is made from the computation for an the amount of water that can pass over the crest of a wall of finite height. Previous experiments have focused on overtopping rates rather than volumes. However volumes per wave are better indicators of the likely damage from overtopping. The results for overtopping volume per wave show a roughly exponential decaying dependence on the height of the wall above the still water level, in general agreement with experimental results for overtopping rates. Results are given for waves of differing height and also for various sizes of foundation berm in front of the wall. It is found that berm dimensions can strongly influence overtopping volumes by changing the behaviour of the reflecting wave.

The preceding chapters are brought together in the final sections. The hydrodynamic parameters used in the design of coastal structures are generally based on empirical formulae extrapolated from small scale experiments. The inclusion of surface tension allows us to perform the overtopping calculations for clean water at length scales commonly used in wave experiments. We find that at such scales surface tension can strongly affect the overtopping volumes and nondimensional run-up heights. This has significant implications for the validity of empirical formulae based

on laboratory experiments for much of the parameter range.

Bibliography

[1] AIRY, G.B. (1845) Tides and waves. *Encyclopaedia metropolitana.*

[2] ALLSOP, N.W.H., BESLEY, P., MADURINI, L. (1995) Overtopping performance and composite breakwaters, sea-walls and low reflection alternatives. *Final proceedings MCS-Project: Monolithic (Vertical) Coastal Structures.*

[3] ASTON, P.J (1993) Understanding the global solutions of the capillary gravity wave problem. *Wave Motion* **19** 113-141.

[4] BARNES, T., BROCCHINI, M., PEREGRINE, D.H. & STANSBY (1996) Modelling post-wave breaking, turbulence and vorticity. *Proc. Int. Conf. Coast. Eng.* (to appear).

[5] BAKER, G.R., MERION, D.I. & ORSZAG, S.A. (1981) Applications of a generalised vortex method to nonlinear free surface flow. *3rd Intnl. Conf. on Num. Ship Hydrodynamics, Paris.*

[6] BATCHELOR, G.K. (1967) An introduction to fluid dynamics. Cambridge U.P.

[7] BOUSSINESQ, J. (1872) Théorie des ondes et de remous qui se propagent. *J. Math. Pures. Appl.* **17**(2) 55-108.

[8] BENJAMIN, B.T. (1982) The solitary wave with surface tension. *Quart. Appl. Math.* **40** 231-234.

[9] CHANG, J.H., WAGNER, R.N. & YUEN, H.C. (1978) Measurement of high frequency capillary waves on steep gravity waves. *J. Fluid Mech.* **86** 401-413.

[10] CHEN, B., & SAFFMAN, P.G. (1980) Steady gravity-capillary waves on deep water. II. Numerical results for finite amplitude. *Stud. Appl. Maths.* **62** 95-111.

[11] CHESTER, W. (1968) Resonant oscillations of water waves. I. Theory. *Proc. Roy Soc A* **306** 5-22.

[12] CHESTER, W. & BONES, J.A. (1968) Resonant oscillations of water waves. II. Experiment. *Proc. Roy Soc A* **306** 23-39.

[13] CONCUS, P. (1962) Standing capillary-gravity waves of finite amplitude. *J.Fluid Mech.* **14** 568-576.

[14] CONCUS, P. (1964) Standing capillary-gravity waves of finite amplitude: Corrigendum. *J.Fluid Mech.* **19** 264-266.

[15] COOKER, M. (1990) The interaction between steep water waves and coastal structures. *PhD. thesis*, Univ. Bristol.

[16] COOKER, M. & PEREGRINE, D.H (1990) A model for breaking wave impact pressures. *Proc. 22nd Int. Conf. Coastal Eng.* ASCE, Delft. 1473-1486.

[17] COOKER, M., PEREGRINE, D.H., VIDAL, C. & DOLD, J.W. (1990) The interaction between a solitary wave and a submerged semi-circular cylinder. *J.Fluid Mech.* **215** 1-22.

[18] COOKER, M., WEIDMAN, P.D. & BALE, D.S. (1997) Reflection of a high amplitude solitary wave at a wall. *J.Fluid Mech.* to appear.

[19] COX, C.S. (1958) Measurement of slopes of high frequency wind-waves. *J. Mar. Res.* **16** 199-225.

[20] CRAIG, W. & STERNBERG, P. (1988) Symmetry of solitary waves. *Comm. Part. Diff. Eqs.* **13**(5) 603-633.

[21] CRAPPER, G.D. (1957) An exact solution for progressive capillary waves of arbitrary amplitude. *J. Fluid Mech.* **2** 532-540.

[22] CRAPPER, G.D. (1970) Non-linear capillary waves generated by steep gravity waves. *J. Fluid Mech.* **40** 149-159.

[23] CRAPPER, G.D. (1984) An introduction to water waves. Ellis Horwood Ltd.

[24] DAVIES, A.G. (1980) Field observations of the threshold of sand motion in a transitional wave boundary layer. *Coastal Eng.*, **4** 23-46.

[25] DIAS, F. (1994) Capillary gravity periodic and solitary waves. *Phys. Fluids* **6**(7) 2239-2241.

[26] DIAS, F., MENASCE, D. & VANDEN-BROECK, J-M. (1996) Numerical study of capillary gravity solitary waves. *Euro. J. Mech* **B** *Fluids* **15**(1) 17-36.

[27] DOLD, J.W. (1992) An efficient surface-integral algorithm applied to unsteady gravity waves. *J. Comp. Phys.* **103** 90-114.

[28] DOLD, J.W. & PEREGRINE, D.H. (1986) An efficient boundary integral method for steep unsteady surface waves. *Numerical methods for fluid dynamics II*, Ed. Morton, K.W., Baines, M.J. 671-679. Oxford.U.P.

[29] DUNCAN, J.H., PHILOMIN, V., BEHRES, M. & KIMMEL, J. (1994) The formation of spilling breaking water waves. *Phys. Fluids* **6**(8) 2558-2560.

[30] EBUCHI, N., KAWAMURA, H., & TOBA, Y. (9187) Fine structure of laboratory wind wave surfaces studies using an optical method. *Boundary-Layer Met.* **39** 133-151.

[31] FENTON, J.D. & RIENECKER, M.M. (1982) A Fourier method for solving nonlinear water wave problems: applications to solitary wave interactions. *J. Fluid Mech.* **118** 411-443.

[32] FRANCO, L. (1993) Overtopping of vertical face breakwaters: results of model tests and admissible overtopping rates. *Proc. First Workshop Monolithic (Vertical) Coastal Structures Project.*, Madrid.

[33] FRANCO, L. (1994) Further results of hydraulic model tests on wave overtopping probability distribution of overtopping volumes per wave *Proc. Second Workshop MSC-Proj.*, Milan.

[34] FRANCO, L., DE GERLONI, M., VAN DER MEER, J.W. (1994) Wave overtopping on vertical and composite breakwaters. *24th International Conference on Coastal Engineering, Kobe*, Japan.

[35] FULTZ, D. (1962) An experimental note on finite amplitude standing gravity waves. *J. Fluid Mech.* **13** 193-212.

[36] GRILLI, S.G. & SVENDSEN, I.A. (1990) Corner problems and global accuracy in the boundary element solution of nonlinear wave flows. *J. Engineering Analysis with Boundary Elements* **7**(4). 178-195.

[37] HALLERMEIER, R.J. (1982) Oscillatory bed-load transport: data review and simple formulation. *Continental Shelf Res.* **1** 159-190.

[38] HOGAN, S.J. (1979) Some effects of surface tension on steep water waves. *J. Fluid Mech.* **91** 167-180.

[39] HOGAN, S.J. (1980) Some effects of surface tension on steep water waves. Part 2. *J. Fluid Mech.* **96** 417-445.

[40] HOGAN, S.J. (1981) Some effects of surface tension on steep water waves. Part 3. *J. Fluid Mech.* **110** 381-410.

[41] HOGAN, S.J. (1988) The superharmonic normal mode instabilities of nonlinear deep water capillary waves. *J. Fluid Mech.* **190** 165-177.

[42] HUGHES, S.A. (1992) Estimating Wave-induced bottom velocities at a vertical wall. *ASCE Jour. Waterway Port Coastal and Ocean Eng.* **118** 175-192.

[43] HUNTER, J.K., & VANDEN-BROECK, J-M. (1983) Solitary and periodic gravity-capillary waves of finite amplitude. *J. Fluid Mech.* **134** 205-219.

[44] GODA, Y. (1985) Random seas and design of maritime structures. Univ. of Tokyo press

[45] IOOSS, G. & KIRCHGÄSSNER, K. (1990) Bifurcation d'ondes solitaires en présence d'une faible tension superficielle. *C. R. Acad. Sci.*, Paris. **311** (I) 265.

[46] IWAGAKI, Y.,TSUCHICA, Y., INOUE,M. (1966) On the effect of wind on wave overtopping on vertical sea walls. *Bull. Disas. Prev. Res. Inst. Kyoto Univ.* Vol. 16, Part 1. **105** 11-30.

[47] JAHNE & RIEMER (1995) Two-dimensional wave number spectra of small scale water surface waves. *J. Geophys. Res.* **95** (C7) 11531-11546.

[48] JUHL, J. (1995) Wave overtopping of vertical walls and influence of wind. *Proc. First Workshop Monolithic Coastal Structures Project.*

[49] JUHL, J. & SLOTH, P. (1994) Wave overtopping of breakwater under oblique waves. *24th Int. Conf. on Coast. Eng.*, ASCE, Kobe. 324-325.

[50] KING, D.B & SEYMOUR, J.R. (1989) State of the art in oscillatory sediment transport models. Near shore sediment transport. Ed., Seymour, R.J. 371-385.

[51] KINNERSLEY, W. (1976) Exact large amplitude capillary waves on sheets of fluids. *J. Fluid Mech.* **77** 229-241.

[52] KINSMAN, B. (1965) Wind waves, their generation and propagation on the ocean surface. Prentice-Hall, Inc., NJ. USA.

[53] KOGA, M. (1982) Bubble entrainment in breaking wind waves. *Tellus* **34** 481-489.

[54] KORTEWEG, D. & DE VRIES, G. (1895) On the change of form of long waves advancing in a rectangular canal, and on a new type of long stationary wave. *Phil. Mag.* **39**(5) 422-443.

[55] LAMB, H. (1932) Hydrodynamics. Cambridge U.P.

[56] LEVI-CIVITA, T. (1925) Détermination rigoureuse des ondes permanentes d'ampleur finie. *Math. Ann.* **93** 264-314.

[57] LONGUET-HIGGINS, M.S. (1963) Generation of capillary waves by steep gravity waves. *J. Fluid Mech.* **16** 138-159.

[58] LONGUET-HIGGINS, M.S. (1983) Bubbles, breaking waves and hyperbolic jets at a free surface. *J. Fluid Mech.* **127** 103-121.

[59] LONGUET-HIGGINS, M.S. (1986) Bifurcation and instability in gravity waves. *Proc. Roy. Soc. Lond.* A **403** 167-187.

[60] LONGUET-HIGGINS, M.S. (1987) The propagation of short surface waves on longer gravity waves. *J. Fluid Mech.* **177** 293-306.

[61] LONGUET-HIGGINS, M.S. (1988) Limiting forms for capillary-gravity waves. *J. Fluid Mech.* **194** 351-375.

[62] LONGUET-HIGGINS, M.S. (1989) Capillary-gravity waves of solitary type on deep water. *J. Fluid Mech.* **200** 451-478.

[63] LONGUET-HIGGINS, M.S. (1992a) Capillary rollers and bores. *J. Fluid Mech.* **240** 659-679.

[64] LONGUET-HIGGINS, M.S. (1992b) Theory of weakly damped Stokes waves: a new formulation and its physical interpretation. *J. Fluid Mech.* **285** 319-324.

[65] LONGUET-HIGGINS, M.S. (1995) Parasitic capillary waves: a direct calculation. *J. Fluid Mech.* **301** 79-107.

[66] LONGUET-HIGGINS, M.S. (1996) Capillary Jumps. *J. Phys. Ocean.* (to appear)

[67] LONGUET-HIGGINS, M.S. & CLEAVER, R.P. (1994) Crest instabilities of gravity waves. Part I. The almost highest wave. *J. Fluid Mech.* **258** 115-129.

[68] LONGUET-HIGGINS, M.S., CLEAVER, R.P. & FOX, M.J.H.(1994) Crest instabilities of gravity waves. Part II. Matching and asymptotic analysis. *J. Fluid Mech.* **259** 333-344.

[69] LONGUET-HIGGINS, M.S. & STEWART, R.W. (1964) Radiation stresses in water waves; a physical discussion, with applications. *Deep-Sea Res.* **11** 529-562.

[70] McGOLDRICK, L.F. (1965) Resonant interactions amoung capillary-gravity waves. *J. Fluid Mech.* **21** 305-331.

[71] McGOLDRICK, L.F. (1970) An experiment on second-order capillary-gravity resonant wave interactions. *J. Fluid Mech.* **40** 251-271.

[72] MARCHANT, T.R. & ROBERTS, A.J. (1987) Properties of short-crested waves in water of finite depth. *J. Aust. Math. Soc.* B **29** 103-125.

[73] MADSEN, O.S. (1974) Stability of a sand bed under breaking waves. *Proc. 14th Conf. Coastal Eng.*, Copenhagen. Vol **2**, Chap 45. 776-794.

[74] MADSEN, O.S. & GRANT, W.D. (1976) Quantitative description of sediment transport by waves. *Proc. 15th Conf. Coastal Eng.* 1093-1112.

[75] MERCER, G.N. & ROBERTS, A.J. (1992) Standing waves in deep water. Their stability and extreme form. *Phys. Fluids* A **4** 259-269.

[76] MERCER, G.N. & ROBERTS, A.J. (1994) The form of standing waves on finite depth water. *Wave Motion* **19** 233-244.

[77] MUNK, W. (1955) High frequency spectrum of ocean waves. *J. Mar. Res* **14** 302-314.

[78] NAGAI, S. (1969) Pressures of standing waves on vertical wall. *J. of the Waterways and Harbours division*, ASCE. 53-76.

[79] NAGAI, S. (1973) Wave forces on structures. *Advances in Hydroscience.* **9** ed. Chow, V.T. Acad. Press.

[80] O'DONOGHUE, T. & GOLDSWORTHY, C.J. (1995) Random wave kinematics in front of sea walls. *Proc. Coastal Structures and Breakwaters, London,* UK.

[81] OUMERACI, H. (1994) Scour in front of vertical breakwaters - Review of problems. *Proceedings of International Workshop on Wave barriers in Deep waters, Yokosuka,* Japan.

[82] OUMERACI, H., ALLSOP, W., DE GROOT, M., CROUCH, R., VRIJLING, H. (1996) Probabilistic Design Tools for Vertical Breakwaters - Newsletter 4 *MAS3 - CT95 - 0041 Project report.*

[83] PENNY, W.G. & PRICE, A.T. (1952) Finite periodic stationary gravity waves in a perfect fluid. Part II. *Phil. Trans. Roy. Soc. Lond. A* **244** 254-284.

[84] PERLIN, M., LIN, H. & TING, C-L. (1993) On parasitic capillary waves generated by steep gravity waves: an experimental investigation with spatial and temporal measurements. *J. Fluid Mech.* **255** 597-620.

[85] PHILLIPS, O.M. (1981) The dispersion of short wavelets in the presence of a dominant long wave. *J. Fluid Mech.* **107** 465-485.

[86] PRUD'HOMME, J.O. & PEREZ, J.B. (1992) Overtopping on a vertical-faced breakwater. *Proc. 23rd Int. Conf. Coast. Eng,* Italy. 375-376.

[87] RAYLEIGH, J.W.S. (1876) *Phil. Mag.* **5** 257-279.

[88] RAYLEIGH, J.W.S. (1890) On the tension of water surfaces, clean and contaminated, investigated by the method of ripples. *Phil. Mag.* **30** 386.

[89] RAYLEIGH, J.W.S. (1915) Deep water waves, progressive or stationary to the third order approximation. *Proc. Roy. Soc. Lond.* A **91** 345-353.

[90] RUSSELL, J.S. (1844) Report on the committee on waves. *Proc. Brit. Ass. Adv. Sci.*, 7th meeting. 311-390.

[91] RUVINSKY, K.D. & FREYDMAN, G.I. (1981) On the generation of capillary-gravity waves by steep gravity waves. *Izves., Atmos. and Oceanic Phys.* **17**(7) 548-553.

[92] RUVINSKY, K.D., FELDSTEIN, F.I. & FREYDMAN, G.I. (1991) Numerical simulations of the quasi-stationary stage of ripple excitation by steep gravity-capillary waves. *J. Fluid Mech.* **230** 339-353.

[93] SACHS, R.L. (1991) On the existence of small amplitude solitary waves with strong surface tension. *Jour. Diff. Equ.* **90** 31-51.

[94] SCHOOLEY, A.H. (1958) Profiles of wind generated water waves in the capillary-gravity transition region. *J. Mar. Res.* **16** 100-108.

[95] SCHWARTZ, L.W. & VANDEN-BROECK, J-M. (1979) Numerical solution of the exact equations for capillary-gravity waves. *J. Fluid Mech.* **95** 119-139.

[96] SCHWARTZ, L.W. & WHITNEY, A.K. (1981) A semi-analytic solution for nonlinear standing waves in deep water. *J. Fluid Mech.* **107** 147-.

[97] SEKERZ-ZENKOVITCH, Y.I. (1956) On the theory of stationary capillary waves of finite amplitude on the surface of a heavy fluid. *Dokl. Akad. Nauk.* **109** 913-918.

[98] SEN, D. (1992) Interaction of steep waves with vertical walls. *ASCE Jour. Waterway, Port, Coastal & Ocean Engineering.* **118** 453-473.

[99] SHINBROT, M. (1981) The solitary wave with surface tension. *Quart. Appl. Math,* **39** 287-291.

[100] SHYU, J-H. & PHILLIPS, O.M. (1990) The blockage of gravity and capillary waves by longer waves and currents. *J. Fluid Mech.* **217** 115-141.

[101] SOULSBY, R.L. & DYER, K.R. (1981) The form of the near-bed velocity profile in tidally accelerating flow. *J. Geophys. Res.* **86** (C9). 8067-8074.

[102] STOKES, G.G. (1849) . *Trans. Camb. Phil. Soc.* **8** 449; reprinted in *Mathematical and Physical Papers,* Vol. **1** 210. Cambridge U.P.

[103] STOKES, G.G. (1847) On the theory of oscillatory waves. *Trans. Camb. Phil. Soc.* **8** 441-455; reprinted in *Mathematical and Physical Papers,* Vol. **1** 314-326. Cambridge U.P.

[104] TADJBAKHSH, I. & KELLER, J.B. (1960) Standing surface waves of finite amplitude. *J. Fluid Mech.* **8** 442-451.

[105] TANAKA, M. (1983) The stability of steep gravity waves. *J. Phys. Soc. Japan.* **52** 3047-3055.

[106] TANAKA, M. (1986) The stability of solitary waves. *Phys. Fluids.* **29** 650-655.

[107] TAYLOR, G.I. (1953) An experimental study of standing waves. *Proc. Roy. Soc.* A **243** 44-59.

[108] TAYLOR, G.I. (1959) The dynamics of thin sheets of fluids II. Waves on fluid sheets. *Proc. Roy. Soc.* A **253** 296-312.

[109] TELES DA SILVA, A.F. & PEREGRINE, D.H. (1988) Steep, steady surface waves on water of finite depth with constant vorticity. *J. Fluid Mech.* **195** 281-302.

[110] VANDEN-BROECK, J-M. (1991) Elevation solitary waves with surface tension. *Phys. Fluids A* **3** (11) 2659-2663.

[111] VANDEN-BROECK, J-M. & DIAS (1992) Gravity-capillary solitary waves in water of infinite depth and related free surface flows. *J. Fluid Mech.* **240** 549-557.

[112] VANDEN-BROECK, J-M. & SCHWARTZ, L.W. (1981) Numerical calculation of standing waves in water of arbitrary uniform depth. *Phys. Fluids A* **24** 812-815.

[113] DE WAAL, J.P. (1993) Influence of wind on wave overtopping of vertical walls. *Proc. 1st Workshop Monolithic Coastal Structures Project.*, Madrid. Part 1: Reports and papers.

[114] DE WAAL, J.P. (1994) Wave overtopping of vertical coastal structures. Influence of wave breaking and wind. *Proc. 2nd Workshop Monolithic Coastal Structures Project.*, Milan. Part 2: Reports and papers.

[115] DE WAAL, J.P. & VAN DER MEER, J.W (1992) Wave run-up and overtopping on coastal structures. *Proc. 23rd Int. Conf. Coastal Eng.*, Italy.

[116] WILTON, J.R. (1915) On ripples. *Phil. Mag.* **29** 688-700.

[117] YAMAMOTO, Y. & HORIKAWA, K. (1992) New methods to evaluate run up height and wave overtopping. *Proc. 23rd Int. Conf. Coast. Eng.*, Italy.

UNIVERSITY
OF BRISTOL
LIBRARY